frontiers | Research Topics

Insights in cardiovascular therapeutics 2022

Edited by
Xiaofeng Yang and Yuling Zhang

Published in
Frontiers in Cardiovascular Medicine

ISSN 1664-8714
ISBN 978-2-8325-2314-8
DOI 10.3389/978-2-8325-2314-8

About Frontiers

Frontiers is more than just an open access publisher of scholarly articles: it is a pioneering approach to the world of academia, radically improving the way scholarly research is managed. The grand vision of Frontiers is a world where all people have an equal opportunity to seek, share and generate knowledge. Frontiers provides immediate and permanent online open access to all its publications, but this alone is not enough to realize our grand goals.

Frontiers journal series

The Frontiers journal series is a multi-tier and interdisciplinary set of open-access, online journals, promising a paradigm shift from the current review, selection and dissemination processes in academic publishing. All Frontiers journals are driven by researchers for researchers; therefore, they constitute a service to the scholarly community. At the same time, the *Frontiers journal series* operates on a revolutionary invention, the tiered publishing system, initially addressing specific communities of scholars, and gradually climbing up to broader public understanding, thus serving the interests of the lay society, too.

Dedication to quality

Each Frontiers article is a landmark of the highest quality, thanks to genuinely collaborative interactions between authors and review editors, who include some of the world's best academicians. Research must be certified by peers before entering a stream of knowledge that may eventually reach the public - and shape society; therefore, Frontiers only applies the most rigorous and unbiased reviews. Frontiers revolutionizes research publishing by freely delivering the most outstanding research, evaluated with no bias from both the academic and social point of view. By applying the most advanced information technologies, Frontiers is catapulting scholarly publishing into a new generation.

What are Frontiers Research Topics?

Frontiers Research Topics are very popular trademarks of the *Frontiers journals series*: they are collections of at least ten articles, all centered on a particular subject. With their unique mix of varied contributions from Original Research to Review Articles, Frontiers Research Topics unify the most influential researchers, the latest key findings and historical advances in a hot research area.

Find out more on how to host your own Frontiers Research Topic or contribute to one as an author by contacting the Frontiers editorial office: frontiersin.org/about/contact

Insights in cardiovascular therapeutics: 2022

Topic editors

Xiaofeng Yang — Temple University, United States

Yuling Zhang — Sun Yat-sen Memorial Hospital, China

Citation

Yang, X., Zhang, Y., eds. (2023). *Insights in cardiovascular therapeutics: 2022*. Lausanne: Frontiers Media SA. doi: 10.3389/978-2-8325-2314-8

Table of contents

frontiers | Frontiers in Cardiovascular Medicine

TYPE Editorial
PUBLISHED 18 April 2023
DOI 10.3389/fcvm.2023.1184030

OPEN ACCESS

EDITED BY
Hong S. Lu,
University of Kentucky, United States

*CORRESPONDENCE
Xiaofeng Yang
xiao-feng.yang@temple.edu

RECEIVED 10 March 2023
ACCEPTED 06 April 2023
PUBLISHED 18 April 2023

CITATION
Xu K, Zhang Y, Saaoud F, Shao Y, Lu Y, Jiang X, Wang H and Yang X (2023) Editorial: Insights in cardiovascular therapeutics 2022—cardiovascular innate immunity.
Front. Cardiovasc. Med. 10:1184030.
doi: 10.3389/fcvm.2023.1184030

Editorial: Insights in cardiovascular therapeutics 2022—cardiovascular innate immunity

Keman Xu[1], Yuling Zhang[2], Fatma Saaoud[1], Ying Shao[1], Yifan Lu[1], Xiaohua Jiang[1,3], Hong Wang[3] and Xiaofeng Yang[1,3]*

[1]Cardiovascular Research Center, Departments of Cardiovascular Sciences and Biomedical Education and Data Sciences, Temple University Lewis Katz School of Medicine, Philadelphia, PA, United States, [2]Department of Cardiology, Sun Yat-sen Memorial Hospital, Zhongshan University, Guangzhou, China, [3]Centers for Metabolic Disease Research, Department of Cardiovascular Sciences, Temple University Lewis Katz School of Medicine, Philadelphia, PA, United States

KEYWORDS

cardiovascular disease, Innate immunity, trained immunity, endothelial cell, innate immune cell

Editorial on the Research Topic
Insights in cardiovascular therapeutics 2022—cardiovascular innate immunity

Introduction

Thanks to the efforts and support of the authors and editorial team, our Research topic entitled "*Insights in Cardiovascular Therapeutics: 2022*" in the Frontiers in Cardiovascular Medicine, Cardiovascular Pharmacology and Drug Discovery Section has achieved great success and attracted more than 13,500 views in the past 12 months. Within this topic, we highlight nine original research papers published related to cardiovascular tissue injury and remodeling, cardiovascular innate immunity, trained immunity, and recent advances in cardiovascular therapies. These highlights may serve as the foundation for new developments in cardiovascular pharmacology and drug discovery areas. Looking ahead to 2023, we will continue our work to provide an outstanding platform for cardiologists, translational cardiovascular scientists, and cardiovascular pharmacological scientists to share new findings in clinical cardiology, cardiovascular pharmacology and drug discovery, and translational cardiovascular therapeutics.

Trained immunity is a novel mechanism underlying the pathogenesis of cardiovascular diseases

Cardiovascular diseases (CVDs) represent a leading cause of death worldwide. However, the specific mechanisms and potential treatment options for CVDs have yet to be fully addressed. Noteworthy, chronic non-resolving low-grade inflammation is known to be a major feature in the pathogenesis of CVDs (1). Increasing evidence indicates that the innate immune system contributes to CVD development (2–4). Recently, it has been

discovered that innate immune cells can produce a long-lasting proinflammatory phenotype after certain stimulations by either exogenous pathogen-associated molecular patterns (PAMPs)/damage-associated molecular patterns (DAMPs) or endogenous metabolic stress-derived stimuli (2, 5). This persistent hyperactivation of the innate immune system is referred to trained immunity (also termed as innate immune memory) (4, 6–14).

Trained immunity is a functional status of enhanced innate immune/proinflammatory responses *via* metabolic reprogramming in generating methyl, acetyl, and other chemical moieties (15), which induces long-term epigenetic reprogramming around the promoters of inflammatory genes (8, 16). These epigenetic changes are associated with immune protection against infections or exacerbated inflammations (11) after re-stimulation (14). In contrast to the adaptive immune system, trained immunity lacks antigen-specific recognition (17–19), but leads to a cross-reaction and protects against different pathogens other than the one to which it was initially exposed (3). Nevertheless, as with adaptive immunity (20), innate immune cells may develop immunological memory after encountering a specific insult to adjust their response to subsequent stimulations (14). Innate immune cells that have been "trained" respond more effectively to the possibility of re-stimulation by the same or different insults. One of the other differences between adaptive immune memory and innate immune memory is that special subsets of adaptive immune cells carry out memory functions (21), whereas innate immune memory is the functional status of all innate immune cells experienced metabolic reprogramming (4). Trained immunity serves as a new mechanism underlying chronic metabolic cardiovascular diseases. In addition, trained immunity can be a qualification criteria for environmental, metabolic, and infectious stimuli to become significant cardiovascular disease risk factors such as hyperlipidemia (22–27), hyperglycemia (28–30), hyperhomocysteinemia (31, 32), cigarette smoke (12, 33, 34), hypertension, infections (11, 35), metabolic syndrome, and obesity (23, 36, 37), which are different from insignificant endogenous metabolites and compounds in the foods in inducing trained immunity and enhancing inflammation (8, 33).

Cardiovascular structural cell types, such as endothelial cells and vascular smooth muscle cells, serve as innate immune cells

As mentioned above, trained immunity is inseparable from innate immune cells. Classically, phagocytes (macrophages and neutrophils), mast cells, dendritic cells, basophils, eosinophils, natural killer (NK) cells, and innate lymphoid cells are identified as innate immune cells (38). Despite their various types, innate immune cells share a common feature: they are all monocytic and antigen-presenting white blood cells. This type of innate immune cell functionalized the role of cell migration and engulfment in cellular interaction during the immune process or inflammation. With the intensive study of the immune system, scientists discovered that innate immune cells are not limited to white blood cells. However, stressful circumstances could transform somatic cells into innate immune cells. Endothelial cells (ECs), the innermost layer of the vessel wall, play a critical role in maintaining cardiovascular homeostasis in health or contributing to the pathological mechanisms in multiple CVDs (39–41). In 2013 (*Journal of Hematology and Oncology* (42, 43), we proposed a new concept: that endothelial cells (ECs) actively participate in innate and adaptive immune responses and carry out all the innate immune functions, the same as prototypical innate immune cell macrophages (44, 45). Therefore, we classified ECs as novel immune cells. The same qualities expressed in traditional innate immune cells are also present in ECs, such as danger associated molecular patterns (DAMPs)/pathogen-associated molecular patterns (PAMPs)-sensing; secretions of cytokines, chemokines, and secretomes (35); phagocytic function; antigen presentation; pro/anti-inflammatory; immunosuppression; migration; plasticity; and heterogeneity (43). Forming the trained phenotype requires metabolic reprogramming, including transitioning from oxidative phosphorylation (OXPHOS) to enhanced glycolysis (13). Oxidized low-density lipoprotein (ox-LDL) (46), a well-established risk factor for CVD, plays a key role in the induction of trained immunity. Evidence reports that ox-LDL mediates immunologic memory in ECs by switching OXPHOS to glycolysis, *via* significantly increases the enrichment of histone 3 lysine 27 trimethylation/histone 3 lysine 27 acetylation (H3K27m3/H3K27ac) and H3K14ac (8) at the enhancers or promoters of proinflammatory cytokines, such as interleukin (IL) 6 and IL8, through mammalian target of rapamycin- hypoxia-inducible factor 1 alpha (mTOR-HIF1α) signaling in ECs (47). In addition to ox-LDL, reactive oxygen species (ROS) (48) are the upstream activator of the leucine-rich repeats (LRR) containing domain, nucleotide oligomerization domain (NOD), and pyrin domain-containing protein 3 (NLRP3) caspase 1 inflammasome, which has a positive correlation with trained immunity activation. Taken together, trained immunity in ECs is functional for inflammation effectiveness and transition to chronic inflammation (4).

In addition, vascular pathologies reshape vascular smooth muscle cells (VSMCs) into six different phenotypes, including contractile, mesenchymal, fibroblast, macrophage (innate immune cell prototype) (49), foam cell-like, osteochondrogenic-like, myofibroblast-like (50), osteogenic, and adipocyte in response to stimulations of DAMPs/PAMPs (51). We also reported that chronic kidney disease -uremic toxins (52) activate the VSMC phenotypic switch (53) and the proinflammatory caspase-1-inflammasome pathway (innate immune sensors) (5) to promote neointima hyperplasia in the carotid artery (54). Others have also reported that ox-LDL induces trained innate immunity in human coronary VSMCs (55). Taken together, we propose a new concept: that VSMCs in pathologies are an innate immune cell type.

TABLE 1 Nine highly viewed research papers, published in our special topic entitled "Insights in Cardiovascular Therapeutics: 2022", are summarized.

Disease model	Therapeutic study	Experimental Outcomes	Reference
Coronary artery disease after percutaneous coronary intervention (PCI)	Long term beta-blocker maintenance with stable CAD after PCI with DES stent	No Clinic improvement outcomes	(Lee et al.)
Diabetic mice ($Lepr^{db}$)	Treated alternate day fasting for 12 weeks	Improve endothelial function and reduce fasting blood glucose level	(Cui et al.)
Murine hind limb gangrene model	E-selectin/AAV2/2 gene therapy	Reduced gangrene severity	(Ribieras et al.)
IL12p40-/- mouse model	LPS-induced cardiac dysfunction	IL12p40 deletion aggravated LPS-induced cardiac injury	(Liu et al)
Patients undergoing non-cardiac surgery (MINS)	Midazolam administration	Midazolam may not pose a significant risk for MINS	(Prin et al.)
Chronic kidney disease patients	The contribution of CKD-associated factors to the chronic remodeling of veins	Age and diabetes are the most important risk factors for chronic development of venous intimal hyperplasia and fibrosis independent of CKD status	(Labissiere et al.)
Patients with DES	Compared long DES vs. spot DES for FP lesion longer than 150mm	Long DES were more effective than spot DES for treating long FP lesion	(Park et al.)
Diabetic mice db/db mice	Agonistic analog of growth hormone-releasing hormone, GHRH-A MR409 injection	GHRH-A MR409 can effectively attenuate vascular calcification and protect against EC dysfunction	(Ren et al.)
Patients with Cocoon patent foramen ovale occluder	To assess the preliminary efficacy and safety profile of PFO closure with Cocoon device in an Italian multi-center registry	Percutaneous closure of PFO with Cocoon Occluder provided satisfactory procedural and mid-term clinical follow-up results in a real world registry.	(Testa et al.)

Nine research papers related to therapeutic studies in cardiovascular diseases, inflammation, and trained immunity have been published

Academic research plays a vital role in identifying new therapeutic targets, including understanding target biology and the connections between novel therapeutic targets and disease states. CVDs, as diseases with high mortality and morbidity, have long been the subject of research by scientists or medical experts seeking potential therapies. A comprehensive analysis of trained immunity in relation to CVD might offer novel perspectives on the pathophysiology of the disease and new treatment options. Cui et al. reported that alternate-day fasting (ADF) reduced fasting blood glucose levels and improved endothelium (EC) function in diabetic mice, indicating the therapeutic potential of blocking novel trained immunity-related metabolic pathways, including glycolysis. Ribieras et al. proved that cell adhesion molecule secretion from ECs is critical for inflammation and neovascularization in areas of wound healing and ischemia. Liu et al. demonstrated that interleukin-12 (IL12)p40, the common subunit of IL12 and IL23, was associated with the classic trained immunity stimuli: LPS-induced cardiac injury; Ren et al. showed that the agonistic analog of growth hormone-releasing hormone (GHRH-A) MR409, can effectively attenuate vascular calcification and trained immunity mediator ROS expression and improve EC function and diabetics. **Table 1** summarizes nine significant studies on our research topic.

Author contributions

KX carried out literature collections and drafted the manuscript. YZ, FS, YS, YL, XJ, and HW provided editing input. XY supervised and edited the manuscript. All authors listed have made a substantial, direct, and intellectual contribution to the work and approved it for publication. All authors contributed to the article and approved the submitted version.

Conflict of interest

The authors declare that the research was conducted in the absence of any commercial or financial relationships that could be construed as a potential conflict of interest.

Publisher's note

References

1. Yang XF, Yin Y, Wang H. VASCULAR INFLAMMATION AND ATHEROGENESIS ARE ACTIVATED VIA RECEPTORS FOR PAMPs AND SUPPRESSED BY REGULATORY T CELLS. *Drug Discov Today Ther Strateg.* (2008) 5:125–42. doi: 10.1016/j.ddstr.2008.11.003

2. Flores-Gomez D, Bekkering S, Netea MG, Riksen NP. Trained immunity in atherosclerotic cardiovascular disease. *Arterioscler Thromb Vasc Biol.* (2021) 41:62–9. doi: 10.1161/ATVBAHA.120.314216

3. Zieleniewska NA, Kazberuk M, Chlabicz M, Eljaszewicz A, Kaminski K. Trained immunity as a trigger for atherosclerotic cardiovascular disease-A literature review. *J Clin Med.* (2022) 11(12):3369. doi: 10.3390/jcm11123369

4. Drummer C, Saaoud F, Shao Y, Sun Y, Xu K, Lu Y, et al. Trained immunity and reactivity of macrophages and endothelial cells. *Arterioscler Thromb Vasc Biol.* (2021) 41:1032–46. doi: 10.1161/ATVBAHA.120.315452

5. Yin Y, Pastrana JL, Li X, Huang X, Mallilankaraman K, Choi ET, et al. Inflammasomes: sensors of metabolic stresses for vascular inflammation. *Front Biosci.* (2013) 18:638–49. doi: 10.2741/4127

6. Drummer CIV, Saaoud F, Sun Y, Atar D, Xu K, Lu Y, et al. Hyperlipidemia may synergize with hypomethylation in establishing trained immunity and promoting inflammation in NASH and NAFLD. *J Immunol Res.* (2021) 2021:3928323. doi: 10.1161/ATVBAHA.120.315452

7. Zhong C, Yang X, Feng Y, Yu J. Trained immunity: an underlying driver of inflammatory atherosclerosis. *Front Immunol.* (2020) 11:284. doi: 10.3389/fimmu.2020.00284

8. Lu Y, Sun Y, Drummer IV C, Nanayakkara GK, Shao Y, Saaoud F, et al. Increased acetylation of H3K14 in the genomic regions that encode trained immunity enzymes in lysophosphatidylcholine-activated human aortic endothelial cells—novel qualification markers for chronic disease risk factors and conditional DAMPs. *Redox Biol.* (2019) 24:101221. doi: 10.1016/j.redox.2019.101221

9. Fagenson AM, Xu K, Saaoud F, Nanayakkara G, Jhala NC, Liu L, et al. Liver ischemia reperfusion injury, enhanced by trained immunity, is attenuated in caspase 1/caspase 11 double gene knockout mice. *Pathogens.* (2020) 9(11):879. doi: 10.3390/pathogens9110879

10. Li X, Fang P, Sun Y, Shao Y, Yang WY, Jiang X, et al. Anti-inflammatory cytokines IL-35 and IL-10 block atherogenic lysophosphatidylcholine-induced, mitochondrial ROS-mediated innate immune activation, but spare innate immune memory signature in endothelial cells. *Redox Biol.* (2020) 28:101373. doi: 10.1016/j.redox.2019.101373

11. Shao Y, Saredy J, Xu K, Sun Y, Saaoud F, Drummer C, et al. Endothelial immunity trained by coronavirus infections, DAMP stimulations and regulated by anti-oxidant NRF2 may contribute to inflammations, myelopoiesis, COVID-19 cytokine storms and thromboembolism. *Front Immunol.* (2021) 12:653110. doi: 10.3389/fimmu.2021.653110

12. Shao Y, Saaoud F, Cornwell W, Xu K, Kirchhoff A, Lu Y, et al. Cigarette smoke and morphine promote treg plasticity to Th17 via enhancing trained immunity. *Cells.* (2022) 11(18):2810. doi: 10.3390/cells11182810

13. Saaoud F, Liu L, Xu K, Cueto R, Shao Y, Lu Y, et al. Aorta- and liver-generated TMAO enhances trained immunity for increased inflammation via ER stress/mitochondrial ROS/glycolysis pathways. *JCI Insight.* (2023) 8(1):e158183. doi: 10.1172/jci.insight.158183

14. Ochando J, Mulder WJM, Madsen JC, Netea MG, Duivenvoorden R. Trained immunity—basic concepts and contributions to immunopathology. *Nat Rev Nephrol.* (2023) 19:23–37. doi: 10.1038/s41581-022-00633-5

15. Huang Z, Song S, Zhang X, Zeng L, Sun A, Ge J. Metabolic substrates, histone modifications, and heart failure. *Biochim Biophys Acta Gene Regul Mech.* (2023) 1866:194898. doi: 10.1016/j.bbagrm.2022.194898

16. Millan-Zambrano G, Burton A, Bannister AJ, Schneider R. Histone post-translational modifications—cause and consequence of genome function. *Nat Rev Genet.* (2022) 23:563–80. doi: 10.1038/s41576-022-00468-7

17. Yang F, Chen IH, Xiong Z, Yan Y, Wang H, Yang XF. Model of stimulation-responsive splicing and strategies in identification of immunogenic isoforms of tumor antigens and autoantigens. *Clin Immunol.* (2006) 121:121–33. doi: 10.1016/j.clim.2006.06.007

18. Yang F, Yang XF. New concepts in tumor antigens: their significance in future immunotherapies for tumors. *Cell Mol Immunol.* (2005) 2:331–41.

19. Ng B, Yang F, Huston DP, Yan Y, Yang Y, Xiong Z, et al. Increased noncanonical splicing of autoantigen transcripts provides the structural basis for expression of untolerized epitopes. *J Allergy Clin Immunol.* (2004) 114:1463–70. doi: 10.1016/j.jaci.2004.09.006

20. Xu K, Yang WY, Nanayakkara GK, Shao Y, Yang F, Hu W, et al. GATA3, HDAC6, and BCL6 regulate FOXP3+ treg plasticity and determine treg conversion into either novel antigen-presenting cell-like treg or Th1-treg. *Front Immunol.* (2018) 9:45. doi: 10.3389/fimmu.2018.00045

21. Shen H, Wu N, Nanayakkara G, Fu H, Yang Q, Yang WY, et al. Co-signaling receptors regulate T-cell plasticity and immune tolerance. *Front Biosci (Landmark Ed).* (2019) 24:96–132. doi: 10.2741/4710

22. Yin Y, Li X, Sha X, Xi H, Li YF, Shao Y, et al. Early hyperlipidemia promotes endothelial activation via a caspase-1-sirtuin 1 pathway. *Arterioscler Thromb Vasc Biol.* (2015) 35:804–16. doi: 10.1161/ATVBAHA.115.305282

23. Virtue A, Johnson C, Lopez-Pastrana J, Shao Y, Fu H, Li X, et al. MicroRNA-155 deficiency leads to decreased atherosclerosis, increased white adipose tissue obesity, and non-alcoholic fatty liver disease: a NOVEL MOUSE MODEL OF OBESITY PARADOX. *J Biol Chem.* (2017) 292:1267–87. doi: 10.1074/jbc.M116.739839

24. Mai J, Nanayakkara G, Lopez-Pastrana J, Li X, Li YF, Wang X, et al. Interleukin-17A promotes aortic endothelial cell activation via transcriptionally and post-translationally activating p38 MAPK pathway. *J Biol Chem.* (2016) 291(10):4939–54. doi: 10.1074/jbc.M115.690081

25. Li X, Shao Y, Sha X, Fang P, Kuo YM, Andrews AJ, et al. IL-35 (Interleukin-35) suppresses endothelial cell activation by inhibiting mitochondrial reactive oxygen Species-mediated site-specific acetylation of H3K14 (histone 3 lysine 14). *Arterioscler Thromb Vasc Biol.* (2018) 38:599–609. doi: 10.1161/ATVBAHA.117.310626

26. Saaoud F, Wang J, Iwanowycz S, Wang Y, Altomare D, Shao Y, et al. Bone marrow deficiency of mRNA decaying protein tristetraprolin increases inflammation and mitochondrial ROS but reduces hepatic lipoprotein production in LDLR knockout mice. *Redox Biol.* (2020) 37:101609. doi: 10.1016/j.redox.2020.101609

27. Shao Y, Yang WY, Saaoud F, Drummer IV C, Sun Y, Xu K, et al. IL-35 promotes CD4 + Foxp3+ tregs and inhibits atherosclerosis via maintaining CCR5-amplified treg-suppressive mechanisms. *JCI Insight.* (2021) 6(19):e152511. doi: 10.1172/jci.insight.152511

28. Fang P, Zhang D, Cheng Z, Yan C, Jiang X, Kruger WD, et al. Hyperhomocysteinemia potentiates hyperglycemia-induced inflammatory monocyte differentiation and atherosclerosis. *Diabetes.* (2014) 63(12):4275–90. doi: 10.2337/db14-0809

29. Yan Y, Xiong Z, Zhang S, Song J, Huang Y, Thornton AM, et al. CD25high T cells with a prolonged survival inhibit development of diabetes. *Int J Immunopathol Pharmacol.* (2008) 21:767–80. doi: 10.1177/039463200802100401

30. Fang P, Li X, Shan H, Saredy JJ, Cueto R, Xia J, et al. Ly6C(+) inflammatory monocyte differentiation partially mediates hyperhomocysteinemia-induced vascular dysfunction in type 2 diabetic db/db mice. *Arterioscler Thromb Vasc Biol.* (2019) 39:2097–119. doi: 10.1161/ATVBAHA.119.313138

31. Jamaluddin MD, Chen I, Yang F, Jiang X, Jan M, Liu X, et al. Homocysteine inhibits endothelial cell growth via DNA hypomethylation of the cyclin agene. *Blood.* (2007) 110:3648–55. doi: 10.1182/blood-2007-06-096701

32. Jamaluddin MS, Yang X, Hyperhomocysteinemia WH. DNA Methylation and vascular disease. *Clin Chem Lab Med.* (2007) 45:1660–6. doi: 10.1515/CCLM.2007.350

33. Saaoud F, Shao Y, Cornwell W, Wang H, Rogers T, Yang X. Cigarette smoke modulates inflammation and immunity via ROS-regulated trained immunity and trained tolerance mechanisms. *Antioxid Redox Signaling.* (2022). doi: 10.1089/ars.2022.0087

34. Shao Y, Cornwell W, Xu K, Kirchhoff A, Saasoud F, Lu Y, et al. Chronic exposure to the combination of cigarette smoke and morphine decreases CD4(+) regulatory T cell numbers by reprogramming the treg cell transcriptome. *Front Immunol.* (2022) 13:887681. doi: 10.3389/fimmu.2022.887681

35. Lu Y, Sun Y, Xu K, Saaoud F, Shao Y, Drummer C, et al. Aorta in pathologies may function as an immune organ by upregulating secretomes for immune and vascular cell activation, differentiation and trans-differentiation-early secretomes may serve as drivers for trained immunity. *Front Immunol.* (2022) 13:858256. doi: 10.3389/fimmu.2022.858256

36. Johnson C, Drummer C, Virtue A, Gao T, Wu S, Hernandez M, et al. Increased expression of resistin in MicroRNA-155-deficient white adipose tissues may be a possible driver of metabolically healthy obesity transition to classical obesity. *Front Physiol.* (2018) 9:1297. doi: 10.3389/fphys.2018.01297

37. Johnson C, Drummer IV C, Shan H, Shao Y, Sun Y, Lu Y, et al. A novel subset of CD95(+) pro-inflammatory macrophages overcome miR155 deficiency and may serve as a switch from metabolically healthy obesity to metabolically unhealthy obesity. *Front Immunol.* (2020) 11:619951. doi: 10.3389/fimmu.2020.619951

38. Holmgren K. Urinary calculi and urinary tract infection. A clinical and microbiological study. *Scand J Urol Nephrol Suppl.* (1986) 98:1–71.

39. Rubanyi GM. The role of endothelium in cardiovascular homeostasis and diseases. *J Cardiovasc Pharmacol.* (1993) 22(Suppl 4):S1–14. doi: 10.1097/00005344-199322004-00002

40. Xu K, Saaoud F, Yu S, Ct D, Shao Y, Sun Y, et al. Monocyte adhesion assays for detecting endothelial cell activation in vascular inflammation and atherosclerosis. *Methods Mol Biol.* (2022) 2419:169–82. doi: 10.1007/978-1-0716-1924-7_10

41. Xu K, Shao Y, Saaoud F, Gillespie A, Drummer C, Liu L, et al. Novel knowledge-based transcriptomic profiling of lipid lysophosphatidylinositol-induced endothelial cell activation. *Front Cardiovasc Med.* (2021) 8:773473. doi: 10.3389/fcvm.2021.773473

42. Mai J, Virtue A, Shen J, Wang H, Yang XF. An evolving new paradigm: endothelial cells–conditional innate immune cells. *J Hematol Oncol.* (2013) 6:61. doi: 10.1186/1756-8722-6-61

43. Shao Y, Saredy J, Yang WY, Sun Y, Lu Y, Saaoud F, et al. Vascular endothelial cells and innate immunity. *Arterioscler Thromb Vasc Biol.* (2020) 40:e138–52. doi: 10.1161/ATVBAHA.120.314330

44. Lai B, Wang J, Fagenson A, Sun Y, Saredy J, Lu Y, et al. Twenty novel disease group-specific and 12 new shared macrophage pathways in eight groups of 34

diseases including 24 inflammatory organ diseases and 10 types of tumors. *Front Immunol*. (2019) 10:2612. doi: 10.3389/fimmu.2019.02612

45. Drummer C, Saaoud F, Jhala NC, Cueto R, Sun Y, Xu K, et al. Caspase-11 promotes high-fat diet-induced NAFLD by increasing glycolysis, OXPHOS, and pyroptosis in macrophages. *Front Immunol*. (2023) 14:1113883. doi: 10.3389/fimmu.2023.1113883

46. Sun Y, Lu Y, Saredy J, Wang X, Drummer IV C, Shao Y, et al. ROS Systems are a new integrated network for sensing homeostasis and alarming stresses in organelle metabolic processes. *Redox Biol*. (2020) 37:101696. doi: 10.1016/j.redox.2020.101696

47. Sohrabi Y, Lagache SMM, Voges VC, Semo D, Sonntag G, Hanemann I, et al. OxLDL-mediated immunologic memory in endothelial cells. *J Mol Cell Cardiol*. (2020) 146:121–32. doi: 10.1016/j.yjmcc.2020.07.006

48. Li X, Fang P, Li Y, Kuo YM, Andrews AJ, Nanayakkara G, et al. Mitochondrial reactive oxygen Species mediate lysophosphatidylcholine-induced endothelial cell activation. *Arterioscler Thromb Vasc Biol*. (2016) 36:1090–100. doi: 10.1161/ATVBAHA.115.306964

49. Bennett MR, Sinha S, Owens GK. Vascular smooth muscle cells in atherosclerosis. *Circ Res*. (2016) 118:692–702. doi: 10.1161/CIRCRESAHA.115.306361

50. Grootaert MOJ, Bennett MR. Vascular smooth muscle cells in atherosclerosis: time for a re-assessment. *Cardiovasc Res*. (2021) 117:2326–39. doi: 10.1093/cvr/cvab046

51. Yap C, Mieremet A, de Vries CJM, Micha D, de Waard V. Six shades of vascular smooth muscle cells illuminated by KLF4 (kruppel-like factor 4). *Arterioscler Thromb Vasc Biol*. (2021) 41:2693–707. doi: 10.1161/ATVBAHA.121.316600

52. Sun Y, Johnson C, Zhou J, Wang L, Li YF, Lu Y, et al. Uremic toxins are conditional danger- or homeostasis-associated molecular patterns. *Front Biosci (Landmark Ed)*. (2018) 23:348–87. doi: 10.2741/4595

53. Monroy MA, Fang J, Li S, Ferrer L, Birkenbach MP, Lee IJ, et al. Chronic kidney disease alters vascular smooth muscle cell phenotype. *Front Biosci (Landmark Ed)*. (2015) 20:784–95. doi: 10.2741/4337

54. Ferrer LM, Monroy AM, Lopez-Pastrana J, Nanayakkara G, Cueto R, Li YF, et al. Caspase-1 plays a critical role in accelerating chronic kidney disease-promoted neointimal hyperplasia in the carotid artery. *J Cardiovasc Transl Res*. (2016) 9 (2):135–44. doi: 10.1007/s12265-016-9683-3

55. Schnack L, Sohrabi Y, Lagache SMM, Kahles F, Bruemmer D, Waltenberger J, et al. Mechanisms of trained innate immunity in oxLDL primed human coronary smooth muscle cells. *Front Immunol*. (2019) 10:13. doi: 10.3389/fimmu.2019.00013

frontiers | Frontiers in Cardiovascular Medicine

ORIGINAL RESEARCH
published: 17 May 2022
doi: 10.3389/fcvm.2022.878003

Long-Term Beta-Blocker Therapy in Patients With Stable Coronary Artery Disease After Percutaneous Coronary Intervention

Seung-Jun Lee[1†], Dong-Woo Choi[2,3†], Choongki Kim[4], Yongsung Suh[5], Sung-Jin Hong[1], Chul-Min Ahn[1], Jung-Sun Kim[1], Byeong-Keuk Kim[1], Young-Guk Ko[1], Donghoon Choi[1], Eun-Cheol Park[2], Yangsoo Jang[6], Chung-Mo Nam[2] and Myeong-Ki Hong[1*]*

[1] Severance Cardiovascular Hospital, Yonsei University College of Medicine, Seoul, South Korea, [2] Department of Preventive Medicine, Yonsei University College of Medicine, Seoul, South Korea, [3] Cancer Big Data Center, National Cancer Control Institute, National Cancer Center, Goyang, South Korea, [4] Seoul Hospital, Ewha Womans University College of Medicine, Seoul, South Korea, [5] Myongji Hospital, Hanyang University College of Medicine, Goyang, South Korea, [6] CHA Bundang Medical Center, CHA University College of Medicine, Seongnam, South Korea

OPEN ACCESS

Edited by:
Xiaofeng Yang,
Temple University, United States

Reviewed by:
Yifan Lu,
Temple University, United States
Jing-Song Ou,
The First Affiliated Hospital of Sun Yat-sen University, China

***Correspondence:**
Myeong-Ki Hong
mkhong61@yuhs.ac
Chung-Mo Nam
cmnam@yuhs.ac

[†] These authors have contributed equally to this work

Specialty section:
This article was submitted to Cardiovascular Therapeutics, a section of the journal Frontiers in Cardiovascular Medicine

Received: *11 March 2022*
Accepted: *15 April 2022*
Published: *17 May 2022*

Citation:
Lee S-J, Choi D-W, Kim C, Suh Y, Hong S-J, Ahn C-M, Kim J-S, Kim B-K, Ko Y-G, Choi D, Park E-C, Jang Y, Nam C-M and Hong M-K (2022) Long-Term Beta-Blocker Therapy in Patients With Stable Coronary Artery Disease After Percutaneous Coronary Intervention. Front. Cardiovasc. Med. 9:878003. doi: 10.3389/fcvm.2022.878003

Background: It is unclear whether beta-blocker treatment is advantageous in patients with stable coronary artery disease (CAD) who underwent percutaneous coronary intervention (PCI). We evaluated the clinical impact of long-term beta-blocker maintenance in patients with stable CAD after PCI with drug-eluting stent (DES).

Methods: From a nationwide cohort database, we identified the stable CAD patients without current or prior history of myocardial infarction or heart failure who underwent DES implantation. An intention-to-treat principle was used to analyze the impact of beta-blocker treatment on long-term outcomes of major adverse cardiovascular events (MACE) composed of cardiovascular death, myocardial infarction, and hospitalization with heart failure.

Results: After stabilized inverse probability of treatment weighting, a total of 78,380 patients with stable CAD was enrolled; 45,746 patients with and 32,634 without beta-blocker treatment. At 5 years after PCI with a 6-month quarantine period, the adjusted incidence of MACE was significantly higher in patients treated with beta-blockers [10.0 vs. 9.1%; hazard ratio (HR) 1.11, 95% CI 1.06–1.16, $p < 0.001$] in an intention-to-treat analysis. There was no significant difference in all-cause death between patients treated with and without beta-blockers (8.1 vs. 8.2%; HR 0.99, 95% CI 0.94–1.04, $p = 0.62$). Statistical analysis with a time-varying Cox regression and rank-preserving structure failure time model revealed similar results to the intention-to-treat analysis.

Conclusions: Among patients with stable CAD undergoing DES implantation, long-term maintenance with beta-blocker treatment might not be associated with clinical outcome improvement.

Trial Registration: ClinicalTrial.gov (NCT04715594).

Keywords: percutaneous coronary intervention, coronary artery disease, beta-blocker, drug-eluting stents, treatment outcome

INTRODUCTION

Beta-blockers are considered the primary choice in long-term maintenance drug therapy in patients with coronary artery disease, based on positive evidence for improving clinical outcomes in patients with acute myocardial infarction (MI) (1, 2) or heart failure (3). Long-term beta-blocker maintenance is associated with reduced mortality after percutaneous coronary intervention (PCI) in patients with acute MI (4). However, there is a lack of evidence supporting the beneficial impact of long-term beta-blocker treatment in patients with stable coronary artery disease (CAD) (5). Randomized clinical studies, which usually enroll small patient numbers (6), and observational studies (7, 8) have found no significant benefit to beta-blocker treatment in reducing mortality or ischemic events among patients with stable CAD. Furthermore, published data evaluating the clinical benefits of beta-blocker treatment in patients with stable CAD under the specific situation of post-PCI with drug-eluting stents (DES) is very rare. Using a nationwide cohort database, we sought to investigate the clinical impact of long-term beta-blocker maintenance in patients with stable CAD after PCI with DES.

MATERIALS AND METHODS

Study Design and Data

This study was a nationwide retrospective analysis of the National Health Claims database established by the National Health Insurance Service (NHIS) of Korea, which contains claimed medical costs, detailed information on prescribed drugs including the number of pills and drug dosage, and medical history presented as International Classification of Diseases, Tenth Revision (ICD-10) codes. A majority (97.1%) of the Korean population is required to subscribe to the NHIS, which is the sole insurer managed by the Korean government. Considering that the NHIS also covers information for the remaining population (2.9%) categorized as medical aid subjects, this cohort is considered to represent the entire Korean population (9). This study was approved by the Institutional Review Board of our institute. Informed consent was waived because personal information was masked after cohort generation according to strict confidentiality guidelines of the Korean Health Insurance Review and Assessment Service. This study is registered at ClinicalTrial.gov (NCT04715594). We were also provided with death certificates including ICD-10 codes from the National Institute of Statistics of Korea.

Study Population

Among the 52 million citizens included in the NHIS database, we identified 214,340 patients (≥20 years old) who underwent DES implantation between January 2005 and December 2015, in Korea (CONNECT DES cohort registry). Patients with current (n = 22,079) or prior (n = 43,637) history of MI, history of heart failure (n = 31,310), or history of atrial fibrillation (n = 4,671) were excluded from this study. Furthermore, patients with missing covariates were excluded (n = 376). Patients with an insufficient period of beta-blocker prescription (<90 days, n = 32,573) or those with any clinical event (n = 1,555) during 180 days of quarantine were also excluded from the analyses. Consequently, the remaining 78,139 patients with stable CAD that was treated with DES implantation were included in the analysis of this study (**Figure 1**).

Study Procedures and Outcomes

To emulate a randomized clinical trial that compares the impact of long-term beta-blocker treatment in patients with stable CAD, we used an intention-to-treat design for beta-blocker treatment, defined as a prescription of more than a 90-day supply of beta-blocker during 180 days of quarantine since index PCI. Types of prescribed beta-blockers are presented in **Supplementary Table 1**. We utilized ICD-10 codes, fee-for-service, and prescribed medication codes provided by the NHIS database and death certificates provided by the National Statistical Office. The primary outcome of interest was major adverse cardiovascular events (MACE) composed of cardiovascular death, MI, and hospitalization with heart failure for 5 years after PCI with 6 months of quarantine. Secondary outcomes were all-cause death and the individual MACE components. Cardiovascular death was ascertained from the National Statistical Office of Korea, which provided death certificates with an accuracy of 92% for the specific causes of death (9–11). Cardiovascular death was identified by a death certificate with at least one cardiovascular-related diagnosis (acute MI, stroke, heart failure, or sudden cardiac death). MI was defined by the ICD-10 codes corresponding to acute MI (10) and satisfaction of one or more of the following conditions: (1) concurrent presence of claims for coronary angiography, (2) admission *via* the emergency department, or (3) cardiac biomarkers tested more than 4 times. A detailed description of each clinical outcome, including the definition of hospitalization due to heart failure, is presented in **Supplementary Table 2**. Additionally, we included baseline comorbidities and drug prescription status before PCI for propensity score calculation, and stabilized inverse probability of treatment weights (IPTW) was used to accounting for differences in baseline characteristics, medical history, and confounding bias (**Supplementary Table 3**).

Statistical Analysis

Continuous variables are reported as mean and SD, and dichotomous variables are presented as frequency and percentage. To minimize the effect of confounding bias, we calculated the IPTW using the propensity score, which was calculated by logistic regression with covariates of age, sex, history of comorbidities and medications, and year of PCI (**Supplementary Table 4**). We also stabilized IPTW by multiplying it by the marginal probability of receiving treatment. The effect size difference between the two groups for all comorbidities and medications was calculated using standardized mean difference and Kernel density plots. Standardized mean difference values above 0.2 were regarded as a potential

Abbreviations: CAD, coronary artery disease; CI, confidence interval; DES, drug-eluting stent; HR, hazard ratio; IPTW, inverse probability of treatment weights; MACE, major adverse cardiovascular events; MI, myocardial infarction; NHIS, national health insurance service; PCI, percutaneous coronary intervention; RPSFT, rank-preserving structural failure times.

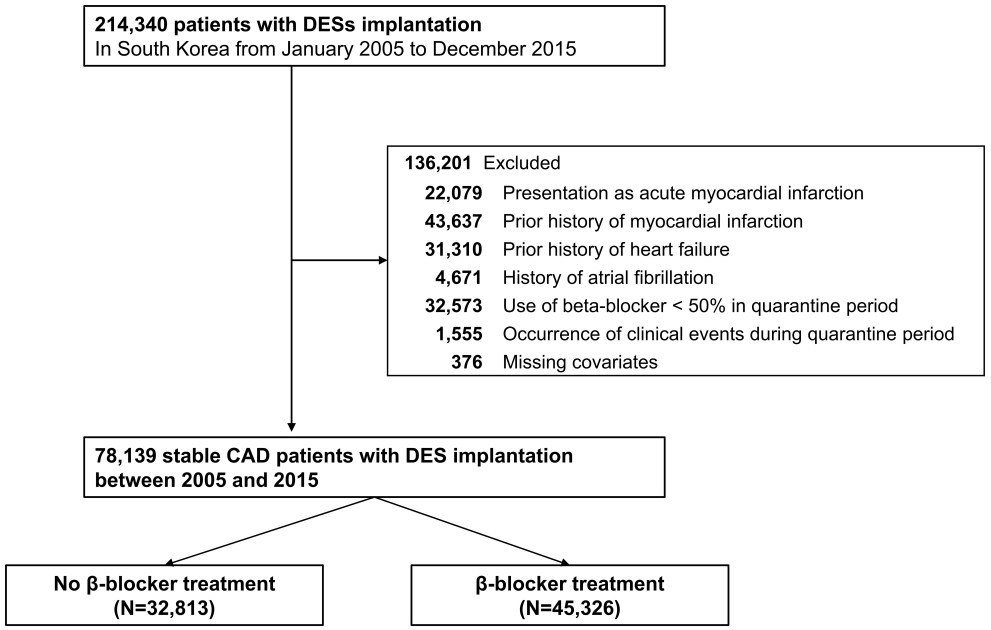

FIGURE 1 | Flow chart of the study population. CAD, coronary artery disease; DES, drug-eluting stent.

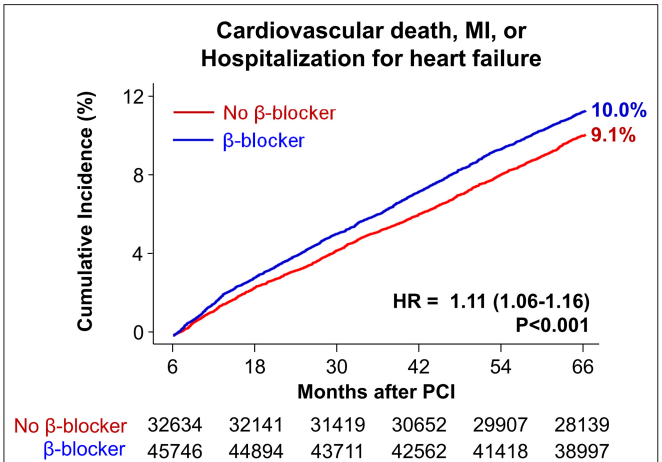

FIGURE 2 | Time-to-event curves for major adverse cardiovascular events for 5 years after PCI. The cumulative incidence of major adverse cardiovascular events for 5 years after PCI. HR, hazard ratio; MI, myocardial infarction; PCI, percutaneous coronary intervention.

imbalance between the two groups. Cumulative incidence curves and the rate of clinical outcomes of interest during follow-up were plotted using the Kaplan–Meier method. The adjusted hazard ratio (HR) for each clinical outcome of interest was calculated using a Cox proportional hazard regression model. A cause-specific hazard model was used to consider death as a competing risk when comparing the incidences of cardiovascular death, MI, and hospitalization due to heart failure. We further conducted sensitivity analyses to assess the robustness of the main results. First, the heterogeneity of treatment effects in subgroups was assessed using interaction terms in a Cox proportional hazard model. Second, to estimate the effect of continuous treatment, the rank-preserving structural failure times (RPSFT) model was used (12). This method estimates counterfactual event times that would have occurred if patients had not switched treatments (13). It also uses a counterfactual framework to estimate the common causal effect of the treatment using a grid search method and may be associated with low bias when a large number of patients switch treatments (14, 15). Since the RPSFT model was designed originally for analysis of a randomized controlled trial with frequent the crossover between treatment groups (15), our observational study utilized the RPSFT model after propensity score-matching to establish homogenous covariate balance at baseline between patients treated with and without beta-blocker (**Supplementary Table 4**). Third, we performed a time-varying Cox regression in which treatment (with or without beta-blocker) was a time-dependent variable considering switch between treatments in real-world practice. Among the patients who were assigned to the beta-blocker treatment group during a quarantine period, those with discontinuation of beta-blocker for ≥90 days were considered unexposed during the interval. Fourth, we conducted an intention-to-treat analysis by assigning patients treated with beta-blockers for more than 1 day during the quarantine period, instead of 90 days, to the treatment group. Fifth, we defined the intention-to-treat group as a prescription of more than a 16-day supply of beta-blocker in the 30-day quarantine period after PCI because the 180-day observational period used in the main

Covariates	β-Blockers		No β-Blockers		Hazard ratio (95% CI)	P for interaction
	Patient N	5-year MACE	Patient N	5-year MACE		
Age						
< 75 years	38881	3,020 (7.8)	27565	1,917 (7.0)	1.13 (1.06-1.19)	0.54
≥ 75 years	6865	1,534 (22.4)	5069	1,042 (20.6)	1.09 (1.01-1.18)	
Sex						
Male	29809	2,911 (9.8)	21411	1,876 (8.8)	1.12 (1.06-1.19)	0.35
Female	15937	1,643 (10.3)	11223	1,082 (9.7)	1.07 (0.99-1.16)	
Hypertension						
No	10361	804 (7.8)	7315	522 (7.1)	1.09 (0.98-1.22)	0.84
Yes	35385	3,750 (10.6)	25319	2,347 (9.6)	1.11 (1.05-1.17)	
Diabetes mellitus						
No	30229	2,547 (8.4)	21624	1,612 (7.5)	1.14 (1.07-1.21)	0.13
Yes	15517	2,007 (12.9)	11010	1,346 (12.2)	1.06 (0.99-1.14)	
Prior CVA						
No	37816	3,370 (8.9)	27083	2,169 (8.0)	1.12 (1.06-1.18)	0.29
Yes	7930	1,184 (14.9)	5551	789 (14.2)	1.06 (0.97-1.16)	

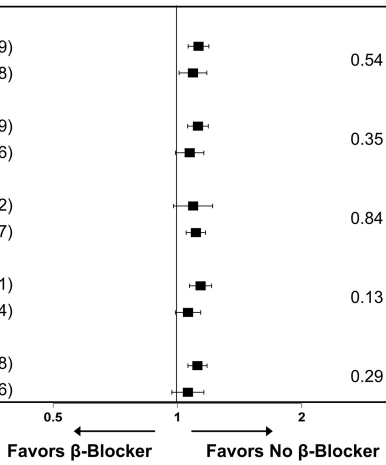

FIGURE 3 | Subgroup analysis for major adverse cardiovascular events. Numbers and percentages show the number of patients at risk, number of events, and the incidence rate of major adverse cardiac events 5 years after drug-eluting stent implantation. CI, confidence interval; CVA, cerebrovascular accidents; MACE, major adverse cardiovascular events.

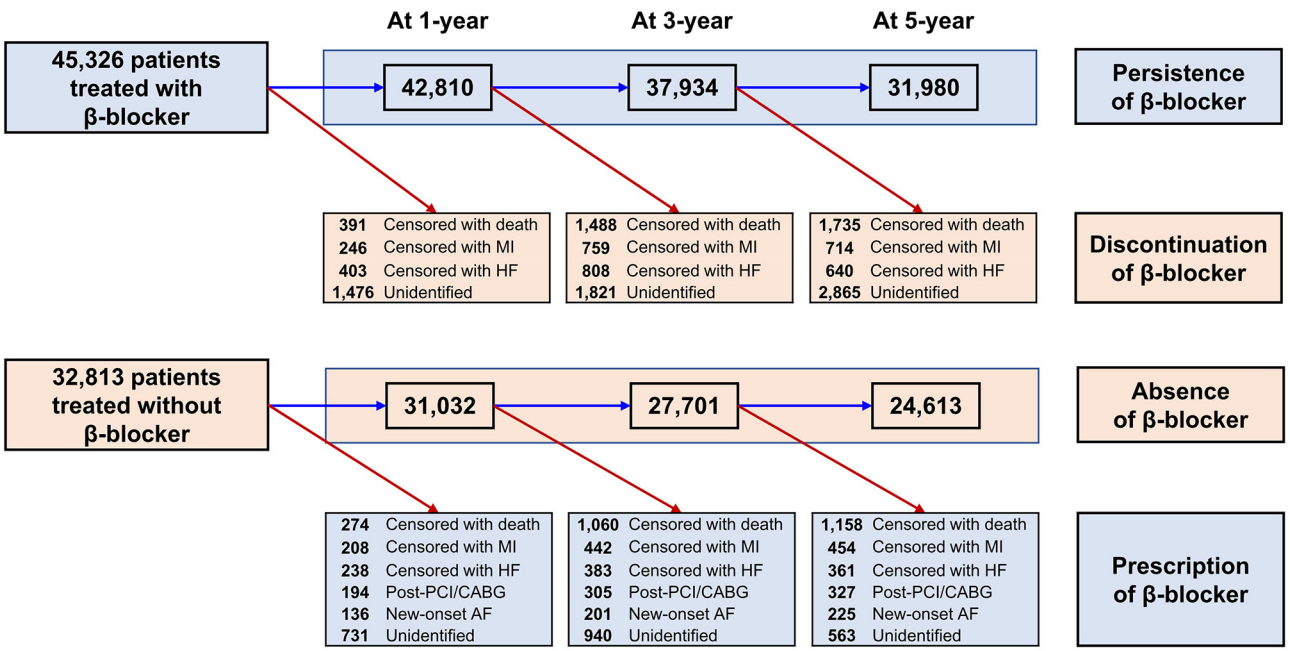

FIGURE 4 | Temporal trends in change of beta-blocker prescription. AF, atrial fibrillation; CABG, coronary artery bypass graft surgery; HF, heart failure; MI, myocardial infarction; PCI, percutaneous coronary intervention.

analysis could have masked the occurrence of adverse clinical events early after DES implantation.

All tests were two-sided and a p-value <0.05 was considered statistically significant. Statistical analyses were conducted using SAS version 9.4 (SAS Institute, Cary, NC, USA) and R version 3.6 with "RPSFTM" and "survival" packages (The R Foundation, www.R-project.org).

RESULTS

Baseline demographics and medical history of the cohort population before and after stabilized IPTW are presented in **Table 1**. After weighting, 78,380 DES-treated patients were included: 45,746 with and 32,634 without beta-blocker treatment. After stabilized IPTW, there was no evidence of inequality in baseline demographic characteristics or medical history

TABLE 1 | Baseline characteristics and medications in all patients.

Characteristics	Before stabilized IPTW (*N* = 78,139)			After stabilized IPTW (*N* =7 8,380)		
	No β-blocker (*N* = 32,813)	β-blocker (*N* = 45,326)	SMD	No β-blocker (*N* = 32,634)	β-blocker (*N* = 45,746)	SMD
Age, years	63.6 ± 10.2	63.8 ± 10.1	0.021	63.8 ± 10.2	63.8 ± 10.2	0.008
Female	10,109 (30.8)	16,460 (36.3)	0.117	11,223 (34.4)	15,937 (34.8)	0.009
Comorbidity						
Hypertension	23,651 (72.1)	36,785 (81.2)	0.216	25,319 (77.6)	35,385 (77.4)	0.006
Dyslipidemia	18,751 (57.1)	23,619 (52.1)	0.101	17,721 (54.3)	24,791 (54.2)	0.002
Chronic kidney disease with severe renal impairment*	1,177 (3.6)	2,510 (5.5)	0.094	1,636 (5.0)	2,159 (4.7)	0.014
Diabetes mellitus	10,490 (32.0)	15,752 (34.8)	0.059	11,010 (33.7)	15,517 (33.9)	0.004
Chronic liver disease	8,587 (26.2)	10,584 (23.4)	0.065	8,029 (24.6)	11,229 (24.5)	0.001
Chronic pulmonary disease	9,969 (30.4)	12,215 (26.9)	0.076	9,445 (28.9)	13,202 (28.9)	0.002
Peripheral arterial occlusive disease	2,442 (7.4)	2,911 (6.4)	0.040	2,289 (7.0)	3,259 (7.1)	0.004
Prior malignancy	2,384 (7.3)	3,009 (6.6)	0.025	2,277 (7.0)	3,159 (6.9)	0.003
Prior stroke or TIA	5,350 (16.3)	7,447 (16.4)	0.003	5,551 (17.0)	7,930 (17.3)	0.009
Prior ICH	300 (0.9)	448 (1.0)	0.008	321 (1.0)	473 (1.0)	0.005
Prior PCI or CABG	639 (1.8)	957 (2.1)	0.007	624 (1.9)	933 (2.0)	0.005
Osteoporosis	4,917 (15.0)	6,769 (14.9)	0.001	4,977 (15.3)	7,042 (15.4)	0.004
Thyroid disorder	1,837 (5.6)	2,249 (5.0)	0.028	1,691 (5.2)	2,393 (5.2)	0.002
Charlson comorbidity index	2.6 ± 2.1	2.5 ± 2.2	0.047	2.6 ± 2.2	2.5 ± 2.2	0.011
Medication before PCI						
Aspirin	18,133 (55.3)	27,769 (61.3)	0.122	18,876 (57.8)	26,089 (57.0)	0.016
Clopidogrel	11,657 (35.5)	16,285 (35.9)	0.008	11,348 (34.8)	15,574 (34.0)	0.015
β-Blocker	9,440 (28.8)	42,527 (93.8)	1.794	21,635 (66.3)	30,126 (65.9)	0.009
RAAS blockade	16,090 (49.0)	29,474 (65.0)	0.327	18,817 (57.7)	26,400 (57.7)	0.001
Procedural information						
Number of stents	1.2 ± 0.4	1.2 ± 0.4	0.022	1.2 ± 0.4	1.2 ± 0.4	0.002
Type of DES						
First-generation DES†	6,779 (20.7)	15,004 (33.1)	0.283	8,797 (27.0)	12,254 (26.8)	0.004
Next-generation DES	26,034 (79.3)	30,322 (66.9)		23,837 (73.0)	33,492 (73.2)	
DAPT duration post-PCI, days	907.3 ± 581.9	934.8 ± 577.8	0.047	913.6 ± 582.1	933.5 ± 577.7	0.032
Year of PCI						
2005	1,752 (5.3)	4,839 (10.7)	0.416	2,562 (7.8)	3,702 (8.1)	0.019
2006	1,918 (5.8)	4,327 (9.5)		2,484 (7.6)	3,458 (7.6)	
2007	1,274 (3.9)	2,916 (6.4)		1,721 (5.3)	2,367 (5.2)	
2008	1,876 (5.7)	3,594 (7.9)		2,221 (6.8)	3,026 (6.6)	
2009	2,305 (7.0)	4,421 (9.8)		2,787 (8.5)	3,789 (8.3)	
2010	2,831 (8.6)	5,003 (11.0)		3,301 (10.1)	4,522 (9.9)	
2011	2,947 (9.0)	3,678 (8.1)		2,865 (8.8)	4,027 (8.8)	
2012	2,737 (8.3)	2,942 (6.5)		2,438 (7.5)	3,445 (7.5)	
2013	3,091 (9.4)	3,256 (7.2)		2,734 (8.4)	3,886 (8.5)	
2014	5,479 (16.7)	4,993 (11.0)		4,443 (13.6)	6,335 (13.8)	
2015	6,603 (20.1)	5,357 (11.8)		5,078 (15.6)	7,192 (15.7)	

Values are presented as the mean ± SD or n (%).IPTW, inverse probability of treatment weighting; SMD, standardized mean difference; TIA, transient ischemic attack; ICH, intracranial hemorrhage; PCI, percutaneous coronary intervention; CABG, coronary artery bypass graft; DES, drug-eluting stent; DAPT, dual antiplatelet therapy; RAAS, renin-angiotensin-aldosterone-system.

**Chronic kidney disease with advanced stage requiring intensive medical therapy and financial assistance from health insurance.*

† First-generation drug-eluting stent indicates Cypher and Taxus.

TABLE 2 | Risks of primary and secondary outcomes at 5 years after percutaneous coronary intervention between patients prescribed with or without β-blocker after stabilized inverse probability of treatment weighting.

	No β-blocker (*N* = 32,634)	β-blocker (*N* = 45,746)	Risk difference (95% CI)	Hazard ratio (95% CI)	*p*-value
Major adverse cardiovascular event*	2,958 (9.1)	4,554 (10.0)	0.9 (0.5 to 1.3)	1.11 (1.06–1.16)	<0.001
All-cause death	2,688 (8.2)	3,722 (8.1)	−0.1 (-0.5 to 0.3)	0.99 (0.94–1.04)	0.62
Cardiovascular death	1,934 (5.9)	2,697 (5.9)	0.0 (-0.4 to 0.3)	1.00 (0.94–1.06)	0.88
Myocardial infarction	1,189 (3.6)	1,717 (3.8)	0.1 (-0.2 to 0.4)	1.03 (0.96–1.11)	0.42
Hospitalization for heart failure	1,018 (3.1)	1,879 (4.1)	1.0 (0.7 to 1.3)	1.32 (1.23–1.43)	<0.001

Composite of cardiovascular death, myocardial infarction, and hospitalization for heart failure.

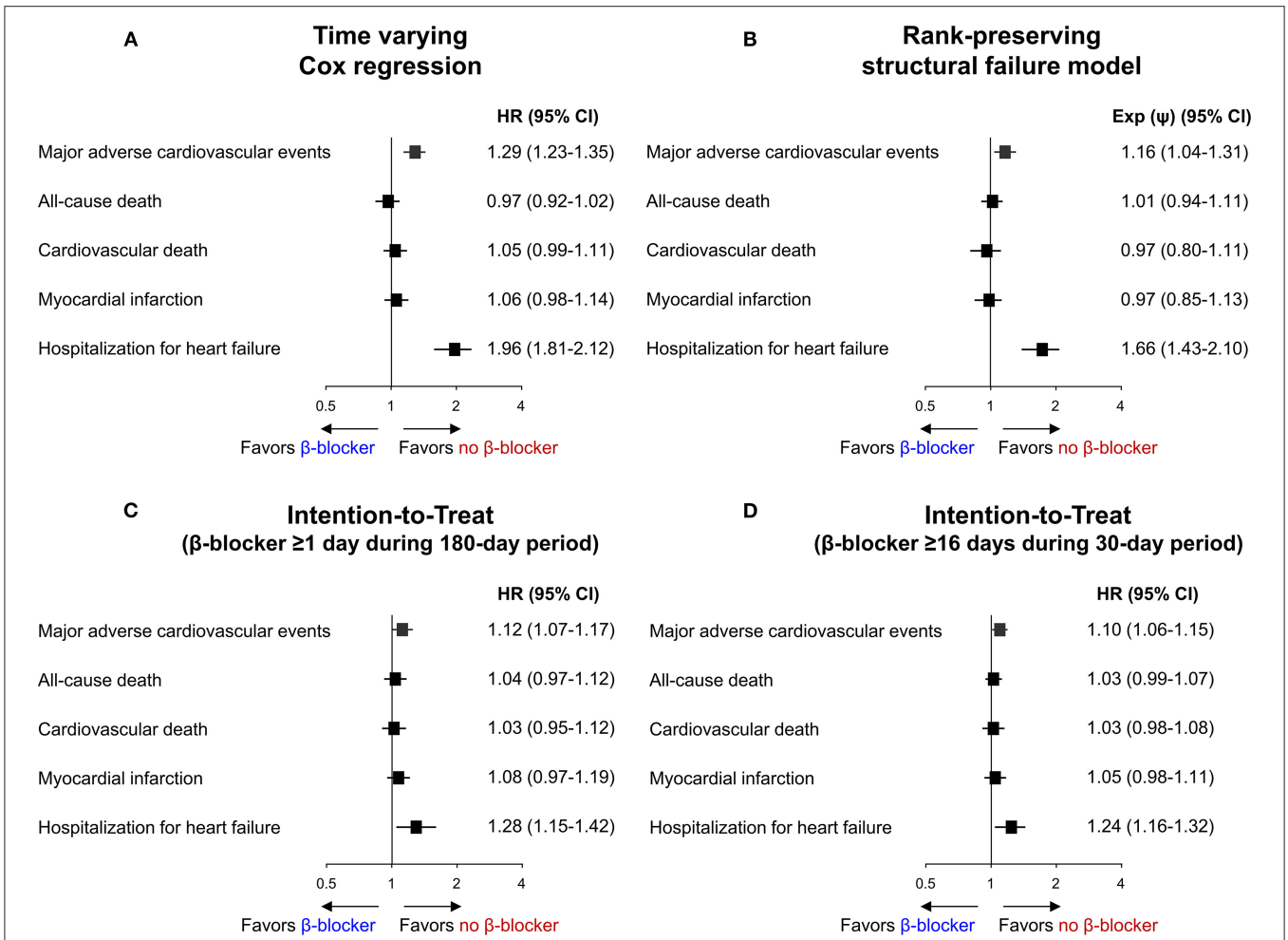

FIGURE 5 | Sensitivity analysis for primary and secondary outcomes. Risk of primary and secondary outcomes according to beta-blocker treatment analyzed by **(A)** Time varying Cox regression, **(B)** Rank-preserving structural failure model, and **(C,D)** Intention-to-Treat method. CI, confidence interval; HR, hazard ratio. Exp (ψ) indicates an increase/decrease in survival in the non-treatment group.

between the two groups (all standardized mean difference <0.1, **Supplementary Figures 1, 2**). The incidence and relative hazards of primary and secondary outcomes are presented in **Table 2**, **Figure 2**, and **Supplementary Figure 3**. At 5 years after PCI with 6 months of quarantine, the adjusted incidence rate of MACE was significantly higher in patients treated with beta-blockers (10.0 vs. 9.1% in those without beta-blocker treatment; HR 1.11, 95% CI 1.06–1.16, $p < 0.001$, **Figure 2**) in an intention-to-treat analysis (**Table 2** and **Supplementary Table 5**). There was no significant difference in all-cause death between patients treated with and without beta-blocker (8.1 vs. 8.2%; HR 0.99, 95% CI 0.94–1.04, $p = 0.62$, **Supplementary Figure 3**), As for the individual components of MACE, there was no significant association between beta-blocker treatment and risk

of cardiovascular death (5.9 vs. 5.9% in those without beta-blocker treatment; HR 1.00, 95% CI 0.94–1.06, $p = 0.88$) or MI (3.8 vs. 3.6% in those without beta-blocker treatment; HR 1.03, 95% CI 0.96–1.11, $p = 0.42$), while the adjusted hospitalization rate due to heart failure was significantly higher in patients treated with beta-blockers (4.1 vs. 3.1% in those without beta-blocker treatment; HR 1.32, 95% CI 1.23–1.43, $p < 0.001$) (**Table 2**). Consistent findings were observed regardless of DAPT duration (**Supplementary Table 6**). In a subgroup analysis, there was no significant interaction between the baseline comorbidities and beta-blocker treatment for a 5-year occurrence of MACE (**Figure 3**) or all-cause mortality (**Supplementary Figure 4**). There was no significant difference in treatment effect according to the generation of beta-blockers (**Supplementary Table 7**). During a 5-year follow-up period, there were frequent changes in the prescribed beta-blocker status during follow-up (**Figure 4**). Among 45,326 patients initially treated with beta-blocker before stabilized IPTW weighting, administration of beta-blocker was discontinued in 6,162 (13.6%) without adverse cardiovascular events such as death, MI, or heart failure. Of the 32,813 patients initially treated without beta-blocker, 3,622 (11.0%) started taking beta-blocker during the 5-year follow-up period and showed no MI or heart failure. To take into account frequent cross-over between the treatment groups, we performed additional statistical analyses with time-varying Cox regression (**Figure 5A**) and RPSFT models (**Figure 5B**), which demonstrated no statistically significant impact of beta-blocker treatment on the occurrence of all-cause death, cardiovascular death, or MI, whereas beta-blocker treatment was associated with a higher incidence rate of MACE or hospitalization for heart failure. Consistent findings were obtained when patients treated with beta-blocker for more than 1 day during 180 days of quarantine were considered as a treatment group (**Figure 5C**) or when the prescription status of beta-blocker within a 30-day period, instead of a 180-day quarantine period, after index PCI was applied (**Figure 5D**).

DISCUSSION

This nationwide cohort analysis evaluated the association between long-term beta-blocker treatment and clinical outcomes including mortality in patients with stable CAD after DES implantation. Taking advantage of the unique feature of the Korean NHIS database that accurately tracks all medication information over the entire study period, we could analyze the clinical impact of long-term beta-blocker administration in real-world practice by emulating the intention-to-treat manner of a randomized controlled trial. Furthermore, we applied time-varying Cox regression analysis and the RPSFT model to account for switching between treatment strategies, which is typical in real-world practice. The major findings of our study are as follows: (1) in patients with stable CAD after DES implantation, long-term maintenance treatment with beta-blockers was not associated with improvement of clinical outcomes, and (2) sensitivity analyses that considered switching between treatment strategies revealed consistent findings of a negligible impact of beta-blocker on clinical outcomes.

Long-term maintenance beta-blocker treatment after PCI in patients with MI or heart failure is recommended highly based on a large body of evidence that the treatment reduces mortality and morbidity (4, 16). This benefit mainly relies on the heart rate lowering property that decreases oxygen requirements, and negative inotropic effects that mitigate adverse cardiac remodeling and ventricular arrhythmia (17). Furthermore, in a COURAGE (Clinical Outcomes Utilizing Revascularization and Aggressive Drug Evaluation) trial, which demonstrated comparable effects of optimal medical therapy to PCI in stable CAD patients, beta-blockers were a mainstay drug treatment prescribed in 87% of patients enrolled in the trial (18).

There are two published studies that evaluated the association between beta-blocker treatment at discharge and clinical outcomes in stable CAD patients undergoing PCI without prior history of MI or heart failure. One registry study ($n = 5,288$) reported that beta-blocker treatment at discharge was associated with a significantly increased risk of cardiac death/MI during a 3-year follow-up after index PCI (HR 1.48, 95% CI 1.05–2.10, $p = 0.02$) (19). Another registry study with a larger number of patients ($n = 122,734$) reported no significant association between beta-blocker treatment at discharge and mortality or MI at 3-year follow-up (8). In addition, discharge with beta-blocker treatment was associated with more frequent readmission due to heart failure (8). However, these two studies did not provide detailed information on the prescribed beta-blocker status during the 3-year follow-up (8, 19). Because continuous beta-blocker prescription status after discharge during long-term follow-up was not evaluated clearly, the impact of drug switch during the follow-up period was not addressed (8, 19).

To minimize potential sources for bias, we excluded patients with concomitant indications for beta-blocker treatment such as MI, heart failure, or atrial fibrillation. Next, we emulated randomized controlled trials using intention-to-treat analysis with a 180-day quarantine period to assign treatment groups and the stabilized IPTW model to adjust for baseline differences. Furthermore, taking advantage of the unique strength of the NHIS database of Korea, which enables tracking and tracing of complete medication information during an entire follow-up period, we compared the main results with those of sensitivity analyses using the time-varying Cox regression and RPSFT model, which consider switches between treatment groups during follow-up. Finally, to compensate for the possible immortal time bias caused by 6 months of quarantine without clinical events, we set a quarantine period of 1 month as a sensitivity analysis. Results from observational studies cannot be used to establish causality, and residual perturbations can persist after propensity score weighting. However, despite the heterogeneity of treatment groups, various sensitivity analyses confirmed consistency compared with the main analysis.

In our analysis, 14% of patients initially treated with beta-blocker after DES implantation eventually discontinued the drug without the occurrence of significant clinical events. In fact, patients who are prescribed beta-blocker can complain of numerous side effects such as fatigue, bradycardia, depression,

hypotension, bronchospasm, peripheral vasoconstriction, or postural hypotension, which usually leads to discontinuation of beta-blocker treatment. Furthermore, chronic beta-blocker use has been associated with lipid profile deterioration and new-onset diabetes (20–22). One study reported that beta-blocker treatment increased serum triglyceride level, decreased HDL cholesterol level, and increased plasma small dense LDL, resulting in an atherogenic lipoprotein phenotype (23). A meta-analysis that included 94,492 hypertensive patients treated with beta-blocker has suggested a positive association between beta-blocker treatment and new-onset diabetes (21). Furthermore, non-selective beta-blockers can cause coronary artery spasms by inhibiting β-adrenergic mediated vasodilation (24). Concerns for possible side effects of long-term beta-blocker administration weaken the rationale for routine use of beta-blocker in specific patients with stable CAD after PCI with DES.

LIMITATIONS

This study has several limitations. First, in this nationwide cohort based on claims data, the systolic function of the left ventricle before PCI and during the follow-up period are not included; thus, patients with borderline left ventricular systolic function or reduced left ventricular systolic function without heart failure diagnosis could be included. Furthermore, in the administrative database, heart failure with preserved ejection fraction could have been underdiagnosed (25). Second, considering the nature of retrospective data based on claims, the findings presented in this study cannot be used to establish causal associations, and residual confounding variables could persist even after stabilized IPTW. Third, we adopted the RPSFT model to correct for frequent changes in beta-blocker prescription. Since the RPSFT is a statistical model typically applied to the analysis of randomized controlled trials, caution is needed in interpreting the findings obtained through this analysis despite the 1:1 propensity score matching for the establishment of RPSFT.

CONCLUSIONS

Among patients with stable CAD undergoing DES implantation, long-term maintenance with beta-blocker treatment was associated with an increased occurrence of MACE. Beta-blocker treatment may not be recommended as a maintenance drug therapy in specific patients with stable CAD after index PCI.

DATA AVAILABILITY STATEMENT

The datasets generated for the analyses are not publicly available because of strict government restrictions. Requests to access these datasets should be directed to M-KH, mkhong61@yuhs.ac.

ETHICS STATEMENT

The studies involving human participants were reviewed and approved by Yonsei University Health System Institutional Review Board. The Ethics Committee waived the requirement of written informed consent for participation.

AUTHOR CONTRIBUTIONS

S-JL, D-WC, YS, CK, S-JH, C-MA, J-SK, B-KK, Y-GK, DC, E-CP, YJ, C-MN, and M-KH contributed to the conception and design. S-JL and M-KH wrote the study protocol. D-WC and C-MN performed the programming to extract the data from the NHIS database. C-MN and M-KH had full access to all the data in the study and take responsibility for the integrity of the data and the accuracy of the data analysis. S-JL, D-WC, C-MN, and M-KH verified the data and conducted all analyses. YS, CK, S-JH, C-MA, J-SK, B-KK, Y-GK, DC, E-CP, and YJ provided a critical review of the manuscript. All authors read and approved the final publication.

FUNDING

This work was supported by the Cardiovascular Research Center, Seoul, Korea.

SUPPLEMENTARY MATERIAL

The Supplementary Material for this article can be found online at: https://www.frontiersin.org/articles/10.3389/fcvm.2022.878003/full#supplementary-material

REFERENCES

1. Puymirat E, Riant E, Aissaoui N, Soria A, Ducrocq G, Coste P, et al. β blockers and mortality after myocardial infarction in patients without heart failure: multicentre prospective cohort study. *BMJ.* (2016) 354i4801 doi: 10.1136/bmj.i4801
2. Ibanez B, James S, Agewall S, Antunes MJ, Bucciarelli-Ducci C, Bueno H, et al. 2017 ESC guidelines for the management of acute myocardial infarction in patients presenting with ST-segment elevation: the task force for the management of acute myocardial infarction in patients presenting with ST-segment elevation of the European Society of Cardiology (ESC). *Eur Heart J.* (2018) 39:119–77. doi: 10.1093/eurheartj/ehx393
3. Yancy CW, Jessup M, Bozkurt B, Butler J, Casey DE Jr, Colvin MM, et al. 2017 ACC/AHA/HFSA focused update of the 2013 ACCF/AHA guideline for the management of heart failure: a report of the American College of Cardiology/American Heart Association task force on clinical practice guidelines and the Heart Failure Society of America. *J Am Coll Cardiol.* (2017) 70:776–803. doi: 10.1161/CIR.0000000000000509
4. Kim J, Kang D, Park H, Kang M, Park TK, Lee JM, et al. Long-term beta-blocker therapy and clinical outcomes after acute myocardial infarction in patients without heart failure: nationwide cohort study. *Eur Heart J.* (2020) 41:3521–29. doi: 10.1093/eurheartj/ehaa376
5. Ohman EM. CLINICAL PRACTICE. Chronic stable angina. *N Engl J Med.* (2016) 374:1167–76. doi: 10.1056/NEJMcp1502240
6. Huang HL, Fox KA. The impact of beta-blockers on mortality in stable angina: a meta-analysis. *Scott Med J.* (2012) 57:69–75. doi: 10.1258/smj.2011.011274
7. Bangalore S, Steg G, Deedwania P, Crowley K, Eagle KA, Goto S, et al. β-Blocker use and clinical outcomes in stable

outpatients with and without coronary artery disease. *JAMA.* (2012) 308:1340–49. doi: 10.1001/jama.2012.12559
8. Motivala AA, Parikh V, Roe M, Dai D, Abbott JD, Prasad A, et al. Predictors, trends, and outcomes (among older patients≥ 65 years of age) associated with beta-blocker use in patients with stable angina undergoing elective percutaneous coronary intervention: insights from the NCDR registry. *JACC Cardiovasc Interv.* (2016) 9:1639–48. doi: 10.1016/j.jcin.2016.05.048
9. Choi EK. Cardiovascular research using the Korean national health information database. *Korean Circ J.* (2020) 50:754–72. doi: 10.4070/kcj.2020.0171
10. You SC, Rho Y, Bikdeli B, Kim J, Siapos A, Weaver J, et al. Association of ticagrelor vs clopidogrel with net adverse clinical events in patients with acute coronary syndrome undergoing percutaneous coronary intervention. *JAMA.* (2020) 324:1640–50. doi: 10.1001/jama.2020.16167
11. Won TY, Kang BS, Im TH, Choi HJ. The study of accuracy of death statistics. *J Korean Soc Emerg Med.* (2007) 18:256–62.
12. Toh S, Hernán MA. Causal inference from longitudinal studies with baseline randomization. *Int J Biostat.* (2008) 4:22 doi: 10.2202/1557-4679.1117
13. Morden JP, Lambert PC, Latimer N, Abrams KR, Wailoo AJ. Assessing methods for dealing with treatment switching in randomised controlled trials: a simulation study. *BMC Med Res Methodol.* (2011) 11:4. doi: 10.1186/1471-2288-11-4
14. Gold MR, Padhiar A, Mealing S, Sidhu MK, Tsintzos SI, Abraham WT. Long-term extrapolation of clinical benefits among patients with mild heart failure receiving cardiac resynchronization therapy: analysis of the 5-year follow-up from the REVERSE study. *JACC Heart Fail.* (2015) 3:691–700. doi: 10.1016/j.jchf.2015.05.005
15. Jönsson L, Sandin R, Ekman M, Ramsberg J, Charbonneau C, Huang X, et al. Analyzing overall survival in randomized controlled trials with crossover and implications for economic evaluation. *Value Health.* (2014) 17:707–13. doi: 10.1016/j.jval.2014.06.006
16. Collet JP, Thiele H, Barbato E, Barthélémy O, Bauersachs J, Bhatt DL, et al. 2020 ESC guidelines for the management of acute coronary syndromes in patients presenting without persistent ST-segment elevation. *Eur Heart J.* (2021) 42:1289–367. doi: 10.1093/eurheartj/ehaa909
17. McAlister FA, Wiebe N, Ezekowitz JA, Leung AA, Armstrong PW. Meta-analysis: β-blocker dose, heart rate reduction, and death in patients with heart failure. *Ann Intern Med.* (2009) 150:784–94. doi: 10.7326/0003-4819-150-11-200906020-00006
18. Boden WE, O'Rourke RA, Teo KK, Hartigan PM, Maron DJ, Kostuk WJ, et al. Optimal medical therapy with or without PCI for stable coronary disease. *N Engl J Med.* (2007) 356:1503–16. doi: 10.1056/NEJMoa070829
19. Ozasa N, Morimoto T, Bao B, Furukawa Y, Nakagawa Y, Kadota K, et al. β-blocker use in patients after percutaneous coronary interventions: one size fits all? Worse outcomes in patients without myocardial infarction or heart failure. *Int J Cardiol.* (2013) 168:774–9. doi: 10.1016/j.ijcard.2012.10.001
20. Weir MR, Moser M. Diuretics and beta-blockers: is there a risk for dyslipidemia? *Am Heart J.* (2000) 139:174–83. doi: 10.1016/S0002-8703(00)90325-9
21. Bangalore S, Parkar S, Grossman E, Messerli FH. A meta-analysis of 94,492 patients with hypertension treated with beta blockers to determine the risk of new-onset diabetes mellitus. *Am J Cardiol.* (2007) 100:1254–62. doi: 10.1016/j.amjcard.2007.05.057
22. Elliott WJ, Meyer PM. Incident diabetes in clinical trials of antihypertensive drugs: a network meta-analysis. *Lancet.* (2007) 369:201–7. doi: 10.1016/S0140-6736(07)60108-1
23. Rosenblit PD. Common medications used by patients with type 2 diabetes mellitus: what are their effects on the lipid profile? *Cardiovasc Diabetol.* (2016) 15:95. doi: 10.1186/s12933-016-0412-7
24. Japanese beta-Blockers and Calcium Antagonists Myocardial Infarction (JBCMI) investigators. Comparison of the effects of beta blockers and calcium antagonists on cardiovascular events after acute myocardial infarction in Japanese subjects. *Am J Cardiol.* (2004) 93:969–73. doi: 10.1016/j.amjcard.2004.01.006
25. McCormick N, Lacaille D, Bhole V, Avina-Zubieta JA. Validity of heart failure diagnoses in administrative databases: a systematic review and meta-analysis. *PLos ONE.* (2014) 9:e104519. doi: 10.1371/journal.pone.0104519

Conflict of Interest: The authors declare that the research was conducted in the absence of any commercial or financial relationships that could be construed as a potential conflict of interest.

Publisher's Note: All claims expressed in this article are solely those of the authors and do not necessarily represent those of their affiliated organizations, or those of the publisher, the editors and the reviewers. Any product that may be evaluated in this article, or claim that may be made by its manufacturer, is not guaranteed or endorsed by the publisher.

frontiers | Frontiers in Cardiovascular Medicine

ORIGINAL RESEARCH
published: 26 May 2022
doi: 10.3389/fcvm.2022.925080

Alternate Day Fasting Improves Endothelial Function in Type 2 Diabetic Mice: Role of Adipose-Derived Hormones

Jian Cui[1,2,3], Sewon Lee[2,3,4], Yan Sun[1], Cuihua Zhang[2,3†], Michael A. Hill[2,3], Yuhang Li[1] and Hanrui Zhang[2,3,5*]*

[1] School of Traditional Chinese Medicine, Beijing University of Chinese Medicine, Beijing, China, [2] Dalton Cardiovascular Research Center, School of Medicine, University of Missouri, Columbia, MO, United States, [3] Department of Medical Pharmacology and Physiology, School of Medicine, University of Missouri, Columbia, MO, United States, [4] Division of Sport Science, College of Arts and Physical Education, Incheon National University, Incheon, South Korea, [5] Department of Medicine, Division of Cardiology, Cardiometabolic Genomics Program, Columbia University Irving Medical Center, New York, NY, United States

OPEN ACCESS

Edited by:
Xiaofeng Yang,
Temple University, United States

Reviewed by:
Hong S. Lu,
University of Kentucky, United States
Jingyan Han,
Boston University, United States

***Correspondence:**
Yuhang Li
liyuhang@bucm.edu.cn
Hanrui Zhang
hz2418@cumc.columbia.edu

[†] Deceased

Specialty section:
This article was submitted to Cardiovascular Therapeutics, a section of the journal Frontiers in Cardiovascular Medicine

Received: 21 April 2022
Accepted: 02 May 2022
Published: 26 May 2022

Citation:
Cui J, Lee S, Sun Y, Zhang C, Hill MA, Li Y and Zhang H (2022) Alternate Day Fasting Improves Endothelial Function in Type 2 Diabetic Mice: Role of Adipose-Derived Hormones. Front. Cardiovasc. Med. 9:925080. doi: 10.3389/fcvm.2022.925080

Introduction: Intermittent fasting, including alternate day fasting (ADF), has grown in popularity as it can produce clinically significant metabolic benefits and is often considered to be easier to adhere to than other types of diets such as chronic calorie restriction. However, the effects of ADF on diabetes-associated vascular dysfunction, and the role of adipose-derived hormones, i.e., adipokines, in mediating its effects, remain largely unknown.

Objective: We aimed to test the hypothesis that ADF protects against diabetes-associated endothelial dysfunction, at least partly through modulating adipokine profiles.

Methods: Control mice (*m Lepr^{db}*) and diabetic mice (*Lepr^{db}*) were treated with 12-weeks of ADF. Glucose metabolism, endothelial function, and adipokine profile were assessed.

Results: ADF reduced fasting blood glucose level and homeostatic model assessment for insulin resistance (HOMA-IR), and improved insulin sensitivity. ADF improved endothelium-dependent vasorelaxation of small mesenteric arteries (SMA) of *Lepr^{db}* mice. The improvement in endothelial function was largely attenuated by incubation with the nitric oxide synthase inhibitor, L-NAME. These ADF-induced metabolic and vascular benefits were accompanied by increased circulating adiponectin. Adenovirus-mediated adiponectin supplementation improved endothelial function in *Lepr^{db}* mice, supporting endothelial protective roles in diabetes-associated endothelial dysfunction. Protein tyrosine nitration is a post-translational modification that serves as a marker of oxidative stress. Nitrotyrosine protein levels in SMA and mesenteric adipose tissue (MAT) were elevated in *Lepr^{db}* mice. ADF reduced nitrotyrosine protein in SMA, but not in MAT, of *Lepr^{db}* mice.

Conclusion: ADF exerts metabolic and endothelial protective benefits. The improvement of endothelial function was partly mediated by increased adiponectin, representing an important mechanism for the beneficial vascular effects resulting from ADF.

Keywords: adipose, adipokines, diabetes, diet, endothelial function, alternate day fasting, adiponectin

INTRODUCTION

Obesity and diabetes are associated with an increased risk of cardiovascular diseases, which remain the leading cause of death globally (1). Lifestyle modification improves metabolic syndrome and associated systemic inflammation and cardiovascular dysfunction (1). Dietary intervention represents an effective lifestyle modification strategy in the management of obesity and type 2 diabetes (2, 3). Calorie restriction, a form of dietary intervention that involves a reduced daily caloric intake, exerts physiological benefits with extended longevity and decreased risks for many age-related diseases in model organisms and humans (3). Despite the well-known benefits, long-term energy restriction is unlikely to be a feasible lifestyle modification strategy in humans due to poor sustained adherence (3).

Intermittent fasting has grown in popularity in the past few years (4–7). Multiple clinical trials support that short-term intermittent fasting can produce clinically significant metabolic benefits in obese subjects (5). Compared with traditional forms of dietary intervention such as chronic calorie restriction that generally require individuals to vigilantly monitor energy intake, intermittent fasting is often considered to be easier in regard to adherence (8). An intermittent fasting regimen can be defined as periods of fasting alternating with periods of eating. Some of the most studied intermittent fasting methods include alternate day fasting (ADF) (0–500 kcal per fast day alternating with *ad libitum* intake on feast days), the 5:2 fasting (two fast days and five feast days per week), and time-restricted fasting (eating only within a prescribed window of time each day) (5).

Despite the recent surge in popularity, there are limited clinical studies on the effects of long-term intermittent energy restriction in patients with type 2 diabetes (5). Encouragingly, a recent randomized clinical trial in subjects with type 2 diabetes compared an intermittent energy restriction diet (the participants followed 500–600 kcal per day for 2 non-consecutive days per week while following their usual diet for the other 5 days) or a continuous energy restriction diet (1200–1500 kcal per day followed for 7 days per week) for 12 months. The results supported that intermittent energy restriction is an effective alternative strategy for the reduction of hemoglobin A1c (HbA1c) and is comparable to continuous energy restriction in these patients (9).

With the promising results, further clinical and experimental studies are required to explore the benefits and mechanisms of intermittent fasting in type 2 diabetes and associated cardiovascular complications. Mice that are homozygous for the diabetes spontaneous mutation ($Lepr^{db}$) have been widely used to model type 2 diabetes (10, 11). Indeed, experimental studies in $Lepr^{db}$ mice support that intermittent fasting improved glycemic control, lipid dysregulation (12, 13), hepatic steatosis (14), retinopathy (15), and cognitive impairment (16). However, if and how intermittent fasting may rescue vascular dysfunction in type 2 diabetes has not been studied. Furthermore, adipose-derived hormones, i.e., adipokines, have been implicated to be altered in type 2 diabetes and contribute to impaired endothelial function (17–19). Adiponectin is an adipocyte-derived hormone that increases with weight loss and protects the endothelium by decreasing oxidative stress and inflammation (20–23). Leptin and resistin, in contrast, are adipokines that are positively correlated to body weight and fat mass (24), and weight loss decreased their levels (25). Leptin and resistin have been implicated to cause endothelial dysfunction by promoting oxidative stress (17, 19). In view of this, it is plausible to speculate that weight loss strategies, such as ADF, would increase adiponectin and decrease leptin and resistin concentrations. In turn, the improvements in adipokine profiles may have a protective effect on the vasculature resulting in improved endothelial function.

Here we aimed to determine the effects of ADF on glucose metabolism and endothelial function, and the involvement of adipokines, in type 2 diabetic mice and their respective non-diabetic controls. We hypothesized that ADF regulates the adipokine profile, particularly adiponectin, which exerts vascular protective effects in type 2 diabetic mice with ADF. To test this hypothesis, heterozygote control mice ($m\ Lepr^{db}$) and homozygote type 2 diabetic mice ($Lepr^{db}$) were treated with ADF for 12 weeks. We determined: (1) if and how ADF affects weight loss, glucose metabolism, and insulin sensitivity in type 2 diabetic mice; (2) if and how ADF affects circulating adipokines and their expression in adipose tissue; (3) how ADF rescues endothelial dysfunction, and if and how adipokines, including adiponectin, resistin, and leptin, modulated by ADF may contribute to the vascular benefits of ADF; and (4) whether and to what extent ADF influences glucose metabolism and vascular function in non-diabetic control mice.

MATERIALS AND METHODS

Animal Models and Treatment

The procedures followed were in accordance with approved guidelines set by the Animal Care Committee at the University of Missouri (Columbia, MO, United States). Mice were purchased from the Jackson Laboratory (Bar Harbor, ME,

Abbreviations: ACh, acetylcholine; ADF, alternate-day fasting; MAT, mesenteric adipose tissue; NO, nitric oxide; PE, phenylephrine; SMA, small mesenteric artery; SNP, sodium nitroprusside.

United States). Homozygote type 2 diabetic mice (*Lepr^{db}*; BKS.Cg-*Dock7^{m}* + / + *Lepr^{db}*J, JAX 000642, black and obese) are wildtype for *Dock7* and homozygous for *Lepr^{db}* (10, 11). The heterozygote control mice (*m Lepr^{db}*, black and lean) from the colony are heterozygous for *Dock7^{m}* and heterozygous for *Lepr^{db}*. Because of the sterility of *Lepr^{db}* homozygotes, the misty (*Dock7^{m}*) mutation has been incorporated into stocks for maintenance of the diabetes mutation (10, 11). The repulsion double heterozygote facilitates the identification of heterozygotes for breeding (10, 11). Mice that are homozygous for *Dock7^{m}* and wildtype for *Lepr* from the colony (gray and lean) are discarded (10, 11). The *Lepr^{db}* mice demonstrate morbid obesity, chronic hyperglycemia, and are polyphagic, polydipsic, and polyuric (10, 11). Heterozygotes control mice (*m Lepr^{db}*) are normal in body weight, blood glucose, and plasma insulin (10, 11).

Mice were maintained on a standard rodent diet. Twelve to sixteen week-old, male, 20–35 g *m Lepr^{db}*, and 40–60 g *Lepr^{db}* mice were used in this study. Mice were fed *ad libitum* on alternate days and then moved to a separate cage without food (starting at 9 a.m.) for 24 h to prevent food from being stored in the bedding. Mice were maintained on a 12-hour light/dark cycle and between 18–23°C according to animal protocols and NIH guidelines. To determine the effects of recombinant resistin treatment, *Lepr^{db}* mice were treated with murine recombinant resistin (Biovision, Cat# 4560-100, 15 μg/per mouse/day, i.p. injection, for 4 days) as previously described (26).

Measurement of Body Weight and Abdominal Girth

Body weight was determined using an electronic balance. Abdominal girth was measured with the use of a soft ruler (27).

Measurement of Blood Parameters

After animals were anesthetized with pentobarbital sodium (50 mg/kg i.p.), whole blood samples were obtained from the vena cava. A whole blood sample was held for 30 min at room temperature to allow clotting. The sample was centrifuged at 2,000–3,000 *g* for 10 min at 4°C; the serum was transferred to separate tubes without disturbing blood clots and stored at −80°C until analysis. Commercial ELISA kits were used to measure serum levels of adiponectin (Millipore, EZMADP-60K), resistin (R&D, MRSN00), and leptin (Millipore, EZML-82K) (28). Similarly, total cholesterol levels were assessed using spectrophotometric assays (Biovision, K603-100) according to the manufacturer's instructions (28).

Measurement of Homeostatic Model Assessment for Insulin Resistance

Fasting blood glucose levels were measured by OneTouch Ultramini glucometer (LifeScan). Fasting serum insulin level was measured with the use of a commercial kit (ALPCO, 80-INSMSU-E01). Insulin resistance was determined by the homeostatic model assessment for insulin resistance; homeostatic model assessment for insulin resistance (HOMA-IR) using the following formula: HOMA-IR = (glucose [mmol/L]) × (insulin [mU/L])/22.5 (21).

Insulin Tolerance Test

Mice were fasted overnight and weighed. The tail was nicked with a fresh razor blade by horizontal cut of the tip and a OneTouch Ultramini glucometer was used to measure baseline blood glucose after overnight fasting. 1.0 unit per kg body weight of diluted porcine insulin (Sigma-Aldrich, St. Louis, MO, United States, I5523) was subsequently injected into the intraperitoneal cavity. Blood glucose was sampled from the tail of each mouse by gently massaging a small drop of blood onto the glucometer strip at 0 (baseline), 15, 30, 60, and 90 min following insulin injection (29).

Adenovirus-Mediated Gene Transfer

Adenovirus vector containing the gene for full-length mouse adiponectin (Ad-APN) was generously gifted by Dr. Shinji Kihara (Department of Internal Medicine and Molecular Science, University of Osaka, Osaka, Japan) (30). HEK-293 AD cells were passaged two to three times before infection and cultured until the floating monolayer was 90–100% confluent. Cells were replenished with 15 ml new growth media containing 10% FBS per 75-cm^2 flask with either Ad-APN or adenovirus containing β-galactosidase (Ad-βgal) added to the culture. After 24 h, 10 ml growth media was added to the culture flask, and the viruses were allowed to produce for another 24 h. When all cells were floating, the culture flask was gently shaken, and all media, including the cells, were transferred to a 50-ml sterile tube, which was centrifuged at 1,000 *g* for 5 min. The cell pellet was then resuspended in 0.8 ml culture medium. The adenoviruses were released from the cells by repeated freeze-thaw cycles using liquid nitrogen. After centrifugation at 10,000 *g* for 10 min, the supernatant was collected for immediate purification of adenoviruses using a commercial purification kit (Cell Biolabs, San Diego, CA, United States). The concentration of purified adenovirus was measured using the commercial QuickTiter Adenovirus Titer Immunoassay Kit (Cell Biolabs, San Diego, CA, United States) according to the manufacturer's instructions. Either Ad-APN or Ad-βgal at 1×10^9 plaque-forming units was injected intravenously *via* the tail vein of *m Lepr^{db}* and *Lepr^{db}* mice. All mice were euthanized 7 days after virus injection. Mice that did not show an increase in serum adiponectin levels (as measured by ELISA) were excluded from the functional assessment (20).

Functional Assessment of Small Mesenteric Arteries

Mesenteric arteries (first order of main branches) with internal diameter of 200–250 μm were cut into 2 mm long rings and mounted in a Myograph 610M (ADInstruments, Colorado Springs, CO, United States) (31). The passive tension-internal circumference was determined by stretching to achieve an internal circumference equivalent to 60–70% of that of the blood vessel under a transmural pressure of 100 mmHg. Vessels were maintained in Physiological Saline Solution (PSS) bubbled with 95% O_2–5% CO_2 at 37°C for the remainder of the experiment. PSS contained 118.99 mM NaCl, 4.69 mM KCl, 1.18 mM KH_2PO4, 1.17 mM $MgSO_4 \bullet 7H_2O$, 2.50 mM $CaCl_2 \bullet 2H_2O$, 14.9 mM $NaHCO_3$, 5.5 mM D-Glucose, and 0.03 mM

EDTA. After an equilibration period of 45 min, vessels were precontracted with 1 μmol/L phenylephrine (PE). A cumulative dose–response curve was obtained by adding acetylcholine (ACh, 1 nmol/L–10 μmol/L) and sodium nitroprusside (SNP, 1 nmol/L–10 μmol/L). Relaxation at each concentration was measured and expressed as the percentage of force generated in response to 1 μmol/L PE. NO availability was evaluated by ACh concentration-response curve repeated after incubation with the NO synthase inhibitor N-Nitro-L-arginine methyl ester (L-NAME, 100 μM, 20 min). PE-induced vasoconstriction was evaluated by cumulative addition of PE (1 nmol/L to 10 μmol/L). The contraction induced by PE was normalized to the maximal force of contraction induced by 120 mM of KCl (27, 32).

Determination of mRNA Expression by Real-Time Polymerase Chain Reaction

Total RNA was extracted from 10 mg of mesenteric adipose tissue (MAT) using RNeasy Lipid Tissue Mini Kit (Qiagen, Valencia, CA, United States) (27, 32). The quality and quantity of total RNA were determined using a Nanodrop ND-1000 Spectrophotometer (Nano Drop Technologies, Wilmington, DE). Total RNA (1.0 μg) was processed directly to cDNA synthesis using SuperScript™ III Reverse Transcriptase (Invitrogen, Grand Island, NY, United States). Quantitative real-time PCR analyses were performed using an i-Cycler (I-Q5, Bio-Rad Laboratories, Hercules, CA, United States). Reactions were carried out in triplicate in a total volume of 25 μl using SYBR green qPCR Master Mix (Invitrogen, Grand Island, NY, United States). The $2^{-\Delta\Delta C_T}$ method ($-\Delta\Delta C_T = C_{T,\text{target gene}} - C_{T,\text{Actb}}$, where C_T is threshold cycle) was used to analyze the change of target gene expression. The housekeeping gene *Actb* was used for internal normalization. Mean C_T values for both the target and internal control genes were determined. Results are presented as fold change of transcripts for target normalized to internal reference (*Actb*), compared with *m Lepr*^{db} (defined as 1.0 fold) (27, 32). The primer sets were designed by Primer3 (33): mouse *Adipoq* (forward primer: 5′-AGGTTGGATGGCAGGC-3′ and reverse primer: 5′-GTCTCACCCTTAGGACCAAGAA-3′), *Retn* (forward primer: 5′- TTCCTTGTCCCTGAACTGCT-3′ and reverse primer: 5′-CAAGACTGCTGTGCCTTCTG-3′), *Lep* (forward primer: 5′- TGTCCAGGGTTGATCTCACA-3′and reverse primer: 5′- TCCCACTGGAACAAAACTCC-3′), and *Actb* (forward primer: 5′-GCTCTTTTCCAGCCTTCCTT-3′ and reverse primer: 5′-CTTCTGCATCCTGTCAGCAA-3′) (20). The efficiency of the PCR reaction was determined using a dilution series of a standard MAT sample.

Protein Expression by Western Blot Analyses

In total, 10 mg of MAT, or 4-6 branches of small mesenteric arteries (SMA) were homogenized in lysis buffer (Cellytic™ MT Mammalian Tissue Lysis/Extraction Reagent, Sigma-Aldrich, St. Louis, MO, United States). Protein concentration was assessed using BCA™ Protein Assay Kit (ThermoScientific, Rockford, IL, United States), and equal amounts of protein were separated by SDS-PAGE and transferred to PVDF membranes (Bio-Rad, Hercules, CA, United States). Protein expression was detected using anti-nitrotyrosine primary antibody (Abcam, Cat#ab7048, 1:500) anti-tubulin primary antibody (Abcam, Cat#ab6160, 1:5,000), Horseradish peroxidase-conjugated secondary antibodies were used. Signals were visualized by enhanced chemiluminescence (Santa Cruz Biotechnology, Santa Cruz, CA, United States), scanned densitometrically using Fuji LAS3000 and quantified with Multigauge software (Fujifilm). The relative amounts of protein expression were quantified to those of the corresponding *m Lepr*^{db} control, which was set to a value of 1.0 (27, 32).

Data Analysis

All data were presented as mean ± SEM except as specifically stated. For insulin tolerance tests and vasomotor responses under various dosages, two-way repeated ANOVA was used to determine how the responses were affected by two factors (ADF × Time as the repeated measure for insulin tolerance tests, and ADF × dosage as the repeated measure for vasomotor responses), followed by the *post hoc* Tukey's test for multiple comparisons. For other data obtained from the four groups (*m Lepr*^{db}, *m Lepr*^{db} + ADF, *Lepr*^{db}, *Lepr*^{db} + ADF), one-way ANOVA was used to compare the groups defined by one factor, followed by the *post hoc* Fisher's Least Significant Difference test for multiple comparisons. Statistical analyses were performed using SPSS11.5. Significance was accepted at $P < 0.05$. The sample size was empirically determined based on our previous studies examining the metabolic and endothelial function of *Lepr*^{db} mice and their respective *m Lepr*^{db} control mice (20, 27, 28, 32, 34, 35). Mice were grouped by genotype and weight-matched thus not randomized. Blinded analysis was not performed because of feasibility.

RESULTS

The Effects of Alternate Day Fasting on Body Weight, Abdominal Girth, Fasting Total Cholesterol, Fasting Glucose, Fasting Insulin, and Homeostatic Model Assessment for Insulin Resistance in Control and Diabetic Mice

Mice on the ADF diet were allowed to eat *ad libitum* for one day, and then given no food the next day. This regimen was maintained for 12 weeks. Meanwhile, mice without ADF were continually allowed to feed *ad libitum*. Food intake was measured on the feast day for mice with or without ADF once per week. ADF led to a net reduction of food intake at 41.8 ± 4.1% in *m Lepr*^{db} mice and 40.2 ± 4.7% in *Lepr*^{db} mice. As expected, the *Lepr*^{db} diabetic mice showed higher body weight, abdominal girth, total cholesterol, blood glucose, insulin, and HOMA-IR than the *m Lepr*^{db} control mice. In *m Lepr*^{db} control mice, 12-week ADF reduced body weight, abdominal girth, and insulin. Although ADF modestly reduced total cholesterol, glucose, and HOMA-IR in *m Lepr*^{db} control mice, the *P*-values were greater than 0.05, we thus cannot conclude that significant differences

TABLE 1 | Basic characteristics.

	m Lepr^{db}	*m Lepr^{db}* + ADF	*Lepr^{db}*	*Lepr^{db}* + ADF
Body weight, g	30.88 ± 0.51	27.38 ± 0.63*#	55.95 ± 1.38*	53.73 ± 0.49*
Abdominal girth, cm	8.68 ± 0.15	8.05 ± 0.21*#	12.10 ± 0.07*	12.02 ± 0.07*
Total cholesterol, mg/dl	158.46 ± 24.27	131.73 ± 11.12#	213.37 ± 20.15*	173.78 ± 14.87
Blood glucose, mg/dl	183.80 ± 17.98	150.00 ± 7.28#	489.60 ± 58.25*	182.25 ± 23.83#
Insulin, ng/ml	1.69 ± 0.32	0.29 ± 0.05*#	2.94 ± 0.45*	2.86 ± 0.46*
HOMA-IR	21.58 ± 4.69	3.06 ± 0.67#	101.12 ± 21.68*	37.45 ± 9.20#

*Data represent mean ± SEM. n = 6 mice. *P < 0.05 vs. m Lepr^{db} control mice, # p < 0.05 vs. Lepr^{db} diabetic mice.*

exist. In *Lepr^{db}* mice, ADF did not significantly reduce body weight, abdominal girth, and total cholesterol. ADF, however, remarkably reduced blood glucose and HOMA-IR without affecting insulin levels (**Table 1**), supporting the profound effects of ADF on improving glucose metabolism despite the lack of effects on weight loss in diabetic mice.

Alternate Day Fasting Improved Insulin Sensitivity in Both Control and Diabetic Mice

We further determined how ADF affects insulin sensitivity by performing an insulin tolerance test. As expected, the *Lepr^{db}* diabetic mice showed impaired insulin sensitivity. ADF improved insulin sensitivity in both *m Lepr^{db}* control mice and *Lepr^{db}* diabetic mice (**Figure 1**).

Alternate Day Fasting Rescued Endothelial Dysfunction of Small Mesenteric Arteries in Diabetic Mice

SMA represent resistance arteries contributing to vascular resistance and regulation of blood flow. Acetylcholine (ACh)-induced endothelium-dependent vasorelaxation was impaired in SMA of *Lepr^{db}* diabetic mice vs. *m Lepr^{db}* control mice. ADF remarkably improved the endothelial function of diabetic mice (**Figure 2A**). Sodium nitroprusside (SNP)-induced endothelium-independent vasorelaxation (**Figure 2C**) and phenylephrine (PE)-induced vasoconstriction (**Figure 2D**) were comparable among groups. Incubation with the nitric oxide synthase inhibitor (L-NAME) largely attenuated the ADF-induced improvement of endothelial function in diabetic mice (**Figure 2B**). In *m Lepr^{db}* mice, ADF also showed a trend toward increasing the % of maximal relaxation at an ACh concentration of 10^{-7} mol/L. ADF did not affect endothelium-independent vasorelaxation or PE-induced vasoconstriction in *m Lepr^{db}* control mice (**Figure 2**).

Alternate Day Fasting Modulates Circulating Adipokine Profile and Their Expression by Adipose Tissue

Adiponectin levels were lower in the serum of *Lepr^{db}* mice, and ADF increased serum adiponectin back to the level of *m Lepr^{db}* control mice (**Figure 3A**). Serum resistin was lower in *Lepr^{db}* mice than in *m Lepr^{db}* control mice. ADF increased resistin in both *m Lepr^{db}* control mice and *Lepr^{db}* diabetic mice (**Figure 3B**). As expected, *Lepr^{db}* mice showed dramatically increased serum leptin, i.e., hyperleptinemia due to the lack of leptin receptor. ADF reduced serum leptin in *m Lepr^{db}* control mice, yet further increased serum leptin in *Lepr^{db}* mice (**Figure 3C**).

Adipose tissue is the primary source of adipokines released into circulation (36). We further determined mRNA expression of these adipokines in MAT. Consistent with the trend of circulating adipokine levels, *Lepr^{db}* mice showed increased *Lep* mRNA (encoding leptin) in MAT (**Figure 3F**), while reduced *Retn* mRNA (encoding resistin) (**Figure 3E**) compared with *m Lepr^{db}* control mice. *Adipoq* mRNA (encoding adiponectin) in MAT was not statistically different between *m Lepr^{db}* and *Lepr^{db}* mice (**Figure 3D**). ADF increased *Adipoq* mRNA in MAT of *m Lepr^{db}* control mice, though circulating adiponectin in *m Lepr^{db}* control mice was not altered by ADF (**Figure 3D**), likely suggesting post-transcriptional regulatory mechanisms limiting a further increase in circulating levels. ADF further increased *Lep* mRNA in the MAT of *m Lepr^{db}* control mice, though serum leptin was reduced by ADF (**Figure 3E**).

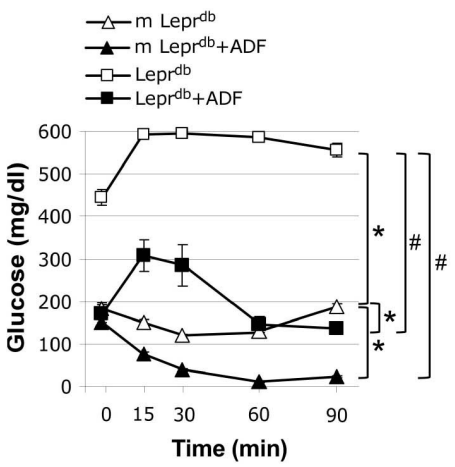

FIGURE 1 | Alternate day fasting (ADF) improved insulin sensitivity in both *m Lepr^{db}* and *Lepr^{db}* mice. Insulin tolerance tests revealed that diabetic mice (*Lepr^{db}*) had impaired glucose metabolism compared with control mice (*m Lepr^{db}*). Twelve weeks of alternate-day fasting (ADF) improved insulin sensitivity in both *Lepr^{db}* and *m Lepr^{db}* mice. Data represent mean ± SEM. *n* = 6 *m Lepr^{db}*, 6 *m Lepr^{db}* + ADF, 6 *Lepr^{db}*, and 5 *Lepr^{db}* + ADF. *$P < 0.05$ vs. *m Lepr^{db}* control mice, # $p < 0.05$ vs. *Lepr^{db}* diabetic mice.

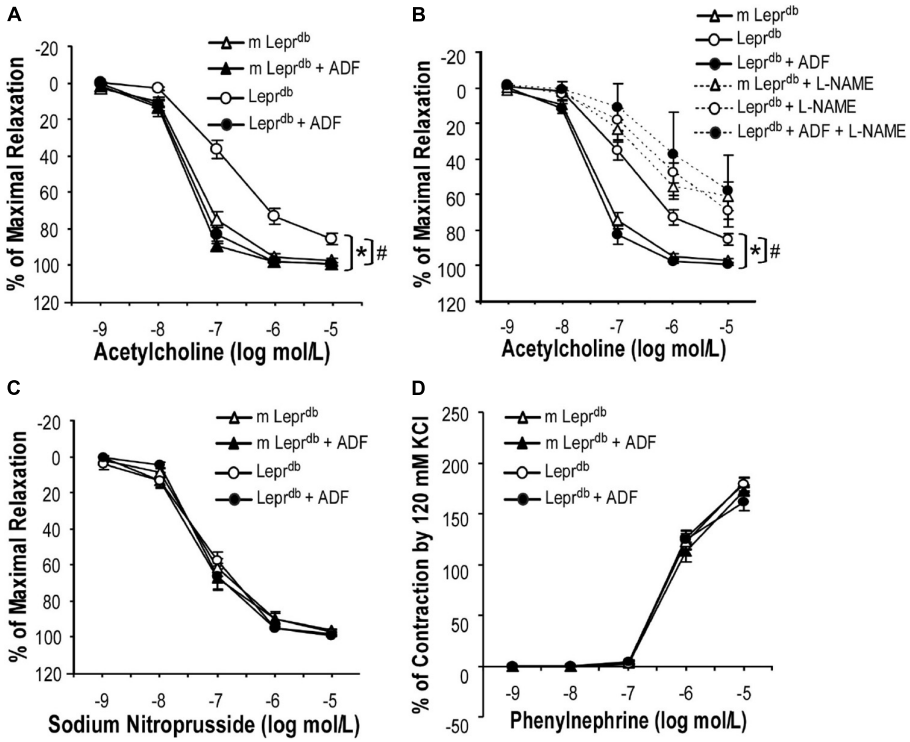

FIGURE 2 | ADF improved endothelium-dependent vasorelaxation without affecting endothelium-independent vasorelaxation or phenylephrine-induced vasoconstriction of small mesenteric arteries (SMA) in type 2 diabetic mice. **(A)** Acetylcholine (ACh)-induced endothelium-dependent vasorelaxation of SMA was impaired in *Lepr*^{db} mice. Twelve weeks of ADF in *Lepr*^{db} (*Lepr*^{db} + ADF) restored endothelium-dependent vasorelaxation back to the level of *m Lepr*^{db} control mice. **(B)** Incubation with the nitric oxide synthase inhibitor (L-NAME) largely attenuated ADF-induced improvement of endothelial function in diabetic mice. **(C)** Sodium Nitroprusside (SNP)-induced endothelium-independent vasorelaxation of SMA was comparable among groups. **(D)** Phenylephrine (PE)-induced vasoconstriction of SMA was comparable among groups. Data represent mean ± SEM. $n = 5$ mice per group with 1–2 rings per mouse. *$P < 0.05$ vs. *m Lepr*^{db} control mice, # $p < 0.05$ vs. *Lepr*^{db} diabetic mice.

Overall, in *Lepr*^{db} mice, adipokine levels in the serum and MAT showed consistent directionality following ADF. In *m Lepr*^{db} control mice, however, the increase in MAT mRNA expression of *Adipoq* and *Lep* did not correlate with change in the circulation, likely suggesting possible feedback mechanisms to maintain homeostasis in non-diabetic control mice.

The Endothelial Protective Effects of Alternate Day Fasting Were Partly Mediated Through Enhanced Adiponectin

To determine if ADF improved endothelium-dependent vasorelaxation through modulating adipose-derived hormones, we treated control and diabetic mice with adenovirus expressing adiponectin (Ad-APN) or β-galactosidase (Ad-βgal) as the control. As we have previously described (20), mice were euthanized one week after adenovirus treatment and increased circulating adiponectin levels were confirmed by ELISA. Indeed, adiponectin supplementation partly improved endothelium-dependent vasorelaxation in *Lepr*^{db} mice (**Figure 4A**), without affecting endothelium-independent vasorelaxation (**Figure 4B**). To dissect if other adipokines were also involved in ADF-mediated endothelial protective effects, *Lepr*^{db} mice were treated with recombinant murine resistin (15 μg/mouse/day for 4 days, i.p.) according to a previously published protocol (26). The short-term treatment of resistin did not impair or improve endothelium-dependent or -independent vasorelaxation (**Figures 4C,D**), suggesting that short-term resistin administration may not affect vascular function. Similarly, *Lepr*^{db} mice showed increased circulating leptin due to leptin receptor deficiency. Circulating leptin was further enhanced by ADF, suggesting that an increase in circulating leptin itself was unlikely to prevent the vascular benefits of ADF. Thus, our study provided some mechanistic insights into the contribution of adipokines to ADF-mediated vascular effects in type 2 diabetes.

The Effects of Alternate Day Fasting on the Expression of Nitrotyrosine Protein, a Marker of Oxidative Stress, in Small Mesenteric Arteries and Mesenteric Adipose Tissue

Nitrotyrosine protein levels were elevated in both SMA and MAT of *Lepr*^{db} diabetic mice compared with *m Lepr*^{db} control

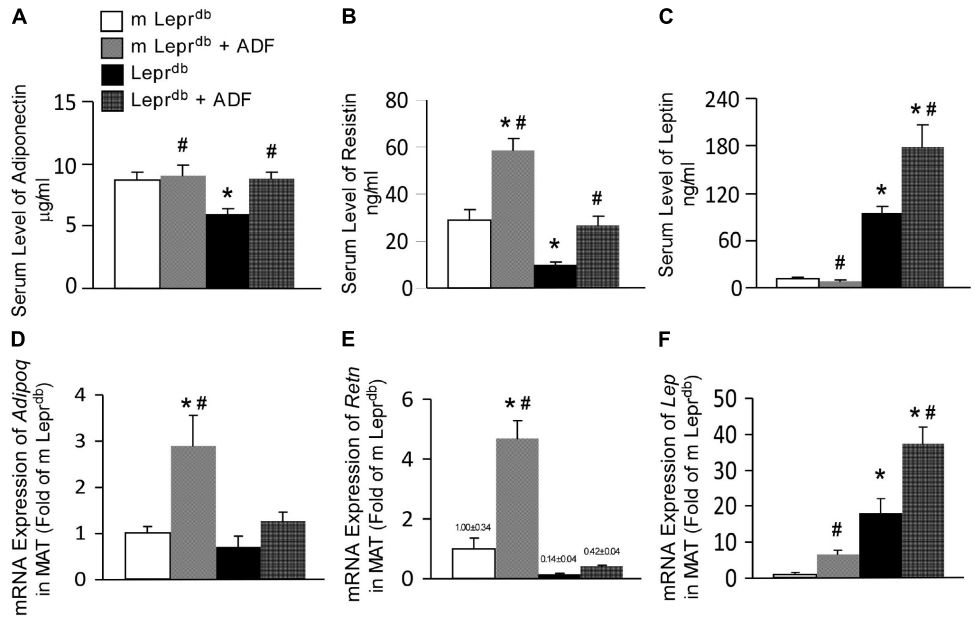

FIGURE 3 | ADF modulated circulating levels and adipose expression of key adipokines, including adiponectin, resistin, and leptin in mesenteric adipose tissue (MAT) of both *m Lepr^{db}* and *Lepr^{db}* mice. Circulating levels of adiponectin **(A)**, resistin **(B)**, and leptin **(C)** were determined by ELISA. mRNA expression of *Adipoq* **(D)**, *Retn* **(E)**, and *Lep* **(F)** were determined by qRT-PCR in mesenteric adipose tissue (MAT). Data represent mean ± SEM. n = 6 *m Lepr^{db}*, 6 *m Lepr^{db}* + ADF, 6 *Lepr^{db}*, and 5 *Lepr^{db}* + ADF. *$P < 0.05$ vs. *m Lepr^{db}* control mice, # $p < 0.05$ vs. *Lepr^{db}* diabetic mice.

mice. ADF reduced SMA nitrotyrosine protein levels in *Lepr^{db}* diabetic mice without affecting that in the *m Lepr^{db}* control mice (**Figure 5A**). ADF, however, did not significantly decrease MAT nitrotyrosine protein levels (**Figure 5B**).

DISCUSSION

Studies demonstrate that intermittent fasting improves cardiometabolic risk factors such as blood pressure, levels of low-density lipoprotein cholesterol and triglycerides, insulin resistance, and HbA1c (5). A better understanding of how intermittent fasting affects cardiovascular function and the underlying mechanisms will facilitate its clinical application in obesity and diabetes-associated cardiovascular complications. Our study revealed the profound benefits of ADF in rescuing endothelial dysfunction. The benefits are at least partly mediated through enhanced adiponectin, while resistin and leptin were unlikely to be involved. Adiponectin thus provides a mechanistic link between the role of ADF in regulating adipokine profile and endothelial function in type 2 diabetes. ADF reduced the marker of oxidative stress in resistance arteries but not adipose tissue, suggesting tissue-specific regulatory roles by ADF. ADF may also exert metabolic and vascular benefits in non-obese control mice. Overall, our data support that ADF presents as promising lifestyle intervention for treating diabetes-associated endothelial dysfunction.

Intermittent fasting is emerging as a popular alternative dietary intervention strategy. Despite limited numbers of clinical trials directly comparing the long-term effects of intermittent fasting and daily calorie restriction, current evidence supports equivalent or superior metabolic benefits of intermittent fasting (5). Comparative studies in a 12-month study of insulin-resistant participants support that ADF may produce greater reductions in fasting insulin and insulin resistance compared with calorie restriction despite similar decreases in body weight (37). Experimental studies in C57BL/6J mice suggested that ADF produces similar beneficial modulation of body fat distribution and adiponectin levels as does daily calorie restriction (38). In *Lepr^{db}* type 2 diabetic mice and streptozotocin-treated type 1 diabetic mice treated with a fasting-mimicking diet, both intermittent fasting and continuous calorie restriction significantly reduced fasting blood glucose levels and improved insulin sensitivity. Yet, intermittent fasting performed significantly better than continuous calorie restriction in improving glycemic control and insulin sensitivity in *Lepr^{db}* type 2 diabetic mice (39). Clinical studies, conducted over multiple years, that directly compare different regimens will provide important insights into the long-term cardiometabolic benefits of these diets.

There are currently no clinical studies determining the vascular benefits of long-term ADF in patients with diabetes. Clinical trials of short-term ADF, e.g., 8–12 weeks, have, however, provided promising evidence. In obese subjects (n = 32), ADF with a low-fat diet, but not a high-fat diet, for 8-weeks showed improved brachial artery flow-mediated vasodilation (40). Increases in adiponectin were positively associated with augmented flow-mediated vasodilation post-ADF in those subjected to ADF with the low-fat diet (40). ADF also reduced plasma resistin and leptin, which were not

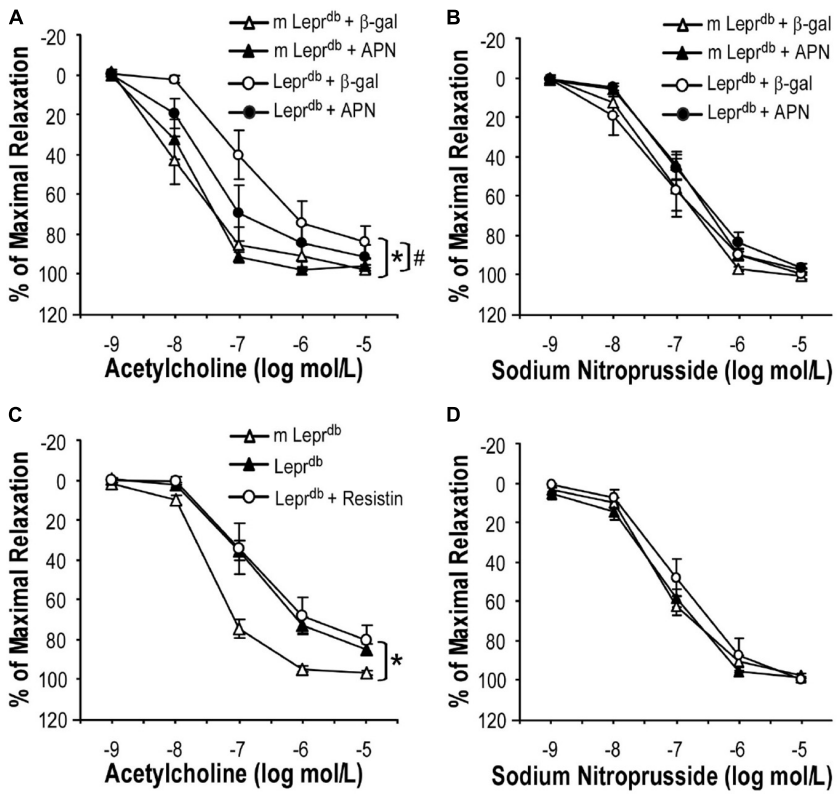

FIGURE 4 | The effects of adipokines on endothelium-dependent vasorelaxation of SMA. **(A)** Adenovirus-mediated adiponectin supplementation improved ACh-induced endothelium-dependent vasorelaxation of SMA in *Lepr*^{db} mice, without affecting SNP-induced endothelium-independent vasorelaxation **(B)**. Data represent mean ± SEM. $n = 5$ mice per group with 1–2 rings per mouse. **(C,D)** Treatment with recombinant resistin did not affect endothelium-dependent or endothelium-independent vasorelaxation of SMA. Data represent mean ± SEM. $n = 6$ *m Lepr*^{db}, 6 *Lepr*^{db}, 4 *Lepr*^{db} + resistin with 1–2 rings per mouse. *$P < 0.05$ vs. *m Lepr*^{db} control mice, # $p < 0.05$ vs. *Lepr*^{db} diabetic mice.

correlated with changes in flow-mediated vasodilation (40). In a study involving 54 obese non-diabetic subjects with an 8-week ADF protocol, brachial artery flow-mediated vasodilation was positively correlated to adiponectin concentrations (41). Another study involving 64 obese subjects supported that a 12-week period of ADF improved brachial artery flow-mediated vasodilation (42). Our experimental data strongly support the profound endothelial protective effects of ADF in mice modeling severe type 2 diabetes. To our knowledge, this is the first experimental study determining the role of ADF in diabetes-associated vascular dysfunction. The above clinical studies in obese subjects and our experimental study in type 2 diabetic mice provide premises to further explore the clinical benefits of long-term ADF in diabetes-associated cardiovascular complications.

Our study has shed light on the mechanisms of the endothelial protective effects of ADF partly through enhanced circulating adiponectin. Adiponectin is well known for its anti-inflammatory and anti-oxidative roles in endothelial cells (43) and its protective effects against neointimal formation in response to vascular injury (44) and atherosclerosis (45). Our previous work has also supported that adiponectin abates diabetes-induced endothelial dysfunction by suppressing oxidative stress, adhesion molecules, and inflammation in type 2 diabetic mice (20). Specifically, adenovirus-mediated adiponectin supplementation improved endothelium-dependent vasorelaxation of aortas in *Lepr*^{db} mice (20). Adiponectin supplementation reduced aortic nitrotyrosine protein levels, *via* suppressing protein expression of gp91^{phox}, an NADPH oxidase subunit, and increasing protein expression of SOD3, an antioxidant enzyme (20). Aortic expression of inflammatory genes, *Tnf*, *Il6*, and *Icam1*, was also suppressed by adiponectin supplementation (20). These pathways are likely responsible for the endothelial protective and anti-oxidative effects of adiponectin in mesenteric arteries of *Lepr*^{db} mice undergoing ADF. The adiponectin-independent endothelial protective and anti-oxidative effects of ADF remain to be further dissected, and we speculate that the metabolic benefits of ADF may play important roles.

Alternate day fasting exerts profound metabolic benefits in both control and diabetic mice with remarkably improved glycemic control and insulin sensitivity. The effects of ADF on weight loss and visceral adiposity were, however, modest. In particular, ADF led to ∼4% weight loss in *Lepr*^{db} mice that did not reach statistical significance (**Table 1**). Consistent with our observation, an independent study also suggested that a 13-week period of intermittent fasting, using a fasting mimicking diet

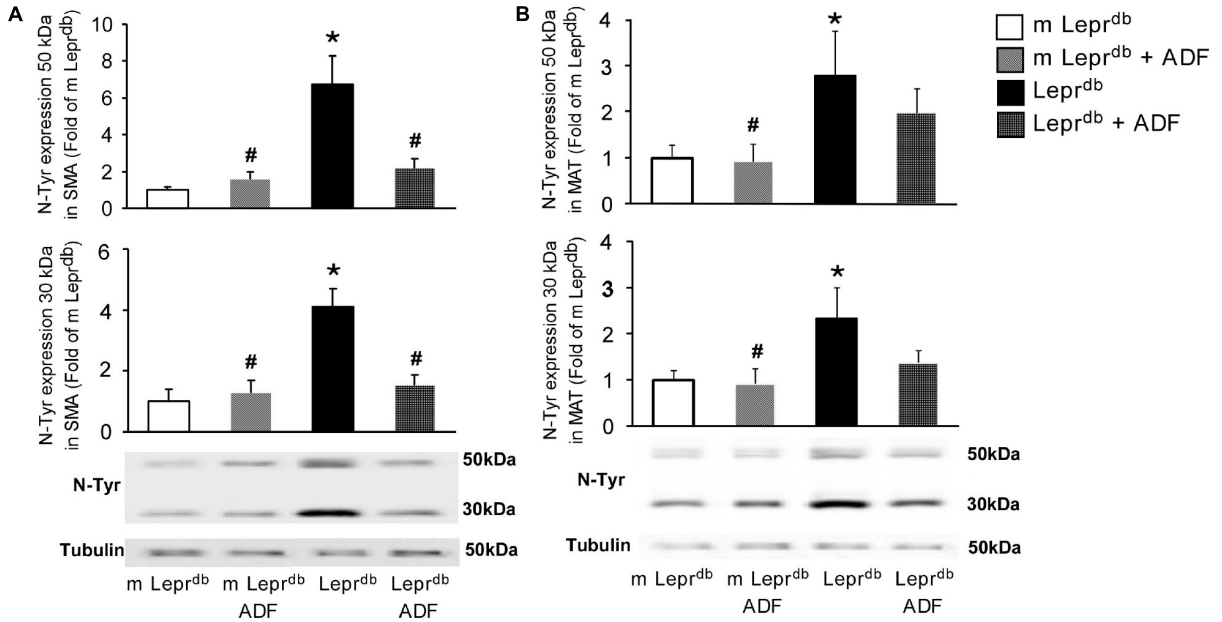

FIGURE 5 | ADF reduced nitrotyrosine protein levels in SMA, but not MAT, of *Lepr*^{db} mice. **(A)** Nitrotyrosine protein levels were higher in SMA of *Lepr*^{db} mice. ADF reduced nitrotyrosince protein in SMA of *Lepr*^{db} mice. $n = 4$ mice per group. **(B)** Nitrotyrosine protein levels were higher in MAT of *Lepr*^{db} mice. ADF did not alter nitrotyrosince protein in MAT of *Lepr*^{db} mice. $n = 6$ mice per group. *$P < 0.05$ vs. *m Lepr*^{db} control mice, # $p < 0.05$ vs. *Lepr*^{db} diabetic mice.

protocol, improved glucose homeostasis in *Lepr*^{db} mice without causing weight loss (39). Our previous study examining the effects of bariatric surgery in *Lepr*^{db} mice demonstrated a ∼15–18% weight reduction following gastric bypass surgery that was accompanied by significantly improved glycemic control and insulin sensitivity (27). Thus, the metabolic benefits of ADF in *Lepr*^{db} diabetic mice are likely not entirely dependent on weight loss effects. Since the *Lepr*^{db} mice resemble severe type 2 diabetes, whether ADF may also exert limited benefits in weight management in patients with type 2 diabetes, despite profound metabolic effects, should be studied clinically. In *m Lepr*^{db} control mice, ADF led to statistically significant weight loss (∼11%, **Table 1**), and further improved glucose metabolism with a trend toward improved endothelial function. Further, the benefits of ADF in non-obese, healthy humans thus may also warrant further investigation.

There are many questions that remain to be explored. Future studies may further elucidate if the knockout of adiponectin abolishes the vascular protective effects of ADF, the involvement of other adipokines, and the molecular mechanisms by which ADF modulates adipokine expression and secretion. Comparative studies are required to tackle how different intermittent fasting regimens affect metabolic, vascular, and hormonal parameters. Findings generated from such studies could inform whether one regimen is superior to the others and elucidate the mechanisms that underlie the cardiometabolic benefits. The discovery of pharmacological agents mimicking fasting can potentially provide novel therapeutic strategies. A potential limitation of the present studies is that they were performed only in male mice and mesenteric resistance arteries. Given possible sexual dimorphism in regard to obesity/diabetes-related macrovascular and microvascular disease, it will be important to extend our observations to females and in multiple vascular beds, such as aorta and coronary arteries, as well as the microvasculature.

CONCLUSION

In summary, our study examined the role and mechanisms of ADF in diabetes-associated endothelial dysfunction using murine models of type 2 diabetes. We have revealed that ADF in type 2 diabetic mice exerts profound endothelial protective effects, partly through modulating the adipose-derived hormone, adiponectin. Thus, this study improves our understanding of how ADF affords significant protection against endothelial dysfunction partly by regulating adipose-derived hormones. Our work also elaborated on the metabolic benefits and potential cardiovascular protective actions of ADF in the management of type 2 diabetes.

DEDICATION

The manuscript is in memory of Dr. Cuihua Zhang, who was deceased on October 1, 2011.

DATA AVAILABILITY STATEMENT

The raw data supporting the conclusions of this article will be made available by the authors, without undue reservation.

ETHICS STATEMENT

The animal study was reviewed and approved by the Animal Care Committee at the University of Missouri (Columbia, MO, United States).

AUTHOR CONTRIBUTIONS

JC, HZ, and CZ conceived the study. JC, SL, and HZ performed the experiments. JC and HZ analyzed the data. JC, YL, and HZ interpreted results of experiments and drafted the manuscript. JC, YS, and HZ prepared the tables and figures. JC, SL, YS, MH, YL, and HZ edited and revised the manuscript. All authors contributed to the article and approved the submitted version.

FUNDING

This work was supported by R01-HL-077566 (to CZ) and R01-HL-085119 (to CZ and MH).

REFERENCES

1. Powell-Wiley TM, Poirier P, Burke LE, Després JP, Gordon-Larsen P, Lavie CJ, et al. Obesity and cardiovascular disease: a scientific statement from the american heart association. *Circulation.* (2021) 143:e984–1010. doi: 10.1161/cir.0000000000000973
2. Varady KA, Cienfuegos S, Ezpeleta M, Gabel K. Cardiometabolic benefits of intermittent fasting. *Annu Rev Nutr.* (2021) 41:333–61. doi: 10.1146/annurev-nutr-052020-041327
3. Flanagan EW, Most J, Mey JT, Redman LM. Calorie restriction and aging in humans. *Annu Rev Nutr.* (2020) 40:105–33. doi: 10.1146/annurev-nutr-122319-034601
4. Santos HO, Genario R, Tinsley GM, Ribeiro P, Carteri RB, Coelho-Ravagnani CF, et al. A scoping review of intermittent fasting, chronobiology, and metabolism. *Am J Clin Nutr.* (2022) 115:991–1004. doi: 10.1093/ajcn/nqab433
5. Varady KA, Cienfuegos S, Ezpeleta M, Gabel K. Clinical application of intermittent fasting for weight loss: progress and future directions. *Nat Rev Endocrinol.* (2022) 18:309–21. doi: 10.1038/s41574-022-00638-x
6. Vasim I, Majeed CN, DeBoer MD. Intermittent fasting and metabolic health. *Nutrients.* (2022) 14:631. doi: 10.3390/nu14030631
7. Zang B-Y, He L-X, Xue L. Intermittent fasting: potential bridge of obesity and diabetes to health? *Nutrients.* (2022) 14:981. doi: 10.3390/nu14050981
8. Martens CR, Seals DR. Practical alternatives to chronic caloric restriction for optimizing vascular function with ageing. *J Physiol.* (2016) 594:7177–95. doi: 10.1113/jp272348
9. Carter S, Clifton PM, Keogh JB. Effect of intermittent compared with continuous energy restricted diet on glycemic control in patients with type 2 diabetes: a randomized noninferiority trial. *JAMA Netw Open.* (2018) 1:e180756. doi: 10.1001/jamanetworkopen.2018.0756
10. Chen H, Charlat O, Tartaglia LA, Woolf EA, Weng X, Ellis SJ, et al. Evidence that the diabetes gene encodes the leptin receptor: identification of a mutation in the leptin receptor gene in Db/Db mice. *Cell.* (1996) 84:491–5. doi: 10.1016/s0092-8674(00)81294-5
11. Chua SC Jr., Chung WK, Wu-Peng XS, Zhang Y, Liu SM, Tartaglia L, et al. Phenotypes of mouse diabetes and rat fatty due to mutations in the Ob (Leptin) receptor. *Science.* (1996) 271:994–6. doi: 10.1126/science.271.5251.994
12. Zhou J, Jiang Z, Lin Y, Li C, Liu J, Tian M, et al. The daily caloric restriction and alternate-day fasting ameliorated lipid dysregulation in type 2 diabetic mice by downregulating hepatic pescadillo 1. *Eur J Nutr.* (2022). doi: 10.1007/s00394-022-02850-x [Epub ahead of print].
13. Zhang H, Zhang W, Yun D, Li L, Zhao W, Li Y, et al. Alternate-day fasting alleviates diabetes-induced glycolipid metabolism disorders: roles of Fgf21 and bile acids. *J Nutr Biochem.* (2020) 83:108403. doi: 10.1016/j.jnutbio.2020.108403
14. Kim KE, Jung Y, Min S, Nam M, Heo RW, Jeon BT, et al. Caloric restriction of Db/Db mice reverts hepatic steatosis and body weight with divergent hepatic metabolism. *Sci Rep.* (2016) 6:30111. doi: 10.1038/srep30111
15. Beli E, Yan Y, Moldovan L, Vieira CP, Gao R, Duan Y, et al. Restructuring of the gut microbiome by intermittent fasting prevents retinopathy and prolongs survival in Db/Db mice. *Diabetes.* (2018) 67:1867–79. doi: 10.2337/db18-0158
16. Liu Z, Dai X, Zhang H, Shi R, Hui Y, Jin X, et al. Gut microbiota mediates intermittent-fasting alleviation of diabetes-induced cognitive impairment. *Nat Commun.* (2020) 11:855. doi: 10.1038/s41467-020-14676-4
17. Zhang H, Zhang C. Adipose "Talks" to distant organs to regulate insulin sensitivity and vascular function. *Obesity (Silver Spring).* (2010) 18:2071–6. doi: 10.1038/oby.2010.91
18. Zhang H, Zhang C. Regulation of microvascular function by adipose tissue in obesity and type 2 diabetes: evidence of an adipose-vascular loop. *Am J Biomed Sci.* (2009) 1:133. doi: 10.5099/aj090200133
19. Zhang H, Cui J, Zhang C. Emerging role of adipokines as mediators in atherosclerosis. *World J Cardiol.* (2010) 2:370–6. doi: 10.4330/wjc.v2.i11.370
20. Lee S, Zhang H, Chen J, Dellsperger KC, Hill MA, Zhang C. Adiponectin abates diabetes-induced endothelial dysfunction by suppressing oxidative stress, adhesion molecules, and inflammation in type 2 diabetic mice. *Am J Physiol Heart Circ Physiol.* (2012) 303:H106–15. doi: 10.1152/ajpheart.00110.2012
21. Zhang H, Park Y, Zhang C. Coronary and aortic endothelial function affected by feedback between adiponectin and tumor necrosis factor α in type 2 diabetic mice. *Arterioscler Thromb Vasc Biol.* (2010) 30:2156–63. doi: 10.1161/atvbaha.110.214700
22. Lee S, Park Y, Dellsperger KC, Zhang C. Exercise training improves endothelial function via adiponectin-dependent and independent pathways in type 2 diabetic mice. *Am J Physiol Heart Circ Physiol.* (2011) 301:H306–14. doi: 10.1152/ajpheart.01306.2010
23. Reinehr T, Roth C, Menke T, Andler W. Adiponectin before and after weight loss in obese children. *J Clin Endocrinol Metab.* (2004) 89:3790–4. doi: 10.1210/jc.2003-031925
24. Zorena K, Jachimowicz-Duda O, Ślęzak D, Robakowska M, Mrugacz M. Adipokines and obesity. Potential link to metabolic disorders and chronic complications. *Int J Mol Sci.* (2020) 21:3570. doi: 10.3390/ijms21103570
25. Varady KA, Tussing L, Bhutani S, Braunschweig CL. Degree of weight loss required to improve adipokine concentrations and decrease fat cell size in severely obese women. *Metabolism.* (2009) 58:1096–101. doi: 10.1016/j.metabol.2009.04.010
26. Steppan CM, Bailey ST, Bhat S, Brown EJ, Banerjee RR, Wright CM, et al. The hormone resistin links obesity to diabetes. *Nature.* (2001) 409:307–12. doi: 10.1038/35053000
27. Zhang H, Wang Y, Zhang J, Potter BJ, Sowers JR, Zhang C. Bariatric surgery reduces visceral adipose inflammation and improves endothelial function in type 2 diabetic mice. *Arterioscler Thromb Vasc Biol.* (2011) 31:2063–9. doi: 10.1161/atvbaha.111.225870
28. Chen X, Zhang H, McAfee S, Zhang C. The reciprocal relationship between adiponectin and lox-1 in the regulation of endothelial dysfunction in apoe knockout mice. *Am J Physiol Heart Circ Physiol.* (2010) 299:H605–12. doi: 10.1152/ajpheart.01096.2009
29. Ste Marie L, Palmiter RD. Norepinephrine and epinephrine-deficient mice are hyperinsulinemic and have lower blood glucose. *Endocrinology.* (2003) 144:4427–32. doi: 10.1210/en.2003-0561
30. Matsuda M, Shimomura I, Sata M, Arita Y, Nishida M, Maeda N, et al. Role of adiponectin in preventing vascular stenosis. the missing link of adipo-vascular axis. *J Biol Chem.* (2002) 277:37487–91. doi: 10.1074/jbc.M206083200
31. Su J, Lucchesi PA, Gonzalez-Villalobos RA, Palen DI, Rezk BM, Suzuki Y, et al. Role of advanced glycation end products with oxidative stress in resistance artery dysfunction in type 2 diabetic mice. *Arterioscler Thromb Vasc Biol.* (2008) 28:1432–8. doi: 10.1161/ATVBAHA.108.167205
32. Zhang H, Potter BJ, Cao JM, Zhang C. Interferon-gamma induced adipose tissue inflammation is linked to endothelial dysfunction in type 2 diabetic

mice. *Basic Res Cardiol.* (2011) 106:1135–45. doi: 10.1007/s00395-011-0212-x
33. Untergasser A, Cutcutache I, Koressaar T, Ye J, Faircloth BC, Remm M, et al. Primer3–new capabilities and interfaces. *Nucleic Acids Res.* (2012) 40:e115. doi: 10.1093/nar/gks596
34. Zhang H, Zhang J, Ungvari Z, Zhang C. Resveratrol improves endothelial function: role of tnf{alpha} and vascular oxidative stress. *Arterioscler Thromb Vasc Biol.* (2009) 29:1164–71. doi: 10.1161/atvbaha.109.187146
35. Chen X, Zhang H, Hill MA, Zhang C, Park Y. Regulation of coronary endothelial function by interactions between Tnf-A, Lox-1 and adiponectin in apolipoprotein e knockout mice. *J Vasc Res.* (2015) 52:372–82. doi: 10.1159/000443887
36. Zhao S, Kusminski CM, Scherer PE. Adiponectin, leptin and cardiovascular disorders. *Circ Res.* (2021) 128:136–49. doi: 10.1161/circresaha.120.314458
37. Gabel K, Kroeger CM, Trepanowski JF, Hoddy KK, Cienfuegos S, Kalam F, et al. Differential effects of alternate-day fasting versus daily calorie restriction on insulin resistance. *Obesity (Silver Spring).* (2019) 27:1443–50. doi: 10.1002/oby.22564
38. Varady KA, Allister CA, Roohk DJ, Hellerstein MK. Improvements in body fat distribution and circulating adiponectin by alternate-day fasting versus calorie restriction. *J Nutr Biochem.* (2010) 21:188–95. doi: 10.1016/j.jnutbio.2008.11.001
39. Wei S, Zhao J, Bai M, Li C, Zhang L, Chen Y. Comparison of glycemic improvement between intermittent calorie restriction and continuous calorie restriction in diabetic mice. *Nutr Metab (Lond).* (2019) 16:60. doi: 10.1186/s12986-019-0388-x
40. Klempel MC, Kroeger CM, Norkeviciute E, Goslawski M, Phillips SA, Varady KA. Benefit of a low-fat over high-fat diet on vascular health during alternate day fasting. *Nutr Diabet.* (2013) 3:e71. doi: 10.1038/nutd.2013.14
41. Hoddy KK, Bhutani S, Phillips SA, Varady KA. Effects of different degrees of insulin resistance on endothelial function in obese adults undergoing alternate day fasting. *Nutr Healthy Aging.* (2016) 4:63–71. doi: 10.3233/nha-1611
42. Bhutani S, Klempel MC, Kroeger CM, Trepanowski JF, Phillips SA, Norkeviciute E, et al. Alternate day fasting with or without exercise: effects on endothelial function and adipokines in obese humans. *e-SPEN J.* (2013) 8:e205–9. doi: 10.1016/j.clnme.2013.07.005
43. Goldstein BJ, Scalia R. Adiponectin: a novel adipokine linking adipocytes and vascular function. *J Clin Endocrinol Metab.* (2004) 89:2563–8. doi: 10.1210/jc.2004-0518
44. Kubota N, Terauchi Y, Yamauchi T, Kubota T, Moroi M, Matsui J, et al. Disruption of adiponectin causes insulin resistance and neointimal formation. *J Biol Chem.* (2002) 277:25863–6. doi: 10.1074/jbc.C200251200
45. Okamoto Y, Kihara S, Ouchi N, Nishida M, Arita Y, Kumada M, et al. Adiponectin reduces atherosclerosis in apolipoprotein e-deficient mice. *Circulation.* (2002) 106:2767–70. doi: 10.1161/01.cir.0000042707.50032.19

Conflict of Interest: The authors declare that the research was conducted in the absence of any commercial or financial relationships that could be construed as a potential conflict of interest.

Publisher's Note: All claims expressed in this article are solely those of the authors and do not necessarily represent those of their affiliated organizations, or those of the publisher, the editors and the reviewers. Any product that may be evaluated in this article, or claim that may be made by its manufacturer, is not guaranteed or endorsed by the publisher.

frontiers | Frontiers in Cardiovascular Medicine

ORIGINAL RESEARCH
published: 16 June 2022
doi: 10.3389/fcvm.2022.929466

E-Selectin/AAV2/2 Gene Therapy Alters Angiogenesis and Inflammatory Gene Profiles in Mouse Gangrene Model

Antoine J. Ribieras[1], Yulexi Y. Ortiz[1], Yan Li[1], Carlos T. Huerta[1], Nga Le[1], Hongwei Shao[1], Roberto I. Vazquez-Padron[1,2], Zhao-Jun Liu[1,2] and Omaida C. Velazquez[1,2]**

[1] Division of Vascular Surgery, DeWitt Daughtry Family Department of Surgery, University of Miami Miller School of Medicine, Miami, FL, United States, [2] Vascular Biology Institute, University of Miami Miller School of Medicine, Miami, FL, United States

OPEN ACCESS

Edited by:
Bin Ren,
University of Alabama at Birmingham, United States

Reviewed by:
Li Li,
Wayne State University, United States
Adam Beck,
University of Alabama at Birmingham, United States
Baohui Xu,
Stanford University, United States

***Correspondence:**
Omaida C. Velazquez
ovelazquez@med.miami.edu
Zhao-Jun Liu
zliu@med.miami.edu

Specialty section:
This article was submitted to Cardiovascular Therapeutics, a section of the journal Frontiers in Cardiovascular Medicine

Received: *26 April 2022*
Accepted: *26 May 2022*
Published: *16 June 2022*

Citation:
Ribieras AJ, Ortiz YY, Li Y, Huerta CT, Le N, Shao H, Vazquez-Padron RI, Liu Z-J and Velazquez OC (2022) E-Selectin/AAV2/2 Gene Therapy Alters Angiogenesis and Inflammatory Gene Profiles in Mouse Gangrene Model. Front. Cardiovasc. Med. 9:929466. doi: 10.3389/fcvm.2022.929466

For patients with chronic limb-threatening ischemia and limited revascularization options, alternate means for therapeutic angiogenesis and limb salvage are needed. E-selectin is a cell adhesion molecule that is critical for inflammation and neovascularization in areas of wound healing and ischemia. Here, we tested the efficacy of modifying ischemic limb tissue by intramuscular administration of E-selectin/AAV2/2 (adeno-associated virus serotype 2/2) to modulate angiogenic and inflammatory responses in a murine hindlimb gangrene model. Limb appearance, reperfusion, and functional recovery were assessed for 3 weeks after induction of ischemia. Mice receiving E-selectin/AAV2/2 gene therapy had reduced gangrene severity, increased limb and footpad perfusion, enhanced recruitment of endothelial progenitor cells, and improved performance on treadmill testing compared to control group. Histologically, E-selectin/AAV2/2 gene therapy was associated with increased vascularity and preserved myofiber integrity. E-selectin/AAV2/2 gene therapy also upregulated a panel of pro-angiogenic genes yet downregulated another group of genes associated with the inflammatory response. This novel gene therapy did not induce adverse effects on coagulability, or hematologic, hepatic, and renal function. Our findings highlight the potential of E-selectin/AAV2/2 gene therapy for improving limb perfusion and function in patients with chronic limb-threatening ischemia.

Keywords: E-selectin (CD62E), gene therapy, angiogenesis, chronic limb-threatening ischemia, peripheral artery disease, gangrene

INTRODUCTION

Peripheral artery disease (PAD) affects 200 million people globally, up to 10% of whom suffer from its most severe form, chronic limb-threatening ischemia (CLTI) (1). CLTI is characterized by hemodynamic compromise to the lower extremities leading to ischemic rest pain, gangrene, or non-healing wounds (2). It is a condition associated with decreased quality of life, increased risk for amputation, and increased 5-year mortality (2). Beyond risk factor optimization (i.e., smoking cessation, lipid-lowering therapy, glycemic control), surgical revascularization with open bypass or endovascular intervention remains the cornerstone of therapy (3). However, these therapies often require repeated procedures, and many patients still suffer limb loss to amputation. For the

30% of CLTI patients who are not candidates for or have failed prior revascularization attempts, alternate methods are needed to improve perfusion to the extremities (1). In addition, it is postulated that adding pro-angiogenic regenerative approaches could improve overall long-term limb salvage over standard of care only. To this end, several gene- and cell-based products have been tested for therapeutic angiogenesis in preclinical animal models and clinical trials. Among gene therapies, previously studied constructs have largely been formulated as naked DNA plasmids encoding soluble angiogenic factors, notably vascular endothelial growth factor (VEGF) (4–6), hepatocyte growth factor (HGF) (7, 8), and fibroblast growth factor (FGF) (9–11). These therapies have shown promise for improving hemodynamic parameters and ulcer healing in CLTI, but without clear benefit on major amputation rates, amputation-free survival, or overall survival in randomized controlled studies (12).

To address the treatment gap in CLTI, we have previously studied the cell adhesion molecule (CAM), E-selectin, as a novel target for therapeutic angiogenesis (13, 14). E-selectin is a multifunctional CAM expressed by activated endothelium that mediates rolling and extravasation of neutrophils and monocytes, thereby playing an important role in inflammatory, immunologic, and thrombotic processes. More recently, the pro-angiogenic actions of E-selectin signaling have also been elucidated. In response to tissue injury, release of cytokines/chemokines, including stromal cell-derived factor 1α (SDF-1α), induces local endothelial expression of membrane-bound E-selectin and systemic reciprocal E-selectin ligand expression on endothelial progenitor cells (EPCs) in the bone marrow *via* C-X-C motif chemokine receptor 4 (CXCR4) (15). Thus, SDF-1α initiates an E-selectin/E-selectin ligand signaling cascade that mobilizes bone marrow-derived EPCs to areas of wound healing and ischemia where these cells can then contribute to vasculogenesis and neovascularization (16). Our previous work in murine hindlimb ischemia models showed that local overexpression of E-selectin by intramuscular gene transfer can be used to make the tissue microenvironment more receptive to EPCs, potentiating the endogenous angiogenic response with corresponding benefits on wound healing (13) and footpad tissue loss (14). This focus on modification of cell-bound adhesion *via* E-selectin is the major novelty introduced by our work. In contrast to most clinical trials of gene-based therapeutic angiogenesis, our prior studies of E-selectin gene therapy used an adeno-associated virus (AAV) delivery vector to provide higher transduction efficiency than naked plasmids with lower immunogenicity than adenoviral vectors (17). Several AAV serotypes exist with diverse tissue tropisms based on capsid- and tissue-specific differences in cellular uptake and intracellular trafficking (18). In our previous work, we employed serotype AAV2/9 due to its known tropism for muscle, both cardiac and skeletal (19). On the other hand, serotype AAV2/2 has been the most widely studied with broad tissue tropism toward skeletal muscle, neurons, vascular smooth muscle cells, and hepatocytes, as well as favorable *in vitro* transduction efficiency (20). Intramuscular AAV2/2 therapies have been used in Phase I studies to treat hemophilia B and α_1-antitrypsin deficiency (21, 22), and both AAV2/2 and AAV2/9-based gene therapies are currently approved by the United States Food and Drug Administration.

As such, the goals of this study were to evaluate the efficacy of E-selectin/AAV2/2 (E-sel/AAV2/2), a novel gene construct for therapeutic angiogenesis, for improving limb salvage, reperfusion, and function in a clinically relevant murine gangrene model. Additionally, we sought to characterize the temporal expression of E-selectin in response to ischemia, both in treated and untreated muscle, as well as the downstream angiogenic and inflammatory responses induced by E-sel/AAV2/2 gene therapy.

MATERIALS AND METHODS

Production of Adeno-Associated Vectors

Murine *E-selectin* and *LacZ* genes were inserted into multiple cloning sites in the pZac vector (13). After confirmation by gene sequencing, E-selectin/pZac and LacZ/pZac plasmids were sent to the University of North Carolina Gene Therapy Vector Core where AAV serotype 2/2 was prepared by three-plasmid transfection into HEK293 cells (23). Quality assurance and control testing was performed by PCR quantification of genomes and infectivity titer.

Administration of E-Sel/AAV2/2 Gene Therapy

All animal experiments described were approved by the University of Miami Institutional Animal Care and Use Committee under protocol 19-163. To account for the lag time between injections and tissue transgene expression, gene therapy was administered 4 and 2 days prior to surgery, as well as on the day of left femoral artery and vein coagulation. Total dose was 1×10^{11} viral genome divided across the 3 days and diluted in 100 μL phosphate-buffered saline (PBS) per dose per mouse. While anesthetized with inhaled isoflurane 1.5–2% and oxygen at 2 L/min, E-sel/AAV2/2 ($N = 31$, 17 female) and LacZ/AAV2/2 ($N = 23$, 12 female) were administered with a 31-gauge needle *via* intramuscular (IM) injections of 20 μL each into the left adductor group (2), lateral thigh (1), and medial (1) and lateral (1) gastrocnemius.

Induction of Hindlimb Gangrene

FVB/NJ male and female mice (001800, Jackson Laboratory, Bar Harbor, ME) aged 10–12 weeks were anesthetized by intraperitoneal (IP) injection of 80 mg/kg ketamine and 5 mg/kg xylazine diluted in PBS. Hair was removed from bilateral groins and hindlimbs and the left groin was prepped with chlorohexidine. A 1 cm incision was made in the left groin and the subcutaneous fat dissected laterally off the inguinal ligament. The femoral sheath was pierced with fine forceps and the femoral nerve gently dissected from the femoral vessels. After identifying the lateral circumflex femoral artery (LCFA), an electrocautery device was used to coagulate and transect both the femoral artery and vein just proximal to the LCFA. In similar fashion, the femoral vessels were divided more distally between the superficial caudal epigastric artery and the saphenopopliteal bifurcation, taking care not to injure the femoral nerve. After ensuring

hemostasis, the wound was closed with 5-0 absorbable suture. To further increase tissue oxidative stress, N_ω-Nitro-L-arginine methyl ester hydrochloride (L-NAME) (N5751, Sigma-Aldrich, St. Louis, MO), a competitive inhibitor of nitric oxide synthase, was dissolved in PBS and administered 2 h preoperatively and on postoperative days (POD) 1–3 *via* IP injection (40 mg/kg per injection).

Laser Doppler Perfusion Imaging

Hindlimb perfusion was assessed using a moorLDI laser Doppler perfusion imaging (LDPI) device running version 5 software (Moor Instruments, Wilmington, DE). Mice were anesthetized with inhaled isoflurane 1.5–2% and oxygen at 2 L/min and placed in prone position with the extremities taped in place on a black foam mat with a temperature-controlled heating pad. Perfusion index was calculated as the ratio of mean flux values from the left/ischemic relative to right/non-ischemic hindlimb.

Faber Hindlimb Ischemia Scoring

Footpad tissue loss was evaluated by Faber hindlimb ischemia scoring on POD 1–3, 7, 14, and 21. Faber scores range from 0 to 12 with 0 to 5 corresponding to the number of ischemic nails, 6–10 corresponding to 1–5 ischemic digits, and 11–12 reflecting partial or complete foot atrophy (24). Functionally, there is an important distinction between ischemia of nails compared to digits, so we defined severe gangrene as Faber score >5 and evaluated presence or absence of severe gangrene as a separate outcome.

Treadmill Exhaustion Testing

Mice ($N = 9$ per group) were trained to run on an Exer 3/6 treadmill (Columbus Instruments, Columbus, OH) during four separate sessions spanning over 2 weeks preoperatively. For training sessions, mice walked on the treadmill with a 10° incline at a speed of 10 m/min for 10 min and then 15 m/min for 5 min with shocks enabled at 1 Hz. After the training period, mice were randomly separated into two groups. For treadmill exhaustion testing, mice were placed on the treadmill and allowed to acclimate with the belt off and shocks on for 5 min. The treadmill was then started at a speed of 5 m/min at a 10° incline and speed was ramped up by 1 m/min^2. Distance recording started when speed reached 10 m/min, after which speed was further increased to 15 m/min after 5 min, and then incrementally increased by 3 m/min every 5 min thereafter until maximum speed of 30 m/min. Exhaustion was defined as 40 shocks, at which point shocks were disabled and total walking distance was recorded. Treadmill exhaustion testing was performed on POD 7, 10, 14, and 21.

DiI Perfusion and Confocal Laser Scanning Microscopy

To assess neovascularization in calf muscle, intracardiac perfusion of the lipophilic carbocyanine dye 1,1'-dioctadecyl-3,3,3',3'-tetramethylindocarbocyanine perchlorate (DiI) was performed on POD 22 ($N = 6$ per group). DiI solution (D282, Invitrogen/Thermo Fisher Scientific, Waltham, MA), diluent, and fixative were prepared, and the perfusion apparatus was assembled according to previously published protocols (25–27). After euthanasia by CO_2 overdose, the thoracic cavity was exposed, and the right atrial appendage incised while inserting the 25-gauge butterfly needle of the perfusion apparatus into the left ventricle. Sequentially, 4 mL of PBS, 10 mL of DiI, and 10 mL of 10% neutral-buffered formalin were injected after which the left and right calf muscles were harvested. Tissues were kept in fixative overnight before proceeding to imaging. To mount tissues, the entire calf muscle was sandwiched between two glass microscope slides and compressed using small binder clips. A Leica TCS SP5 (Leica Microsystems, Wetzlar, Germany) inverted confocal microscope was used to image tissues under 5X magnification. To control for technical errors during perfusion, we imaged bilateral gastrocnemius muscles and calculated the ratio of vessel density between left/ischemic and right/non-ischemic hindlimbs. Quantification of tissue vascularity was performed in Fiji (National Institutes of Health, Bethesda, MD).

Histological Examination

On POD 21, mice underwent euthanasia and intracardiac perfusion with 10% neutral-buffered formalin prior to harvesting the left and right adductor and calf muscles. Tissue samples were embedded in paraffin and sectioned. Slides were deparaffinized, hydrated, washed, and stained with hematoxylin (95057-844, VWR, Radnor, PA) and eosin (95057-848, VWR). Slides were imaged with a Leica DFC295 (Leica Microsystems) under 20X and 40X magnification. To measure myofiber cross-sectional area, 2 sections per animal ($N = 5$ per group) were imaged under 20X magnification with a Zeiss Axio Observer inverted microscope (ZEISS, Oberkochen, Germany). Four muscle fiber perimeters were traced per image and the cross-sectional area was calculated in ZEN software (version 3.3, ZEISS). Results are expressed both in terms of absolute myofiber cross-sectional area and relative to that of non-ischemic muscle.

Immunofluorescence Assays

Immunofluorescence studies were performed in calf muscle harvested on POD 21 to evaluate for expression of E-selectin and presence of EPCs and inflammatory cells. Slides were deparaffinized per standard protocol and antigen retrieval was performed in EDTA buffer (pH 9.0) at 120°C for 10 min. Slides were then washed in distilled water and permeabilized with 0.25% Triton-X100 TBS for 15 min. Tissue was incubated with Protein Block (ab64226, Abcam, Cambridge, United Kingdom) for 1 h. Slides were then incubated overnight at 4°C with conjugated primary antibodies, including E-selectin/CD62E Alexa Fluor 488 (5 μg/mL) (NB110-85473AF488, Novus Biologicals, Littleton, CO), CD31/PECAM-1 Alexa Fluor 647 (5 μg/mL) (NB600-1475AF647, Novus Biologicals), KDR/VEGFR-2 Alexa Fluor 647 (5 μg/mL) (NBP1-43300AF647, Novus Biologicals), CD34 AF488 (5 μg/mL) (SC-18917AF488, Santa Cruz Biotechnology, Dallas, TX) CD3 FITC (5 μg/mL) (11-0032-82, eBioscience/Thermo Fisher Scientific), and unconjugated Mac-2/Galectin-3 (5 μg/mL) (125401, BioLegend, San Diego, CA) followed by Alexa Fluor 594 goat anti-rat IgG (2 μg/mL) (A11007, Invitrogen). To confirm antibody specificity, isotype-matched negative controls were performed using rat IgG2a, kappa monoclonal antibody (ab18450, Abcam)

(5 μg/mL) with Alexa Fluor 594 goat anti-rat IgG (2 μg/mL) as secondary antibody (**Supplementary Figure 1**). Slides were imaged with an Axio Observer inverted microscope (ZEISS). For each stain, 4 images were acquired at 20X magnification from 4 sections per animal ($N = 5$ per group) and cell counting or quantification of mean fluorescence intensity was performed in Fiji.

RT-qPCR, PCR Arrays, and Bioinformatics Analysis

Thigh and calf muscles were harvested at specified time points postoperatively and total RNA was isolated after tissue homogenization in TRIzol reagent (15596018, Invitrogen/Thermo Fisher Scientific) according to manufacturer instructions. Total RNA was reverse transcribed using RT^2 First Strand Kit (Qiagen, Venlo, Netherlands). Real-time reverse transcription quantitative polymerase chain reaction (RT-qPCR) was performed using RT^2 SYBR Green qPCR Mastermix (330500, Qiagen) and primers for *E-sel* (*Sele*, NM_0113435, assay ID Mm.PT.58.11296882) and *Rplp0* (NM_007475, assay ID Mm.PT.58.43894205) as housekeeping gene (Integrated DNA Technologies, Coralville, IA). PCR arrays assessing 84 genes related to angiogenesis (RT^2 Profiler PCR Array Mouse Angiogenesis, GeneGlobe ID PAMM-024Z, Qiagen) and inflammation (RT^2 Profiler PCR Array Mouse Inflammatory Cytokines & Receptors, GeneGlobe ID PAMM-011Z, Qiagen) were performed according to manufacturer instructions using a Bio-Rad CFX96 Touch Real-Time PCR Detection System (Bio-Rad Laboratories, Hercules, CA). Data were analyzed using the ΔCt method ($2^{-\Delta\Delta Ct}$) method and RT-qPCR and PCR arrays were performed in duplicate using samples from 3 to 6 mice per group. For bioinformatics analysis, raw expression (Ct) values were normalized to housekeeping genes (*Actb, B2m, Gapdh, Gusb, Hsp90ab1*) using R Statistical Software (R Core Team 2021) "NormqPCR" (28). Then, -ΔCt values were analyzed for differential expression using R "limma" (29), and raw *P*-values based on empirical Bayes moderated *t*-statistics were adjusted for multiple testing with Benjamini & Hochberg false discovery rate correction (30).

Evaluation of Coagulation and Hematologic, Hepatic, and Renal Function

Intracardiac blood samples collected on POD 21 were sent for complete blood count and comprehensive metabolic panel. To evaluate for prothrombotic effect of E-selectin/AAV2/2, blood samples were collected on POD 7 in tubes containing 3.2% sodium bicarbonate in 9:1 ratio and centrifuged at 3,000 rpm for 10 min. The supernatant plasma was collected and used for enzyme-linked immunosorbent assay (ELISA) quantification of D-dimer levels per the kit protocol (LS-F6179-1, LifeSpan BioSciences, Seattle, WA) using a previously determined optimal sample dilution of 1:1,000.

Statistics

Statistical analyses were performed using GraphPad Prism (version 9.0.1, GraphPad Software, San Diego, CA). All continuous data were normally distributed according to Shapiro-Wilk test and compared using Student's *t*-test for two variables and ANOVA for greater than two variables. Categorical outcomes between two groups were compared using Chi-square test. Data are presented as mean ± standard error (SEM) and results with $P < 0.05$ considered statistically significant.

RESULTS

E-Sel/AAV2/2 Gene Therapy Provides High-Level and Durable Tissue Transgene Expression

To account for the lag time between AAV injection and tissue transgene expression, our protocol called for gene therapy administration 4 and 2 days preoperatively, and immediately prior to induction of hindlimb ischemia. A total of 1×10^{11} viral genome divided across 3 doses of either E-sel/AAV2/2 or LacZ/AAV2/2 serving as control was administered to 5 sites in the left thigh adductor and calf muscles. Expression of transgene, *E-selectin* mRNA (*E-sel*), in hindlimb tissues was measured by RT-qPCR. Relative to non-ischemic hindlimb, endogenous *E-sel* levels in untreated ischemic muscle at various time points after femoral artery and vein coagulation were 2.10 ± 1.97 on POD 7, 0.84 ± 1.08 on POD 14, 1.54 ± 1.40 on POD 21, and 1.09 ± 1.22 on POD 35 (**Figure 1A**). While there was a trend toward increased *E-sel* levels above baseline on POD 7, this result was not statistically significant ($P = 0.085$). Moreover, any endogenous elevation in tissue *E-sel* was transient with a rapid decline to baseline levels by POD 14 which persisted through POD 35.

On the other hand, quantification of *E-sel* levels by RT-qPCR in muscle harvested from ischemic limbs treated with E-sel/AAV2/2 revealed high-level *E-sel* transgene expression by POD 7 compared to endogenous *E-sel* levels (**Figure 1B**). Additionally, *E-sel* levels following treatment with AAV2/2 serotype further increased from POD 7 (17.86 ± 2.331) to POD 21 (21.66 ± 1.53) although this difference was not statistically significant ($P = 0.613$) (**Figure 1C**). We also found comparable transduction efficiency of *E-sel* transgene expression between AAV2/2 (17.86 ± 2.33) and AAV2/9 serotypes (26.35 ± 2.14) on POD 7 ($P = 0.299$) (**Figure 1D**). Immunofluorescence analysis (IFA) confirmed significantly greater E-sel expression as measured by mean fluorescence intensity (MFI) in muscle treated with E-sel/AAV2/2 compared to LacZ/AAV2/2 (1.031 ± 0.249 vs. 0.144 ± 0.025, $P = 0.008$; **Figures 1E,F**). Thus, both assays used to detect E-sel gene expression and protein levels demonstrated that intramuscularly administered E-sel/AAV2/2 provides high-level and durable tissue transgene expression in ischemic limb muscle. Additionally, on IFA, E-sel/AAV2/2 gene therapy was associated with increased capillary density as measured by CD31 MFI (1.884 ± 0.486 vs. 0.605 ± 0.144, $P = 0.036$) and an elevated E-selectin to CD31 MFI ratio (0.569 ± 0.121 vs. 0.229 ± 0.021, $P = 0.024$; **Figure 1E**), suggesting a pro-angiogenic effect of E-sel/AAV2/2 gene therapy that is consistent with further observations in this study.

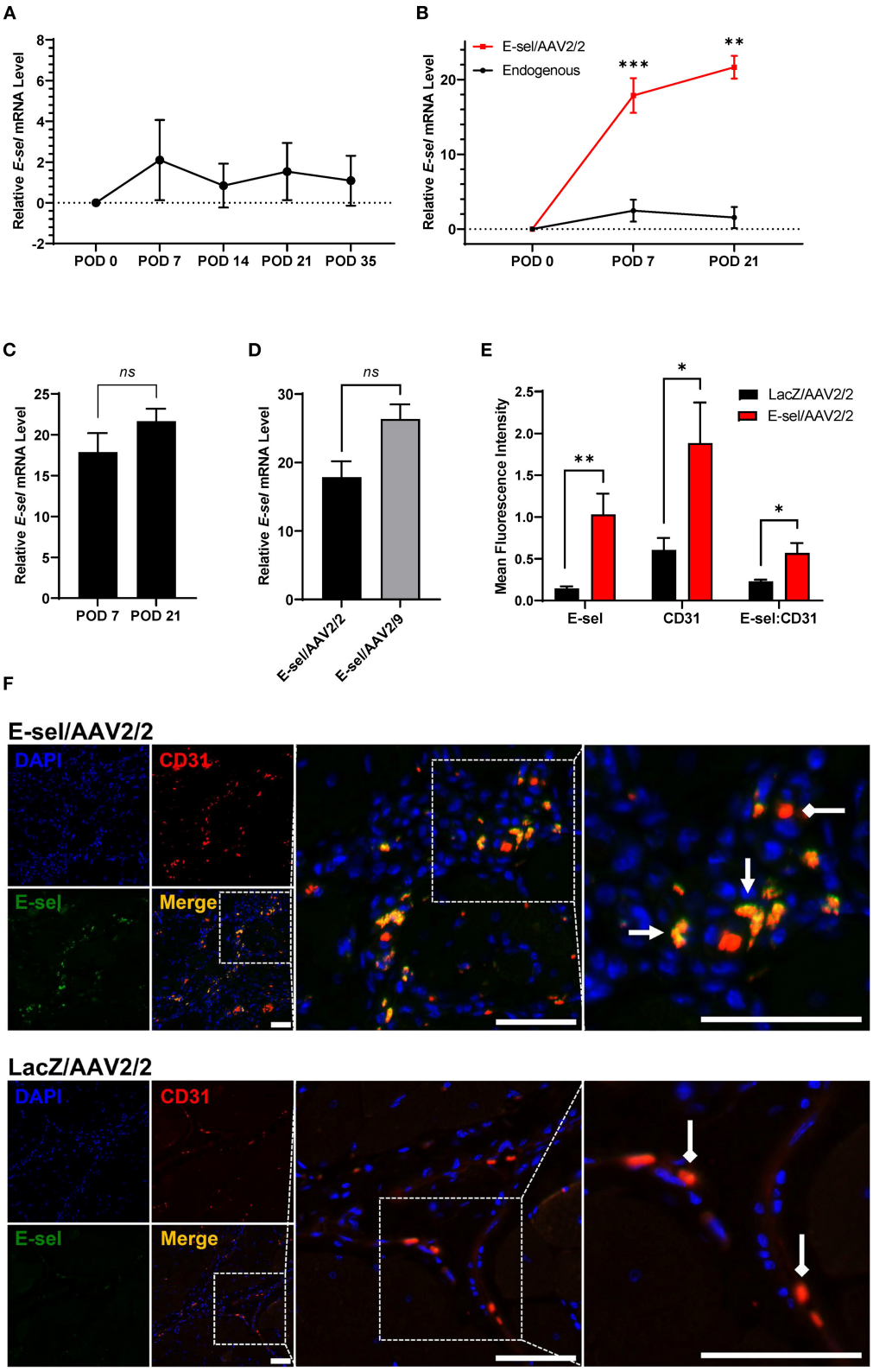

FIGURE 1 | High-level E-selectin expression by E-sel/AAV2/2 treatment in ischemic limb tissues. **(A)** Endogenous *E-sel* mRNA measured by RT-qPCR is transiently upregulated in untreated ischemic muscle normalized to untreated non-ischemic muscle. **(B)** Relative *E-sel* mRNA in E-sel/AAV2/2-treated ischemic muscle

(Continued)

FIGURE 1 | normalized to LacZ/AAV2/2-treated ischemic muscle (red) demonstrates high-level *E-sel* expression compared to endogenous levels in untreated ischemic muscle (black). **(C)** *E-sel* mRNA levels are stable from 1 to 3 weeks after treatment with E-sel/AAV2/2. **(D)** Comparison of *E-sel* mRNA expression by AAV2/2 and AAV2/9 vectors demonstrating no significant difference on POD 7. **(E)** Quantification and **(F)** representative images of immunofluorescence staining for CD31 (red) and E-selectin (green) showing enhanced colocalization (yellow) of these markers in muscle treated with E-sel/AAV2/2 (pointed arrowheads) compared to CD31 staining in absence of E-selectin positivity in muscle treated with LacZ/AAV2/2 (diamond arrowheads). Scale bars represent 50 μm. Data are presented as mean ± SEM where $^{*}P < 0.05$, $^{**}P < 0.01$, $^{***}P < 0.001$, and *ns*, not significant ($P > 0.05$).

E-Sel/AAV2/2 Gene Therapy Promotes Pro-angiogenic Response and Increases Footpad Reperfusion and Calf Muscle Vascularity

To measure the angiogenic effect of E-sel/AAV2/2 gene therapy, we quantified ischemic limb reperfusion on LDPI and visualized skeletal muscle vascularity by whole-body DiI perfusion and subsequent confocal microscopy of resected ischemic calf muscles. On LDPI, a significant improvement in footpad perfusion index, expressed as the ratio of blood flow of the ischemic relative to non-ischemic limb, was observed with E-sel/AAV2/2 therapy compared to LacZ/AAV2/2 control starting on POD 7 (0.213 ± 0.014 vs. 0.135 ± 0.016, $P < 0.001$) with a continued steady increase through the study endpoint on POD 21 (0.425 ± 0.024 vs. 0.222 ± 0.017, $P < 0.001$; **Figures 2A,B**). Because LDPI measurements primarily reflect blood flow *via* larger caliber arteries, we also examined small blood vessel and capillary density in the treated limb tissues by whole-body DiI perfusion and subsequent laser scanning confocal microscopy of resected calf muscles which allows for high-resolution, three-dimensional visualization of tissue vasculature (27). Imaging of ischemic gastrocnemius muscle after DiI perfusion on POD 22 showed that mean vessel density was significantly greater in mice treated with E-sel/AAV2/2 (0.579 ± 0.099) compared to LacZ/AAV2/2 controls (0.317 ± 0.054) ($P = 0.042$; **Figures 2C,D**), further providing evidence that E-sel/AAV2/2 gene therapy is pro-angiogenic and can increase footpad reperfusion and vessel density in treated ischemic limb tissues.

To further investigate the pro-angiogenic effect of E-sel/AAV2/2 gene therapy, we carried out an angiogenesis-focused PCR array analysis to quantitatively assess 84 genes comprising a panel of growth factors, cytokines, cell adhesion molecules, and transcription factors known to play a role in angiogenesis and arteriogenesis (RT^2 Profiler PCR Array Mouse Angiogenesis, GeneGlobe ID PAMM-024Z, Qiagen). Bioinformatic analysis was then performed using PCR array data to generate corresponding angiogenesis heatmaps (**Figure 2E**). The complete list of angiogenesis-related genes analyzed is available in **Supplementary Figure 2**. PCR array analysis demonstrated a robust angiogenic gene expression profile in ischemic muscle treated with E-sel/AAV2/2 compared to LacZ/AAV2/2 with upregulation of 14/84 genes (16.7%). Genes that were modulated more than two-fold are shown in **Table 1**. Taken together, these results demonstrated that E-sel/AAV2/2 gene therapy initiates a robust local angiogenic response with upregulation of diverse pro-angiogenesis genes.

E-Sel/AAV2/2 Gene Therapy Promotes Recruitment of EPCs to Ischemic Tissue

E-selectin has previously been demonstrated to be involved in recruitment of EPCs (15, 16). To further elucidate the mechanism underlying therapeutic angiogenesis induced by E-sel/AAV2/2 gene therapy in ischemic hindlimb, we therefore assessed recruitment of EPCs into E-sel/AAV2/2-treated vs. LacZ/AAV2/2-treated ischemic calf muscle using IFA. To identify EPCs in ischemic calf muscle, we stained for CD34 (hematopoietic cell marker carried by circulating stem/progenitor cells) and KDR (kinase insert domain receptor, also known as VEGFR-2 or vascular endothelial growth factor receptor 2, an endothelial cell marker; **Figure 3A**). In limb tissues harvested on POD 7, we found no significant difference in EPC numbers in muscle treated with E-sel/AAV2/2 compared to LacZ/AAV2/2 (14.0 ± 7.2 cells/mm^2 vs. 18.5 ± 6.7 cells/mm^2, $P = 0.670$). By POD 21, however, IFA demonstrated significantly more $CD34^+/KDR^+$ colocalization in ischemic tissue treated with E-sel/AAV2/2 compared to LacZ/AAV2/2 (63.9 ± 10.9 cells/mm^2 vs. 17.3 ± 2.2 cells/mm^2, $P = 0.003$), indicating enhanced EPC recruitment in the treatment group (**Figure 3B**). Globally, ischemic tissue from LacZ/AAV2/2-treated mice demonstrated sparse foci of EPC recruitment, whereas in E-sel/AAV2/2-treated limb muscle, there were consistently several large foci of EPC enrichment. We found no appreciable numbers of $CD34^+/KDR^+$ cells in non-ischemic limb muscle from either group. The data, hence, suggested that E-sel/AAV2/2-induced therapeutic angiogenesis is mediated, at least in part, by increasing recruitment of circulating EPCs to ischemic tissues where these cells can then participate in neovascularization.

E-Sel/AAV2/2 Gene Therapy Reduces Severity of Tissue Loss and Incidence of Severe Gangrene

To evaluate the therapeutic effect of E-sel/AAV2/2 gene therapy on severity of tissue loss, we monitored and recorded Faber scores at prespecified time points. The Faber hindlimb ischemia score is an established and popular grading scheme used to assess severity of tissue loss in hindlimb ischemia models (24). Examples of Faber scores 1–12 are shown in **Figure 4A**. A Faber score of 0 reflects a normal foot without any ischemic nails or digits. Mice treated with E-sel/AAV2/2 or LacZ/AAV2/2 were visually inspected on POD 1–3 and weekly through POD 21. Mean Faber scores were consistently lower for E-sel/AAV2/2-treated mice compared to LacZ/AAV2/2 controls starting on POD 7 (4.45 ± 0.53 vs. 6.35 ± 0.74, $P = 0.042$) and through POD 21 (3.84 ± 0.55 vs. 6.13 ± 0.71, $P = 0.014$; **Figures 4B,C**), indicating overall reduced tissue loss severity in the treatment group. Because

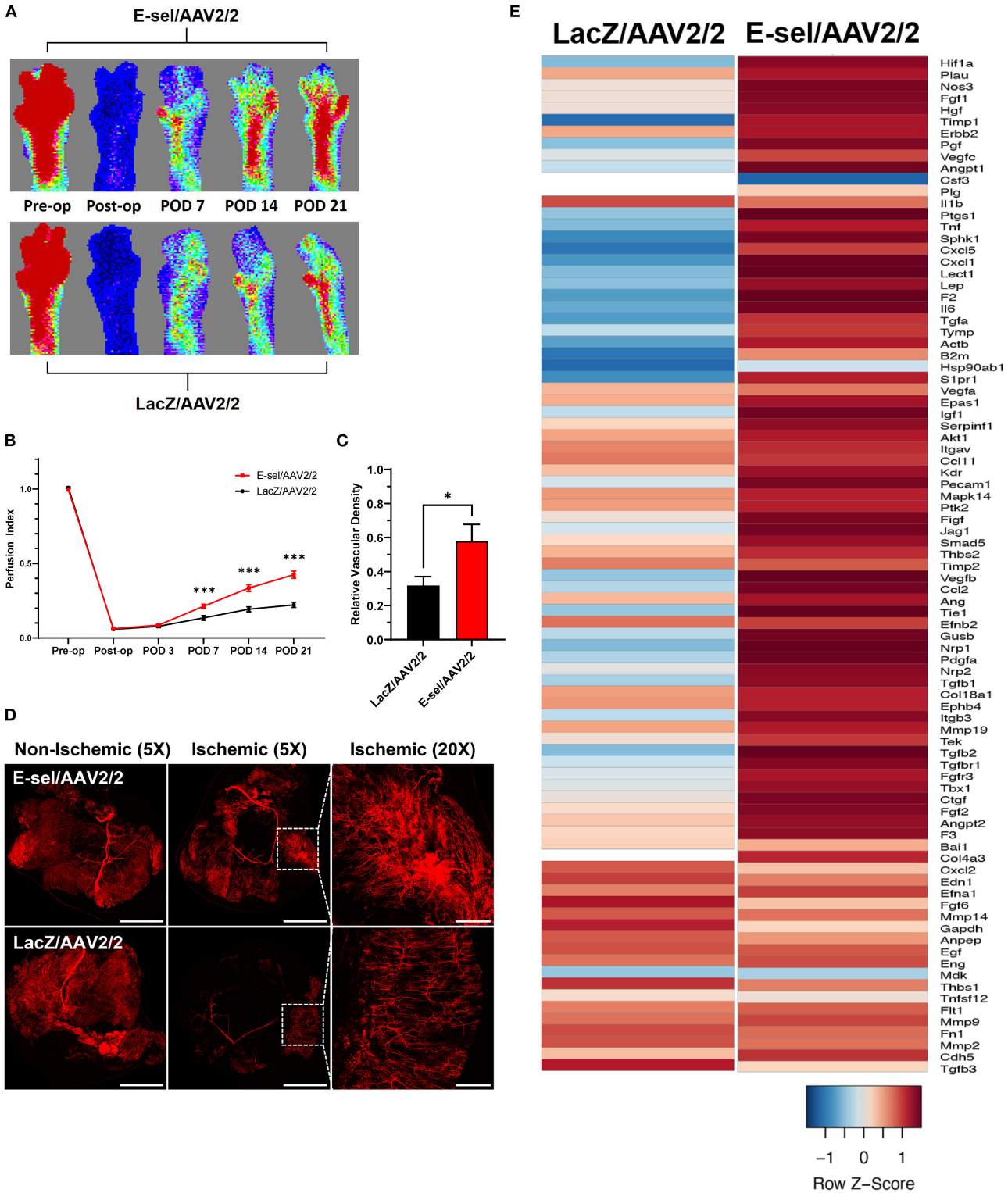

FIGURE 2 | Hindlimb reperfusion and angiogenesis gene profile is enhanced by E-sel/AAV2/2. **(A)** Representative laser Doppler perfusion images and **(B)** quantification of perfusion indices demonstrating improved recovery of footpad perfusion in mice treated with E-selectin/AAV2/ compared to LacZ/AAV2/2. **(C)** Quantification and **(D)** representative confocal microscopy images of calf muscle following whole-body perfusion with DiI to stain the peripheral vasculature on POD 22. Scale bars represent 5 and 1 mm for 5X and 20X images, respectively. **(E)** PCR array demonstrating upregulation of several angiogenesis genes in muscle treated with E-sel/AAV2/2 compared to LacZ/AAV2/2 control vector. Data are presented as mean ± SEM where $^{*}P < 0.05$ and $^{***}P < 0.001$.

TABLE 1 | Name and function of angiogenesis genes modulated by intramuscular E-selectin/AAV2/2 gene therapy.

Gene	Name	Fold-change in mRNA level	Function
Lep	Leptin	9.48 ± 0.65	Adipokine with anti-obesity effect involved in wound healing and angiogenesis (36, 37)
Il6	Interleukin 6	4.24 ± 0.39	Cytokine with acute pro-angiogenic and chronic anti-angiogenic properties (35, 36)
Tnf	Tumor necrosis factor	3.94 ± 0.93	Cytokine involved in inflammatory angiogenesis (46, 47)
Tymp	Thymidine phosphorylase	3.63 ± 0.73	PD-ECGF, improves perfusion in rabbit hindlimb ischemia model (38)
Tgfa	Transforming growth factor α	3.31 ± 0.97	Binds EGFR, involved in post-infarct angiogenesis in the brain (48)
S1pr1	Sphingosine-1-phosphate receptor 1	2.90 ± 0.82	Receptor for S1P, involved in pericyte and vascular smooth muscle cell recruitment (49–53)
Timp1	Tissue inhibitor of metalloproteinase 1	2.61 ± 0.06	Involved in remodeling of ECM by regulating MMP activity (54)
Pgf	Placental growth factor	2.49 ± 0.73	Improves perfusion and exercise tolerance in rabbit hindlimb ischemia model (39)
Sphk1	Sphingosine kinase 1	2.27 ± 0.20	Phosphorylates sphingosine to S1P, involved in ischemic preconditioning-induced cardioprotection (55)
Itgb3	Integrin β3	2.23 ± 0.87	Pro-angiogenic adhesion molecule involved in endothelial cell adhesion and migration (41)
Tbx1	T-box 1	2.19 ± 0.94	Transcription factor required for organization and differentiation of vascular networks (56, 57)
Ccl2	C-C motif chemokine ligand 2	2.14 ± 0.69	MCP-1, involved in monocyte recruitment and required for arteriogenesis (40)
Hif1a	Hypoxia-inducible factor 1α	2.09 ± 0.81	Primary hypoxia response element leading to VEGF gradient expression (58)
Fgfr3	Fibroblast growth factor receptor 3	2.06 ± 0.93	Receptor for FGF, involved in vascular development (59)

Data are presented as mean ± SD. PD-ECGF, platelet-derived endothelial cell growth factor; EGFR, epidermal growth factor receptor; S1P, sphingosine-1-phosphate; ECM, extracellular matrix; MMP, matrix metalloproteinase; MCP-1, monocyte chemoattractant protein 1; VEGF, vascular endothelial growth factor; FGF, fibroblast growth factor.

of the significant functional difference between ischemic nails (Faber score 1–5) and ischemic/necrotic digits (Faber score 6–12), we further categorized limb outcomes as mild and severe gangrene according to these cutoff values. By POD 21, incidence of severe gangrene, defined as Faber score greater than 5, was 29% (9/31) in the E-sel/AAV2/2 group compared to 61% (14/23) in the LacZ/AAV2/2 group ($P = 0.027$), corresponding to an absolute risk reduction of 31.8% and relative risk of 0.478 (95% confidence interval 0.248–0.889; **Figure 4D**). Overall, these data quantifying gross limb appearance showed that E-sel/AAV2/2 gene therapy reduces severity of limb tissue loss and incidence of severe gangrene, demonstrating its efficacy for limb salvage.

E-Sel/AAV2/2 Gene Therapy Preserves Histological Integrity and Improves Function of Ischemic Muscle

To test the effect of E-sel/AAV2/2 gene therapy on recovery of ischemic limb function, we conducted mouse treadmill exhaustion testing at prespecified postoperative time points. Preoperatively, mice were trained to run on a treadmill during 4 training sessions spread across 2 weeks. Trained mice were then randomly separated into two groups for E-sel/AAV2/2 and LacZ/AAV2/2 treatment, respectively. Following induction of hindlimb gangrene, both groups suffered significant reduction in exercise capacity. Walking/running distance on treadmill exhaustion testing then progressively improved for both groups but starting on POD 7 (231 ± 4 vs. 179 ± 17 m, $P = 0.001$) and through POD 21 (675 ± 58 vs. 532 ± 27 m, $P = 0.043$), performance was significantly better in the E-sel/AAV2/2-treated group compared to LacZ/AAV2/2-treated controls (**Figure 5D**). To address the pathophysiological basis of improved limb function, we performed histological analysis of calf skeletal muscle harvested on POD 21. On hematoxylin and eosin (H&E) staining, myocyte integrity was better preserved in the E-sel/AAV2/2-treated group compared to LacZ/AAV2/2-treated controls, as demonstrated by increased absolute myofiber size (1,872 ± 119 vs. 1,121 ± 75 μm, $P < 0.001$) and that relative to non-ischemic calf muscle (0.907 ± 0.029 vs. 0.637 ± 0.040, $P < 0.001$; **Figures 5A–C**). Myofiber size in non-ischemic muscle was not significantly different between groups (2,078 ± 162 vs. 1,772 ± 97 μm, $P = 0.145$; **Figure 5B**). Our data thus revealed that E-sel/AAV2/2 gene therapy improves functional recovery of ischemia-injured limbs and gangrenous footpads by reducing skeletal muscle atrophy.

Effects of E-Sel/AAV2/2 Gene Therapy on Inflammation, Coagulation, and Hematologic, Hepatic, and Renal Function

The above data indicate a pro-angiogenic role of E-selectin for therapeutic angiogenesis. Since E-selectin is also known to be involved in inflammation and thrombosis, we addressed

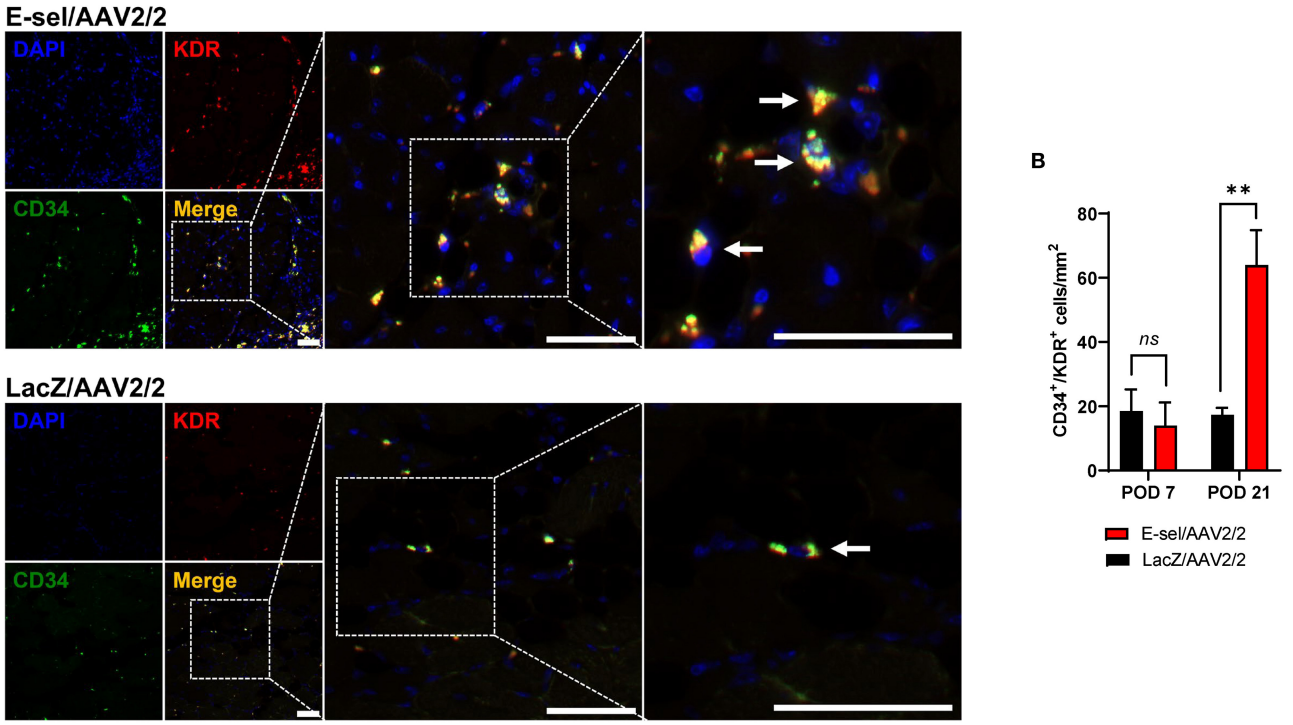

FIGURE 3 | Recruitment of endothelial progenitor cells (EPCs) to ischemic muscle is enhanced by E-sel/AAV2/2. **(A)** Representative immunofluorescence images demonstrating enhanced colocalization (yellow) of EPC markers CD34 (green) and KDR/VEGFR-2 (red) on POD 21 in muscle treated with E-sel/AAV2/2 compared to LacZ/AAV2/2. EPCs indicated by pointed arrowheads. Scale bars represent 50 μm. **(B)** Counting of cells co-staining for CD34 and KDR/VEGFR-2 revealed similar EPC numbers in the acute phase of ischemia (POD 7) but enhanced recruitment of EPCs by POD 21 in muscle treated with E-sel/AAV2/2 compared to LacZ/AAV2/2. Data are presented as mean ± SEM where $^{**}P < 0.01$ and *ns*, not significant ($P > 0.05$).

potential effects of intramuscularly administered E-sel/AAV2/2 gene therapy on inflammation and thrombosis as well as general toxicity in our mouse hindlimb gangrene model. To assess whether E-sel/AAV2/2 gene therapy induced a pro-inflammatory response in ischemic tissue, we conducted pathway-focused PCR array analysis to specifically test levels of 84 genes related to the inflammatory response. Total RNA samples extracted from ischemic limb tissue on POD 21 were subjected to RT-qPCR array analysis (RT^2 Profiler PCR Array Mouse Inflammatory Cytokines & Receptors, GeneGlobe ID PANZ-011Z, Qiagen). Although there was evidence of both upregulation of certain genes (21/84, 25%) and downregulation of others (27/84, 32%), there were overall more genes related with inflammation that were downregulated with E-sel/AAV2/2 therapy compared to LacZ/AAV2/2. As visualized by heatmap analysis (**Figure 6A**), these results indicated an overall "cooling" or dampening effect of E-sel/AAV2/2 gene therapy on tissue inflammatory gene profile. The complete list of analyzed genes related to inflammation is available in **Supplementary Figure 3**. Using IFA, inflammation was further assessed by counting the number of T cells ($CD3^+$) and macrophages (Mac-2/Galectin-3^+) infiltrated in treated ischemic limb tissues. In both E-sel/AAV2/2-treated and LacZ/AAV2/2-treated ischemic limb muscle, $CD3^+$ cells were sparse (23 ± 4 vs. 27 ± 1 cells/mm^2, $P = 0.403$; **Figures 6B,D**). Moreover, the number of Mac-2^+ macrophages was similar between E-sel/AAV2/2-treated and LacZ/AAV2/2-treated muscle (41 ± 17 vs. 38 ± 14 cells/mm^2, $P = 0.877$; **Figures 6C,E**), indicating that E-sel/AAV2/2 gene therapy did not exert a pro-inflammatory effect on POD 21.

Routine blood tests were performed to assess hematologic, hepatic, and renal function. Blood sampling on POD 21 revealed no differences in hematologic, hepatic, or renal function panels between mice treated with E-sel/AAV2/2, LacZ/AAV2/2, or PBS (**Table 2**), indicating that locally administered E-sel/AAV2/2 gene therapy does not appear to cause systemic toxicity. To test potential effect of E-sel/AAV2/2 gene therapy on thrombosis, we quantified serum D-dimer levels on POD 7. ELISA revealed that D-dimer was elevated above normal levels (250 ng/mL) in E-sel/AAV2/2-treated mice, but also LacZ/AAV2/2 and PBS controls. However, there was no significant difference in D-dimer levels between E-sel/AAV2/2-treated mice and those that received LacZ/AAV2/2 or PBS vehicle (**Table 2**). Thus, increased D-dimer levels may be related to recent surgical procedure or intramuscular injection but were not uniquely attributable to E-sel/AAV2/2 gene therapy. Collectively, our data showed that locally administered E-sel/AAV2/2 gene therapy alters

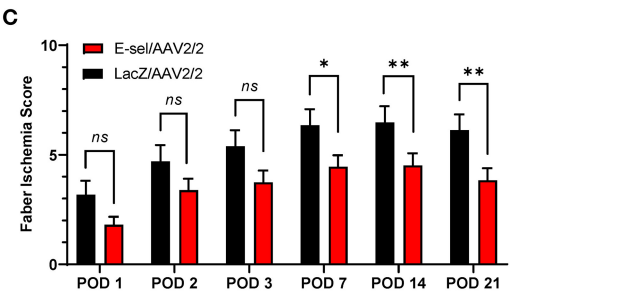

D

Gene Therapy	Mild or no gangrene	Severe gangrene
E-sel/AAV/2/2	22/31 (71%)	9/31 (29%)
LacZ/AAV2/2	9/23 (39%)	14/23 (61%)

$P = .027$

FIGURE 4 | Limb tissue loss and incidence of severe gangrene is reduced by E-sel/AAV2/2 gene therapy. **(A)** Representative photos illustrating range of

(Continued)

FIGURE 4 | Faber ischemia scores 1–12. **(B)** Representative images of footpads obtained on POD 14 in mice treated with E-sel/AAV2/2 and LacZ/AAV2/2. **(C)** Mean Faber ischemia scores up to POD 21 after induction of hindlimb ischemia are significantly lower in mice treated with E-sel/AAV2/2 compared to LacZ/AAV2/2. **(D)** Proportion of mice with severe gangrene (Faber score >5) on POD 14. Data are presented as mean ± SEM where $*P < 0.05$, $**P < 0.01$, and *ns*, not significant ($P > 0.05$).

the inflammatory gene profile of ischemic muscle but does not induce T cell or macrophage infiltration, thrombosis, or systemic toxicity.

DISCUSSION

Our prior work on E-selectin vascular regenerative approaches indicated a beneficial effect on murine limb revascularization. In this study, we demonstrate for the first time that *in vivo* direct E-sel/AAV2/2 gene therapy results in dramatic changes of the tissue angiogenesis and inflammatory gene profiles. These major findings are associated with more effective recruitment of EPCs to the compromised ischemic limb. In addition, the phenotype of the treated animals indicates significantly improved recovery in laser Doppler perfusion and capillary density with associated reduction in tissue loss. The absolute risk reduction provided by E-sel/AAV2/2 gene therapy regarding development of severe gangrene, which we defined as digital or foot necrosis (Faber score >5), was 32%. This effect size suggests a number needed to treat on the order of 3–4. While these results are not directly translatable to human subjects, the observed reduction in mean tissue loss severity and overall incidence of severe gangrene in this study demonstrates promise for local E-selectin-based gene therapy as a potential treatment for limb-threatening ischemia.

PAD/CLTI is a chronic disease in which buildup of atherosclerotic plaque typically occurs over many years. This gradual occlusive process allows for adaptation of skeletal muscle to tissue hypoxia, and how well individuals can compensate explains some of the variability in symptoms experienced by patients with PAD/CLTI. In this chronic setting, limb tissue may become more tolerant to tissue hypoxia and respond differently than it does to an acute ischemic insult. While our findings corroborate prior studies indicating that E-selectin is acutely upregulated following induction of ischemia, expression of E-selectin in chronically ischemic tissue is not well-characterized. Like others, we found that endogenous E-selectin levels rapidly return to baseline within 7 days and remain at this level afterwards (31). Such a transient and modest elevation of E-selectin is an acute response to tissue ischemia and likely insufficient to initiate or support an adequate angiogenic response essential for rescuing and repairing chronically ischemia-injured tissue. Therefore, increasing tissue levels of E-selectin and prolonging its expression, particularly in the vasculature, can aid in mounting a therapeutic angiogenic response.

The present construct, E-sel/AAV2/2, achieved stable transgene expression 20-fold higher than LacZ/AAV2/2 control

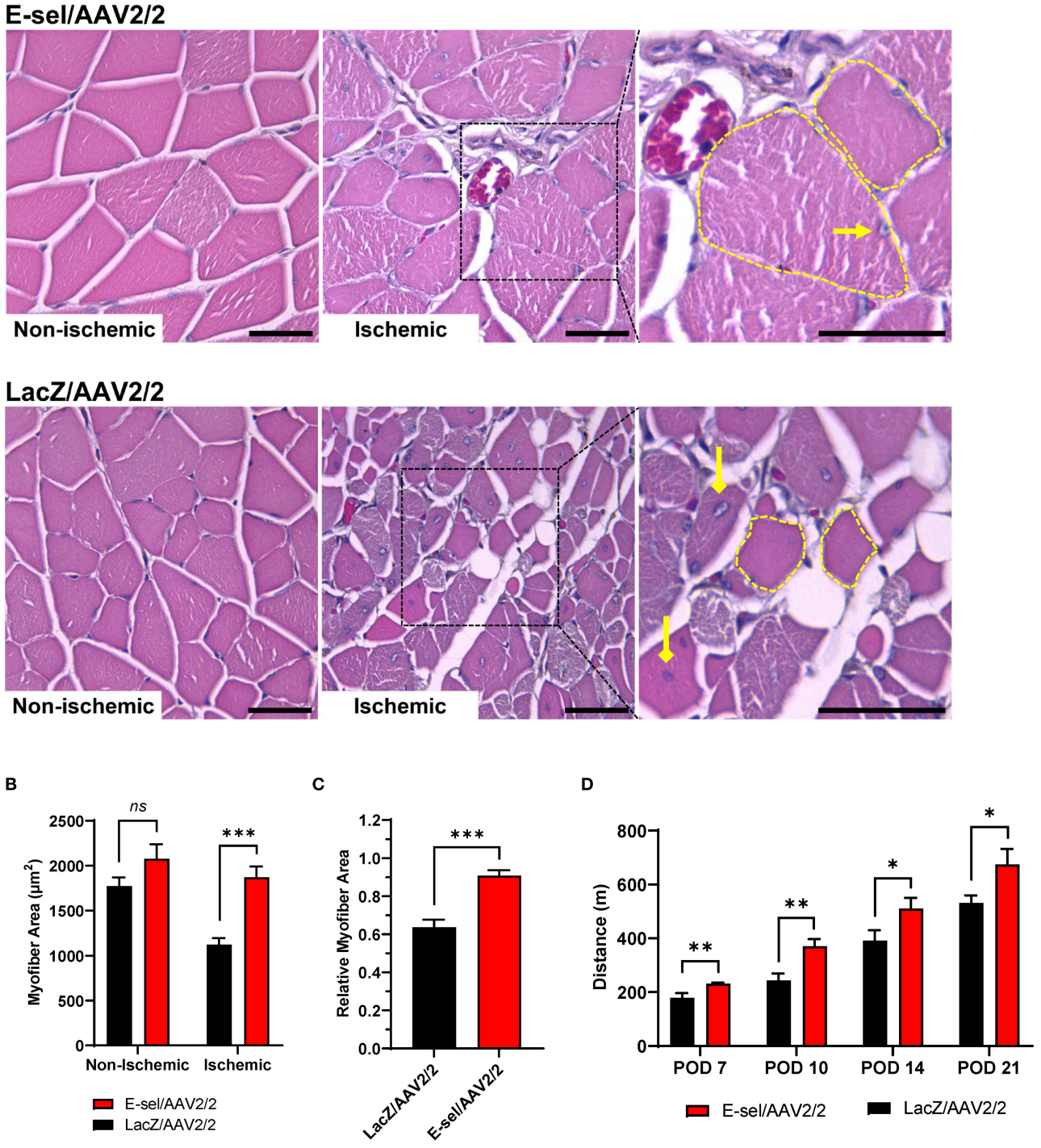

FIGURE 5 | E-sel/AAV2/2 gene therapy is associated with preserved myofiber integrity and improved functional recovery in ischemic hindlimb. **(A)** Representative H&E sections demonstrating better-preserved muscle integrity with larger myofiber size (dashed yellow line) and peripherally located nuclei (pointed arrowhead) in E-sel/AAV2/2-treated muscle compared to shrunken (dashed yellow line), eosinophilic necrotic fibers and centrally located nuclei (diamond arrowheads) observed in muscle treated with LacZ/AAV2/2. Scale bars represent 25 μm. **(B)** Measurement of myofiber cross-sectional area demonstrating reduced myofiber size in LacZ/AAV2/2-treated compared to E-sel/AAV2/2-treated ischemic muscle. Non-ischemic myofiber size is comparable across groups. **(C)** Relative myofiber size in ischemic muscle compared to non-ischemic muscle is significantly larger after treatment with E-sel/AAV2/2 compared to LacZ/AAV2/2. **(D)** Mean distance walked on treadmill exhaustion testing at various timepoints postoperatively. Data are presented as mean ± SEM where $^{*}P < 0.05$, $^{**}P < 0.01$, $^{***}P < 0.001$, and *ns*, not significant ($P > 0.05$).

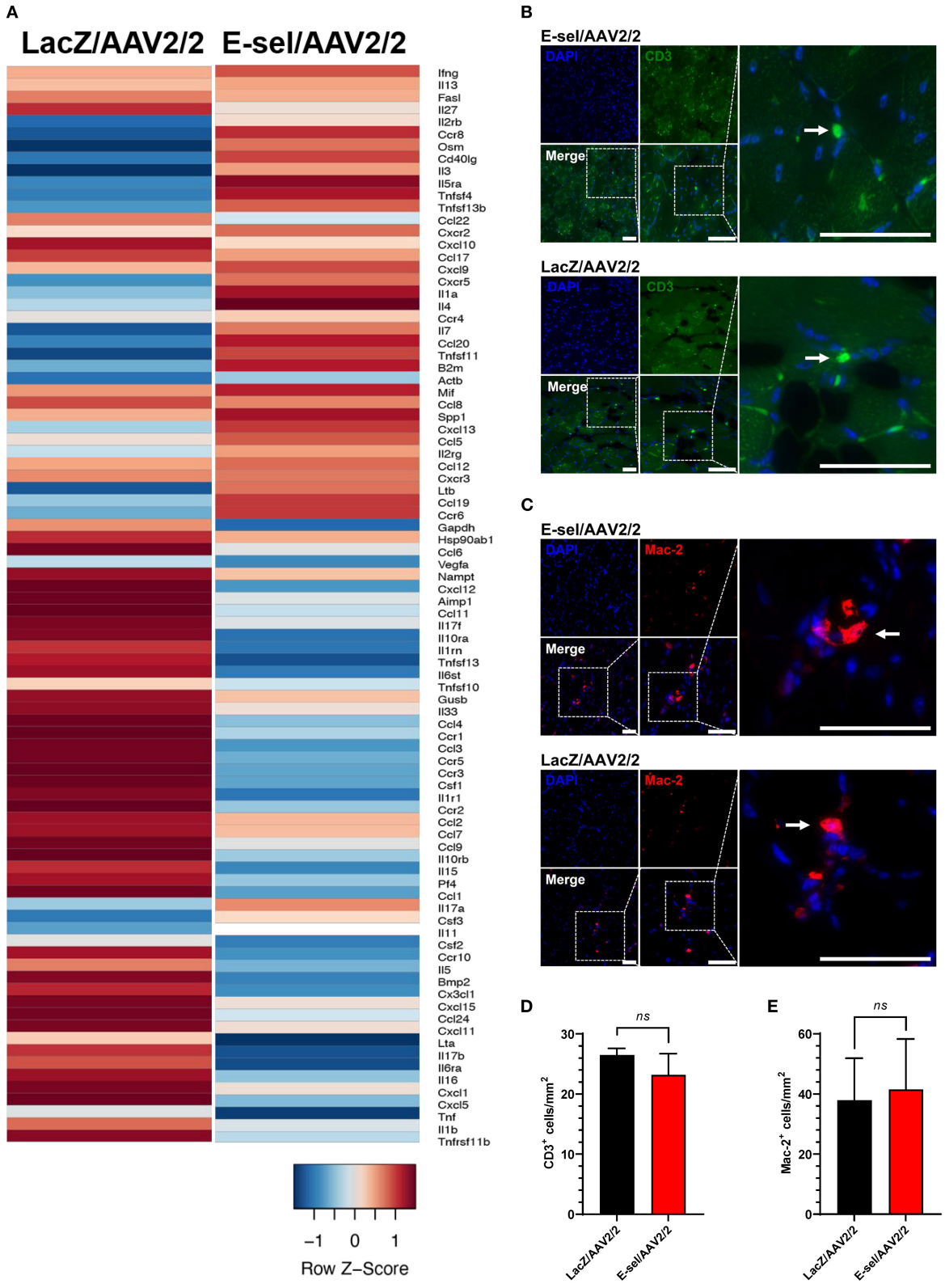

FIGURE 6 | E-sel/AAV2/2 modulates inflammatory gene profile in ischemic muscle without inducing significant inflammatory cell recruitment. **(A)** PCR array from muscle harvested on POD 21 demonstrating an overall downregulation of inflammatory genes by E-sel/AAV2/2 gene therapy. **(B)** Representative immunofluorescence images of ischemic muscle stained for CD3, a marker of T cells (pointed arrowheads), and **(C)** Mac-2/Galectin-3, a marker of macrophages (pointed arrowheads). **(D)** Counting of $CD3^+$ and **(E)** Mac-2^+ cells demonstrating no significant difference in T cell or macrophage recruitment to ischemic muscle treated with E-sel/AAV2/2 and LacZ/AAV2/2. Scale bars represent 50 μm. Data are presented as mean ± SEM and *ns*, not significant ($P > 0.05$).

TABLE 2 | Serum D-dimer levels on POD 7 and complete blood count and liver and renal function tests obtained on POD 21 in mice treated with E-sel/AAV2/2, LacZ/AAV2/2, and PBS.

Test	E-sel/AAV2/2	LacZ/AAV2/2	PBS	Normal range	*P*
D-dimer (ng/mL)	587 ± 97	476 ± 61	635 ± 101	<250	*ns*
Hematocrit (%)	51.0 ± 3.6	51.5 ± 3.3	49.2 ± 1.0	34–50	*ns*
Hgb (g/dL)	12.0 ± 0.7	11.9 ± 0.5	11.3 ± 0.2	12.8–16.1	*ns*
WBC (x$10^3/\mu L$)	3.5 ± 1.6	2.1 ± 0.7	3.5 ± 4.6	4.5–9.1	*ns*
Platelets (x$10^3/\mu L$)	939 ± 64	989 ± 56	1,009 ± 267	100–250	*ns*
BUN (mg/dL)	20 ± 4	16 ± 1	21 ± 3	18–29	*ns*
Creatinine (mg/dL)	0.1 ± 0.1	0.1 ± 0	0.1 ± 0	0.1–0.4	*ns*
CPK (U/L)	37 ± 6	32 ± 5	50 ± 9	50–114	*ns*
Protein, total (g/dL)	5.1 ± 0.4	5.3 ± 0.6	4.8 ± 0.2	4.6–6.9	*ns*
Albumin (g/dL)	2.5 ± 0.3	2.5 ± 0.3	2.4 ± 0.2	2.5–4.8	*ns*
Bilirubin, total (mg/dL)	0.3 ± 0.2	0.3 ± 0.2	0.5 ± 0.2	0.1–0.9	*ns*
AST (U/L)	64 ± 17	75 ± 18	58 ± 3	50–270	*ns*
ALT (U/L)	39 ± 1	34 ± 7	34 ± 2	29–77	*ns*
ALP (U/L)	94 ± 7	96 ± 9	78 ± 7	51–285	*ns*

PBS, phosphate-buffered saline; Hgb, hemoglobin; WBC, white blood cell count; BUN, blood urea nitrogen; CPK, creatine phosphokinase; AST, aspartate transaminase; ALT, alanine transaminase; ALP, alkaline phosphatase. Data are presented as mean ± SD where ns, not significant (P > 0.05).

vector up to 3 weeks after therapy. IFA then confirmed endothelial expression of E-selectin and increased capillary density, as measured by CD31 positivity, in ischemic muscle treated with E-sel/AAV2/2. The primary mechanism by which we hypothesize E-selectin overexpression promotes angiogenesis is through recruitment of EPCs and perhaps other tissue repair cells to areas of ischemia and wound healing. In humans, EPCs were first characterized as $CD34^+/KDR^+$ cells but are now known to comprise a diverse population of cells expressing a variety of cell surface markers as they differentiate into mature endothelial cells (32–34). Homing of EPCs to areas of wound healing is mediated by SDF-1α-induced E-selectin/E-selectin ligand interactions on activated endothelium and circulating EPCs, respectively (15, 16). By increasing levels of vascular E-selectin in the ischemic tissue microenvironment, E-sel/AAV2/2 may help to potentiate and prolong the innate response to ischemia, thereby increasing post-natal vasculogenesis with subsequent benefit on skeletal muscle vascularity. Consistently, treatment with E-sel/AAV2/2 was associated with histological preservation of myofiber size and integrity which translated to improved exercise capacity on treadmill exhaustion testing.

While our findings demonstrated significantly enhanced EPC recruitment with E-sel/AAV2/2, there may be other mechanisms mediating the pro-angiogenic effects of E-selectin. Beyond homing of EPCs to areas of ischemia, our PCR array data show that local E-selectin overexpression induces a robust angiogenic response with upregulation of several growth factors, cytokines, cell adhesion molecules, and transcription factors. Of these, leptin (*Lep*) was the most significantly upregulated gene in ischemic muscle treated with E-sel/AAV2/2. Leptin is an adipokine that acts systemically as a satiety signal but has also been implicated in wound healing (35) and post-natal angiogenesis (36). Under physiological conditions, adipocytes in perivascular adipose tissue help to regulate vascular tone by releasing vasoactive molecules, including leptin, and these vasodilatory mechanisms may be impaired due to leptin-resistance associated with obesity (37). Additionally, perivascular cells expressing platelet-derived growth factor receptor α (PDGFRα) and PDGFRβ within skeletal muscle are leptin-producing and have been shown to induce production of VEGF-A by skeletal muscle cells (36). Other notable factors upregulated by E-sel/AAV2/2 included thymidine phosphorylase (platelet-derived endothelial cell growth factor, PD-ECGF) and placental growth factor (PGF) which have been shown to improve perfusion and exercise tolerance in rabbit hindlimb ischemia models (38, 39), as well as monocyte chemoattractant protein 1 (MCP-1) and integrin β3, which are critical for monocyte recruitment and arteriogenesis (40) and endothelial cell adhesion, migration, and endothelial tube formation, respectively (41). Future studies, including validation of angiogenic factor protein levels, are needed to better elucidate the mechanisms underlying therapeutic angiogenesis induced by E-sel/AAV2/2 gene therapy. Moreover, the beneficial effects observed on skeletal muscle histology and function warrant more detailed investigations into the effects of E-selectin on myocyte regeneration and mitochondrial metabolism.

Our preliminary safety data did not demonstrate a difference between mice treated with E-sel/AAV2/2, LacZ/AAV2/2 control vector, or PBS vehicle with regards to hematologic, hepatic, or renal function panels. However, D-dimer levels were elevated on POD 7 in E-selectin/AAV2/2-treated, as well as LacZ/AAV2/2 and PBS controls. These results likely indicate that neither E-selectin nor AAV2/2 vector alone was responsible for this effect. As we did not observe any evidence of microvascular thrombosis on histological examination, the supranormal D-dimer levels likely reflect recent surgical intervention. Of note, coagulation of the femoral vein in conjunction with the femoral artery was performed due to ease of the operation and may be

clinically relevant as chronic venous insufficiency is a common comorbidity in patients with PAD (42). Regarding inflammation, PCR array demonstrated that E-sel/AAV2/2 modulated the inflammatory gene profile of ischemic limb tissue with an overall dampening or "cooling" effect on heatmap analysis. Although Mac-2^+ macrophage infiltration was similar between E-sel/AAV2/2-treated and control tissue, the observed alteration in inflammatory cytokine and receptor gene expression may reflect improvement in the degree of ischemia in the tissue microenvironment, as well as direct downstream effects of E-selectin signaling and indirect paracrine actions of recruited cells. To account for the lag time between injection and transgene expression, our protocol called for administration of gene therapy at 4 and 2 days preoperatively, as well as on day of surgery. It should be noted that even with 3 separate administrations of gene therapy, these all occurred within a 4-day interval. In this short period, the immune system likely recognizes a single antigenic stimulus and does not have sufficient time to mount an antibody response. To this end, we found minimal recruitment of $CD3^+$ T cells in either E-sel/AAV2/2-treated or LacZ/AAV2/2-treated ischemic muscle, indicating that neither E-selectin nor AAV2/2 vector induces a significant viral lymphocytic response, which is consistent with the well-documented low immunogenicity of AAV vectors (17).

The primary limitation of this study is the acuity of arterial disruption and subsequent ischemic injury. In our model, gangrene is induced in FVB mice by femoral artery and vein coagulation with additional administration of a nitric oxide synthase inhibitor to inhibit the endogenous vasodilatory response and increase tissue oxidative stress. Peak severity of tissue loss generally appears within 7–14 days with greatest therapeutic effect observed between 14 and 21 days. To develop a more chronic model of limb ischemia, other groups have used ameroid constrictors to gradually occlude the femoral artery (43, 44). With this technique, ischemia is less severe and associated with reduced inflammation and muscle necrosis compared to acute femoral artery ligation. However, the timing of ischemia onset in this model can be variable. Peak ischemia severity is reached within 14 days but may occur as soon as 3 days postoperatively with necrotic changes observed in BALB/c mice within 5 days (44). Perhaps more reflective of subacute ischemia, adapting this approach to FVB mice, which have intermediate sensitivity to ischemia, could prolong the duration of ischemia compared to C57BL/6 mice while improving the therapeutic window relative to BALB/c mice.

Importantly, our model does not account for comorbid smoking, hypertension, hyperlipidemia, or diabetes, which are common cardiovascular risk factors that also contribute to limb outcomes in PAD/CLTI. We also could not ascertain an independent effect of exercise therapy which is an essential component of management for PAD. In clinical practice, we envision using scoring systems such as the Wound, Ischemia, and foot Infection (WIfI) score (45), which incorporates tissue loss severity, hemodynamic parameters, and presence of infection, along with individual patient-specific factors such as disease etiology (i.e., diabetes, Buerger's disease) and vascular anatomy on angiography, to identify patients at risk of amputation who have exhausted traditional revascularization options and may benefit from angiogenic gene therapy.

While risk factor modification and revascularization remain central to treatment of PAD and CLTI, there is an unmet need for angiogenic therapies in patients with limited surgical revascularization options. Herein, we demonstrate the potential of E-sel/AAV2/2 gene therapy for reducing severity of tissue loss and improving perfusion and function of ischemic limbs. This preclinical study paves the way for studies in larger animal models and clinical trials in patients with inoperable CLTI.

DATA AVAILABILITY STATEMENT

The datasets presented in this study can be found in online repositories. The names of the repository/repositories and accession number(s) can be found below: https://www.ncbi.nlm.nih.gov/geo/, GSE201501.

ETHICS STATEMENT

The animal study was reviewed and approved by the University of Miami Institutional Animal Care and Use Committee under protocol 19-163.

AUTHOR CONTRIBUTIONS

AR: study design, investigation, data analysis, and manuscript writing. YO: investigation, data analysis, and critical review. YL, CH, NL, and HS: investigation and critical review. RV-P: conceptualization and methodology. Z-JL and OV: conceptualization, methodology, manuscript editing, supervision, critical review, and funding acquisition. All authors contributed to the manuscript and approved the submitted version.

FUNDING

This work was supported by grants from the National Institutes of Health [R01DK071084, R01GM081570, and VITA (NHLBI-CSB-HV-2017-01-JS)].

ACKNOWLEDGMENTS

We thank the University of Miami Diabetes Research Institute Analytical Imaging Core Facility for assistance with confocal microscopy and the Biostatistics and Bioinformatics Shared Resource of the Sylvester Comprehensive Cancer Center at the University of Miami for bioinformatics analysis of PCR array data.

SUPPLEMENTARY MATERIAL

The Supplementary Material for this article can be found online at: https://www.frontiersin.org/articles/10.3389/fcvm.2022.929466/full#supplementary-material

REFERENCES

1. Fereydooni A, Gorecka J, Dardik A. Using the epidemiology of critical limb ischemia to estimate the number of patients amenable to endovascular therapy. *Vasc Med.* (2020) 25:78–87. doi: 10.1177/1358863X19878271
2. Conte MS, Bradbury AW, Kolh P, White J V., Dick F, Fitridge R, et al. Global vascular guidelines on the management of chronic limb-threatening ischemia. *J Vasc Surg.* (2019) 69:3S—125S. doi: 10.1016/j.jvs.2019.02.016
3. Farber A, Eberhardt RT. The current state of critical limb ischemia: a systematic review. *JAMA Surg.* (2016) 151:1070–7. doi: 10.1001/jamasurg.2016.2018
4. Baumgartner I, Pieczek A, Manor O, Blair R, Kearney M, Walsh K, et al. Constitutive expression of phVEGF165 after intramuscular gene transfer promotes collateral vessel development in patients with critical limb ischemia. *Circulation.* (1998) 97:1114–23. doi: 10.1161/01.CIR.97.12.1114
5. Isner JM, Baumgartner I, Rauh G, Schainfeld R, Blair R, Manor O, et al. Treatment of thromboangiitis obliterans (Buerger's disease) by intramuscular gene transfer of vascular endothelial growth factor: preliminary clinical results. *J Vasc Surg.* (1998) 28:964–75. doi: 10.1016/S0741-5214(98)70022-9
6. Kusumanto YH, Van Weel V, Mulder NH, Smit AJ, Van Den Dungen JJAM, Hooymans JMM, et al. Treatment with intramuscular vascular endothelial growth factor gene compared with placebo for patients with diabetes mellitus and critical limb ischemia: a double-blind randomized trial. *Hum Gene Ther.* (2006) 17:683–91. doi: 10.1089/hum.2006.17.683
7. Powell RJ, Goodney P, Mendelsohn FO, Moen EK, Annex BH. Safety and efficacy of patient specific intramuscular injection of HGF plasmid gene therapy on limb perfusion and wound healing in patients with ischemic lower extremity ulceration: results of the HGF-0205 trial. *J Vasc Surg.* (2010) 52:1525–30. doi: 10.1016/j.jvs.2010.07.044
8. Morishita R, Shimamura M, Takeya Y, Nakagami H, Chujo M, Ishihama T, et al. Combined analysis of clinical data on HGF gene therapy to treat critical limb ischemia in Japan. *Curr Gene Ther.* (2020) 20:25–35. doi: 10.2174/1566523220666200516171447
9. Comerota AJ, Throm RC, Miller KA, Henry T, Chronos N, Laird J, et al. Naked plasmid DNA encoding fibroblast growth factor type 1 for the treatment of end-stage unreconstructible lower extremity ischemia: preliminary results of a phase I trial. *J Vasc Surg.* (2002) 35:930–6. doi: 10.1067/mva.2002.123677
10. Belch J, Hiatt WR, Baumgartner I, Driver IV, Nikol S, Norgren L, et al. Effect of fibroblast growth factor NV1FGF on amputation and death: a randomised placebo-controlled trial of gene therapy in critical limb ischaemia. *Lancet.* (2011) 377:1929–37. doi: 10.1016/S0140-6736(11)60394-2
11. Nikol S, Baumgartner I, Van Belle E, Diehm C, Visoná A, Capogrossi MC, et al. Therapeutic angiogenesis with intramuscular NV1FGF improves amputation-free survival in patients with critical limb ischemia. *Mol Ther.* (2008) 16:972–8. doi: 10.1038/mt.2008.33
12. Forster R, Liew A, Bhattacharya V, Shaw J, Stansby G. Gene therapy for peripheral arterial disease. *Cochrane Database Syst Rev.* (2018) 10:CD012058. doi: 10.1002/14651858.CD012058
13. Parikh PP, Lassance-Soares RM, Shao H, Regueiro MM, Li Y, Liu ZJ, et al. Intramuscular E-selectin/adeno-associated virus gene therapy promotes wound healing in an ischemic mouse model. *J Surg Res.* (2018) 228:68–76. doi: 10.1016/j.jss.2018.02.061
14. Quiroz HJ, Parikh PP, Lassance-Soares RM, Regueiro MM, Li Y, Shao H, et al. Gangrene, revascularization, and limb function improved with E-selectin/adeno-associated virus gene therapy. *J Vasc Sci.* (2021) 2:20–32. doi: 10.1016/j.jvssci.2020.10.001
15. Liu ZJ, Tian R, An W, Zhuge Y, Li Y, Shao H, et al. Identification of E-selectin as a novel target for the regulation of post-natal neovascularization: implications for diabetic wound healing. *Ann Surg.* (2010) 252:625–34. doi: 10.1097/SLA.0b013e3181f5a079
16. Liu ZJ, Tian R, Li Y, Zhang L, Shao H, Yang C, et al. SDF-1α-induced dual pairs of E-selectin/ligand mediate endothelial progenitor cell homing to critical ischemia. *Sci Rep.* (2016) 6:1–11. doi: 10.1038/srep34416
17. Nayak S, Herzog RW. Progress and prospects: immune responses to viral vectors. *Gene Ther.* (2010) 17:295–304. doi: 10.1038/gt.2009.148
18. Wu Z, Asokan A, Samulski RJ. Adeno-associated virus serotypes: vector toolkit for human gene therapy. *Mol Ther.* (2006) 14:316–27. doi: 10.1016/j.ymthe.2006.05.009
19. Parikh PP, Castilla D, Lassance-Soares RM, Shao H, Regueiro M, Li Y, et al. A reliable mouse model of hind limb gangrene. *Ann Vasc Surg.* (2018) 48:222–32. doi: 10.1016/j.avsg.2017.10.008
20. Gao G, Vandenberghe LH, Alvira MR, Lu Y, Calcedo R, Zhou X, et al. Clades of adeno-associated viruses are widely disseminated in human tissues. *J Virol.* (2004) 78:6381–8. doi: 10.1128/JVI.78.12.6381-6388.2004
21. Manno CS, Chew AJ, Hutchison S, Larson PJ, Herzog RW, Arruda VR, et al. AAV-mediated factor IX gene transfer to skeletal muscle in patients with severe hemophilia B. *Blood.* (2003) 101:2963–72. doi: 10.1182/blood-2002-10-3296
22. Brantly ML, Spencer LT, Humphries M, Conlon TJ, Spencer CT, Poirier A, et al. Phase I trial of intramuscular injection of a recombinant adeno-associated virus serotype 2 α1-antitrypsin (AAT) vector in AAT-deficient adults. *Hum Gene Ther.* (2006) 17:1177–86. doi: 10.1089/hum.2006.17.1177
23. Clément N, Grieger JC. Manufacturing of recombinant adeno-associated viral vectors for clinical trials. *Mol Ther Methods Clin Dev.* (2016) 3:16002. doi: 10.1038/mtm.2016.2
24. Chalothorn D, Clayton JA, Zhang H, Pomp D, Faber JE. Collateral density, remodeling, and VEGF-A expression differ widely between mouse strains. *Physiol Genomics.* (2007) 30:179–91. doi: 10.1152/physiolgenomics.00047.2007
25. Li Y, Song Y, Zhao L, Gaidosh G, Laties AM, Wen R. Direct labeling and visualization of blood vessels with lipophilic carbocyanine dye DiI. *Nat Protoc.* (2008) 3:1703–8. doi: 10.1038/nprot.2008.172
26. Boden J, Wei J, McNamara G, Layman H, Abdulreda M, Andreopoulos F, et al. Whole-mount imaging of the mouse hindlimb vasculature using the lipophilic carbocyanine dye DiI. *Biotechniques.* (2012) 53:3–6. doi: 10.2144/000113907
27. Ribieras AJ, Ortiz YY, Shrestha S, Huerta CT, Shao H, Boulina ME, et al. High-resolution three-dimensional imaging of the footpad vasculature in a murine hindlimb gangrene model. *J Vis Exp.* (2022) 181:e63284. doi: 10.3791/63284
28. Perkins JR, Dawes JM, McMahon SB, Bennett DLH, Orengo C, Kohl M. ReadqPCR and NormqPCR: R packages for the reading, quality checking normalisation of RT-qPCR quantification cycle (Cq) data. *BMC Genomics.* (2012) 13:296. doi: 10.1186/1471-2164-13-296
29. Smyth GK. Linear models and empirical bayes methods for assessing differential expression in microarray experiments. *Stat Appl Genet Mol Biol.* (2004) 3:3. doi: 10.2202/1544-6115.1027
30. Benjamini Y, Hochberg Y. Controlling the false discovery rate: a practical and powerful approach to multiple testing. *J R Stat Soc Ser B Methodol.* (1995) 57:289–300. doi: 10.1111/j.2517-6161.1995.tb02031.x
31. Oh IY, Yoon CH, Hur J, Kim JH, Kim TY, Lee CS, et al. Involvement of E-selectin in recruitment of endothelial progenitor cells and angiogenesis in ischemic muscle. *Blood.* (2007) 110:3891–9. doi: 10.1182/blood-2006-10-048991
32. Asahara T, Murohara T, Sullivan A, Silver M, Van Der Zee R, Li T, et al. Isolation of putative progenitor endothelial cells for angiogenesis. *Science.* (1997) 275:964–7. doi: 10.1126/science.275.5302.964
33. Friedrich EB, Walenta K, Scharlau J, Nickenig G, Werner N. CD34-/CD133+/VEGFR-2+ endothelial progenitor cell subpopulation with potent vasoregenerative capacities. *Circ Res.* (2006) 98:20–5. doi: 10.1161/01.RES.0000205765.28940.93
34. Fadini GP, Losordo D, Dimmeler S. Critical re-evaluation of endothelial progenitor cell phenotypes for therapeutic and diagnostic use. *Circ Res.* (2012) 110:624–37. doi: 10.1161/CIRCRESAHA.111.243386
35. Frank S, Stallmeyer B, Kämpfer H, Kolb N, Pfeilschifter J. Leptin enhances wound re-epithelialization and constitutes a direct function of leptin in skin repair. *J Clin Invest.* (2000) 106:501–9. doi: 10.1172/JCI9148
36. Nwadozi E, Ng A, Strömberg A, Liu H yi, Olsson K, Gustafsson T, et al. Leptin is a physiological regulator of skeletal muscle angiogenesis and is locally produced by PDGFRα and PDGFRβ expressing perivascular cells. *Angiogenesis.* (2019) 22:103–15. doi: 10.1007/s10456-018-9641-6
37. Xia N, Li H. The role of perivascular adipose tissue in obesity-induced vascular dysfunction. *Br J Pharmacol.* (2017) 174:3425–42. doi: 10.1111/bph.13650
38. Yamada N, Li W, Ihaya A, Kimura T, Morioka K, Uesaka T, et al. Platelet-derived endothelial cell growth factor gene therapy for limb ischemia. *J Vasc Surg.* (2006) 44:1322–8. doi: 10.1016/j.jvs.2006.07.051
39. Korpisalo P, Rissanen TT, Bengtsson T, Liimatainen T, Laidinen S, Karvinen H, et al. Therapeutic angiogenesis with placental growth factor improves

exercise tolerance of ischaemic rabbit hindlimbs. *Cardiovasc Res.* (2008) 80:263–70. doi: 10.1093/cvr/cvn195
40. Schirmer SH, Buschmann IR, Jost MM, Hoefer IE, Grundmann S, Andert JP, et al. Differential effects of MCP-1 and leptin on collateral flow and arteriogenesis. *Cardiovasc Res.* (2004) 64:356–64. doi: 10.1016/j.cardiores.2004.06.022
41. Mahabeleshwar GH, Feng W, Reddy K, Plow EF, Byzova T V. Mechanisms of integrin-vascular endothelial growth factor receptor cross-activation in angiogenesis. *Circ Res.* (2007) 101:570–80. doi: 10.1161/CIRCRESAHA.107.155655
42. Ammermann F, Meinel FG, Beller E, Busse A, Streckenbach F, Teichert C, et al. Concomitant chronic venous insufficiency in patients with peripheral artery disease: insights from MR angiography. *Eur Radiol.* (2020) 30:3908–14. doi: 10.1007/s00330-020-06696-x
43. Yang Y, Tang G, Yan J, Park B, Hoffman A, Tie G, et al. Cellular and molecular mechanism regulating blood flow recovery in acute versus gradual femoral artery occlusion are distinct in the mouse. *J Vasc Surg.* (2008) 48:1546–58. doi: 10.1016/j.jvs.2008.07.063
44. McClung JM, McCord TJ, Southerland K, Schmidt CA, Padgett ME, Ryan TE, et al. Subacute limb ischemia induces skeletal muscle injury in genetically susceptible mice independent of vascular density. *J Vasc Surg.* (2016) 64:1101–11. doi: 10.1016/j.jvs.2015.06.139
45. Mills JL, Conte MS, Armstrong DG, Pomposelli FB, Schanzer A, Sidawy AN, et al. The society for vascular surgery lower extremity threatened limb classification system: Risk stratification based on Wound, Ischemia, and foot Infection (WIfI). *J Vasc Surg.* (2014) 59:220–34. doi: 10.1016/j.jvs.2013.08.003
46. Goukassian DA, Qin G, Dolan C, Murayama T, Silver M, Curry C, et al. Tumor necrosis factor-α receptor p75 is required in ischemia-induced neovascularization. *Circulation.* (2007) 115:752–62. doi: 10.1161/CIRCULATIONAHA.106.647255
47. Huang H, Huang Q, Wang F, Milner R, Li L. Cerebral ischemia-induced angiogenesis is dependent on tumor necrosis factor receptor 1-mediated upregulation of α5β1 and αVβ3 integrins. *J Neuroinflamm.* (2016) 13:1–12. doi: 10.1186/s12974-016-0697-1
48. Leker RR, Toth ZE, Shahar T, Cassiani-Ingoni R, Szalayova I, Key S, et al. Transforming growth factor α induces angiogenesis and neurogenesis following stroke. *Neuroscience.* (2009) 163:233–43. doi: 10.1016/j.neuroscience.2009.05.050
49. Liu Y, Wada R, Yamashita T, Mi Y, Deng CX, Hobson JP, et al. Edg-1, the G protein-coupled receptor for sphingosine-1-phosphate, is essential for vascular maturation. *J Clin Invest.* (2000) 106:951–61. doi: 10.1172/JCI10905
50. Allende ML, Yamashita T, Proia RL. G-protein-coupled receptor S1P1 acts within endothelial cells to regulate vascular maturation. *Blood.* (2003) 102:3665–7. doi: 10.1182/blood-2003-02-0460
51. Oyama O, Sugimoto N, Qi X, Takuwa N, Mizugishi K, Koizumi J, et al. The lysophospholipid mediator sphingosine-1-phosphate promotes angiogenesis in vivo in ischaemic hindlimbs of mice. *Cardiovasc Res.* (2008) 78:301–7. doi: 10.1093/cvr/cvn002
52. Walter DH, Rochwalsky U, Reinhold J, Seeger F, Aicher A, Urbich C, et al. Sphingosine-1-phosphate stimulates the functional capacity of progenitor cells by activation of the CXCR4-dependent signaling pathway *via* the S1P3 receptor. *Arterioscler Thromb Vasc Biol.* (2007) 27:275–82. doi: 10.1161/01.ATV.0000254669.12675.70
53. Williams PA, Stilhano RS, To VP, Tran L, Wong K, Silva EA. Hypoxia augments outgrowth endothelial cell (OEC) sprouting and directed migration in response to sphingosine-1-phosphate (S1P). *PLoS ONE.* (2015) 10:e0123437. doi: 10.1371/journal.pone.0123437
54. Mandel ER, Uchida C, Nwadozi E, Makki A, Haas TL. Tissue inhibitor of metalloproteinase 1 influences vascular adaptations to chronic alterations in blood flow. *J Cell Physiol.* (2017) 232:831–41. doi: 10.1002/jcp.25491
55. Jin ZQ, Goetzl EJ, Karliner JS. Sphingosine kinase activation mediates ischemic preconditioning in murine heart. *Circulation.* (2004) 110:1980–9. doi: 10.1161/01.CIR.0000143632.06471.93
56. Chen L, Fulcoli FG, Tang S, Baldini A. Tbx1 regulates proliferation and differentiation of multipotent heart progenitors. *Circ Res.* (2009) 105:842–51. doi: 10.1161/CIRCRESAHA.109.200295
57. Cioffi S, Martucciello S, Fulcoli FG, Bilio M, Ferrentino R, Nusco E, et al. Tbx1 regulates brain vascularization. *Hum Mol Genet.* (2014) 23:78–89. doi: 10.1093/hmg/ddt400
58. Apte RS, Chen DS, Ferrara N. VEGF in signaling and disease: beyond discovery and development. *Cell.* (2019) 176:1–35. doi: 10.1016/j.cell.2019.01.021
59. Yu P, Wilhelm K, Dubrac A, Tung JK, Alves TC, Fang JS, et al. FGF-dependent metabolic control of vascular development. *Nature.* (2017) 545:224–8. doi: 10.1038/nature22322

Conflict of Interest: Z-JL and OV along with the University of Miami hold intellectual property of the AAV engineered E-selectin vector and have been licensed to Ambulero, Inc.

The remaining authors declare that the research was conducted in the absence of any commercial or financial relationships that could be construed as a potential conflict of interest.

Publisher's Note: All claims expressed in this article are solely those of the authors and do not necessarily represent those of their affiliated organizations, or those of the publisher, the editors and the reviewers. Any product that may be evaluated in this article, or claim that may be made by its manufacturer, is not guaranteed or endorsed by the publisher.

frontiers | Frontiers in Cardiovascular Medicine

TYPE Original Research
PUBLISHED 16 September 2022
DOI 10.3389/fcvm.2022.950029

OPEN ACCESS

EDITED BY
Xiaofeng Yang,
Temple University, United States

REVIEWED BY
Alec Schmaier,
Beth Israel Deaconess Medical Center and Harvard Medical School, United States
Dorit Avni,
Migal - Galilee Research Institute, Israel

*CORRESPONDENCE
Jun Wan
whuwanjun@163.com
Jing Ye
whuyejing@163.com

†These authors have contributed equally to this work

SPECIALTY SECTION
This article was submitted to Cardiovascular Therapeutics, a section of the journal Frontiers in Cardiovascular Medicine

RECEIVED 22 May 2022
ACCEPTED 24 August 2022
PUBLISHED 16 September 2022

CITATION
Liu M, Wang Z, Zhang J, Ye D, Wang M, Xu Y, Zhao M, Feng Y, Lu X, Pan H, Pan W, Wei C, Tian D, Li W, Lyu J, Ye J and Wan J (2022) IL-12p40 deletion aggravates lipopolysaccharide-induced cardiac dysfunction in mice.
Front. Cardiovasc. Med. 9:950029.
doi: 10.3389/fcvm.2022.950029

IL-12p40 deletion aggravates lipopolysaccharide-induced cardiac dysfunction in mice

Menglin Liu[1†], Zhen Wang[2†], Jishou Zhang[2†], Di Ye[2], Menglong Wang[2], Yao Xu[2], Mengmeng Zhao[2], Yongqi Feng[2], Xiyi Lu[2], Heng Pan[2], Wei Pan[2], Cheng Wei[2], Dan Tian[1], Wenqiang Li[1], Jingjun Lyu[1], Jing Ye[2*] and Jun Wan[2*]

[1]Department of Emergency, Renmin Hospital of Wuhan University, Wuhan, China, [2]Department of Cardiology, Renmin Hospital of Wuhan University, Wuhan, China

Background: Cardiac dysfunction is one of the most common complications of sepsis and is associated with the adverse outcomes and high mortality of sepsis patients. IL-12p40, the common subunit of IL-12 and IL-23, has been shown to be involved in a variety of inflammation-related diseases, such as psoriasis and inflammatory bowel disease. However, the role of IL-12p40 in lipopolysaccharide (LPS)-induced cardiac dysfunction remains obscure. This study aimed to explore the role of IL-12p40 in LPS-induced cardiac dysfunction and its potential mechanisms.

Methods: In this study, mice were treated with LPS and the cardiac expression of IL-12p40 was determined. Then, IL-12p40$^{-/-}$ mice were used to detect the role and mechanisms of IL-12p40 in LPS-induced cardiac injury. In addition, monocytes were adoptively transferred to IL-12p40$^{-/-}$ mice to explore their effects on LPS-induced cardiac dysfunction.

Results: The results showed that cardiac IL-12p40 expression was significantly increased after treated with LPS. In addition, IL-12p40 deletion significantly aggravated LPS-induced cardiac dysfunction, evidenced by the increased serum levels of cardiomyocyte injury markers and heart injury scores, as well as by the deteriorated cardiac function. Moreover, IL-12p40 deletion increased LPS-induced monocyte accumulation and cardiac expression of inflammatory cytokines, as well as enhanced the activation of the NF-κB and MAPK pathways. Furthermore, adoptive transfer WT mouse monocytes to IL-12p40$^{-/-}$ mice alleviated LPS-induced cardiac dysfunction and decreased the phosphorylation of p65.

Conclusion: IL-12p40 deletion significantly aggravated LPS-induced cardiac injury and cardiac dysfunction in mice by regulating the NF-κB and MAPK signaling pathways, and this process was related to monocytes. Therefore, IL-12p40 show a protective role in SIC, and IL-12p40 deficiency or anti-IL-12p40 monoclonal antibodies may be detrimental to patients with SIC.

KEYWORDS

sepsis, IL-12p40 deletion, cardiac dysfunction, monocytes, LPS

Introduction

Sepsis is a systemic inflammatory response syndrome (SIRS) caused by severe infection, surgery, burns, trauma, etc., characterized by an imbalance between inflammatory and anti-inflammatory responses in the body. It can cause septic shock and multiple organ dysfunction syndrome (MODS). Sepsis-induced cardiac dysfunction (SIC) is the most common complication in clinical sepsis and is associated with adverse outcomes and high mortality in sepsis patients (1, 2). It is mainly characterized by ventricular enlargement, myocardial contraction and/or diastolic dysfunction (3). Although numerous studies have paved the way to understand the underlying pathogenesis of SIC (4), the specific mechanism is still not clear. Some studies have reported that the potential mechanism of SIC is a result of the complex interaction of inflammation, oxidative stress, autophagy and apoptosis (4–6) rather than due to a single factor alone.

Previous studies have shown that cytokines participate in the pathological process of sepsis by regulating the immune–inflammatory response of the body. Feng et al. reported that the patients with severe sepsis and septic shock had significantly high serum levels of IL-6 and IL-18 (7). Furthermore, Huan et al. reported that the expression level of IL-35 was decreased in mouse heart tissue after treatment with LPS (8). Therefore, some researchers have attempted modulate these cytokines to reduce the disadvantages of the sepsis-related host response. Panacek et al. found that the anti-TNF-α antibody afelimomab can significantly decrease the 28-day mortality rate of sepsis patients whose serum IL-6 level is over 1,000 pg/ml (9). Moreover, the anti-IL-6 receptor (IL-6R) antibody tocilizumab can improve the prognosis of critical COVID-19 patients, as it can bind to IL-6R and block downstream signal transduction (10).

IL-12p40 is the common subunit of IL-12 and IL-23, which are the proinflammatory factors of the IL-12 family. It can be produced by activated inflammatory cells including monocytes, macrophages, dendritic cells (DCs) and neutrophils (11, 12). To date, some studies have explored the roles of IL-12p40 in autoimmune disease (13), inflammatory responses (14), fibrosis (15) and allograft rejection (16). However, in different diseases, the biological effects of IL-12p40 are not fixed and depending on the inflammatory microenvironment (17). Eriksson et al. found that IL-12p40 deletion can protect mice from autoimmune myocarditis (18). Yao et al. reported that IL-12p40 deletion can induces cholangitis and fibrosis in interleukin-2Rα($^{-/-}$) mice (19). Furthermore, Prando et al. found that patients with IL-12p40 deficiency were susceptibility to mycobacterial disease and salmonellosis disease (20). However, whether IL-12p40 plays a role in sepsis and sepsis-induced cardiac dysfunction is unknown. In this study, we aimed to identify the function of IL-12p40 in sepsis-induced cardiac dysfunction and to explore its underlying mechanisms.

Materials and methods

Animals and experimental model

IL-12p40 knockout (IL-12p40$^{-/-}$) mice with a C57BL/6J background were purchased from the Institute of Model Zoology, Nanjing University (imported from the Jackson Laboratory), and wild-type (WT) mice in the same brood were used as controls (21, 22). All mice were housed in the specific-pathogen-free mouse room of Renmin Hospital of Wuhan University, in which the temperature (20–22°C) and humidity (50 ± 5%) were relatively constant, and the mice could freely obtain water and food. The study was approved by the Animal Care and Use Committee of Renmin Hospital of Wuhan University, and the Care and Use of Laboratory Animals were performed in accordance with the NIH Guidelines revised in 2011.

In the first experiment, male WT mice aged 8–10 weeks were randomly divided into a Saline group ($n = 10$) and an LPS group ($n = 30$). Mice in the LPS group were intraperitoneally injected with 10 mg/kg LPS (055:B5, Sigma-Aldrich, USA) (23), while those in the Saline group were intraperitoneally injected with an isovolumetric dose of saline. Every 10 mice in the LPS group were sacrificed with isoflurane at 3, 6, and 12 h after treatment with LPS. Mice in the Saline group were sacrificed in the same way at 6 h after treatment with saline. The heart tissues of all the mice were harvested, and cardiac IL-12p40 expression levels were detected by qRT–PCR and western blotting. In the second experiment, 8- to 10-week-old WT mice and IL-12p40$^{-/-}$ mice were selected and randomly divided into Saline + WT group ($n = 10$), Saline + KO group ($n = 10$), LPS + WT group ($n = 10$) and LPS + KO group ($n = 10$). Mice in the LPS + WT and LPS + KO groups were given LPS at a dose of 10 mg/kg, while those in the other two groups were given an isovolumetric dose of saline. Six hours later, all the mice were anesthetized and underwent cardiac ultrasound. After that, all of them were sacrificed, and serum and heart tissue samples were obtained for further measurement. In the third experiment, 8- to 10-week-old IL-12p40$^{-/-}$ mice were subjected to the adoptive transfer of WT monocytes or IL-12p40$^{-/-}$ monocytes (10^6 cells/mouse) from the tail vein (24). On the second day, all IL-12p40$^{-/-}$ mice that had received WT monocytes or IL-12p40$^{-/-}$ monocytes were divided into KO+WT Mono group ($n = 6$), KO+WT Mono+LPS group ($n = 6$), KO+KO Mono group ($n = 6$) and KO+KO Mono+LPS group ($n = 6$). Then, mice in the KO+WT Mono+LPS and KO+KO Mono+LPS groups received 10 mg/kg LPS, while those in the other two groups received an isovolumetric dose of saline. Six hours later, all the mice were anesthetized and underwent cardiac ultrasound. Then, all of them were sacrificed, and serum and heart tissue samples were obtained for further measurement.

Echocardiography

The cardiac function of mice was evaluated by echocardiography as described in our previous study (25). In brief, transthoracic echocardiography was performed using a Mylab30CV ultrasound (Biosound Esaote), and data on left ventricular end-diastolic diameter (LVEDd), left ventricular end-systolic diameter (LVESd), left ventricular end-diastolic volume (LVEDd), left ventricular end-systolic volume (LVESd), ejection fraction (LVEF) and fractional shortening (LVFS) were obtained for 10–15 cardiac cycles.

Biochemical determination

The creatine kinase-myocardial band (CK-MB) and lactate dehydrogenase (LDH) were assessed as indices of cardiomyocyte injury. Serum concentrations of CK-MB and LDH were detected according to the manufacturer's instructions, and all kits were purchased from Nanjing Jiancheng Bioengineering Institute, China.

Quantitative real-time PCR

Total RNA was extracted from heart tissues using TRIzol reagent and reverse transcribed to cDNA according to a previous protocol (26). Subsequently, quantitative real-time PCR (qRT–PCR) was performed using a LightCycler 480 (Roche, Switzerland) according to the manufacturer's recommendation. The expression of glyceraldehyde-3-phosphate dehydrogenase (GAPDH) was quantified as an internal control. All the primer sequences used in our study are shown in Table 1.

TABLE 1 All the primer sequences in this study.

Gene	Forward primer (5′-3′)	Reverse primer (5′-3′)
ANP	ACCTGCTAGACCACCTGGAG	CCTTGGCTTATCTTCGGTACCGG
BNP	GAGGTCACTCCTATCCTCTGG	GCCATTTCCTCCGACTTTTCTC
IL-1β	GGGCCTCAAAGGAAAGAATC	TACCAGTTGGGGAACTCTGC
IL-6	AGTTGCCTTCTTGGGACTGA	TCCACGATTTCCCAGAGAAC
IL-17	TCCAGAAGGCCCTCAGACTA	AGCATCTTCTCGACCCTGAA
TNF-α	CCCAGGGACCTCTCTCTAATC	ATGGGCTACAGGCTTGTCACT
INF-γ	ACTGGCAAAAGGATGGTGAC	TGAGCTCATTGAATGCTTGG
GAPDH	ACTCCACTCACGGCAAATTC	TCTCCATGGTGGTGAAGACA

Western blot analysis

The extraction of protein from heart tissues and western blotting were performed according to methods described previously (27). In brief, the heart tissues were lysed by RIPA buffer and ultrasound successively. Total protein was collected from each heart sample and quantified with a BCA Protein Assay Kit (Thermo Fisher Scientific). Then, the proteins (50 μg per sample) were separated by SDS-PAGE and transferred to PVDF membranes (Millipore, Beijing, China). The PVDF membranes were then blocked for 1.5 h with specific 5% non-fat dried milk and incubated with primary antibodies overnight at 4°C. The primary antibodies included anti-IL-12p40, anti-Bcl-2, anti-Bax, anti-c-caspase3, anti-STAT1, anti-p-STAT1, anti-p-p65, anti-p65, anti-CD14, anti-CD16, anti-ERK, anti-p-ERK, anti-p38, anti-p-p38, anti-JNK, anti-p-JNK and anti-GAPDH. Finally, the membranes were incubated with secondary antibodies and scanned with an Odyssey infrared imaging system (LI-COR, USA). The protein expression level of GAPDH was used as an internal control to analyse the expression levels of the target proteins.

Histological analysis

Hearts were arrested in 10% KCl solution immediately after being obtained. After fixation with 10% formalin for 48 h, the heart specimens were embedded in paraffin and then sliced into 5-μm sections. The heart injury score and myocardial collagen volume were analyzed by hematoxylin and eosin (HE) staining and masson's trichrome staining, respectively. Moreover, these sections were also subjected to immunofluorescence staining. In brief, the sections were incubated with primary antibodies against CD14 (R&D Systems, USA), against CD16 (R&D Systems, USA) and against p-p65 (Abcam, United Kingdom) overnight at 4°C. Then, the sections were incubated with secondary antibodies [anti-rabbit HRP reagent (Gene Tech, Shanghai, China)] and 40,6-diamidino-2-phenylindole [DAPI (Gene Tech, Shanghai, China)]. All the figures were captured with fluorescence microscope, and Image Pro Plus 6.0 (Media Cybernetics, Bethesda, MD, United States) was used for relative quantification.

TdT-mediated dUTP nick-end labeling (TUNEL) assay

The heart specimens described above were deparaffinized with toluene and dehydrated with ethanol according to the procedures previously described in our previous study (28).

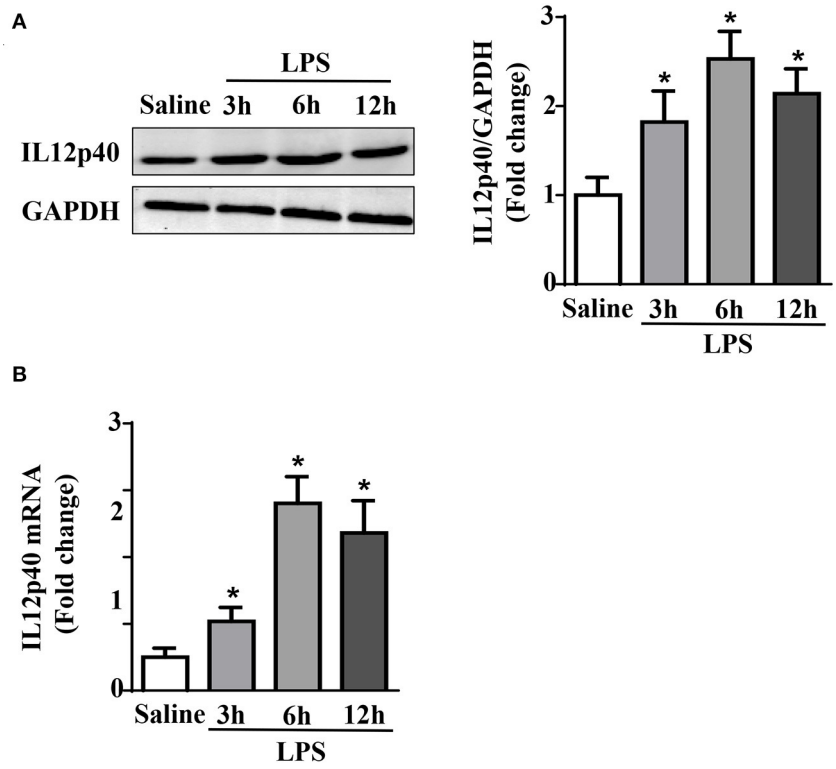

FIGURE 1
LPS treatment increases cardiac IL-12p40 expression in mice. **(A)** Western blot analysis of IL-12p40 protein levels in the hearts of each group ($n = 5$). **(B)** qRT-PCR analysis of IL-12p40 mRNA expression levels in the hearts of each group ($n = 6$). *$P < 0.05$ compared with the Saline group.

Then, a TUNEL kit (Millipore, United States) was used to assess the apoptosis of myocardial tissue.

Flow cytometry

Flow cytometry of mouse spleen tissue was performed as described previously (29). In brief, isolated cell suspensions from spleens were filtered, centrifuged, resuspended and blocked with a CD16/32 antibody. Then, the cell suspensions were stained with primary antibodies for 30 min at 4°C in the dark. Flow cytometry analysis was performed on a BD FACS Calibur flow cytometer (BD Biosciences, San Jose, CA, USA).

Monocyte transduction

Monocytes were obtained according to previous reports (30, 31). Briefly, tibias and femurs were collected from WT and IL-12p40$^{-/-}$ mice. Serum-free α-MEM was injected with a syringe into the bone marrow cavities of tibias and femurs to flush out the cells in the cavities. This process was repeated several times until all the cells in the marrow cavities were flushed out. All bone marrow cell suspensions from IL-12p40$^{-/-}$ mice were collected in a petri dish, while those from WT mice were collected in a separate petri dish. After filtration and centrifugation, bone marrow cell suspensions were lysed with sterile cell lysate. Then, the bone marrow cell suspensions were mixed with FBS, PS and α-MEM and seeded in each well of 6-well culture plates. After overnight incubation in a humid incubator with 5% CO2, the supernatants were discarded from the 6-well culture plates, and the adherent cells were treated for 3 days with monocyte colony-stimulating factor (MC-SF), FBS, PS and α-MEM. All cytokines were purchased from R&D Systems. Monocytes were then cultured in fresh serum-free α-MEM medium at a density of 5×10^6 cells/ml. These monocytes from WT or IL-12p40$^{-/-}$ mice were transferred into each IL-12p40$^{-/-}$ recipient mouse through the tail vein at a dose of 10^6 cells per mouse (24).

Statistics

All the results are presented as the mean ± SD. One-way analysis of variance (ANOVA) or multiactor analysis of variance

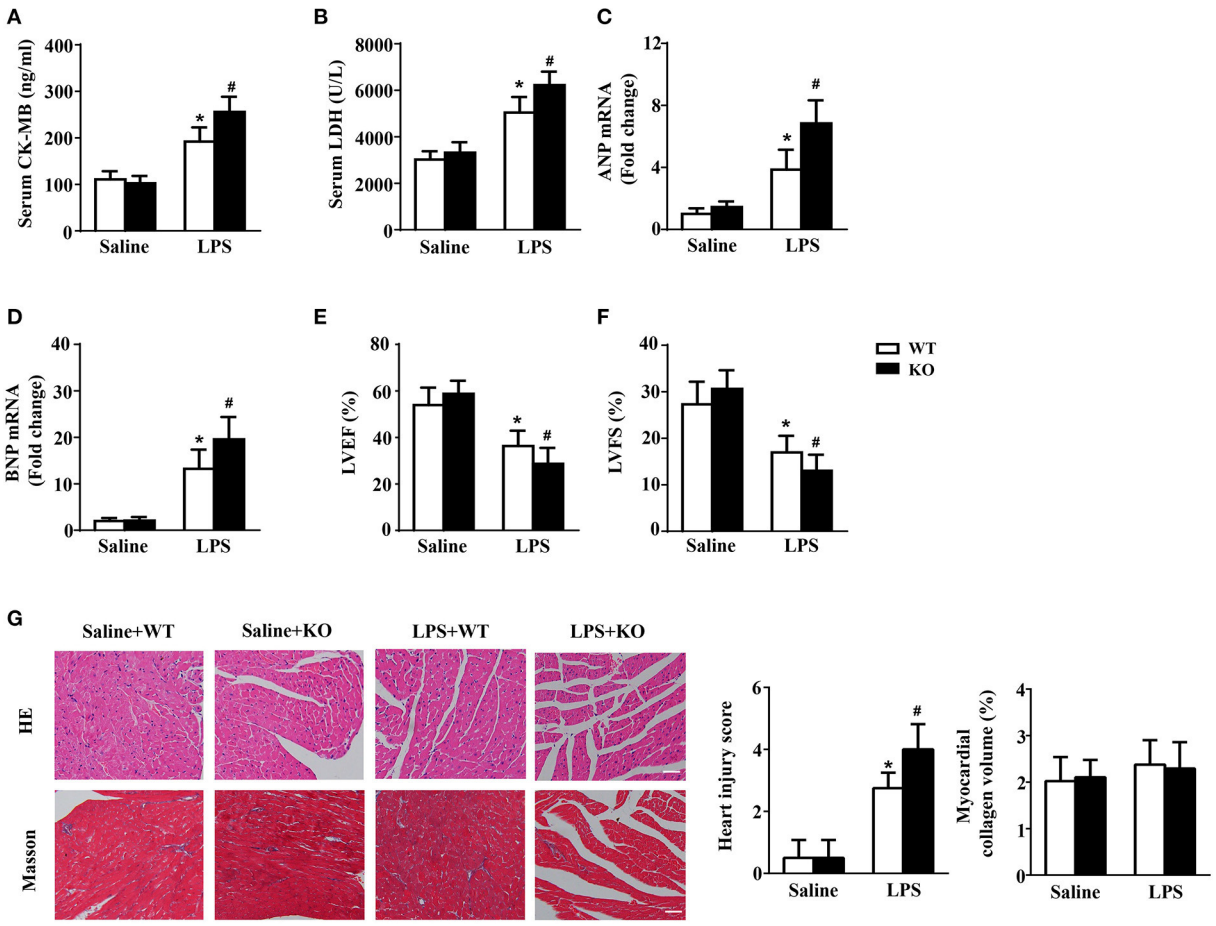

FIGURE 2
IL-12p40 deletion aggravates LPS-induced cardiac injury and cardiac dysfunction in mice. **(A,B)** The levels of LDH and CK-MB in serum of mice in each group ($n = 6$). **(C,D)** qRT-PCR analysis of ANP and BNP mRNA expression levels in the hearts of mice in each group ($n = 6$). **(E,F)** Echocardiography analysis of LVEF and LVFS of mice in each group ($n = 6$). **(G)** HE and masson's trichrome stainings and the quantitative results of heart tissues in each group ($n = 6$; scale bar, 100 μm). *$P < 0.05$ compared with the Saline group. #$P < 0.05$ compared with the LPS+WT group.

was used for comparison of the mean between the groups. A $p < 0.05$ was considered significant.

Results

LPS treatment increases cardiac IL-12p40 expression in mice

The results of qRT-PCR and Western blot showed that within 6 h after treated with LPS, the mRNA and protein levels of IL-12p40 in the mouse myocardium increased gradually. However, after 12 h, both the mRNA and protein levels of IL-12p40 showed downwards trends. Moreover, the mRNA and protein levels of IL-12p40 in mice treated with LPS at 3, 6, and 12 h were significantly different from those in mice in the Saline group (Figure 1).

IL-12p40 deletion aggravates LPS-induced cardiac injury and cardiac dysfunction in mice

The results of biochemical determination showed that treatment with LPS dramatically increased the LDH and CK-MB levels in the serum of mice, and IL-12p40 deletion further increased their levels in mice treated with LPS (Figures 2A,B). The results of qRT-PCR also showed that the levels of ANP and BNP in the cardiac tissue of mice were obviously increased after treatment with LPS and were further increased after IL-12p40 deletion (Figures 2C,D). In addition, the echocardiography results showed that treatment with LPS significantly reduced the LVEF and LVFS of mice; however, IL-12p40 deletion further reduced the LVEF and LVFS of mice (Figures 2E,F). Furthermore, the histological examination revealed that the

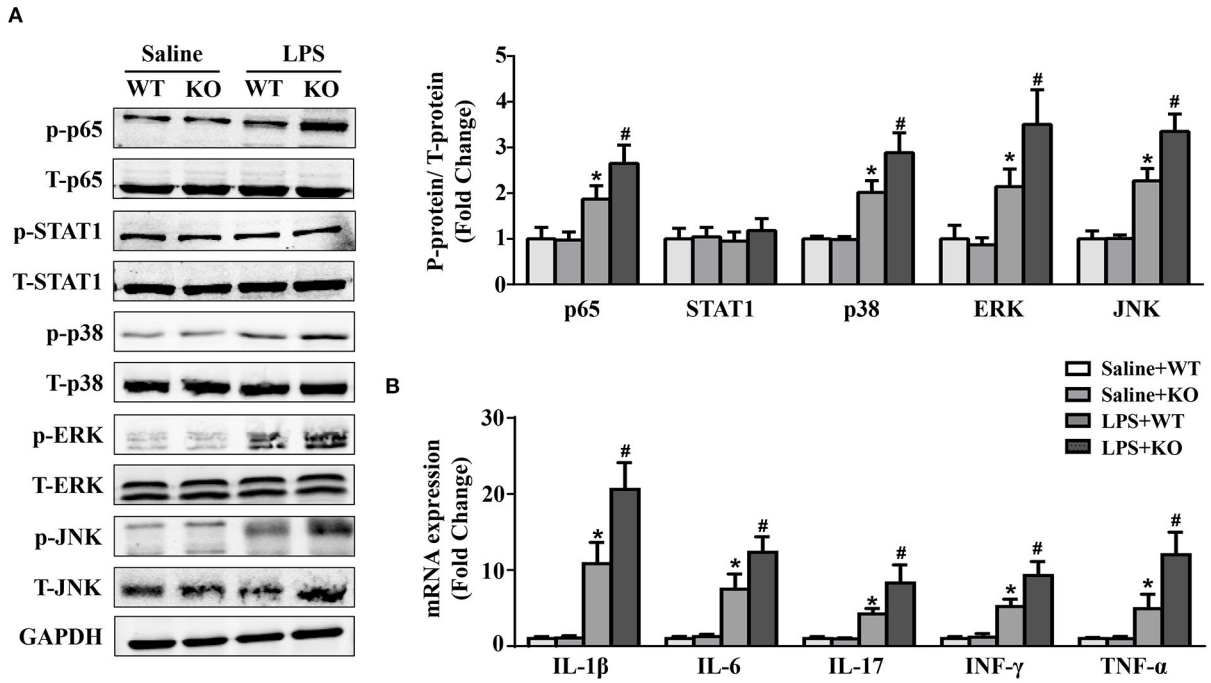

FIGURE 3
IL-12p40 deletion increases the phosphorylation of NF-κB and MAPK signaling pathways and aggravates cardiac inflammation in mice treated with LPS. **(A)** Western blot analysis of T-ERK, p-ERK, T-p38, p-p38, T-JNK, p-JNK, T-STAT1, p-STAT1, T-P65, and p-P65 protein levels in the hearts of mice and the ratios of p-ERK/T-ERK, p-p38/ T-p38, p-JNK/T-JNK, p-P65/T-P65, and p-STAT1/T-STAT1 in each group ($n = 5$). **(B)** qRT-PCR analysis of IL-1β, IL-6, IL-17, TNF-α and INF-γ mRNA expression levels in the hearts of mice in each group ($n = 6$). *$P < 0.05$ compared with the Saline group. #P < 0.05 compared with the LPS+WT group.

heart injury scores of mice treated with LPS were significant higher than those of mice treated with saline, and IL-12p40 deletion could further increase the heart injury scores of mice treated with LPS (Figure 2G). However, there was no significant difference in myocardial collagen volume among all the groups (Figure 2G).

IL-12p40 deletion increases the activation of NF-κB and MAPK signaling pathways and aggravates cardiac inflammation in mice treated with LPS

JAK/STAT1 and NF-κB are the signaling pathways of inflammatory responses, while the MAPK signaling pathway is involved in the pathogenesis of LPS-induced cardiac injury. The results showed that LPS stimulation could significantly increase the phosphorylation of p65, p38, ERK and JNK, which were further increased by IL-12p40 deletion (Figure 3A). However, neither LPS stimulation nor IL-12p40 deletion had significant effect on the phosphorylation of STAT1 (Figure 3A). Furthermore, the qRT–PCR results showed that the mRNA levels of the proinflammatory cytokines IL-1β, IL-6, IL-17, TNF-α, and INF-γ were markedly increased after treatment with LPS (Figure 3B). And IL-12p40 deletion could further increase the mRNA levels of these inflammatory cytokines (Figure 3B).

IL-12p40 deletion increases monocyte infiltration

Monocytes are natural inflammatory cells and are involved in the inflammatory response of sepsis (32, 33). Thus, we also evaluated the infiltration of monocytes in mice. CD14 and CD16 are the surface molecules of monocytes. The immunofluorescence results showed that the infiltration of monocytes in the hearts of mice was significantly increased after treatment with LPS. Interestingly, these changes were obviously exacerbated by IL-12p40 deletion (Figure 4A). Furthermore, the results of flow cytometry also showed that LPS stimulation increased the infiltration of monocytes in the spleen, which was further exacerbated by IL-12p40 deletion (Figure 4B).

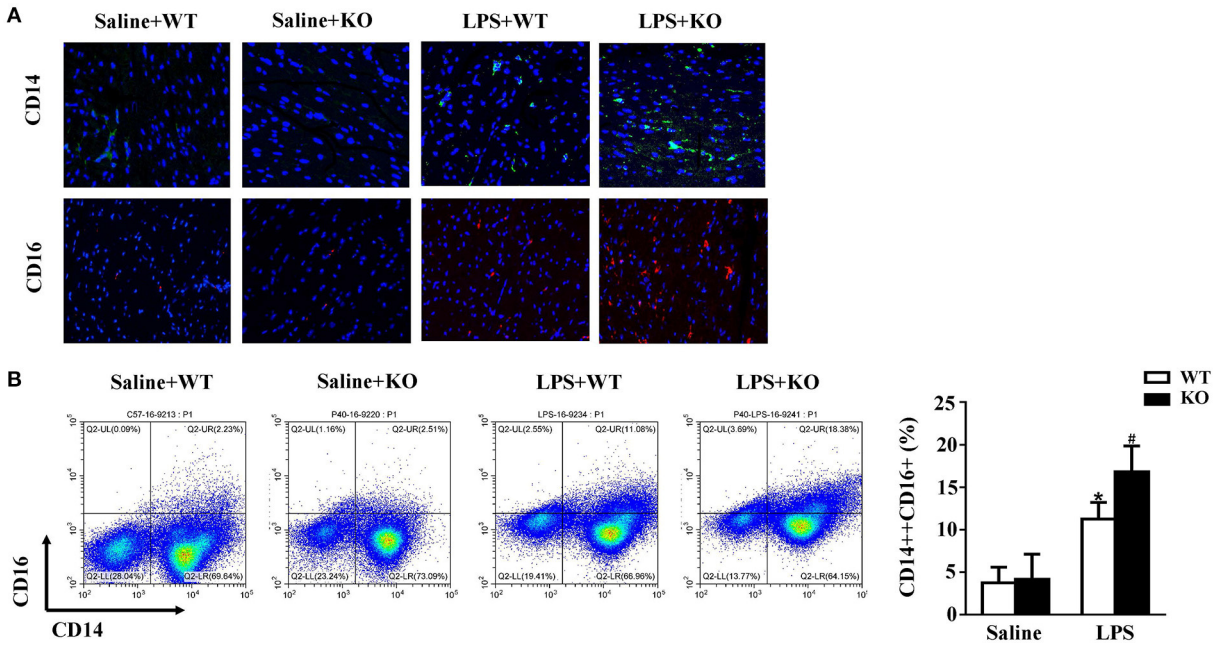

FIGURE 4
IL-12p40 deletion increases monocytes infiltration. **(A)** The immunofluorescence analysis of CD14 and CD16 in heart sections of each group ($n = 6$; scale bar, 50 μm). **(B)** Flow cytometry analysis of CD14++CD16+monocyte percents in spleen tissues of mice in each group ($n = 6$). *$P <$ 0.05 compared with the Saline group. $^{\#}P < 0.05$ compared with the LPS+WT group.

IL-12p40 deletion aggravates LPS-induced myocardial apoptosis

Western blot results showed that LPS stimulation increased the protein expression of Bax and C-caspase3 and decreased the protein expression of Bcl-2 in hearts. These changes were obviously aggravated by IL-12p40 deletion (Figure 5A). Moreover, compared with the saline group, the number of TUNEL-positive cells in the hearts of the LPS group was significantly increased and was further increased by IL-12p40 deletion (Figure 5B).

WT monocyte adoptive transfer alleviates cardiac injury in LPS-treated IL-12p40$^{-/-}$ mice

To explore the effects of exogenous monocytes on LPS-treated IL-12p40$^{-/-}$ mice, WT or IL-12p40$^{-/-}$ mouse monocytes were injected *via* the tail vein prior to LPS or saline treatment. Our results showed that lower levels of LDH and CK-MB in serum and lower mRNA levels of ANP and BNP in the hearts were observed in LPS-treated IL-12p40$^{-/-}$ mice with adoptive transfer of WT monocytes than those in LPS-treated IL-12p40$^{-/-}$ mice with adoptive transfer of IL-12p40$^{-/-}$ monocytes (Figures 6A–D); however, these significant differences were not observed in saline-treated IL-12p40$^{-/-}$ mice (Figures 6A–D). In addition, the echocardiography results also showed that adoptive transfer of WT monocytes could improve cardiac function of LPS-treated IL-12p40$^{-/-}$ mice (Figures 6E,F). Moreover, the results of histological examination indicated that adoptive transfer of WT monocytes can decrease heart injury scores of LPS-treated IL-12p40$^{-/-}$ mice but have no effect on the myocardial collagen volume (Figure 6G).

WT monocyte adoptive transfer alleviates myocardial apoptosis in LPS-treated IL-12p40$^{-/-}$ mice

Adoptive transfer of WT monocytes into LPS-treated IL-12p40$^{-/-}$ mice decreased the protein expression of Bax and C-caspase-3 and increased the protein expression of Bcl-2; however, these significant differences were not observed in saline-treated IL-12P40$^{-/-}$ mice (Figure 7A). In addition, LPS-treated IL-12p40$^{-/-}$ mice with adoptive transfer of WT monocytes exhibited fewer TUNEL-positive cells than those with adoptive transfer of IL-12p40$^{-/-}$ monocytes (Figure 7B).

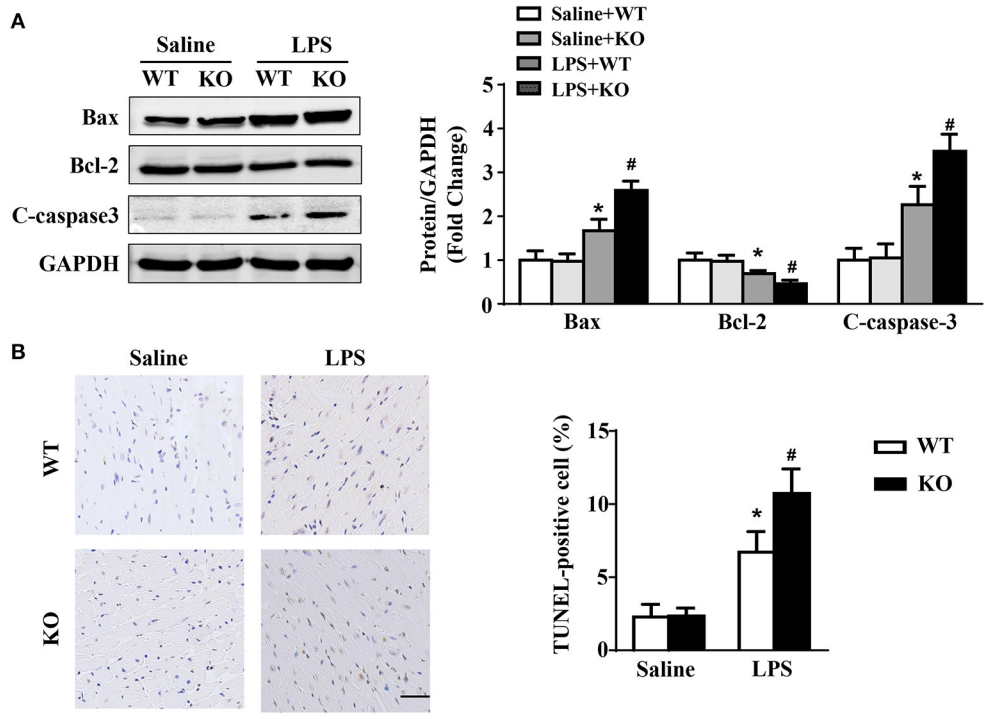

FIGURE 5
IL-12p40 deletion aggravates LPS-induced myocardial apoptosis. **(A)** Western blot analysis of Bax, Bcl-2 and C-caspase-3 protein levels in heart tissues of each group ($n = 5$). **(B)** TUNEL staining and the quantitative results of heart tissues in each group ($n = 6$; scale bar, 50 μm). $^{*}P < 0.05$ compared with the Saline group. $^{\#}P < 0.05$ compared with the LPS+WT group.

WT monocyte adoptive transfer inhibits cardiac inflammation in LPS-treated IL-12p40$^{-/-}$ mice

Compared to the LPS-treated IL-12p40$^{-/-}$ mice with adoptive transfer of IL-12p40$^{-/-}$ monocytes, the levels of p-p65 were significant lower in the hearts of LPS-treated IL-12p40$^{-/-}$ mice with adoptive transfer of WT monocytes (Figure 8A). Moreover, the inhibitory effect of WT monocyte adoptive transfer on inflammation was further confirmed by the results of qRT-PCR, which showed that the mRNA expression of proinflammatory cytokines, including IL-1β, IL-6, IL-17, TNF-α, and INF-γ were significantly down-regulated in LPS-treated IL-12p40$^{-/-}$ mice with adoptive transfer of WT monocytes (Figure 8B).

Discussion

In this study, we explored the effects of IL-12p40 deletion on LPS-induced cardiac dysfunction and elucidated the underlying mechanisms. We found that the expression of IL-12p40 was upregulated in mice after treatment with LPS. In addition, our findings indicated that IL-12p40 deletion aggravated cardiac injury and cardiac dysfunction and increased monocyte infiltration in mice treated with LPS. Moreover, IL-12p40 deletion enhanced the phosphorylation of NF-κB and MAPK signaling pathways, and up-regulated the expression of inflammatory factors. In subsequent experiments, we found that the levels of cardiac inflammation and cardiac injury in LPS-treated IL-12p40$^{-/-}$ mice with adoptive transfer of WT monocytes were lower than those in LPS-treated IL-12p40$^{-/-}$ mice with adoptive transfer of IL-12p40$^{-/-}$ monocytes.

The results of epidemiological statistics showed that ∼40% of patients with sepsis have cardiac dysfunction (34). This type of cardiac dysfunction is caused by sepsis alone and is called SIC. Previous studies have demonstrated that the mortality rate of septic patients with SIC is obviously higher than that of septic patients without SIC (1, 35). Although the underlying mechanisms of SIC have been explored by many studies, these processes are not completely understood. Accumulating evidence indicates that inflammatory reactions are key factors for the initiation and progression of SIC (6). Interleukins (ILs) play an important role in regulating the immune system of human beings. There are more than 40 ILs which can be divided into six families according to their biological functions. IL-12 and IL-23 are the two proinflammatory factors of the IL-12 family and share a common subunit of IL-12p40.

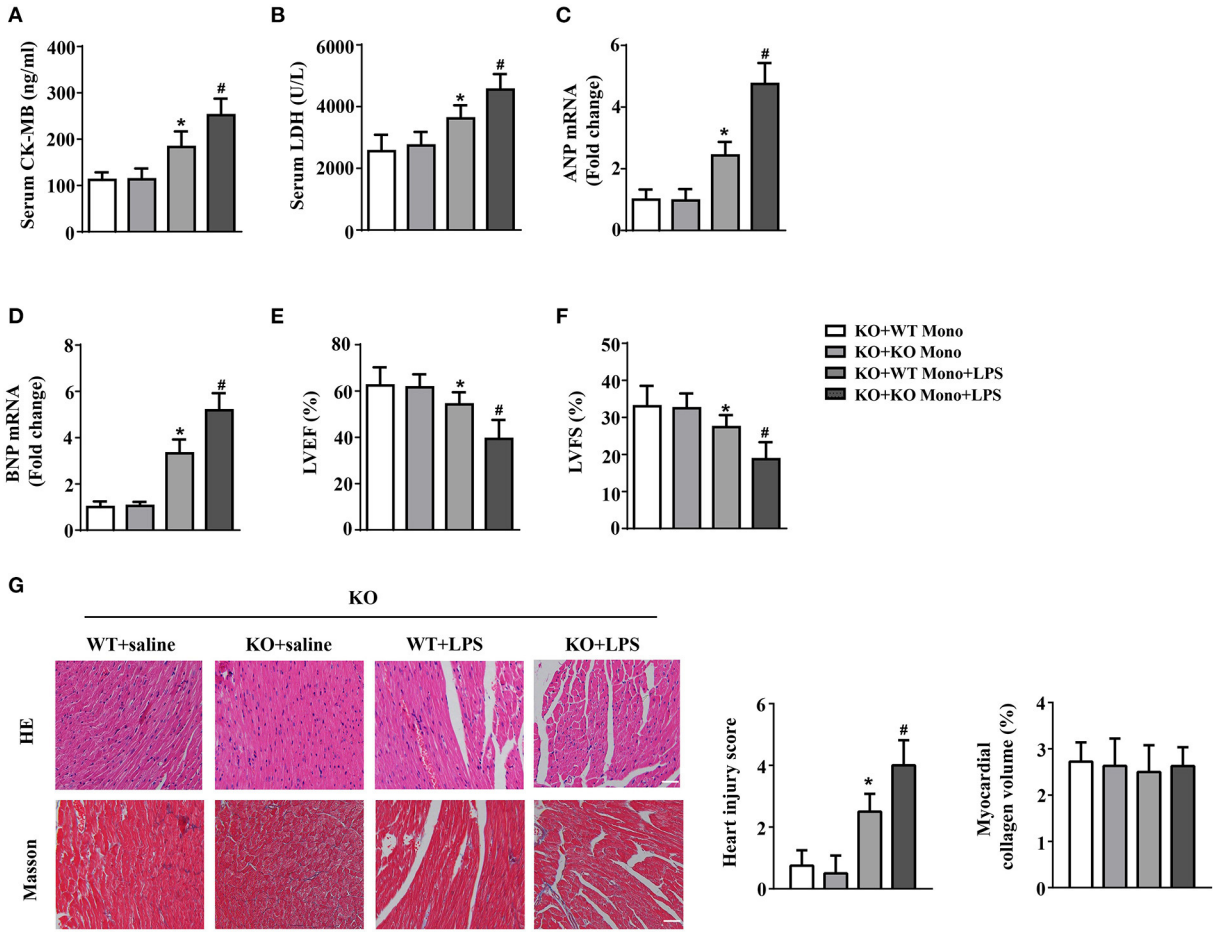

FIGURE 6
WT monocyte adoptive transfer alleviates cardiac injury in LPS-treated IL-12p40$^{-/-}$ mice. **(A,B)** The levels of LDH and CK-MB in serum of mice in each group ($n = 6$). **(C,D)** qRT-PCR analysis of ANP and BNP mRNA expression levels in the hearts of mice in each group ($n = 6$). **(E,F)** Echocardiography analysis of LVEF and LVFS of mice in each group ($n = 6$). **(G)** HE and masson's trichrome stainings and the quantitative results of heart tissues in each group ($n = 6$; scale bar, 100 μm). *$P < 0.05$ compared with the KO+WT Mono group. #$P < 0.05$ compared with the KO+WT Mono+LPS group.

Thus, knocking out or neutralizing the IL-12p40 subunit can counteract the biological effects of both IL-12 and IL-23. To date, there is growing evidence that neutralizing the IL-12p40 subunit can improve the prognosis of many patients with autoimmune diseases by regulating the immune/inflammatory response (36–38). In this study, we detected that IL-12p40 expression in the hearts of mice was upregulated within 6 h after treatment with LPS; however, after 12 h, the expression of IL-12p40 showed a downwards trend. The mechanism of this phenomenon is unclear and may be attributed to the inflammatory overreaction in the early stage of sepsis, followed by immunoparalysis or immunosuppression. Moreover, we also detected that IL-12p40 deletion upregulated the expression of inflammatory factors and aggravated cardiac injury and cardiac dysfunction in mice treated with LPS. Therefore, we speculated that IL-12p40 deletion could aggravate LPS-induced SIC in mice.

The NF-κB pathway is considered an important proinflammatory signaling pathway and can mediate the synthesis of cytokines, including TNF-α, IL-1β, IL-6, IL-8, etc. NF-κB is a heterodimer and p65 is one subunit of it. Sakurai et al. reported that IL-2 deletion leads to the development of inflammatory colitis accompanied by enhanced NF-κB activation (39). In addition, Wang et al. found that sevoflurane can ameliorate LPS-induced inflammatory injury of HK-2 cells by down-regulating the expression of p-p65 (40). MAPK signaling pathway is one of TLR4-related immune signalings and has three major subfamilies, including ERK, JNK and p38 (41). TLR4 is responsible for the recognition of LPS and MAPK signaling pathway is involved in regulating cardiac

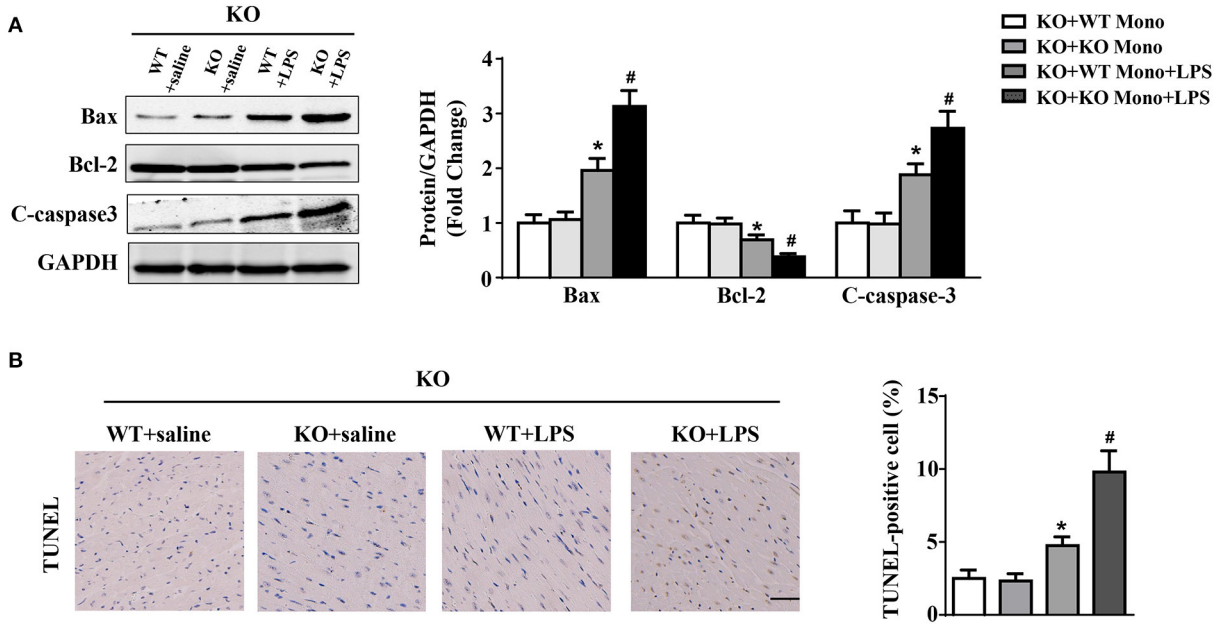

FIGURE 7
WT monocyte adoptive transfer alleviates myocardial apoptosis in LPS-treated IL-12p40$^{-/-}$ mice. **(A)** Western blot analysis of Bax, Bcl-2 and C-caspase-3 protein levels in heart tissues of each group ($n = 5$). **(B)** TUNEL staining and the quantitative results of heart tissues in each group ($n = 6$; scale bar, 50 μm). *$P < 0.05$ compared with the KO+WT Mono group. $^{\#}P < 0.05$ compared with the KO+WT Mono+LPS group.

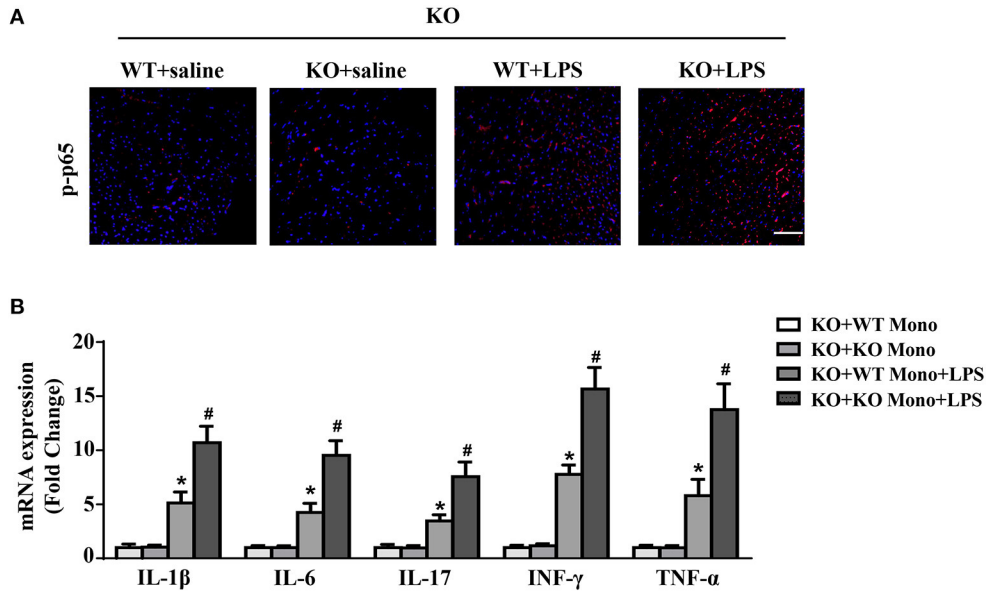

FIGURE 8
WT monocyte adoptive transfer reduces cardiac inflammation in LPS-treated IL-12p40$^{-/-}$ mice. **(A)** The immunofluorescence analysis of p-p65 in heart sections of each group ($n = 6$; scale bar, 50 μm). **(B)** qRT-PCR analysis of IL-1β, IL-6, IL-17, TNF-α, and INF-γ mRNA expression levels in the hearts of mice in each group ($n = 6$). *$P < 0.05$ compared with the KO+WT Mono group. $^{\#}P < 0.05$ compared with the KO+WT Mono+LPS group.

inflammatory responses triggered by LPS (28). STAT1 is an important mediator of biological responses induced by inflammatory activators (42), and the JAK-STAT signaling pathway is known as a mechanism involved in immune regulation (43). In our study, the results indicated that the phosphorylation of p65, p38, ERK, and JNK were significantly increased in mice treated with LPS, and IL-12p40 deletion further exacerbated these changes. However, neither LPS stimulation nor IL-12p40 deletion had significant effect on the phosphorylation of STAT1 in mice. Therefore, IL-12p40 deletion aggravates LPS-induced cardiac dysfunction in mice by activating NF-κB and MAPK signaling pathways but not the JAK-STAT1 signaling pathway.

Monocytes are natural immune cells that can participate in the activation of the innate immune system and release inflammatory cytokines and chemokines after recognized pathogens. The cytokines include TNF-α, IL-1β, IL-6, IL-12, IL-18, and IL-23 (44, 45), while the chemokines include CCL2/MCP-1, CXCL8, CXCL10, CCL18, and CCL20 (46–48). Then, these cytokines and chemokines further activate and recruit other immune cells to the inflammation sites and trigger a series of inflammatory responses (49). In recent years, many studies have reported the role of monocytes in sepsis. Gainaru et al. found that the circulating monocyte count was greatly increased in gram-negative sepsis (32). Raffray et al. observed that zoledronate could rescue immunosuppressed monocytes during acute sepsis and thus may help improve clinical outcomes during severe infection (50). Furthermore, Sáenz et al. reported that we could diagnose severe sepsis in the early stage by analyzing the monocyte immunophenotype (51). In this study, we found that the infiltration of monocytes in mice was significantly increased after treatment with LPS. Moreover, IL-12p40 deletion further increased the infiltration of monocytes in mice treated with LPS.

However, the role of monocytes in LPS-induced cardiac dysfunction in IL-12p40$^{-/-}$ mice still needs to be further verified. In subsequent experiments, we transferred WT and IL-12p40$^{-/-}$ monocytes into different IL-12p40$^{-/-}$ mice treated with LPS. The results indicated that transfer of WT monocytes can significantly alleviate cardiac inflammation and cardiac injury compared with transfer of IL-12p40$^{-/-}$ monocytes. One possible explanation is that WT monocytes can secrete more IL-12 and IL-23 than IL-12p40$^{-/-}$ monocytes, and transfer of WT monocytes can partially offset the loss of the biological effects of IL-12 and IL-23 caused by IL-12p40 deletion. Thus, monocytes can regulate LPS-induced inflammatory responses, cardiac injury and cardiac dysfunction by secreting IL-12 and IL-23, and their functions are different in different environments.

In conclusion, our research indicated that IL-12p40 deletion significantly aggravated LPS-induced cardiac injury and cardiac dysfunction in mice by regulating the NF-κB and MAPK signaling pathways, and this process may be related to monocytes. Therefore, IL-12p40 show a protective role in SIC, and IL-12p40 deficiency or anti-IL-12p40 monoclonal antibodies may be detrimental to patients with SIC.

Data availability statement

The original contributions presented in the study are included in the article/Supplementary material, further inquiries can be directed to the corresponding author/s.

Ethics statement

The animal study was reviewed and approved by Animal Care and Use Committee of Renmin Hospital of Wuhan University.

Author contributions

ML, ZW, and JZ contributed to the experimental design and wrote the manuscript. DY, MW, YX, MZ, JL, and JY contributed to the acquisition and analysis of the data. YF, XL, WP, HP, CW, DT, WL, and JW reviewed the manuscript. All authors contributed to the article and approved the submitted version.

Funding

This work was supported by the National Natural Science Foundation of China (No. 1382070436 to JW).

Conflict of interest

The authors declare that the research was conducted in the absence of any commercial or financial relationships that could be construed as a potential conflict of interest.

Publisher's note

Supplementary material

The Supplementary Material for this article can be found online at: https://www.frontiersin.org/articles/10.3389/fcvm.2022.950029/full#supplementary-material

References

1. Merx MW, Weber C. Sepsis and the heart. *Circulation*. (2007) 116:793–802. doi: 10.1161/CIRCULATIONAHA.106.678359

2. van der Slikke Elisabeth C, An Andy Y, Hancock Robert EW, Bouma Hjalmar R. Exploring the pathophysiology of post-sepsis syndrome to identify therapeutic opportunities. *EBioMedicine*. (2020) 61:103044. doi: 10.1016/j.ebiom.2020.103044

3. Court O, Kumar A, Parrillo JE, Kumar A. Clinical review: myocardial depression in sepsis and septic shock. *Crit Care*. (2002) 6:500–8. doi: 10.1186/cc1822

4. Liu YC, Yu MM, Shou ST, Chai YF. Sepsis-induced cardiomyopathy: mechanisms and treatments. *Front Immunol*. (2017) 8:1021. doi: 10.3389/fimmu.2017.01021

5. Beesley SJ, Weber G, Sarge T, Nikravan S, Grissom CK, Lanspa MJ, et al. Septic cardiomyopathy. *Crit Care Med*. (2018) 46:625–34. doi: 10.1097/CCM.0000000000002851

6. Martin L, Derwall M, Al Zoubi S, Zechendorf E, Reuter DA, Thiemermann C, et al. The septic heart: current understanding of molecular mechanisms and clinical implications. *Chest*. (2019) 155:427–37. doi: 10.1016/j.chest.2018.08.1037

7. Feng M, Sun T, Zhao Y, Zhang H. Detection of serum interleukin-6/10/18 levels in sepsis and its clinical significance. *J Clin Lab Anal*. (2016) 30:1037–43. doi: 10.1002/jcla.21977

8. Hu H, Fu Y, Li M, Xia H, Liu Y, Sun X, et al. Interleukin-35 pretreatment attenuates lipopolysaccharide-induced heart injury by inhibition of inflammation, apoptosis and fibrotic reactions. *Int Immunopharmacol*. (2020) 86:106725. doi: 10.1016/j.intimp.2020.106725

9. Panacek EA, Marshall JC, Albertson TE, Johnson DH, Johnson S, MacArthur RD, et al. Efficacy and safety of the monoclonal anti-tumor necrosis factor antibody F(ab')2 fragment afelimomab in patients with severe sepsis and elevated interleukin-6 levels. *Crit Care Med*. (2004) 32:2173–82. doi: 10.1097/01.CCM.0000145229.59014.6C

10. Xu X, Han M, Li T, Sun W, Wang D, Fu B, et al. Effective treatment of severe COVID-19 patients with tocilizumab. *Proc Natl Acad Sci USA*. (2020) 117:10970–5. doi: 10.1073/pnas.2005615117

11. Trinchieri G, Pflanz S, Kastelein RA. The IL-12 family of heterodimeric cytokines: new players in the regulation of T cell responses. *Immunity*. (2003) 19:641–4. doi: 10.1016/S1074-7613(03)00296-6

12. Trinchieri G. Interleukin-12 and the regulation of innate resistance and adaptive immunity. *Nat Rev Immunol*. (2003) 3:133–46. doi: 10.1038/nri1001

13. Abdi K. IL-12: the role of p40 versus p75. *Scand J Immunol*. (2002) 56:1–11. doi: 10.1046/j.1365-3083.2002.01101.x

14. Walter MJ, Kajiwara N, Karanja P, Castro M, Holtzman MJ. Interleukin 12 p40 production by barrier epithelial cells during airway inflammation. *J Exp Med*. (2001) 193:339–51. doi: 10.1084/jem.193.3.339

15. Huaux F, Lardot C, Arras M, Delos M, Many MC, Coutelier JP, et al. Lung fibrosis induced by silica particles in NMRI mice is associated with an upregulation of the p40 subunit of interleukin-12 and Th-2 manifestations. *Am J Respir Cell Mol Biol*. (1999) 20:561–72. doi: 10.1165/ajrcmb.20.4.3342

16. Mikols CL, Yan L, Norris JY, Russell TD, Khalifah AP, Hachem RR, et al. IL-12 p80 is an innate epithelial cell effector that mediates chronic allograft dysfunction. *Am J Respir Crit Care Med*. (2006) 174:461–70. doi: 10.1164/rccm.200512-1886OC

17. Floss DM, Moll JM, Scheller J. IL-12 and IL-23-close relatives with structural homologies but distinct immunological functions. *Cells*. (2020) 9:2184. doi: 10.3390/cells9102184

18. Eriksson U, Kurrer MO, Sebald W, Brombacher F, Kopf M. Dual role of the IL-12/IFN-gamma axis in the development of autoimmune myocarditis: induction by IL-12 and protection by IFN-gamma. *J Immunol*. (2001) 167:5464–9. doi: 10.4049/jimmunol.167.9.5464

19. Yao Y, Yang W, Yang YQ, Ma HD, Lu FT, Li L, et al. Distinct from its canonical effects, deletion of IL-12p40 induces cholangitis and fibrosis in interleukin-2Rα($^{-/-}$) mice. *J Autoimmun*. (2014) 51:99–108. doi: 10.1016/j.jaut.2014.02.009

20. Prando C, Samarina A, Bustamante J, Boisson-Dupuis S, Cobat A, Picard C et al. Inherited IL-12p40 deficiency: genetic, immunologic, and clinical features of 49 patients from 30 kindreds. *Medicine*. (2013) 92:109–22. doi: 10.1097/MD.0b013e3182963750

21. Wang Z, Liu M, Ye D, Ye J, Wang M, Liu J, et al. Il12a Deletion aggravates sepsis-induced cardiac dysfunction by regulating macrophage polarization. *Front Pharmacol*. (2021) 12:632912. doi: 10.3389/fphar.2021.632912

22. Ye J, Wang Y, Xu Y, Wang Z, Liu L, Wang M, et al. Interleukin-22 deficiency alleviates doxorubicin-induced oxidative stress and cardiac injury via the p38 MAPK/macrophage/Fizz3 axis in mice. *Redox Biol*. (2020) 36:101636. doi: 10.1016/j.redox.2020.101636

23. Li N, Zhou H, Wu H, Wu Q, Duan M, Deng W, Tang Q. STING-IRF3 contributes to lipopolysaccharide- induced cardiac dysfunction, inflammation, apoptosis and pyroptosis by activating NLRP3. *Redox Biol*. (2019) 24:101215. doi: 10.1016/j.redox.2019.101215

24. Yang K, Xu C, Zhang Y, He S, Li D. Sestrin2 suppresses classically activated macrophages-mediated inflammatory response in myocardial infarction through inhibition of mTORC1 signaling. *Front Immunol*. (2017) 8:728. doi: 10.3389/fimmu.2017.00728

25. Ye J, Huang Y, Que B, Chang C, Liu W, Hu H, et al. Interleukin-12p35 knock out aggravates doxorubicin-induced cardiac injury and dysfunction by aggravating the inflammatory response, oxidative stress, apoptosis and autophagy in mice. *EBioMedicine*. (2018) 35:29–39. doi: 10.1016/j.ebiom.2018.06.009

26. Ye D, Wang Z, Ye J, Wang M, Liu J, Xu Y, et al. Interleukin-5 levels are decreased in the plasma of coronary artery disease patients and inhibit Th1 and Th17 differentiation *in vitro*. *Rev Esp Cardiol*. (2020) 73:393–402. doi: 10.1016/j.rec.2019.07.005

27. Wang Z, Ye D, Ye J, Wang M, Liu J, Jiang H, et al. ADAMTS-5 decreases in coronary arteries and plasma from patients with coronary artery disease. *Dis Markers*. (2019) 2019:6129748. doi: 10.1155/2019/6129748

28. Zhang J, Wang M, Ye J, Liu J, Xu Y, Wang Z, et al. The anti-inflammatory mediator resolvin E1 protects mice against lipopolysaccharide-induced heart injury. *Front Pharmacol*. (2020) 11:203. doi: 10.3389/fphar.2020.00203

29. Wang Z, Xu Y, Wang M, Ye J, Liu J, Jiang H, et al. TRPA1 inhibition ameliorates pressure overload-induced cardiac hypertrophy and fibrosis in mice. *EBioMedicine*. (2018) 36:54–62. doi: 10.1016/j.ebiom.2018.08.022

30. Rey-Giraud F, Hafner M, Ries CH. *In vitro* generation of monocyte-derived macrophages under serum-free conditions improves their tumor promoting functions. *PLoS ONE*. (2012) 7:e42656. doi: 10.1371/journal.pone.0042656

31. Italiani P, Boraschi D. From Monocytes to M1/M2 Macrophages: phenotypical vs. functional differentiation. *Front Immunol*. (2014) 5:514. doi: 10.3389/fimmu.2014.00514

32. Gainaru G, Papadopoulos A, Tsangaris I, Lada M, Giamarellos-Bourboulis EJ, Pistiki A. Increases in inflammatory and CD14/CD16/CD45 patrolling monocytes in sepsis: correlation with final outcome. *Crit Care*. (2018) 22:56. doi: 10.1186/s13054-018-1977-1

33. Baudesson de Chanville C, Chousterman BG, Hamon P, Laviron M, Guillou N, Loyher PL, et al. Sepsis triggers a late expansion of functionally impaired tissue-vascular inflammatory monocytes during clinical recovery. *Front Immunol*. (2020) 11:675. doi: 10.3389/fimmu.2020.00675

34. Mayr FB, Yende S, Angus DC. Epidemiology of severe sepsis. *Virulence*. (2014) 5:4–11. doi: 10.4161/viru.27372

35. Vieillard-Baron A, Caille V, Charron C, Belliard G, Page B, Jardin F. Actual incidence of global left ventricular hypokinesia in adult septic shock. *Crit Care Med*. (2008) 36:1701–6. doi: 10.1097/CCM.0b013e318174db05

36. Wong U, Cross RK. Expert opinion on interleukin-12/23 and interleukin-23 antagonists as potential therapeutic options for the treatment of inflammatory bowel disease. *Expert Opin Investig Drugs*. (2019) 28:473–9. doi: 10.1080/13543784.2019.1597053

37. Zabotti A, Goletti D, Lubrano E, Cantini F. The impact of the interleukin 12/23 inhibitor ustekinumab on the risk of infections in patients with psoriatic arthritis. *Expert Opin Drug Saf*. (2020) 19:69–82. doi: 10.1080/14740338.2020.1703946

38. Jeon C, Sekhon S, Yan D, Afifi L, Nakamura M, Bhutani T. Monoclonal antibodies inhibiting IL-12,−23, and−17 for the treatment of psoriasis. *Hum Vaccin Immunother*. (2017) 13:2247–59. doi: 10.1080/21645515.2017.1356498

39. Sakurai H, Hisada Y, Ueno M, Sugiura M, Kawashima K, Sugita T. Activation of transcription factor NF-kappa B in experimental glomerulonephritis in rats. *Biochim Biophys Acta*. (1996) 1316:132–8. doi: 10.1016/0925-4439(96)00022-1

40. Peipei W, Ping W, Miaomiao Y, Shuo W. Sevoflurane ameliorates LPS-induced inflammatory injury of HK-2 cells through Sirtuin1/NF-κB pathway. *Allergol Immunopathol*. (2022) 50:115–23. doi: 10.15586/aei.v50i4.623

41. Zhang WB, Zhang HY, Zhang Q, Jiao FZ, Zhang H, Wang LW, et al. Glutamine ameliorates lipopolysaccharide-induced cardiac dysfunction by regulating the toll-like receptor 4/mitogen-activated

protein kinase/nuclear factor-κB signaling pathway. *Exp Ther Med.* (2017) 14:5825–32. doi: 10.3892/etm.2017.5324

42. Sikorski K, Chmielewski S, Olejnik A, Wesoly JZ, Heemann U, Baumann M, et al. STAT1 as a central mediator of IFNγ and TLR4 signal integration in vascular dysfunction. *JAKSTAT*. (2012) 1:241–9. doi: 10.4161/jkst.22469

43. Liu L, Yue Y, Xiong S. NK-derived IFN-γ/IL-4 triggers the sexually disparate polarization of macrophages in CVB3-induced myocarditis. *J Mol Cell Cardiol*. (2014) 76:15–25. doi: 10.1016/j.yjmcc.2014.07.021

44. Hashimoto D, Miller J, Merad M. Dendritic cell and macrophage heterogeneity *in vivo*. *Immunity*. (2011) 35:323–35. doi: 10.1016/j.immuni.2011.09.007

45. Georgopoulos S, Plows D, Kollias G. Transmembrane TNF is sufficient to induce localized tissue toxicity and chronic inflammatory arthritis in transgenic mice. *J Inflamm*. (1996) 46:86–97.

46. Pavkova Goldbergova M, Lipkova J, Pavek N, Gatterova J, Vasku A, Soucek M, et al. RANTES, MCP-1 chemokines and factors describing rheumatoid arthritis. *Mol Immunol*. (2012) 52:273–8. doi: 10.1016/j.molimm.2012.06.006

47. Schmidt T, Berthold E, Arve-Butler S, Gullstrand B, Mossberg A, Kahn F, et al. Children with oligoarticular juvenile idiopathic arthritis have skewed synovial monocyte polarization pattern with functional impairment-a distinct inflammatory pattern for oligoarticular juvenile arthritis. *Arthritis Res Ther*. (2020) 22:186. doi: 10.1186/s13075-020-02279-9

48. Niu X, Schulert GS. Functional regulation of macrophage phenotypes by MicroRNAs in inflammatory arthritis. *Front Immunol.* (2019) 10:2217. doi: 10.3389/fimmu.2019.02217

49. Ross EA, Devitt A, Johnson JR. Macrophages: the good, the bad, and the gluttony. *Front Immunol*. (2021) 12:708186. doi: 10.3389/fimmu.2021.708186

50. Raffray L, Burton RJ, Baker SE, Morgan MP, Eberl M. Zoledronate rescues immunosuppressed monocytes in sepsis patients. Immunology (2020) 159:88–95. doi: 10.1111/imm.13132

51. Sáenz JJ, Izura JJ, Manrique A, Sala F, Gaminde I. Early prognosis in severe sepsis via analyzing the monocyte immunophenotype. *Intensive Care Med*. (2001) 27:970–7. doi: 10.1007/s001340100962

frontiers | Frontiers in Cardiovascular Medicine

TYPE Original Research
PUBLISHED 19 October 2022
DOI 10.3389/fcvm.2022.1022071

OPEN ACCESS

EDITED BY
Xiaofeng Yang,
Temple University, United States

REVIEWED BY
Masahiko Fujihara,
Kishiwada Tokushukai Hospital, Japan
Yung-Wei Chi,
University of California, Davis, United States
Gopal Chandra Ghosh,
Rabindranath Thakur Diagnostic and Medical Care Center, India

*CORRESPONDENCE
Young-Guk Ko
ygko@yuhs.ac
Dong-Hoon Choi
cdhlyj@yuhs.ac

†These authors have contributed equally to this work and share senior authorship

SPECIALTY SECTION
This article was submitted to Cardiovascular Therapeutics, a section of the journal Frontiers in Cardiovascular Medicine

RECEIVED 18 August 2022
ACCEPTED 26 September 2022
PUBLISHED 19 October 2022

CITATION
Park J-I, Ko Y-G, Lee Y-J, Lee S-J, Hong S-J, Ahn C-M, Kim J-S, Kim B-K, Hong M-K, Yu C-W, Rha S-W, Park J-K, Min P-K, Yoon C-H, Lee S-R, Park S-H and Choi D-H (2022) Long coverage with drug-eluting stents is superior to spot coverage for long femoropopliteal artery disease: PARADE II study.
Front. Cardiovasc. Med. 9:1022071.
doi: 10.3389/fcvm.2022.1022071

Long coverage with drug-eluting stents is superior to spot coverage for long femoropopliteal artery disease: PARADE II study

Jong-Il Park[1], Young-Guk Ko[1*†], Yong-Joon Lee[1], Seung-Jun Lee[1], Sung-Jin Hong[1], Chul-Min Ahn[1], Jung-Sun Kim[1], Byeong-Keuk Kim[1], Myeong-Ki Hong[1], Cheol-Woong Yu[2], Seung-Woon Rha[3], Jong-Kwan Park[4], Pil-Ki Min[5], Chang-Hwan Yoon[6], Sang-Rok Lee[7], Sang-Ho Park[8] and Dong-Hoon Choi[1*†]

[1]Division of Cardiology, Severance Cardiovascular Hospital, Yonsei University College of Medicine, Seoul, South Korea, [2]Division of Cardiology, Korea University Anam Hospital, Seoul, South Korea, [3]Division of Cardiology, Korea University Guro Hospital, Seoul, South Korea, [4]Division of Cardiology, National Health Insurance Service Ilsan Hospital, Gyeonggi-do, South Korea, [5]Division of Cardiology, Yonsei University Gangnam Severance Hospital, Seoul, South Korea, [6]Division of Cardiology, Seoul National University Bundang Hospital, Seongnam-si, South Korea, [7]Division of Cardiology, Jeonbuk National University Hospital, Jeonju-si, South Korea, [8]Division of Cardiology, Soonchunhyang University Cheonan Hospital, Cheonan-si, South Korea

Background: The efficacy of spot stenting using drug-eluting stents (DES) for the treatment of long femoropopliteal (FP) lesion is unknown. This study aimed to compare clinical outcomes of long full coverage vs. spot coverage with DES for long FP artery disease.

Methods: This multicenter randomized trial compared long DES vs. spot DES for FP lesions longer than 150 mm. All lesions were treated with paclitaxel-eluting stents (Zilver PTX). The primary endpoint was primary patency at 12 months.

Results: The study was terminated early after an interim analysis. A total of 103 patients (55 in the long DES group; 48 in the spot DES group) were eligible for analysis. There were no significant differences in baseline and lesion characteristics between groups. Total stent length was longer in the long DES group than in the spot DES group (225.6 ± 67.2 vs. 131.3 ± 48.7 mm, $p < 0.001$). Technical success was achieved in all patients. There was a trend toward a higher primary patency rate at 12 months in the long DES group than in the spot DES group (87.5% vs. 67.5%, $p = 0.120$). The rate of survival free from target lesion revascularization was significantly higher in the long DES group than in the spot DES group (91.7% vs. 72.0%, $p = 0.044$). In multivariate Cox regression analysis, spot DES [hazard ratio (HR) 2.42, 95% confidence interval (CI) 1.14–5.12, $p = 0.021$] and postdilation (HR 0.27, 95% CI 0.09–0.79, $p =$

0.018) were identified as independent predictors for loss of patency at 12 months post-procedure.

Conclusions: Long DES were more effective than spot DES for treating long FP lesions.

Clinical trial registration: Clinicaltrials.gov, identifier: NCT02701881.

KEYWORDS

peripheral artery disease, femoropopliteal artery, drug-eluting stent, patency, restenosis

Introduction

Self-expandable nitinol stents have higher patency rates than balloon angioplasty in femoropopliteal (FP) artery lesions (1, 2). However, restenosis after stenting occurs in 16 to 37% of patients by 1 year as the stent length increases, and this remains a major limitation of bare nitinol stents (3, 4). To reduce restenosis after stenting, drug-eluting stents (DES) were developed and adopted for the treatment of FP lesions. The Zilver PTX Drug-Eluting Stent (Cook Medical, Bloomington, IN, USA) is a self-expanding nitinol stent with a polymer-free paclitaxel coating designed to deliver paclitaxel locally to the vessel wall (5). Almost all of the paclitaxel is released within 72 h and remains in the vascular tissue for up to 56 days (5).

A randomized controlled clinical trial and various registry studies have reported superior efficacy of Zilver PTX, compared with balloon angioplasty or bare nitinol stents (6, 7). However, in FP lesions longer than 150 mm, the rate of restenosis after Zilver PTX implantation is as high as 37% by 1 year (8). The 1-year restenosis rate after full metal jacket stenting using Zilver PTX in lesions longer than 200 mm has been reported as 40%.

In previous studies using bare nitinol stents, spot stenting resulted in more favorable outcomes than long stenting (9, 10). However, the efficacy of spot stenting using DES in long FP lesions is unknown. Thus, the present study was designed to investigate clinical outcomes of long stenting vs. spot stenting using Zilver PTX for the treatment of long FP artery disease.

Materials and methods

Study design

The PARADE II (Comparison of the Primary Long vs. Short Coverage with Drug-Eluting Stents for Long Femoropopliteal Artery Disease II) study was a multicenter randomized controlled clinical trial comparing long DES implantation with full lesion coverage vs. spot DES implantation in patients with symptomatic FP artery disease. The major inclusion criteria were intermittent claudication or symptoms of critical limb-threatening ischemia (CLTI, Rutherford categories 2–5), FP artery lesions with stenosis > 50% and/or lesion length > 150 mm, and at least 1 patent runoff vessel. The major exclusion criteria were age > 85 years, severe CLTI (Rutherford category 6), acute limb ischemia, previous bypass surgery or stenting of the target FP artery, untreated inflow disease of the ipsilateral pelvic arteries (> 50% stenosis or occlusion), diseased distal popliteal artery (P2 or P3 segment) with stenosis > 50%, or a major bleeding event within the previous 2 months.

Based on the sample size calculation, the study was designed to enroll a total of 220 participants, randomized in a 1:1 manner. However, we decided to discontinue study enrollment in August 2019 because interim analysis showed a clinically relevant difference in outcomes between the study groups; the data and safety monitoring board for this study suggested early termination at that time. The trial protocol was approved by the local institutional review board of each participating center and was registered at www.clinicaltrials.gov (NCT02701881).

Interventions

For all procedures, the patients received local anesthesia, which was supplemented with intravenous sedation and analgesia when required. Either ipsilateral or contralateral femoral puncture was performed, depending on the location of the target lesion. A 6F or 7F short introducer sheath (Terumo, Tokyo, Japan) was used for the ipsilateral approach, and a 6F to 7F long sheath (Balkin or Ansel; Cook Inc., Bloomington, IN, USA) was employed for the crossover approach. After the guidewire was passed through the target lesion, web-based randomization was performed. Patients were stratified according to the enrolling site and severity of ischemic symptoms (claudication vs. CTLI) and randomized to either the long stenting or spot stenting group. In cases of total occlusion, both intraluminal and subintimal approaches for

Abbreviations: DES, drug-eluting stents; FP, femoropopliteal; TLR, target lesion revascularization; TASC, Trans-Atlantic Inter-Society Consensus; ABI, ankle-brachial index; CTA, computed tomography angiography; CLTI, chronic limb-threatening ischemia; PTA, percutaneous transluminal angioplasty.

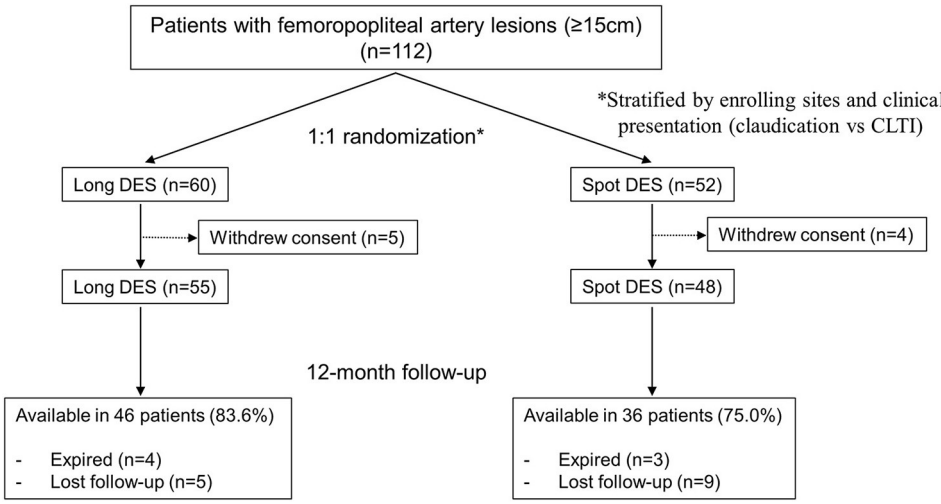

FIGURE 1
Patient flow diagram. CLTI, chronic limb-threatening ischemia; DES, drug-eluting stents.

TABLE 1 Baseline clinical characteristics.

Characteristic	Long DES ($n = 55$)	Spot DES ($n = 48$)	*P*-value
Age (y)	70.8 ± 8.3	71.1 ± 9.2	0.861
Male	47 (85.5)	38 (79.2)	0.402
BMI (kg/m^2)	23.3 ± 3.2	23.0 ± 3.4	0.599
Hypertension	41 (74.5)	37 (77.1)	0.764
Diabetes mellitus	32 (58.2)	31 (64.6)	0.506
Hypercholesterolemia (TC > 200 mg/dL)	18 (32.7)	17 (35.4)	0.458
Chronic kidney disease	13 (23.6)	10 (20.8)	0.917
Hemodialysis	7 (12.7)	4 (8.3)	0.761
Coronary artery disease	29 (52.7)	28 (58.3)	0.568
Current smoker	16 (29.1)	17 (35.4)	0.635
Previous stroke	6 (10.9)	9 (18.8)	0.260
CLTI	17 (31.5)	11 (22.9)	0.333
Medication at discharge			
Aspirin	50 (90.9)	44 (91.7)	0.892
Clopidogrel	50 (90.9)	43 (89.6)	0.821
Cilostazol	21 (38.2)	15 (31.3)	0.462
Warfarin/DOAC	0 (0)	4 (8.3)	0.044
Statin	44 (80.0)	38 (79.2)	0.917

Data are mean ± standard deviation or count (percentage).
BMI, body mass index; CLTI, chronic limb-threatening ischemia; DES, drug-eluting stents; DOAC, direct oral anticoagulant; TC, total cholesterol.

recanalization were permitted. In both groups, predilation of the target lesion was performed prior to stent implantation. In the long DES group, stents were implanted to extend 10 mm proximally and distally from the margins of the target lesion with a luminal narrowing of > 50%. When multiple stents were required, margins of the stents overlapped by at least 10 mm. In the spot DES group, stents were implanted only in those segments with residual stenosis > 30% or a flow-limiting dissection after repeated predilation. In cases of an optimal result after predilation (without significant residual stenosis or flow-limiting dissection), a single stent was implanted to cover the most stenotic segment or the proximal stump of the occlusion before predilation. In both groups, Zilver PTX with a diameter of 5–7 mm was used for stenting at the FP target lesions. Postdilation with an up to 10% oversized balloon was performed when the residual stenosis was > 30%. After the procedure, aspirin (100 mg/day) was maintained indefinitely, and clopidogrel (75 mg/day) was prescribed for at least 6 months.

Follow-up

We followed the patients clinically at 1, 3, 6, 9, 12, and 24 months after the procedure, according to the study schedule. Ankle-brachial index (ABI) was obtained at hospital discharge and at 6, 12, and 24 months post-procedure. An imaging study, such as intra-arterial angiography, computed tomography angiography (CTA), or duplex ultrasound, was performed at 12 months or if there was a > 0.15 decrement in ABI or worsening symptoms, as reflected by a change in Rutherford category.

Study endpoints and definitions

Technical success was defined as recanalization of the target lesion, with residual stenosis of 30% or less and no flow-limiting dissection. The primary endpoint was the primary patency at 12

TABLE 2 Lesion and procedural data.

Variable	Long DES ($n = 55$)	Spot DES ($n = 48$)	*P*-value
TASC II lesion type			0.338
B	2 (3.6)	5 (10.4)	
C	42 (76.4)	36 (75.0)	
D	11 (20.0)	7 (14.6)	
Lesion length (mm)	245.1 ± 58.7	238.6 ± 63.7	0.597
Total occlusion	46 (85.2)	35 (72.9)	0.126
Severe calcification	10 (18.2)	8 (16.7)	0.840
Combined treatment			
Iliac lesion	7 (12.7)	9 (18.8)	0.400
BTK lesion	7 (12.7)	8 (16.7)	0.572
Subintimal approach	28 (50.9)	26 (54.2)	0.741
Atherectomy	2 (3.6)	0 (0)	0.497
Number of implanted stents	2.5 ± 0.8	1.5 ± 0.6	0.024
Total stented length (mm)	225.6 ± 67.2	131.3 ± 48.7	< 0.001
Full lesion coverage with stents	55 (100.0)	7 (14.6)	< 0.001
Postdilation	10 (18.2)	16 (34.0)	0.067
Technical success	55 (100.0)	48 (100.0)	1.000
Pre-procedure ABI	0.62 ± 0.23	0.55 ± 0.21	0.178
Post-procedure ABI	0.87 ± 0.17	0.84 ± 0.19	0.507
Complications			
Major	0 (0)	1 (2.1)	0.466
Access site bleeding	0 (0)	2 (4.2)	0.215
Vascular perforation	0 (0)	0 (0)	-
Distal embolization	1 (1.8)	0 (0)	1.000

Data are mean ± standard deviation or count (percentage).
ABI, ankle-brachial index; BTK, below-the-knee; DES, drug-eluting stents; TASC, Trans-Atlantic Inter-Society Consensus.

months after the procedure, according to the stenting strategy. Primary patency was defined as treated FP lesions without > 50% restenosis, as assessed by an imaging study (intra-arterial angiography, CTA, or duplex ultrasound). A lesion/adjacent segment velocity ratio > 2.4 by duplex was considered indicative of > 50% restenosis (11). The secondary endpoint was freedom from clinically driven target lesion revascularization (TLR). Clinically driven TLR was performed for restenotic lesions with both worsening symptoms and a > 0.15 decrement in ABI. Major complications were defined as any event that was either fatal or required surgical treatment or re-hospitalization within 30 days after the procedure.

Statistical analysis

Continuous data are presented as mean ± standard deviation, and categorical data are presented as count (percentage). Patient, lesion, and procedural data were compared between the 2 groups using the Fisher exact test or $\chi 2$ test for categorical data or the Student's *t*-test for continuous data. We estimated the primary and secondary endpoints using Kaplan-Meier survival analysis and compared the results of the two groups using the log-rank test. We performed univariate analysis using Cox proportional hazards regression to identify potential risk factors (clinical and procedural variables) for restenosis at 12 months post-procedure. Variables achieving a *p*-value < 0.15 in univariate analysis were entered into the multivariate analysis. *P*-values < 0.05 were considered statistically significant. All statistical analyses were performed using SPSS (version 25.0; IBM, Chicago, IL, USA).

Results

Baseline clinical data

From January 2016 through May 2019, a total of 112 patients were enrolled in this study and randomized to either the long DES group or spot DES group. After excluding 9 patients because of inclusion and exclusion criteria violations, 103 patients (55 in the long DES group and 48 in the spot DES group) were included in the final analysis, as shown in Figure 1.

Baseline clinical characteristics are summarized in Table 1. When considering all 103 patients, the mean patient age was 70.9 ± 8.6 years, and the majority (82.5%) of study participants were male. Diabetes mellitus and chronic kidney disease were present in 61.2 and 34.0% of patients, respectively. CLTI was present in 27.2% of participants. Baseline clinical characteristics did not differ significantly between groups. Medications at discharge also did not differ between groups, except for anticoagulants (warfarin or direct oral anticoagulants), which were prescribed more frequently in the spot DES group (0% vs. 8.3%, $p = 0.044$).

Lesion and procedural data

Lesion and procedural characteristics are presented in Table 2. When considering all 103 patients, the mean lesion length was 242.7 ± 64.5 mm. Total occlusion and severely calcified lesions were present in 78.6 and 17.5% of participants, respectively. Lesion length and rates of total occlusion, severely calcified lesions, and Trans-Atlantic Inter-Society Consensus (TASC) II lesion types did not differ significantly between groups.

Procedural success was achieved in all patients. However, 7 patients (14.6%) in the spot DES group underwent unplanned full-lesion stent coverage because of severe dissection. The number of implanted stents was significantly higher (2.5 ± 0.8 vs. 1.5 ± 0.6, $p = 0.024$) and the total stented length was significantly longer (225.6 ± 67.2 mm vs. 131.3 ± 48.7 mm, $p < 0.001$) in the long DES group than in the spot DES

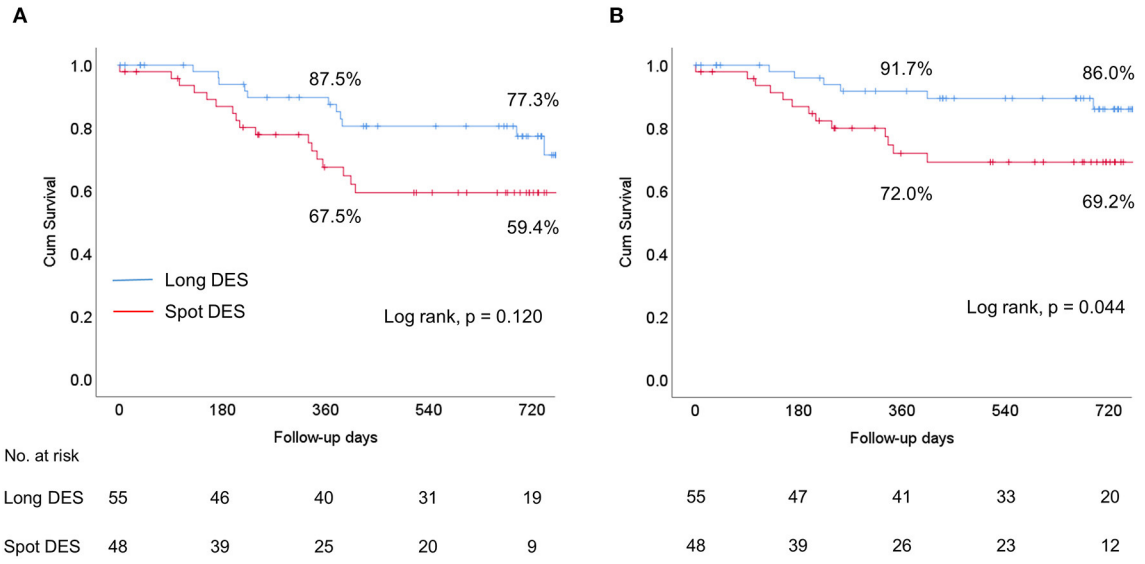

FIGURE 2
Kaplan-Meier survival curves comparing the long drug-eluting stent (DES) group vs. the spot DES group. **(A)** Primary patency. **(B)** Target lesion revascularization (TLR)-free survival. Cum, cumulative.

group. In addition, there was a trend toward more frequent postdilation performed in the short DES group than in the long DES group (34% vs. 18.2%, $p = 0.067$). Atherectomy using Turbohawk (Medtronic, Santa Rosa, CA, USA) was performed in two patients of the long DES group. Embolic protection device was not utilized in this study.

ABI was not significantly different between the two groups before or after the procedure. There were 2 cases of access site bleeding in the spot DES group, 1 of which required surgical repair and was thus considered a major complication. There was 1 case of distal embolization in the long DES group, which was managed with endovascular embolectomy.

Clinical outcomes

The mean duration of clinical follow-up was 535.8 ± 251.2 days. A total of 84 patients completed 1 year of follow-up: 46 in the long DES group and 38 in the spot DES group (Figure 1). In the long DES group, there were 4 deaths (2 from a cardiovascular cause; 2 from an unknown cause) and 5 cases of loss to follow-up. In the spot DES group, there were 3 deaths (1 from a non-cardiovascular cause; 2 from an unknown cause) and 9 cases of loss to follow-up.

There was a trend toward higher primary patency in the long DES group than in the spot DES group (Figure 2A). Specifically, the primary patency rates were 87.5% at 12 months and 77.3% at 24 months in the long DES group and 67.5% at 12 months and 59.4% at 24 months in the spot DES group ($p = 0.120$). Survival free from TLR was significantly higher in the long DES group than in the spot DES group (Figure 2B). Specifically, the TLR-free survival rates were 91.7% at 12 months and 86.0% at 24 months in the long DES group and 72.0% at 12 months and 69.2% at 24 months in the spot DES group ($p = 0.044$). In multivariate Cox regression analysis, spot DES [hazard ratio (HR) 2.42, 95% confidence interval (CI) 1.14–5.12, $p = 0.021$] and postdilation (HR 0.27, 95% CI 0.09–0.79, $p = 0.018$) were identified as independent predictors for loss of patency at 12 months post-procedure (Table 3).

Discussion

The main findings of this study were that the long DES strategy was more effective than the spot DES approach for endovascular treatment of long FP lesions in terms of primary patency and freedom from TLR.

Zilver PTX, a paclitaxel-eluting stent, has shown excellent 12-month primary patency rates ranging from 86.4 to 90.4% in clinical trials with mean FP lesion lengths < 150 mm. However, there have been only a few studies investigating the efficacy of Zliver PTX in very long FP lesions (> 200 mm). A substudy of the Zilver PTX single-arm study involving lesions with a mean length of 226 mm demonstrated a primary patency rate of 77.6% and TLR-free survival rate of 88% at 12 months (12). Other studies reported 12-month primary patency rates ranging from 60 to 74.5% and TLR-free survival rates of 79% and 85.4% for very long lesions (13, 14). Thus, primary patency rates of DES appear to decrease with increasing lesion length.

TABLE 3 Predictors of loss of patency at 12 months in Cox proportional hazards regression analysis.

Factor	Univariate analysis		Multivariate analysis	
	HR (95% CI)	*P*-value	HR (95% CI)	*P*-value
Age	0.98 (0.94–1.02)	0.279		
Male	1.11 (0.42–2.59)	0.829		
Body mass index	1.04 (0.93–1.17)	0.448		
Hypertension	1.21 (0.52–2.84)	0.658		
Diabetes mellitus	1.82 (0.82–4.01)	0.140	1.76 (0.77–4.03)	0.180
Hypercholesterolemia	1.20 (0.55–2.62)	0.652		
Current smokers	1.43 (0.67–3.04)	0.361		
Chronic kidney disease	1.27 (0.59–2.74)	0.538		
Hemodialysis	2.70 (1.02–7.18)	0.046	2.22 (0.80–6.12)	0.124
Coronary artery disease	1.06 (0.51–2.19)	0.872		
Previous stroke	1.24 (0.43–3.58)	0.694		
CLTI	0.87 (0.35–2.14)	0.753		
Pre-procedure ABI	0.66 (0.10–4.50)	0.669		
Lesion length (per 10 mm)	0.97 (0.91–1.04)	0.417		
Total occlusion	1.10 (0.42–2.90)	0.850		
TASC II D lesion	1.50 (0.64–3.53)	0.354		
Subintimal approach	1.08 (0.51–2.29)	0.842		
Combined iliac intervention	0.59 (0.18–1.97)	0.393		
Combined BTK intervention	1.00 (0.35–2.89)	0.997		
Spot DES	1.76 (0.85–3.64)	0.125	2.42 (1.14–5.12)	0.021
Postdilation	0.37 (0.13-1.06)	0.065	0.27 (0.09-0.79)	0.018
Oral anticoagulants	1.57 (0.55–4.47)	0.397		

ABI, ankle-brachial index; BTK, below-the-knee; CI, confidence interval; CLTI, chronic limb-threatening ischemia; DES, drug-eluting stents; HR, hazard ratio; TASC, Trans-Atlantic Inter-Society Consensus.

In the current study, the mean lesion length of the study population was 242 mm, and the primary patency rates for the entire population were 78.0% at 12 months and 68.8% at 24 months. These rates are generally comparable to those of previous studies. However, we found that the primary patency rate at 12 months was well maintained at 87.5% in the long stent group but fell to 67.5% in the spot stent group. There have been only a few studies that reported on the outcomes of spot stenting. In a retrospective study, Tomoi et al. showed a lower 3-year patency rate with spot stenting compared with full coverage stenting for FP lesions (15). However, this study used not only DES but also bare-metal nitinol stent. The study concluded that spot stenting was non-inferior to full coverage stenting for primary patency at lesion length ≥138 mm. By contrast, Iida et al. found in a prospective single-arm study using fluoropolymer-based DES study (Eluvia, Boston Scientific) that spot stenting was associated with an increased risk of 12-month restenosis with odds ratio of 2.44 (16). Whether full jacket stenting was performed in the previous studies is unknown, except for the small retrospective study by Phillips et al. (14). In their study, the 12-month primary patency of full jacket Zilver PTX stenting for lesions > 200 mm was only 60%. Differences in various factors (e.g., baseline clinical and lesion characteristics, medications) may have contributed to discrepancies in results between the present study and previous studies. In particular, differences in the inclusion of distal popliteal artery lesions and in-stent restenosis might have led to varying reported outcomes for Zilver PTX. Stenting in the distal popliteal artery is known to be associated with an increased risk of restenosis (13, 17), and in the present study, we excluded patients with FP lesions involving P2 or P3 popliteal artery segments. By contrast, in the study of Phillips et al., all lesions > 200 mm were TASC II D lesions; thus, it is likely that a large proportion of their study subjects had distal popliteal artery involvement. Additionally, in-stent restenosis accounted for 14.4%−29% of lesions in previous studies, whereas we excluded all patients with in-stent restenosis. Repeated endovascular treatment of in-stent restenosis lesions is associated with generally poorer outcomes than treatment of *de-novo* lesions (18). Our group previously reported that using bare nitinol stents, spot stenting achieved better outcomes than long stenting in the treatment of long FP lesions (9, 10). Therefore, our current results appear to contradict our prior findings. However, there are two principal differences between the present and previous studies. First, DES were used in all

patients in the current study. Second, lesions with distal popliteal artery involvement were excluded in the present study but were included in our previous studies. Compared to bare metal stents, DES have been shown to more effectively inhibit neointimal proliferation in coronary and peripheral arteries and were able to reduce the restenosis rate, even when long "full jacket" stents were implanted (7, 19, 20). However, when DES were implanted in a segment shorter than the total lesion length, there was a higher possibility of restenosis in the non-stented segment treated with balloon angioplasty alone. Furthermore, the stent border zones that were injured by balloon angioplasty but not covered by DES exhibited more active neointimal proliferation and an increased risk of restenosis (21, 22). This phenomenon, known as a geographic miss, has been described as an important factor leading to stent failure in coronary artery interventions and likely accounts for the poorer results with spot stenting in this study. Based on the present study results, spot stenting using DES after plain balloon angioplasty appears to be inappropriate. However, provisional spot stenting after drug-coated balloon (DCB) has shown to be effective according to clinical trials on DCBs for FP artery lesions (23, 24). Thus, it would be interesting to compare DCB with spot stenting vs. full metal jacket stenting using DES in the future studies.

This study has several limitations. First, it was underpowered because of insufficient subject enrollment. This was the consequence of the early termination of the study, which was recommended by the data and safety monitoring board because interim analysis revealed a clinically relevant difference in outcomes between study groups. Second, spot stenting was defined arbitrarily. We did not set a limit on the stented length or stent-to-lesion length ratio. Third, we did not routinely perform intravascular ultrasound during the procedure to verify subintimal passage of the wires. Fourth, the quality of life before and after the intervention was not investigated because there were many elderly patients who could not give an appropriate answer to the questionnaire due to their comorbidities.

Conclusions

Long DES was more effective for treating diffuse long FP lesions than spot DES in terms of primary patency and freedom from TLR. These results suggest that when treating FP disease with DES, lesions should be fully covered by these stents to achieve better outcomes.

Data availability statement

The original contributions presented in the study are included in the article/supplementary material, further inquiries can be directed to the corresponding authors.

Author contributions

Y-GK and D-HC: conception, design, and overall responsibility. J-IP and Y-GK: analysis, interpretation, and writing the article. Y-GK, D-HC, Y-JL, S-JL, S-JH, C-MA, J-SK, B-KK, M-KH, C-WY, S-WR, J-KP, P-KM, C-HY, S-RL, and S-HP: data collection. All authors contributed to the article and approved the submitted version.

Funding

This study was supported by grants from Cook Medical Korea; the Korea Health Technology R&D Project through the Korea Health Industry Development Institute (KHIDI) (No. HI20C1566) and the Bio & Medical Technology Development Program of the National Research Foundation & MSIT (No.2020M3A9I4038455); the Patient-Centered Clinical Research Coordinating Center (PACEN) funded by the Ministry of Health & Welfare, Republic of Korea (HC20C0081); and the Korea Medical Device Development Fund funded by the Korean government (202011B29-03, 202011D12-02) and the Cardiovascular Research Center (Seoul, Korea).

Acknowledgments

The authors thank the investigators, trial and data management staff, and study coordinators.

Conflict of interest

Y-GK and D-HC received institutional research grants from Cook Medical, Medtronic, Boston Scientific, Samjin Pharm, Korea United Pharm, Dong-A Pharm, and Otsuka Korea. None of these companies, including Cook Medical, were involved in developing study protocols or study process of PARADE II.

The remaining authors declare that the research was conducted in the absence of any commercial or financial relationships that could be construed as a potential conflict of interest.

Publisher's note

References

1. Laird JR, Katzen BT, Scheinert D, Lammer J, Carpenter J, Buchbinder M, et al. Nitinol stent implantation versus balloon angioplasty for lesions in the superficial femoral artery and proximal popliteal artery: twelve-month results from the RESILIENT randomized trial. *Circ Cardiovasc Interv.* (2010) 3:267–76. doi: 10.1161/CIRCINTERVENTIONS.109.903468

2. Schillinger M, Sabeti S, Dick P, Amighi J, Mlekusch W, Schlager O, et al. Sustained benefit at 2 years of primary femoropopliteal stenting compared with balloon angioplasty with optional stenting. *Circulation.* (2007) 115:2745–9. doi: 10.1161/CIRCULATIONAHA.107.688341

3. Schillinger M, Sabeti S, Loewe C, Dick P, Amighi J, Mlekusch W, et al. Balloon angioplasty versus implantation of nitinol stents in the superficial femoral artery. *N Engl J Med.* (2006) 354:1879–88. doi: 10.1056/NEJMoa051303

4. Acin F, de Haro J, Bleda S, Varela C, Esparza L. Primary nitinol stenting in femoropopliteal occlusive disease: a meta-analysis of randomized controlled trials. *J Endovasc Ther.* (2012) 19:585–95. doi: 10.1583/JEVT-12-3898R.1

5. Dake MD, Van Alstine WG, Zhou Q, Ragheb AO. Polymer-free paclitaxel-coated Zilver PTX Stents–evaluation of pharmacokinetics and comparative safety in porcine arteries. *J Vasc Interv Radiol.* (2011) 22:603–10. doi: 10.1016/j.jvir.2010.12.027

6. Dake MD, Scheinert D, Tepe G, Tessarek J, Fanelli F, Bosiers M, et al. Nitinol stents with polymer-free paclitaxel coating for lesions in the superficial femoral and popliteal arteries above the knee: twelve-month safety and effectiveness results from the Zilver PTX single-arm clinical study. *J Endovasc Ther.* (2011) 18:613–23. doi: 10.1583/11-3560.1

7. Dake MD, Ansel GM, Jaff MR, Ohki T, Saxon RR, Smouse HB, et al. Durable clinical effectiveness with paclitaxel-eluting stents in the femoropopliteal artery: 5-year results of the zilver PTX randomized trial. *Circulation.* (2016) 133:1472–83. doi: 10.1161/CIRCULATIONAHA.115.016900

8. Iida O, Takahara M, Soga Y, Nakano M, Yamauchi Y, Zen K, et al. 1-year results of the ZEPHYR Registry (zilver PTX for the femoral artery and proximal popliteal artery): predictors of restenosis. *JACC Cardiovasc Interv.* (2015) 8:1105–12. doi: 10.1016/j.jcin.2015.03.022

9. Ko YG, Ahn CM, Rha SW Yu CW, Park SH, Lee SJ, et al. Comparison of spot versus long stenting for femoropopliteal artery disease. *Ann Vasc Surg.* (2019) 58:101–7. doi: 10.1016/j.avsg.2018.11.023

10. Hong SJ, Ko YG, Shin DH, Kim JS, Kim BK, Choi D, et al. Outcomes of spot stenting versus long stenting after intentional subintimal approach for long chronic total occlusions of the femoropopliteal artery. *JACC Cardiovasc Interv.* (2015) 8:472–80. doi: 10.1016/j.jcin.2014.10.016

11. Diehm N, Pattynama PM, Jaff MR, Cremonesi A, Becker GJ, Hopkins LN, et al. Clinical endpoints in peripheral endovascular revascularization trials: a case for standardized definitions. *Eur J Vasc Endovasc Surg.* (2008) 36:409–19. doi: 10.1016/j.ejvs.2008.06.020

12. Bosiers M, Peeters P, Tessarek J, Deloose K, Strickler S. The Zilver® PTX® Single Arm Study: 12-month results from the TASC C/D lesion subgroup. *J Cardiovasc Surg (Torino).* (2013) 54:115–22.

13. Bosiers M, Setacci C, De Donato G, Torsello G, Silveira PG, Deloose K, et al. ZILVERPASS study: ZILVER PTX stent vs. bypass surgery in femoropopliteal lesions. *J Endovasc Ther.* (2020) 27:287–95. doi: 10.1177/1526602820902014

14. Phillips JA, Falls A, Kolluri R, Whipp A, Collins C, Mohir-Sadaai S, et al. Full drug-eluting stent jacket: two-year results of a single-center experience with zilver PTX stenting for long lesions in the femoropopliteal arteries. *J Endovasc Ther.* (2018) 25:295–301. doi: 10.1177/1526602818762805

15. Tomoi Y, Soga Y, Takahara M, Fujihara M, Iida O, Kawasaki D, et al. Spot stenting versus full coverage stenting after endovascular therapy for femoropopliteal artery lesions. *J Vasc Surg.* (2019) 70:1166–76. doi: 10.1016/j.jvs.2018.12.044

16. Iida O, Takahara M, Soga Y, Yamaoka T, Fujihara M, Kawasaki D, et al. 1-year outcomes of fluoropolymer-based drug-eluting stent in femoropopliteal practice: predictors of restenosis and aneurysmal degeneration. *JACC Cardiovasc Interv.* (2022) 15:630–8. doi: 10.1016/j.jcin.2022.01.019

17. Baril DT, Chaer RA, Rhee RY, Makaroun MS, Marone LK. Endovascular interventions for TASC II D femoropopliteal lesions. *J Vasc Surg.* (2010) 51:1406–12. doi: 10.1016/j.jvs.2010.01.062

18. Varela DL, Armstrong EJ. Endovascular management of femoropopliteal in-stent restenosis: a systematic review. *Cardiovasc Revasc Med.* (2019) 20:915–25. doi: 10.1016/j.carrev.2018.10.028

19. Marx SO, Totary-Jain H, Marks AR. Vascular smooth muscle cell proliferation in restenosis. *Circ Cardiovasc Interv.* (2011) 4:104–11. doi: 10.1161/CIRCINTERVENTIONS.110.957332

20. Grube E, Silber S, Hauptmann KE, Mueller R, Buellesfeld L, Gerckens U, et al. TAXUS I: six- and twelve-month results from a randomized, double-blind trial on a slow-release paclitaxel-eluting stent for de novo coronary lesions. *Circulation.* (2003) 107:38–42. doi: 10.1161/01.CIR.0000047700.58683.A1

21. Costa MA, Angiolillo DJ, Tannenbaum M, Driesman M, Chu A, Patterson J, et al. Impact of stent deployment procedural factors on long-term effectiveness and safety of sirolimus-eluting stents (final results of the multicenter prospective STLLR trial). *Am J Cardiol.* (2008) 101:1704–11. doi: 10.1016/j.amjcard.2008.02.053

22. Calvert PA, Brown AJ, Hoole SP, Obaid DR, West NE, Bennett MR. Geographical miss is associated with vulnerable plaque and increased major adverse cardiovascular events in patients with myocardial infarction. *Catheter Cardiovasc Interv.* (2016) 88:340–7. doi: 10.1002/ccd.26275

23. Thieme M, Von Bilderling P, Paetzel C, Karnabatidis D, Perez Delgado J, Lichtenberg M. The 24-month results of the lutonix global SFA registry: worldwide experience with lutonix drug-coated balloon. *JACC Cardiovasc Interv.* (2017) 10:1682–90. doi: 10.1016/j.jcin.2017.04.041

24. Scheinert D, Micari A, Brodmann M, Tepe G, Peeters P, Jaff MR, et al. Drug-Coated balloon treatment for femoropopliteal Artery Disease. *Circ Cardiovasc Interv.* (2018) 11:e005654. doi: 10.1161/CIRCINTERVENTIONS.117.005654

frontiers | Frontiers in Cardiovascular Medicine

TYPE Original Research
PUBLISHED 28 October 2022
DOI 10.3389/fcvm.2022.982209

OPEN ACCESS

EDITED BY
Stéphanie Barrere-Lemaire,
INSERM U1191 Institut de Génomique Fonctionnelle (IGF), France

REVIEWED BY
Germaine Cornelissen Guillaume,
University of Minnesota, United States
Sang-Hwan Do,
Seoul National University Bundang Hospital, South Korea
Kroekkiat Chinda,
Naresuan University, Thailand

*CORRESPONDENCE
Tobias Eckle
tobias.eckle@cuanschutz.edu

SPECIALTY SECTION
This article was submitted to Cardiovascular Therapeutics, a section of the journal Frontiers in Cardiovascular Medicine

RECEIVED 30 June 2022
ACCEPTED 10 October 2022
PUBLISHED 28 October 2022

CITATION
Prin M, Pattee J, Douin DJ, Scott BK, Ginde AA and Eckle T (2022) Time-of-day dependent effects of midazolam administration on myocardial injury in non-cardiac surgery.
Front. Cardiovasc. Med. 9:982209.
doi: 10.3389/fcvm.2022.982209

Time-of-day dependent effects of midazolam administration on myocardial injury in non-cardiac surgery

Meghan Prin, Jack Pattee, David J. Douin, Benjamin K. Scott, Adit A. Ginde and Tobias Eckle*

Department of Anesthesiology, University of Colorado Anschutz Medical Campus, Aurora, CO, United States

Background: Animal studies have shown that midazolam can increase vulnerability to cardiac ischemia, potentially *via* circadian-mediated mechanisms. We hypothesized that perioperative midazolam administration is associated with an increased incidence of myocardial injury in patients undergoing non-cardiac surgery (MINS) and that circadian biology may underlie this relationship.

Methods: We analyzed intraoperative data from the Multicenter Perioperative Outcomes Group for the occurrence of MINS across 50 institutions from 2014 to 2019. The primary outcome was the occurrence of MINS. MINS was defined as having at least one troponin-I lab value $\geq$0.03 ng/ml from anesthesia start to 72 h after anesthesia end. To account for bias, propensity scores and inverse probability of treatment weighting were applied.

Results: A total of 1,773,118 cases were available for analysis. Of these subjects, 951,345 (53.7%) received midazolam perioperatively, and 16,404 (0.93%) met criteria for perioperative MINS. There was no association between perioperative midazolam administration and risk of MINS in the study population as a whole (odds ratio (OR) 0.98, confidence interval (CI) [0.94, 1.01]). However, we found a strong association between midazolam administration and risk of MINS when surgery occurred overnight (OR 3.52, CI [3.10, 4.00]) or when surgery occurred in ASA 1 or 2 patients (OR 1.25, CI [1.13, 1.39]).

Conclusion: Perioperative midazolam administration may not pose a significant risk for MINS occurrence. However, midazolam administration at night and in healthier patients could increase MINS, which warrants further clinical investigation with an emphasis on circadian biology.

KEYWORDS

circadian rhythms, midazolam, chronobiology, MINS, perioperative outcome, general anesthesia, MPOG, large dataset

Introduction

In the perioperative setting for non-cardiac surgery, the incidence of myocardial injury in patients undergoing non-cardiac surgery (MINS) has been reported to be as high as 16% (1). Considering that >300 million surgeries are performed annually, and that changing demographics and evolving medical practices have resulted in an increasing number of surgical patients with elevated cardiovascular risk (2), these estimates are of paramount clinical significance (3). In fact, MINS is associated with substantial mortality. A recent single-center 10-year retrospective analysis reported 30-day mortality of 31% and 1-year mortality of 42% in patients who experienced a perioperative myocardial ischemia (MI) and underwent percutaneous revascularization after non-cardiac surgery (4). Strategies to reduce the incidence of perioperative myocardial ischemia and reperfusion injury are urgently needed (5).

Midazolam, a benzodiazepine which binds to receptor sites in the gamma-aminobutyric acid (GABA) system, first came into use in 1976 and is on the World Health Organization's List of Essential Medicines. It is the most commonly used pre-procedural sedative-hypnotic worldwide (6), but it is also associated with significant clinical complications, which are most clearly described in the critical care literature. A growing body of evidence shows that benzodiazepines are associated with poor patient outcomes including delirium, duration of mechanical ventilation, and ICU length of stay (7). Benzodiazepine infusions, as compared to propofol, are also linked to an increased likelihood of death among patients who receive mechanical ventilation (8). Because of its adverse associations, midazolam is no longer recommended as a first-line sedative on critical care units (9–12). Whether midazolam use prior to surgical procedures is similarly associated with adverse outcomes is unknown.

Recently, our group determined that the circadian rhythm protein Period 2 (PER2) provides robust cardio-protection from myocardial ischemia (MI) in an animal model (13, 14). We also demonstrated that midazolam increases vulnerability to cardiac ischemia by downregulating PER2 (15). Because perioperative MI is the most common perioperative cardiovascular complication and sedative-hypnotics can alter the expression of PER2, a sedative-mediated downregulation of PER2 could be detrimental if myocardial ischemia and reperfusion occurs (16–18). As a first effort in studying this association in humans, we hypothesized that midazolam administration during the perioperative period would be associated with an increased incidence of MINS and that this relationship depends on the 24-h cycle of human circadian physiology.

Materials and methods

Approvals

Approval was obtained, and waiver of written informed consent was granted from the Institutional Review Board [Colorado Multiple Institutional Review Board (COMIRB)] at the University of Colorado Denver, USA (#09-0674). In keeping with the Multicenter Perioperative Outcomes Group Bylaws at the University of Michigan, this study protocol was presented to the Multicenter Perioperative Outcomes Group Perioperative Clinical Research Committee and was approved on August 12, 2019. We followed the Strengthening the Reporting of Observational Studies in Epidemiology (STROBE) checklist in developing this manuscript.

Data source and study inclusion and exclusion criteria

The Multicenter Perioperative Outcomes Group (MPOG) database, as well as methods for data entry, validation, and quality assurance, have been previously described (19) and have been used for multiple published observational studies (20, 21). MPOG data are drawn from cases documented in the Electronic Health Record at participating sites. These data are extracted, standardized, joined to additional laboratory, billing, and diagnosis coding data, and de-identified except for date of service, producing a limited dataset.

Data for 2,740,183 subjects undergoing non-cardiac surgical procedures between 1 January 2014, and 31 December 2019, were obtained from MPOG. Various preoperative demographic and comorbidity variables were available, as were data on the timing and dosage of midazolam administrations and the timing and magnitude of troponin-I lab values. From this sample of 2,740,183 subjects, we excluded all subjects who met one or more of the following exclusion criteria: emergent cases, outpatient procedures, patients admitted for less than 24 h, patients with ASA value 5 or 6, preoperatively intubated patients, patients with preoperative troponin elevation (defined as a recorded troponin I value ≥0.01 ng/ml within 42 days of the start of anesthesia), pre-induction vasopressor or inotrope infusion, intraoperative transfusion >4 units of blood, estimated blood loss >2000 ml, lung-transplant surgery (CPT code between 32850 and 32856), liver-transplant surgery (CPT code between 47133 and 47147), cardiac procedures (CPT code between 33016 and 33999), and individuals under 18 years of age. 2,264,900 subjects remained after applying these exclusion criteria.

Perioperative MINS was defined as having at least one troponin-I lab value ≥0.03 ng/ml in the period from anesthesia start to 72 h after anesthesia end. Perioperative

midazolam administration was defined as having at least one documented midazolam administration in the period from 2 h before anesthesia start to anesthesia end. The mean dose of midazolam was 2.3 mg.

As typical for large observational data extracted from electronic health records, there was some amount of missingness in our data. Of those 2,264,900 subjects who met the inclusion criteria, 9.76% had missing information regarding BMI and 0.05% regarding sex. We opted to only include those subjects without missingness in our analytic dataset. Given that our sample size was substantial, we were not concerned with efficiency loss due to a complete case analysis as opposed to an imputation approach. Recommendations from literature indicate that, as long as there is no missingness in an effect modifier variable (midazolam administration, time of day, or ASA class), complete case analysis will be unbiased regardless of the missingness pattern of the covariate (i.e., missing completely at random, missing at random, or not missing at random) (22). In this case, as BMI was not an effect modifier in our analysis, a complete case analysis will not bias our inference. Our final analytic dataset consisted of 1,773,118 subjects. Of these subjects, 16,404 (0.93%) experienced perioperative MINS, and 951,345 (53.7%) had a perioperative administration of midazolam (mean dose 2.3 mg).

Patient variables

Complete data from the Multicenter Perioperative Outcomes Group database included age, sex, body mass, institution, American Society of Anesthesiologists (ASA; Schaumburg, Illinois) physical status and various comorbidities (**Figure 1**).

Outcomes of interest

The primary outcome of our study was perioperative MINS in relation to human circadian physiology.

Statistical analysis

Data are presented as coefficient estimates (adjusted odds ratios) with confidence intervals. To account for possible bias and confounders in the observational data, propensity scores were used to balance the distribution of baseline covariates between the population with and without perioperative midazolam administration (23, 24). Specifically, the method of inverse probability of treatment weighting was used. The propensity score and the associated inverse probability of treatment weights were estimated in R *via* the "WeightIt" package (version 0.12.0). The propensity score was estimated *via* logistic regression using all baseline covariates as predictors, with no higher-order or interaction effects. A recounting of the baseline covariates and their stratified distribution in the analytic dataset is presented in **Figure 1**. All covariates listed in **Figure 1** were included as predictors in the propensity-score model. Whether or not those covariates listed in **Figure 1** are technically considered confounders or not, however, is immaterial (25). Nevertheless, we note here that their inclusion in the propensity score model and the subsequent reweighting procedure precludes any potential confounding effect of these variables on our inferences of interest. Comorbidities with <5% prevalence were excluded from **Figure 1** and the ensuing propensity-score model. Only covariates that were measured before the administration of midazolam were included in the propensity score model, following established practice (26). This precluded the inclusion of perioperative variables such as intraoperative blood pressure. Balance diagnostics were assessed *via* the "WeightIt" package, and balance was assessed as standardized mean difference <0.1 (25).

For assessing the effect of (binary) midazolam administration on perioperative MINS, we used a weighted logistic regression model with robust variance estimation, implemented in R *via* the "survey" package (version 4.1-1). For this analysis, stabilized inverse probability of treatment weights were used. Circadian physiology analyses, including assessment of potential effect modification of time of day or ASA class on the effect of midazolam administration on perioperative MINS, were conducted using marginal structural models with an interaction effect. The time of day was divided into daytime (between 6:00 and 18:00) and a nighttime period (between 18:00 and 06:00) based on anesthesia start. Marginal structural models were also estimated *via* weighted logistic regression with robust variance estimation *via* the R package "survey." For theses analyses *via* marginal structural models, weights were stabilized as per Section 12.5 of Hernán and Robins (27). This stabilization entails using the ratio of the probability of midazolam administration predicted by the modifier (e.g., time of day or ASA class) to the probability of midazolam administration predicted by all baseline covariates as weights in the marginal structural model. The form of the inverse probability of treatment weights was different for the analysis of the effect of midazolam administration on perioperative MINS and each of the analyses assessing the potential effect modification of time of day or ASA class on the effect of midazolam administration on perioperative MINS.

Per Hernán and Robins, whether the effect of exposure α on the outcome is modified by the particular covariate V while adjusting for the set of baseline covariates L, the following model is used: $E[Y|\alpha, V]$ $\beta_0\beta_1\alpha\beta_2 V\alpha\beta_3 V$ [1]. In order to isolate the causal effect of α (in our context, midazolam administration) on a binary outcome (in our context, MINS) while assessing potential effect modification by V (in our context, either time of day or ASA class), we estimated the above model in a weighted

	No MINS	MINS	SMD
n	1756714	16404	
Male Sex (%)	717723 (40.9)	9131 (55.7)	0.300
Age (mean (SD))	53.78 (18.19)	67.50 (14.31)	0.838
BMI (mean (SD))	29.84 (7.57)	28.81 (7.22)	0.139
ASA Class (%)			
1	51414 (2.9)	45 (0.3)	
2	699160 (39.8)	1650 (10.1)	
3	885152 (50.4)	9945 (60.6)	
4	120988 (6.9)	4764 (29.0)	
Inpatient Admission (%)	1266131 (72.1)	12871 (78.5)	0.148
Congestive Heart Failure (%)	115278 (6.6)	5126 (31.2)	0.664
Cardiac Arrhythmia (%)	295292 (16.8)	8575 (52.3)	0.804
Valvular Disease (%)	85788 (4.9)	3127 (19.1)	0.448
Peripheral Vascular Disorders (%)	127121 (7.2)	3828 (23.3)	0.459
Hypertension with Complications (%)	173025 (9.8)	5650 (34.4)	0.620
Hypertension without Complications (%)	653258 (37.2)	8488 (51.7)	0.296
Other Neurological Disorders (%)	118673 (6.8)	2561 (15.6)	0.284
Chronic Pulmonary Disease (%)	282961 (16.1)	4166 (25.4)	0.231
Diabetes Without Complications (%)	210304 (12.0)	3163 (19.3)	0.202
Hypothyroidism (%)	201509 (11.5)	2489 (15.2)	0.109
Renal Failure (%)	164418 (9.4)	4922 (30.0)	0.538
Liver Disease (%)	99057 (5.6)	1758 (10.7)	0.186
Metastatic Cancer (%)	159952 (9.1)	1827 (11.1)	0.067
Solid Tumor without Metastasis (%)	311463 (17.7)	3254 (19.8)	0.054
Coagulopathy (%)	106204 (6.0)	2908 (17.7)	0.367
Obesity (%)	361473 (20.6)	3343 (20.4)	0.005
Weight Loss (%)	137667 (7.8)	2989 (18.2)	0.312
Fluid and Electrolyte Disorders (%)	302901 (17.2)	8206 (50.0)	0.740
Depression (%)	272719 (15.5)	2841 (17.3)	0.048
Night Procedure (Versus Baseline of 'Day') (%)	160071 (9.1)	1179 (7.2)	0.070
Midazolam Administration (%)	944030 (53.7)	7315 (44.6)	0.184

FIGURE 1
Distribution of the propensity score stratified by whether subjects had perioperative myocardial injury in non-cardiac surgery (MINS). Standardized mean difference (SMD) column represents the standardized mean difference.

logistic regression framework *via* the R package survey (version 4.1-1), where weights are generated *via* propensity scoring. Weights are estimated as follows, per the recommendation of Hernán and Robins:

$$SW^{A}(V) = \frac{f[\alpha|V]}{f[\alpha|L]}[2]$$

We estimated two models in this framework: one to assess whether ASA class modifies the effect of midazolam administration on MINS, and one to assess whether time of day modifies the effect of midazolam administration on MINS. For the ASA model, V is the ASA class (either high: ASA 3 or 4, or ASA low: 1 or 2). For the time-of-day model, V is the time of day (either overnight or day). Thus, for each of these two paradigms, we estimated model [1] *via* weighted logistic regression using weights as described in [2]. For the ASA model, weights as described in [2] are equal to the ratio of the probability of midazolam administration (α) as predicted by ASA class (V) to the probability of midazolam administration as predicted by all baseline covariates including ASA class (L). For the time-of-day model, weights as described in [2] are equal to the ratio of the probability of midazolam administration (α) as predicted by time of day (V) to the probability of midazolam administration as predicted by all baseline covariates including time of day (L).

Power analysis

The large sample size (>1,400,000 non-cardiac patients) and an estimated incidence of 0.4% for MINS provided a >99% power at an alpha of 0.05 to detect any differences between the groups receiving midazolam or not receiving midazolam.

Results

Study populations and outcomes

Of 2,264,900 cases that were eligible for analysis, 491,782 were excluded for missing data. A total of 1,773,118 cases

	No Midazolam	Midazolam	SMD
n	821773	951345	
Male Sex (%)	288050 (35.1)	438804 (46.1)	0.227
Age (mean (SD))	53.10 (20.79)	54.60 (15.60)	0.082
BMI (mean (SD))	29.71 (7.44)	29.94 (7.68)	0.031
ASA.Class (%)			
1	18270 (2.2)	33189 (3.5)	
2	327554 (39.9)	373256 (39.2)	
3	404821 (49.3)	490276 (51.5)	
4	71128 (8.7)	54624 (5.7)	
Inpatient Admission (%)	644169 (78.4)	634833 (66.7)	0.264
Congestive Heart Failure (%)	69936 (8.5)	50468 (5.3)	0.127
Cardiac Arrhythmia (%)	158632 (19.3)	145235 (15.3)	0.107
Valvular Disease (%)	49968 (6.1)	38947 (4.1)	0.091
Peripheral Vascular Disorders (%)	67567 (8.2)	63382 (6.7)	0.059
Hypertension with Complications (%)	99606 (12.1)	79069 (8.3)	0.126
Hypertension without Complications (%)	279919 (34.1)	381827 (40.1)	0.126
Other Neurological Disorders (%)	69135 (8.4)	52099 (5.5)	0.116
Chronic Pulmonary Disease (%)	133125 (16.2)	154002 (16.2)	<0.001
Diabetes without Complications (%)	97123 (11.8)	116344 (12.2)	0.013
Hypothyroidism (%)	96636 (11.8)	107362 (11.3)	0.015
Renal Failure (%)	90637 (11.0)	78703 (8.3)	0.093
Liver Disease (%)	50626 (6.2)	50189 (5.3)	0.038
Metastatic.Cancer (%)	70148 (8.5)	91631 (9.6)	0.038
Solid Tumor without Metastasis (%)	129670 (15.8)	185047 (19.5)	0.096
Coagulopathy (%)	62094 (7.6)	47018 (4.9)	0.108
Obesity (%)	145085 (17.7)	219731 (23.1)	0.135
Weight.Loss (%)	77836 (9.5)	62820 (6.6)	0.106
Fluid and Electrolyte Disorders (%)	161078 (19.6)	150029 (15.8)	0.101
Depression (%)	123653 (15.0)	151907 (16.0)	0.025
Time of Day (%)			
Morning	386155 (47.0)	587852 (61.8)	
Afternoon	323938 (39.4)	341861 (35.9)	
Overnight	111680 (13.6)	21632 (2.3)	

FIGURE 2
Distribution of the propensity score stratified by whether subjects had perioperative midazolam. "SMD" column represents the standardized mean difference. The percentage of patients with a neuromuscular block only were 0.4% in the midazolam group and 1.6% in the non-midazolam group. The lab cTnI (ng/mL), used to define our myocardial injury in non-cardiac surgery (MINS) endpoint, was present in 4.7% of subjects in both the group with and without midazolam.

from 50 institutions were available. Figures 1, 2 describe the distribution of all baseline covariates in the study stratified by whether perioperative MINS occurred, or weather Midazolam was administered, respectively. The unadjusted rate of perioperative MINS in subjects with perioperative midazolam was 7,315 [0.77%], and the rate of MINS in subjects without perioperative midazolam was 9,089 [1.1%]. However, midazolam administration was associated with baseline covariates which indicated that these variables could be confounders. This association is displayed in Figure 3, which shows propensity scores stratified by whether subjects received perioperative midazolam. Therefore, propensity scores were used to balance the distribution of baseline covariates between the population with and without perioperative midazolam administration. Weighting the samples by the inverse probability of treatments successfully accounted for imbalances in the baseline covariates as illustrated in Figure 4. Following propensity score correction, on average, no association between perioperative midazolam administration and the rate of MINS was observed (OR 0.98, CI [0.94, 1.01]).

Based on observations that midazolam alters the risk for myocardial ischemia in a circadian-rhythm-dependent manner, we performed two circadian physiology related analyses: (1) time-of-day dependent effects of midazolam administration on MINS risk, as circadian mechanisms are expected to cause variations in MINS risk throughout a full circadian cycle (24 h); and (2) ASA classification dependent effects of midazolam administration on MINS risk, as higher ASA classification (3+4) include an older population with more comorbidities in whom

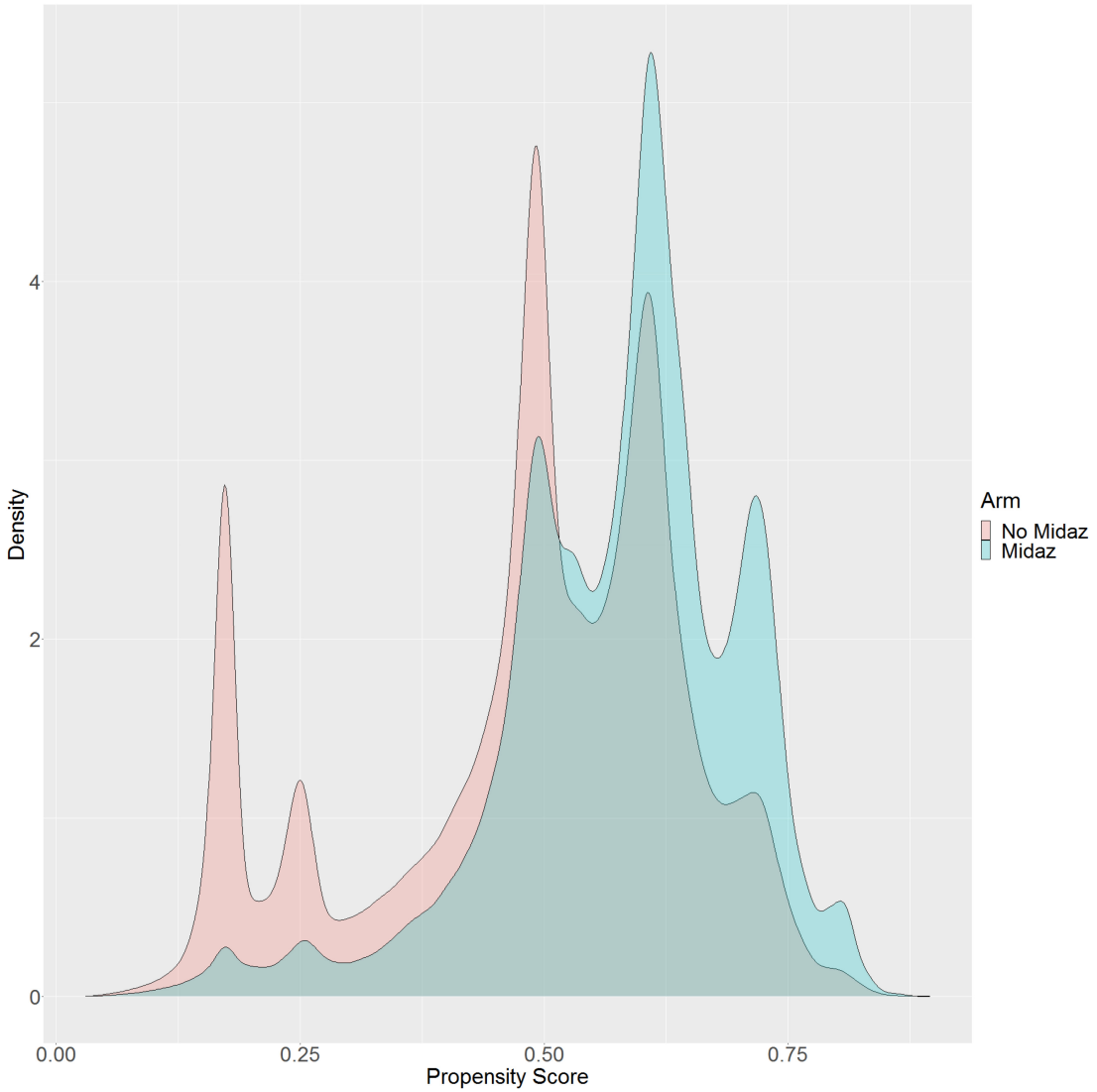

FIGURE 3
Distribution of the propensity score stratified by whether subjects received perioperative midazolam.

circadian rhythms are known to fade and become dysfunctional (28, 29).

As shown in Table 1A the baseline MINS risks significantly varied throughout the day. There was a significantly decreased baseline risk of MINS during overnight when compared to daytime surgeries (OR: 0.52, 95% CI [0.48, 0.56]).

The time-of-day dependent effect of midazolam administration on MINS occurrence is shown in Table 1B. The interaction between time-of-day and midazolam administration was significant (p 2 10^{-16}), demonstrating that the effect of midazolam on MINS occurrence was modified by the time-of-day. While midazolam administration during the daytime decreased the risk for MINS (OR 0.84, 95% CI [0.80, 0.87], the administration of midazolam to individuals who underwent overnight surgery significantly increased the risk for MINS (odds ratio of 3.52 for MINS, 95% CI [3.10, 4.00]), when compared to no midazolam administration. Our nighttime analysis included 161,250 individuals (Figure 1).

Next, we evaluated the effect of the ASA classification on the MINS baseline risk without any midazolam administration. As expected, patients in the ASA 3+4 class had a significantly higher MINS risk than patients in the ASA class 1+2 (OR 7.42, 95% CI [6.84, 8.04], Table 1C).

Finally, we analyzed the relationship between midazolam administration and MINS risk in ASA 1+2 and ASA 3+4 patients (Table 1D). We found a significant interaction between the ASA class and midazolam administration (p 2.8 10^{-7}), demonstrating that the effect of midazolam on MINS occurrence was modified by the ASA class. Indeed, midazolam was associated with a moderately increased

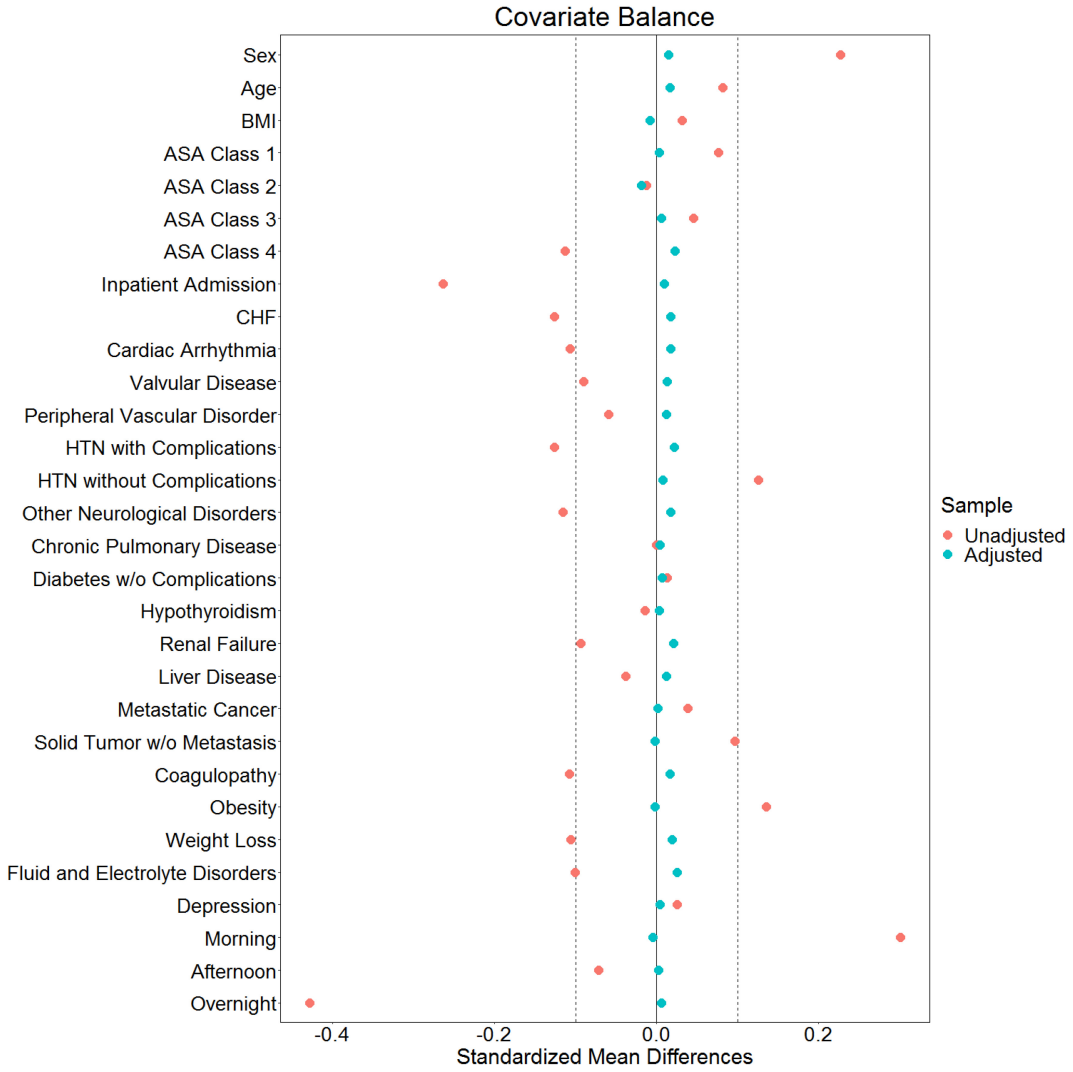

FIGURE 4
Love plot showing baseline imbalances for the covariates of interest and the effectiveness of balancing *via* the inverse probability of treatment weights.

rate of MINS in the low ASA (1+2) class group (OR: 1.25, 95% CI [1.13, 1.39]) who had a total MINS rate of 0.23%. However, the association between midazolam and MINS was substantially attenuated, and in fact changed directions, when a subject was in the high ASA group (3+4), who had a total MINS rate of 1.44%. For a subject in the high ASA group, the administration of midazolam was associated with an odds ratio of 0.94 for MINS (95% CI [0.91, 0.98]).

However, as shown in **Table 1**E,F, the administration of midazolam during overnight surgeries significantly increased the risk for MINS in ASA 1+2 as well as in ASA 3+4 patients (odds ratio of 3.59 for MINS, 95% CI [2.4, 45.38] for ASA 1+2 and odds ratio of 1.67 for MINS, 95% CI [1.46, 1.91] for ASA 3+4), when compared to no midazolam administration.

Discussion

In this study, we examined the relationship between perioperative midazolam administration and MINS. Overall, we did not find an association between midazolam administration and the rate of MINS. However, midazolam administration was associated with an increased risk of MINS when surgeries occurred at night or in healthier patients in the ASA 1+2 class. Interestingly, we found a MINS risk reduction when midazolam was given to higher risk patients (ASA 3+4 class). When assessing the time of day, however, the increased risk of MINS at night was present in both ASA 1+2 and ASA 3+4.

The endogenous circadian clock mechanism involves a cell autonomous transcription–translation feedback loop. During the day, the transcription factor CLOCK interacts with BMAL1

TABLE 1 Effect of circadian physiology on MINS.

(A) Time of day effect on MINS		
No midazolam	Odds ratio	95% Confidence interval
MINS–overnight versus daytime surgery	0.52	[0.48, 0.56]
(B) Time of day effect of midazolam on MINS		
Midazolam vs. *no midazolam*		
MINS during daytime surgery	0.84	[0.80, 0.87]
MINS during overnight surgery	3.52	[3.10, 4.00]
(C) ASA effect only on MINS		
No midazolam		
MINS in ASA 3+4 vs. ASA 1+2	7.42	[6.84, 8.04]
(D) MINS in different ASA classes		
Midazolam vs. *no midazolam*		
MINS in ASA 1+2	1.25	[1.13, 1.39]
MINS in ASA 3+4	0.94	[0.91, 0.98]
(E) Time of day effect of midazolam on MINS in ASA 1+2		
Midazolam vs. *no midazolam*		
MINS during daytime surgery	1.11	[0.998, 0.123]
MINS during overnight surgery	3.59	[2.4, 5.38]
(F) Time of day effect of midazolam on MINS in ASA 3+4		
Midazolam vs. *no midazolam*		
MINS during daytime surgery	0.85	[0.82, 0.88]
MINS during overnight surgery	1.67	[1.46, 1.91]

(A,B) Coefficient estimates and confidence intervals for the marginal structural model assessing the effect modification of time of day on midazolam administration. (C,D) Coefficient estimates and confidence intervals for the marginal structural model assessing the effect modification of the American Society of Anesthesiologists (ASA) class on midazolam administration. (E,F) Coefficient estimates and confidence intervals for the marginal structural model assessing the effect modification of time of day on midazolam administration in ASA 1+2 or ASA 3+4 patients.

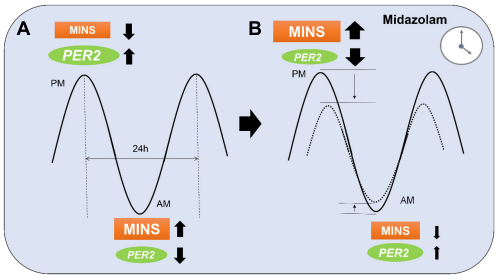

FIGURE 5
Proposed model of midazolam modifying myocardial injury in non-cardiac surgery (MINS) risk during a 24 h period. **(A)** At the peak of PER2 in the evening (p.m.), MINS occurs less frequent than during the PER2 trough in the morning (a.m.). **(B)** Midazolam administration at night might lower the PER2 peak which results in a higher occurrence of MINS. Midazolam administration during the daytime might have opposite effects and lower the PER2 trough resulting in less MINS occurrence. Dotted line indicates MINS risk in patients with midazolam.

to activate transcription of the *Per* and Cryptochrome (*Cry*) genes, resulting in high levels of these transcripts. The resulting PER and CRY proteins translocate to the nucleus to inhibit their own transcription (30). The entire cycle takes approximately 24 h. This process is also active without external cues and takes approximately 25 h in humans (31). Besides autonomous mechanisms, resetting of the circadian clock by photic induction of *Per1* and *Per2* genes is mediated by the binding of phosphorylated CREB (cyclic AMP responsive element-binding protein) to a cAMP-responsive element (CRE) in the respective promoters (32). Since the circadian rhythm in humans is dominantly regulated by sunlight (33), circadian proteins cycle over a 24-h period, reaching their peak expression at night. The incidence of myocardial injury has been found to be lower at night in both mice and humans with an abrupt increase in the early morning hours (6 a.m.) (14). Mouse studies have revealed a reciprocal relationship between myocardial injury and PER2 protein expression (13). In-depth genetic studies in mice have recently identified endothelial PER2 as an endogenous cardioprotective mechanism (14). In keeping with these findings, we found a lower baseline risk for MINS during the night when compared to the day. We also found a correlation between the time of midazolam administration and the risk of MINS. This would support data from animal studies showing a link between midazolam, circadian protein expression, and ischemia, and suggests that midazolam also interferes with the circadian system in humans. Midazolam increases $GABA_A$ signaling, an important component of circadian rhythm protein regulation (34). In fact, $GABA_A$ activation can inhibit the expression of circadian *Per2* mRNA (35). As midazolam could lower the naturally occurring higher nighttime-PER2 levels, it is plausible that the heart could be more susceptible to injury when midazolam is given at night compared to the day. Further, as we also found that midazolam decreased the risk of MINS during the daytime, midazolam might also cause a reduction of the amplitude not only at the peak but also at the trough (**Figure 5**).

The relationship between ASA class and risk of MINS after midazolam exposure may have a similar physiologic basis. Because most medical comorbidities increase in prevalence with age, ASA classes 3 and 4 presumably include an older patient population. Indeed, our ASA 1+2 had a mean age of 45.7 and our ASA 3+4 group had a mean age of 59.9 years. In older adults, the amplitude and peak expression of circadian rhythms decreases by 20 to 40% (36). In addition, animal studies have shown that aging results in the diurnal rhythm amplitude of PER2 (37). Exposures that interfere with circadian protein expression might therefore be more harmful in younger patients who are accustomed to a higher circadian amplitude and baseline expression of circadian proteins. Indeed, we identified a significant increase of MINS in the ASA 1+2 group when midazolam was given perioperatively. Surprisingly, we found a possible protective effect of midazolam in the ASA 3+4 group. Although small, this reduction in risk is harder to explain *via* circadian mechanisms. One possibility is that

administration in patients with many comorbidities resulted in lower cumulative anesthetic doses, reduced stress responses, and more hemodynamic stability during surgery which ultimately could have resulted in fewer cardiac complications. Analyzing ASA 5 and 6 patients could potentially have given more insight into this phenomenon. However, since we excluded ASA 5 and ASA 6 patients due to their emergent and complex status, this will require future evaluation. Regardless, when we considered the time of day, an increased risk of MINS at night was present in both ASA 1+2 and ASA 3+4, suggesting that the time of day had a higher impact on the occurrence of MINS.

Limitations

A limitation of our current study is the retrospective analysis of administrative data which shows associations among variables but not necessarily causal relationships, a common problem of unmeasured confounding. However, propensity scores were used to balance the distribution of baseline covariates between the population with and without perioperative midazolam administration which has been shown to contribute to a more precise estimation of the treatment response (38).

Further, perioperative midazolam could have been administered for a variety of indications other than anxiolysis, including in hemodynamically unstable patients to minimize the use of inhaled agents or more vasodilatory or cardioactive sedative-hypnotics. However, this is likely a small subset of our population and would not explain our finding that midazolam has a time-of-day dependent effect on the rate of MINS.

In addition, other causes of MINS (occurring in the 72-h period after surgery) such as from postoperative ischemia, sepsis, neurogenic cardiomyopathy, etc., might have been missed and could therefore be possible confounders. Again, this would not fully account for the findings of our analyses regarding time-of-day or ASA-class effects.

Finally, MINS was most likely underestimated in our sample as most institutions do not measure postoperative troponin routinely. As a result, our analysis treated any subject without a perioperative troponin-I as negative for perioperative MINS resulting in a MINS rate of 0.93%. However, previous studies have reported a MINS rate of 8.0% among patients that are 45 years or older (39). Given this data, undetected MINS almost certainly occurred in our cohort, but it seems reasonable to assume that undetected MINS was proportionate in individuals with and without midazolam administration.

Conclusion

This large retrospective observational study suggests that perioperative administration of midazolam during nighttime surgeries as well as administration in healthier patients may increase the risk of MINS. The fact that we did not find an overall relationship between perioperative midazolam and MINS but found differences in risk at certain times of day suggests that chronobiology may play an important role in MINS and other perioperative outcomes. Future studies are needed that assess these time-of-day dependent effects.

Data availability statement

The original contributions presented in this study are included in the article/supplementary material, further inquiries can be directed to the corresponding author.

Ethics statement

The studies involving human participants were reviewed and approved by Colorado Multiple Institutional Review Board (COMIRB) at the University of Colorado Denver, United States (#09-0674). Written informed consent for participation was not required for this study in accordance with the national legislation and the institutional requirements.

Author contributions

MP, JP, DD, BS, and AG: wrote the manuscript and analyzed the data. TE: designed the study, wrote the manuscript, and analyzed the data. All authors contributed to the article and approved the submitted version.

Funding

This publication was supported by the National Heart, Lung, and Blood Institute and National Institute of Aging of the National Institutes of Health under Award Numbers: R56HL156955 and R03AG078956. The content is solely the responsibility of the authors and does not necessarily represent the official views of the National Institutes of Health.

Acknowledgments

We gratefully acknowledged the valuable contributions to protocol and final manuscript review by the Multicenter Perioperative Outcomes Group (MPOG) collaborators, including Germaine Cuff, Michael R Mathis, Bhiken I. Naik,

Patrick McCormick, Robert Edward Freundlich, Jochen D. Muehlschlegel, and Nathan Leon Pace.

Conflict of interest

The authors declare that the research was conducted in the absence of any commercial or financial relationships that could be construed as a potential conflict of interest.

Publisher's note

References

1. Puelacher C, Lurati Buse G, Seeberger D, Sazgary L, Marbot S, Lampart A, et al. Perioperative myocardial injury after noncardiac surgery: incidence, mortality, and characterization. *Circulation.* (2018) 137:1221–32. doi: 10.1161/CIRCULATIONAHA.117.030114

2. Gao L, Chen L, He J, Wang B, Liu C, Wang R, et al. Perioperative myocardial injury/infarction after non-cardiac surgery in elderly patients. *Front Cardiovasc Med.* (2022) 9:910879. doi: 10.3389/fcvm.2022.910879

3. Dauerman HL. The expanding universe of perioperative myocardial infarction. *J Am Coll Cardiol.* (2016) 68:339–42. doi: 10.1016/j.jacc.2016.03.601

4. Parashar A, Agarwal S, Krishnaswamy A, Sud K, Poddar KL, Bassi M, et al. Percutaneous intervention for myocardial infarction after noncardiac surgery: patient characteristics and outcomes. *J Am Coll Cardiol.* (2016) 68:329–38. doi: 10.1016/j.jacc.2016.03.602

5. Eltzschig HK, Eckle T. Ischemia and reperfusion–from mechanism to translation. *Nat Med.* (2011) 17:1391–401. doi: 10.1038/nm.2507

6. Matthes K, Urman R, Ehrenfeld J. *Anesthesiology: A Comprehensive Board Review for Primary and Maintenance of Certification*. Oxford: Oxford University Press (2013).doi: 10.1093/med/9780199733859.001.0001

7. Hughes CG, McGrane S, Pandharipande PP. Sedation in the intensive care setting. *Clin Pharmacol.* (2012) 4:53–63. doi: 10.2147/CPAA.S26582

8. Lonardo NW, Mone MC, Nirula R, Kimball EJ, Ludwig K, Zhou X, et al. Propofol is associated with favorable outcomes compared with benzodiazepines in ventilated intensive care unit patients. *Am J Respir Crit Care Med.* (2014) 189:1383–94. doi: 10.1164/rccm.201312-2291OC

9. Gile J, Scott B, Eckle T. The period 2 enhancer nobiletin as novel therapy in murine models of circadian disruption resembling delirium. *Crit Care Med.* (2018) 46:e600–8. doi: 10.1097/CCM.0000000000003077

10. Kudchadkar SR. Benzodiazepines and delirium in the young and old: truth be told or still not sold? *Crit Care Med.* (2017) 45:1562–4. doi: 10.1097/CCM.0000000000002558

11. Zhang Z, Chen K, Ni H, Zhang X, Fan H. Sedation of mechanically ventilated adults in intensive care unit: a network meta-analysis. *Sci Rep.* (2017) 7:44979. doi: 10.1038/srep44979

12. Devlin JW, Skrobik Y, Gélinas C, Needham DM, Slooter AJC, Pandharipande PP, et al. Clinical practice guidelines for the prevention and management of pain, agitation/sedation, delirium, immobility, and sleep disruption in adult patients in the ICU. *Crit Care Med.* (2018) 46:e825–73.

13. Eckle T, Hartmann K, Bonney S, Reithel S, Mittelbronn M, Walker LA, et al. Adora2b-elicited Per2 stabilization promotes a HIF-dependent metabolic switch crucial for myocardial adaptation to ischemia. *Nat Med.* (2012) 18:774–82. doi: 10.1038/nm.2728

14. Oyama Y, Bartman CM, Bonney S, Lee JS, Walker LA, Han J, et al. Intense light-mediated circadian cardioprotection via transcriptional reprogramming of the endothelium. *Cell Rep.* (2019) 28:1471–84.e11. doi: 10.1016/j.celrep.2019.07.020

15. Oyama Y, Bartman CM, Gile J, Sehrt D, Eckle T. The circadian PER2 enhancer Nobiletin reverses the deleterious effects of midazolam in myocardial ischemia and reperfusion injury. *Curr Pharm Des.* (2018) 24:3376–83. doi: 10.2174/1381612824666180924102530

16. Landesberg G, Beattie WS, Mosseri M, Jaffe AS, Alpert JS. Perioperative myocardial infarction. *Circulation.* (2009) 119:2936–44. doi: 10.1161/CIRCULATIONAHA.108.828228

17. Goldman L, Caldera DL, Nussbaum SR, Southwick FS, Krogstad D, Murray B, et al. Multifactorial index of cardiac risk in noncardiac surgical procedures. *N Engl J Med.* (1977) 297:845–50. doi: 10.1056/NEJM197710202971601

18. Brainard J, Gobel M, Scott B, Koeppen M, Eckle T. Health implications of disrupted circadian rhythms and the potential for daylight as therapy. *Anesthesiology.* (2015) 122:1170–5. doi: 10.1097/ALN.0000000000000596

19. Colquhoun DA, Shanks AM, Kapeles SR, Shah N, Saager L, Vaughn MT, et al. Considerations for integration of perioperative electronic health records across institutions for research and quality improvement: the approach taken by the multicenter perioperative outcomes group. *Anesth Analg.* (2020) 130:1133–46. doi: 10.1213/ANE.0000000000004489

20. Bender SP, Paganelli WC, Gerety LP, Tharp WG, Shanks AM, Housey M, et al. Intraoperative lung-protective ventilation trends and practice patterns: a report from the multicenter perioperative outcomes group. *Anesth Analg.* (2015) 121:1231–9. doi: 10.1213/ANE.0000000000000940

21. Colquhoun DA, Naik BI, Durieux ME, Shanks AM, Kheterpal S, Bender SP, et al. Management of 1-lung ventilation-variation and trends in clinical practice: a report from the multicenter perioperative outcomes group. *Anesth Analg.* (2018) 126:495–502. doi: 10.1213/ANE.0000000000002642

22. Choi J, Dekkers OM, Le Cessie S. A comparison of different methods to handle missing data in the context of propensity score analysis. *Eur J Epidemiol.* (2019) 34:23–36. doi: 10.1007/s10654-018-0447-z

23. Pattanayak CW, Rubin DB, Zell ER. Propensity score methods for creating covariate balance in observational studies. *Rev Esp Cardiol.* (2011) 64:897–903. doi: 10.1016/j.rec.2011.06.008

24. Rubin DB. Propensity score methods. *Am J Ophthalmol.* (2010) 149:7–9. doi: 10.1016/j.ajo.2009.08.024

25. Austin PC. Balance diagnostics for comparing the distribution of baseline covariates between treatment groups in propensity-score matched samples. *Stat Med.* (2009) 28:3083–107. doi: 10.1002/sim.3697

26. Austin PC. An introduction to propensity score methods for reducing the effects of confounding in observational studies. *Multivariate Behav Res.* (2011) 46:399–424. doi: 10.1080/00273171.2011.568786

27. Hernán MA, Robins J. *Causal Inference: What If.* Boca Raton, FL: Chapman & Hall/CRC. (2020).

28. Mattis J, Sehgal A. Circadian rhythms, sleep, and disorders of aging. *Trends Endocrinol Metab.* (2016) 27:192–203. doi: 10.1016/j.tem.2016.02.003

29. Sindi S, Pérez LM, Vetrano DL, Triolo F, Kåreholt I, Sjöberg L, et al. Sleep disturbances and the speed of multimorbidity development in old age: results from a longitudinal population-based study. *BMC Med.* (2020) 18:382. doi: 10.1186/s12916-020-01846-w

30. Takahashi JS, Hong HK, Ko CH, McDearmon EL. The genetics of mammalian circadian order and disorder: implications for physiology and disease. *Nat Rev Genet.* (2008) 9:764–75.

31. Aschoff J. Circadian rhythms in man. *Science.* (1965) 148:1427–32. doi: 10.1126/science.148.3676.1427

32. Ginty DD, Kornhauser JM, Thompson MA, Bading H, Mayo KE, Takahashi JS, et al. Regulation of CREB phosphorylation in the suprachiasmatic nucleus by light and a circadian clock. *Science.* (1993) 260:238–41.

33. Roenneberg T, Kumar CJ, Merrow M. The human circadian clock entrains to sun time. *Curr Biol.* (2007) 17:R44–5. doi: 10.1016/j.cub.2006.12.011

34. Myung J, Hong S, DeWoskin D, De Schutter E, Forger DB, Takumi T. GABA-mediated repulsive coupling between circadian clock neurons in the SCN encodes seasonal time. *Proc Natl Acad Sci U.S.A.* (2015) 112:E3920–9.

35. Ehlen JC, Novak CM, Karom MC, Gamble KL, Albers HE. Interactions of GABA A receptor activation and light on period mRNA expression in the suprachiasmatic nucleus. *J Biol Rhythms.* (2008) 23:16–25. doi: 10.1177/0748730407310785

36. Hood S, Amir S. The aging clock: circadian rhythms and later life. *J Clin Invest.* (2017) 127:437–46. doi: 10.1172/JCI90328

37. Duncan MJ, Prochot JR, Cook DH, Tyler Smith J, Franklin KM. Influence of aging on Bmal1 and Per2 expression in extra-SCN oscillators in hamster brain. *Brain Res.* (2013) 1491:44–53. doi: 10.1016/j.brainres.2012.11.008

38. Winger DG, Nason KS. Propensity-score analysis in thoracic surgery: when, why, and an introduction to how. *J Thorac Cardiovasc Surg.* (2016) 151:1484–7. doi: 10.1016/j.jtcvs.2016.02.036

39. Botto F, Alonso-Coello P, Chan MT, Villar JC, Xavier D, Srinathan S, et al. Myocardial injury after noncardiac surgery: a large, international, prospective cohort study establishing diagnostic criteria, characteristics, predictors, and 30-day outcomes. *Anesthesiology.* (2014) 120:564–78.

frontiers | Frontiers in Cardiovascular Medicine

TYPE Original Research
PUBLISHED 07 November 2022
DOI 10.3389/fcvm.2022.1005030

OPEN ACCESS

EDITED BY
Jinfeng Xu,
The University of Hong Kong,
Hong Kong SAR, China

REVIEWED BY
Li Yin,
University of Virginia, United States
Philip Düsing,
University Hospital Bonn, Germany

*CORRESPONDENCE
Laisel Martinez
lmartinez6@med.miami.edu

SPECIALTY SECTION
This article was submitted to Cardiovascular Therapeutics, a section of the journal Frontiers in Cardiovascular Medicine

RECEIVED 27 July 2022
ACCEPTED 10 October 2022
PUBLISHED 07 November 2022

CITATION
Labissiere X, Zigmond ZM, Challa A, Montoya C, Manzur-Pineda K, Abraham A, Tabbara M, Salama A, Pan Y, Salman LH, Yang X, Vazquez-Padron RI and Martinez L (2022) Vein morphometry in end-stage kidney disease: Teasing out the contribution of age, comorbidities, and vintage to chronic wall remodeling. *Front. Cardiovasc. Med.* 9:1005030. doi: 10.3389/fcvm.2022.1005030

Vein morphometry in end-stage kidney disease: Teasing out the contribution of age, comorbidities, and vintage to chronic wall remodeling

Xochilt Labissiere[1], Zachary M. Zigmond[2], Akshara Challa[1], Christopher Montoya[1], Karen Manzur-Pineda[1], Amalia Abraham[1], Marwan Tabbara[1], Alghidak Salama[1], Yue Pan[3], Loay H. Salman[4], Xiaofeng Yang[5], Roberto I. Vazquez-Padron[1,2] and Laisel Martinez[1]*

[1]DeWitt Daughtry Family Department of Surgery, Leonard M. Miller School of Medicine, University of Miami, Miami, FL, United States, [2]Bruce W. Carter Veterans Affairs Medical Center, Miami, FL, United States, [3]Department of Public Health Sciences, Leonard M. Miller School of Medicine, University of Miami, Miami, FL, United States, [4]Division of Nephrology, Albany Medical College, Albany, NY, United States, [5]Lewis Katz School of Medicine, Temple University, Philadelphia, PA, United States

Background: Chronic kidney disease (CKD) is a highly comorbid condition with significant effects on vascular health and remodeling. Upper extremity veins are important in end-stage kidney disease (ESKD) due to their potential use to create vascular accesses. However, unlike arteries, the contribution of CKD-associated factors to the chronic remodeling of veins has been barely studied.

Methods: We measured morphometric parameters in 315 upper extremity veins, 131 (85% basilic) from stage 5 CKD/ESKD patients and 184 (89% basilic) from non-CKD organ donors. Associations of demographic and clinical characteristics with intimal hyperplasia (IH) and medial fibrosis were evaluated using multivariate regression models.

Results: The study cohort included 33% females, 30% blacks, 32% Hispanics, and 37% whites. Over 60% had hypertension, and 25% had diabetes independent of CKD status. Among kidney disease participants, 26% had stage 5 CKD, while 22 and 52% had ESKD with and without history of a previous arteriovenous fistula/graft (AVF/AVG), respectively. Intimal hyperplasia was associated with older age (β = 0.13 per year, confidence interval [CI] = 0.002–0.26), dialysis vintage > 12 months (β = 0.22, CI = 0.09–0.35), and previous AVF/AVG creation (β = 0.19, CI = 0.06–0.32). Upper quartile values of IH were significantly associated with diabetes (odds ratio [OR] = 2.02, CI = 1.08–3.80), which demonstrated an additive effect with previous AVF/AVG history and longer vintage in exacerbating IH. Medial fibrosis also increased as a function of age (β = 0.17, CI = 0.04–0.30) and among patients with diabetes

(β = 0.15, CI = 0.03–0.28). Age was the predominant factor predicting upper quartile values of fibrosis (OR = 1.03 per year, CI = 1.01–1.05) independent of other comorbidities.

Conclusion: Age and diabetes are the most important risk factors for chronic development of venous IH and fibrosis independent of CKD status. Among kidney disease patients, longer dialysis vintage, and history of a previous AVF/AVG are strong predictors of IH.

KEYWORDS

intimal hyperplasia (IH), fibrosis, chronic kidney disease, diabetes, vascular aging

Introduction

Upper extremity vessels are the preferred sites for creation of hemodialysis accesses. Traditional and non-traditional risk factors in chronic kidney disease (CKD) are thought to induce structural changes that lead to wall stiffness and impair vasoactivity, affecting the capacity of vessels to remodel and mature after vascular access creation (1). Unfortunately, most of the mechanisms behind those changes are extrapolated from the arterial system (2–4), despite differences in hemodynamics and structure between arteries and veins. The impact of CKD on chronic remodeling of upper extremity veins remains understudied.

Intimal hyperplasia (IH) and imbalanced extracellular matrix (ECM) remodeling are implicated in the origin and progression of vascular diseases, and in postoperative complications after vascular surgeries (2, 5–10). Concentric development of IH and moderate degree of wall fibrosis are frequently found in veins of CKD patients at the time of hemodialysis access creation (8, 11, 12). Despite mild or no associations of pre-access vein morphometry with arteriovenous fistula (AVF) or graft (AVG) outcomes (8, 11, 13, 14), IH and excessive fibrosis may negatively influence the selection of vessels for vascular access surgeries (15).

In the acute or postoperative scenarios, IH is the main pathophysiological feature in arterial restenosis and vein graft disease (9, 16). Vascular fibrosis underlies post-thrombotic syndrome after deep vein thrombosis (7). Excessive postoperative fibrosis also plays a significant role in maturation failure of newly created AVFs, which is further exacerbated by concurrent IH (8, 17). The chronic and acute/postoperative distinctions are particularly important to the study of vascular remodeling. On one hand, both processes differ in the presence or absence of wall injury, sources of inflammation, and the type of regulatory or healing response. On the other hand, acute remodeling occurs on the fabric of chronically adapted tissues, which may influence the acute response. Importantly, most of our understanding of venous IH and fibrosis applies to the acute and postoperative settings, with limited information about factors contributing to chronic wall changes due to the scarcity of systematic histopathology studies.

In this work, we embarked on a comparative analysis of upper vein morphometry in 131 veins from stage 5 CKD and end-stage kidney disease (ESKD) patients and 184 from non-CKD organ donors with moderate prevalence of other chronic comorbidities. We studied the associations of clinical characteristics with venous morphometry, and the specific roles of CKD and hemodialysis on these vascular changes. To our knowledge, this is the first systematic study of upper extremity veins in more than 300 CKD and non-CKD patients. This information may be valuable for the understanding of mechanisms driving postoperative remodeling of veins after access creation and for the design of preventive treatments and lifestyle interventions to improve vascular health in CKD patients.

Materials and methods

Study subjects and sample collection

The CKD cohort consisted of 131 patients, who were undergoing surgery for AVF creation and enrolled in prospective studies previously reported by us (8, 18). Of these, 34 were classified as stage 5 CKD (CKD5; defined as estimated glomerular filtration rate [eGFR] < 15, not on dialysis) while 97 were hemodialysis-dependent (ESKD). Dialysis vintage was defined as the time between the first day of dialysis and the day of vein collection, minus the time with a functioning kidney transplant. The patients provided written informed consent during their preoperative visit, under a protocol approved by the University of Miami Institutional Review Board and adherent to the Declaration of Helsinki. We obtained a 1–5 mm cross-section of the pre-access vein (111 basilic, 11 cephalic, 5 brachial, and 4 median cubital) that would have been otherwise discarded after AVF creation.

The non-CKD cohort included 184 organ donors whose tissues were donated for research purposes through a collaboration with the Life Alliance Recovery Agency. Cross-sectional samples of upper extremity veins (164 basilic and 20 cephalic veins), approximately 2 cm in length, were obtained post mortem following organ procurement procedures. All veins were collected in RNA*later* (QIAGEN, Germantown, MD) and stored at −80°C. A 1–5 mm cross-section was fixed in 10% neutral formalin (Sigma-Aldrich, St. Louis, MO) before paraffin embedding and sectioning.

Histology and morphometry measurements

Vein sections were stained with Masson's trichrome for gross histomorphometric analysis. Medial fibrosis (% area of collagen), intimal area, and medial area were quantified using ImageJ (National Institutes of Health) and color thresholding methods. Intimal hyperplasia (IH) was calculated as the intima/media area ratio to normalize for vein size differences due to anatomy or tissue shrinkage during formalin fixation and dehydration. Images were acquired using a VisionTek DM01 digital microscope (Sakura Finetek, Torrance, CA). Operators blinded to the clinical data performed image digital processing and morphometric measurements.

Statistical analyses

Statistical analyses were performed using XLSTAT 2020.1.1 (Addinsoft Inc., New York, NY) and GraphPad Prism 8.4.0 (San Diego, CA). Normally distributed data were expressed as mean ± standard deviation (SD) and compared using the Student's *t*-test. When normality criteria were not met, data were expressed as median and interquartile range (IQR) and compared using the Mann-Whitney test or Kruskal-Wallis tests with *post hoc* comparisons. Categorical values were compared using the Fisher's exact test. Associations between binary clinical covariates (positive or negative diagnosis of CKD/ESKD, diabetes, and hypertension) and continuous morphometry data (intima/media area ratio, and medial fibrosis) were evaluated using multivariate general linear regression models adjusted for age, sex, ethnicity/race, comorbidities, and type of vein. In addition, we evaluated associations between clinical covariates and upper quartile morphometry values (Q3-maximum). Continuous data were converted to binary status (1 if $\geq$ Q3, 0 if $<$ Q3) based on the upper quartile values of the overall study population and analyzed using multivariate logistic regression models adjusted for the above characteristics. To examine the additive effects of CKD/ESKD and diabetes on upper quartile morphometry status, we used logistic regression models controlling for age. Results were considered significant when $p < 0.05$.

Results

Characteristics of the study cohort

The overall cohort had a mean age of 49 years (± 15) and was composed of 33% females, 30% non-Hispanic blacks, 32% Hispanics, and 36% whites (**Table 1**). Over 60% of participants were positive for hypertension and 25% had diabetes independent of CKD status. Most of the vessels were basilic veins (275/315, 87%), with minor proportions of cephalic (10%) and brachial or median cubital veins (3%). Because of its deep anatomical location, the predominance of basilic veins ensured that morphometric measurements reflected chronic remodeling as a result of physiological stimuli and not likely due to venipuncture or other vascular injuries.

As expected, the CKD/ESKD subgroup was significantly older than non-CKD participants (56 vs. 45 years, respectively) and had higher prevalence of hypertension (98 vs. 36%) and diabetes (47 vs. 10%). There was also a different ratio of black to white individuals between the CKD/ESKD and non-CKD groups (**Table 1**). Among kidney disease participants, 34/131 (26%) were CKD5, while 29 (22%) and 68 (52%) had ESKD with and without history of a previous AVF/AVG, respectively (**Table 1**). Dialysis vintage ranged from 0.7 to 43.6 (median 4.5, IQR 3.0–11.1) months in ESKD patients without a previous AVF or AVG, and 0.2 to 163 (median 17.3, IQR 9.1–41.6) months in participants with a prior AVF/AVG access. Eighteen patients in the latter group had the previous access in the same arm, 9 in the contralateral arm, and 2 bilaterally. Only 4/97 ESKD participants had history of peritoneal dialysis.

Clinical factors associated with chronic intimal hyperplasia

Intimal hyperplasia defined as intima/media area ratio was quantified in venous cross-sections as a surrogate marker of adaptive cell accumulation and/or survival. This parameter illustrates intimal expansion compared to the media while correcting for the size of the vessel. Intima/media area ratio ranged from 0.00 to 1.50 in the overall cohort (**Figure 1A**). Intimal hyperplasia was significantly higher in CKD/ESKD patients than in non-CKD donors (median 0.32 vs. 0.21, $p < 0.0001$), including patients with CKD5 status, ESKD with and without a previous AVF/AVG, and ESKD with dialysis vintage $>$ 12 months (**Table 2**). After adjusting for additional demographic and clinical characteristics, IH was significantly associated with increasing age ($\beta = 0.13$, $p = 0.046$) and CKD/ESKD ($\beta = 0.18$, $p = 0.025$), specifically with history of a previous AVF/AVG and vintage $>$ 12 months (**Table 3**). An analysis controlling for both AVF/AVG history and vintage was not possible due to collinearity between these variables. Nonetheless, while the association with a previous AVF/AVG

TABLE 1 Baseline characteristics of the study cohorts.

	All (N = 315)	CKD/ESKD (N = 131)	Non-CKD (N = 184)	P-value*
Demographics				
Age (y)–mean ± SD	49.33 ± 14.97	55.79 ± 13.57	44.72 ± 14.22	<0.0001
Female sex (%)	103 (33)	44 (34)	59 (32)	0.81
Hispanic (%)	102 (32)	47 (36)	55 (30)	0.27
Black (%)	95 (30)	68 (52)	27 (15)	0.0001
White (%)	118 (37)	16 (12)	102 (55)	0.0001
Comorbidities/CKD stage				
Hypertension (%)	195 (62)	128 (98)	67 (36)	0.0001
Diabetes (%)	79 (25)	61 (47)	18 (10)	0.0001
CKD/ESKD (%)	131 (42)	131 (100)	–	–
Stage 5 CKD	34 (11)	34 (26)	–	–
ESKD no prior AVF	68 (22)	68 (52)	–	–
ESKD + prior AVF	29 (9)	29 (22)	–	–
Type of vein				
Basilic (%)	275 (87)	111 (85)	164 (89)	0.30
Cephalic (%)	31 (10)	11 (8)	20 (11)	0.57
Other (%) ǂ	9 (3)	9 (7)	–	0.0003

*P-values for CKD/ESKD vs. non-CKD comparisons.
ǂOther types of veins include 4 median cubital and 5 brachial.

could be partly due to hemodynamic effects, longer dialysis vintage by itself was a predictor of IH in ESKD patients without a prior AVF or AVG access (β = 0.36, p = 0.003; **Supplementary Table 1**).

In addition to the associations of age and ESKD subgroups with gradual increases in IH (**Figures 1B,C**), we tested for the relationship of clinical characteristics with upper quartile values (Q3-maximum; IH ≥ 0.042). These represent conditions that exacerbate intimal growth or imbalanced intimal/medial remodeling. Only diabetes was significantly associated with upper quartile IH values in the main logistic regression model (**Table 4** and **Figure 1B**), and further demonstrated a strong additive effect with ESKD plus a prior AVF/AVG (**Table 4** and **Figure 1D** top). Dialysis vintage > 12 months also predicted upper quartile IH values regardless of diabetes status, and diabetes combined with vintage < 12 months (**Table 4** and **Figure 1D** bottom).

Clinical factors associated with chronic medial fibrosis

The percentage of medial fibrosis in venous cross-sections is a surrogate marker of adaptive ECM remodeling. Medial fibrosis ranged from 14.92 to 66.52% in the overall study cohort (**Figure 2A**). Higher medial fibrosis was associated with increasing age (β = 0.17, p = 0.012) and diabetes (β = 0.15, p = 0.018) in multivariate general linear regression models (**Table 3**). In contrast with the increase of venous IH in subgroups of ESKD, the percent of medial fibrosis was similar between CKD/ESKD and non-CKD individuals (**Tables 2**, **3** and **Figure 2A**).

Increasing age was the main predictor of upper quartile values of fibrosis (≥ 46.85%; OR = 1.03 per year, p = 0.013) (**Table 4** and **Figure 2B**). Combined logistic regression models of (+) diabetes/(+) CKD5 were only significantly different with respect to a couple of (–) diabetes models but not with the rest (**Figures 2C,D**), suggesting differential effects of CKD/ESKD stages in ECM remodeling. These analyses demonstrated that age is the primary factor predicting high values of venous fibrosis independent of CKD or diabetes status. **Figure 3** portrays representative pictures of vein morphometry in non-CKD and CKD/ESKD individuals.

Discussion

Intimal hyperplasia and imbalanced ECM remodeling are histopathological changes associated with poor venous health (7, 8, 10, 19, 20). Kidney disease is considered a major contributing factor in the development of these vascular changes (2, 3, 5, 21). However, as various risk factors coexist in CKD patients, it is important to understand the independent contribution of each characteristic to detrimental vascular changes. In this study we evaluated the associations of clinical and demographic characteristics with the morphometry of upper extremity veins. Our findings clarify the role of age, CKD stage, dialysis vintage, vascular access history, hypertension, and diabetes in the chronic remodeling of vessels, and may be applicable to the improvement of vein health in CKD patients.

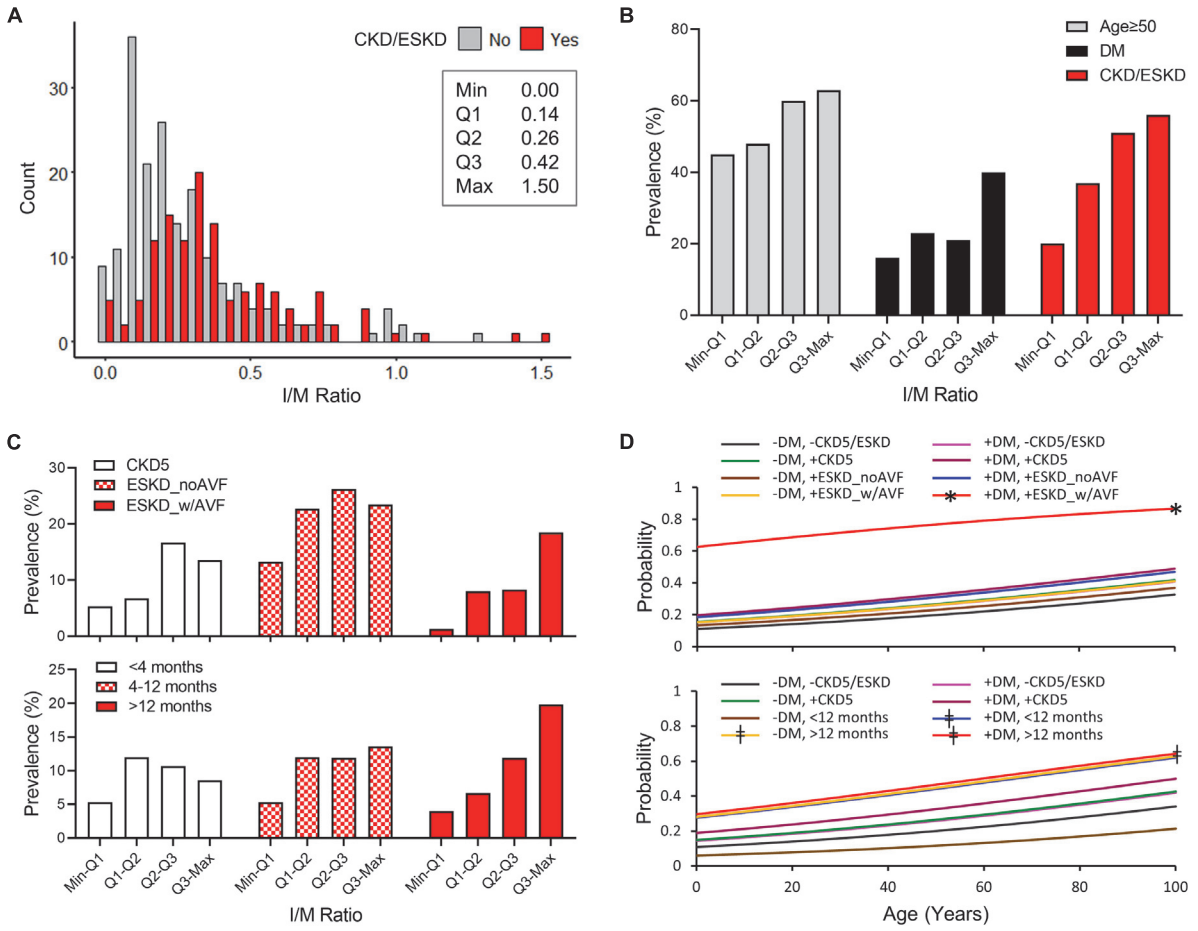

FIGURE 1
Predictors of high intimal hyperplasia (IH) in CKD and non-CKD veins. **(A)** Histogram of IH expressed as intima/media area ratio in CKD/ESKD and non-CKD veins. The minimum, first quartile (Q1), median (Q2), third quartile (Q3), and maximum values are indicated for the overall study cohort. **(B)** Prevalence of age ≥ 50 years, diabetes, and CKD/ESKD per quartile of IH in the overall study cohort. **(C)** Distribution of CKD and ESKD subgroups per quartile of IH according to disease stage and vascular access history (Top) or dialysis vintage (Bottom). **(D)** Probability of IH falling in the upper quartile values (≥0.42) as predicted by age and combined status of diabetes and CKD/ESKD stages. CKD subgroups are separated according to disease stage and vascular access history (Top) or dialysis vintage (Bottom). DM, diabetes; CKD5, stage 5 CKD; ESKD_noAVF, ESKD without previous AVF or AVG; ESKD_w/AVF, ESKD and previous AVF/AVG history. *$p < 0.05$ vs. all individual models, ‡$p < 0.05$ vs. (−) DM/(−)CKD5/ESKD and (−) DM/ < 12 months.

TABLE 2 Morphometric comparisons between the CKD/ESKD and non-CKD cohorts.

	N	Intima/media ratio	*P*-value*	Medial fibrosis (%)	*P*-value*
Non-CKD	184	0.21 [0.11–0.36]	–	41.41 ± 8.04	–
CKD/ESKD	131	**0.32 [0.22–0.51]**	**<0.0001**	41.75 ± 9.03	>0.99
CKD stage 5	34	**0.34 [0.23–0.47]**	**0.0091**	42.20 ± 9.74	>0.99
ESKD by AVF history					
No prior AVF	68	**0.31 [0.21–0.47]**	**0.017**	41.71 ± 8.24	>0.99
With prior AVF	29	**0.43 [0.25–0.59]**	**0.0002**	41.30 ± 10.18	>0.99
ESKD by vintage					
<4 months	29	0.30 [0.22–0.41]	0.29	39.94 ± 7.97	>0.99
4–12 months	34	0.29 [0.20–0.51]	0.26	42.36 ± 8.15	>0.99
>12 months	34	**0.36 [0.26–0.65]**	**0.0001**	42.23 ± 10.11	>0.99

Values presented as mean ± SD or median [interquartile range].
**P*-values vs. non-CKD. Bold values indicate statistical significance.

TABLE 3 Clinical predictors of venous morphometry using multivariate general linear regression models.

	Intima/media area ratio		Medial fibrosis	
	β (95% CI)	*P*-value	β (95% CI)	*P*-value
Main model				
Age (per year)	**0.13 (0.002, 0.26)**	**0.046**	**0.17 (0.04, 0.30)**	**0.012**
Female sex	−0.08 (−0.19, 0.03)	0.133	0.03 (−0.08, 0.14)	0.615
Hispanic	−0.02 (−0.15, 0.11)	0.731	−0.06 (−0.19, 0.07)	0.345
Black	−0.10 (−0.25, 0.04)	0.154	0.09 (−0.06, 0.23)	0.246
Hypertension	−0.01 (−0.16, 0.14)	0.909	−0.04 (−0.19, 0.11)	0.628
Diabetes	0.06 (−0.06, 0.18)	0.333	**0.15 (0.03, 0.28)**	**0.018**
CKD/ESKD	**0.18 (0.02, 0.34)**	**0.025**	−0.11 (−0.27, 0.05)	0.170
Basilic vein	−0.03 (−0.13, 0.09)	0.660	0.03 (−0.08, 0.14)	0.619
CKD subgroup models				
By stage and AVF history				
Age (per year)	**0.13 (0.004, 0.26)**	**0.043**	**0.17 (0.04, 0.30)**	**0.013**
Female sex	−0.09 (−0.21, 0.02)	0.095	0.03 (−0.08, 0.14)	0.624
Hispanic	−0.02 (−0.15, 0.11)	0.758	−0.06 (−0.19, 0.07)	0.344
Black	−0.09 (−0.23, 0.05)	0.224	0.08 (−0.06, 0.23)	0.256
Hypertension	−0.01 (−0.16, 0.14)	0.909	−0.04 (−0.19, 0.12)	0.638
Diabetes	0.06 (−0.07, 0.18)	0.359	**0.15 (0.03, 0.28)**	**0.018**
CKD subgroup				
CKD stage 5	0.12 (−0.01, 0.25)	0.076	−0.06 (−0.20, 0.07)	0.341
ESKD no prior AVF	0.08 (−0.07, 0.23)	0.276	−0.09 (−0.24, 0.06)	0.254
ESKD + prior AVF	**0.19 (0.06, 0.32)**	**0.004**	−0.08 (−0.21, 0.05)	0.250
Basilic vein	−0.04 (−0.15, 0.07)	0.522	0.03 (−0.08, 0.14)	0.606
By stage and vintage				
Age (per year)	**0.14 (0.005, 0.26)**	**0.042**	**0.17 (0.03, 0.30)**	**0.015**
Female sex	−0.10 (−0.21, 0.01)	0.088	0.02 (−0.09, 0.133)	0.705
Hispanic	−0.02 (−0.15, 0.11)	0.763	−0.06 (−0.19, 0.07)	0.345
Black	−0.09 (−0.23, 0.05)	0.210	0.09 (−0.06, 0.23)	0.225
Hypertension	−0.01 (−0.16, 0.14)	0.882	−0.04 (−0.19, 0.12)	0.635
Diabetes	0.07 (−0.05, 0.19)	0.268	**0.15 (0.03, 0.28)**	**0.017**
CKD/ESKD subgroup				
CKD stage 5	0.12 (−0.01, 0.25)	0.079	−0.06 (−0.20, 0.07)	0.344
Vintage < 4 mo.	0.05 (−0.09, 0.18)	0.496	−0.12 (−0.25, 0.01)	0.074
Vintage 4–12 mo.	0.03 (−0.10, 0.17)	0.631	−0.06 (−0.19, 0.08)	0.428
Vintage > 12 mo.	**0.22 (0.09, 0.35)**	**0.001**	−0.04 (−0.17, 0.09)	0.538
Basilic vein	−0.03 (−0.14, 0.08)	0.573	0.03 (−0.08, 0.14)	0.635

Reference levels for binary variables are male sex, white race, non-basilic vein, and negative for hypertension, diabetes, and CKD/ESKD. CI, confidence interval. Bold values indicate statistical significance.

Our analysis of > 300 CKD and non-CKD veins indicates that IH and medial fibrosis are not unique to CKD/ESKD, and that both groups present overlapping ranges of these morphometric parameters. Both IH and medial fibrosis increase over time as a function of age. The positive association of age with both cellular and ECM changes agrees with the concept of vascular aging that is thought to affect arteries and veins (22–24). Age-related alterations in endothelial cells (ECs) and smooth muscle cells (SMCs) induce intimal expansion and wall stiffness in arteries in response to local mechanical, hemodynamic, and neurohumoral stimulations (25, 26). The nature of the stimuli is likely different in veins since they are not subjected to the same hemodynamic conditions and pressure changes as arteries. Nonetheless, there is evidence of endothelial dysfunction and a pro-inflammatory and pro-oxidant phenotype in ECs of aged veins (27–29) that may contribute to maladaptive vascular changes. Dysregulation of the contractile SMC phenotype with age has also been associated with vascular fibrosis and stiffness (26). Specifically in aged veins, higher TGFβ signaling and tissue inhibitors of metalloproteinases (TIMPs), along with

TABLE 4 Clinical predictors of upper quartile (≥ Q3) morphometry values using multivariate logistic regression models.

	Intima/media area ratio ≥ 0.42		Medial fibrosis ≥ 46.85%	
	OR (95% CI)	*P*-value	OR (95% CI)	*P*-value
Main model				
Age (per year)	1.01 (0.99, 1.03)	0.348	**1.03 (1.01, 1.05)**	**0.013**
Female sex	0.81 (0.46, 1.43)	0.470	1.40 (0.80, 2.44)	0.234
Hispanic	0.73 (0.37, 1.46)	0.372	0.75 (0.38, 1.48)	0.408
Black	0.76 (0.35, 1.61)	0.467	1.02 (0.48, 2.15)	0.960
Hypertension	1.03 (0.47, 2.23)	0.944	0.73 (0.34, 1.54)	0.405
Diabetes	**2.02 (1.08, 3.80)**	**0.029**	1.90 (0.99, 3.64)	0.052
CKD/ESKD	1.69 (0.79, 3.63)	0.177	0.92 (0.43, 1.96)	0.824
Basilic vein	1.33 (0.58, 3.04)	0.497	0.57 (0.27, 1.21)	0.146
Additive models				
By stage and AVF history				
Age (per year)	1.01 (0.99, 1.03)	0.188	**1.03 (1.01, 1.05)**	**0.013**
–DM, + CKD5	1.47 (0.46, 4.67)	0.519	0.51 (0.13, 1.98)	0.330
–DM, + ESKD_noAVF	1.20 (0.51, 2.86)	0.673	0.65 (0.26, 1.64)	0.360
–DM, + ESKD_w/AVF	1.43 (0.42, 4.86)	0.563	1.09 (0.32, 3.71)	0.891
+ DM, –CKD5/ESKD	1.42 (0.46, 4.39)	0.546	1.33 (0.45, 3.91)	0.605
+ DM, + CKD5	1.95 (0.65, 5.91)	0.236	2.87 (0.99, 8.28)	0.052
+ DM, + ESKD_noAVF	1.81 (0.74, 4.43)	0.197	1.48 (0.62, 3.56)	0.378
+ DM, + ESKD_w/AVF	**13.19 (3.38, 51.50)**	< **0.001**	0.68 (0.17, 2.66)	0.577
By stage and vintage				
Age (per year)	1.02 (0.99, 1.04)	0.156	**1.03 (1.01, 1.05)**	**0.015**
–DM, + CKD5	1.44 (0.45, 4.60)	0.537	0.51 (0.13, 1.99)	0.335
–DM, < 12 months	0.53 (0.17, 1.64)	0.267	0.78 (0.30, 1.99)	0.598
–DM, > 12 months	**3.25 (1.22, 8.62)**	**0.018**	0.74 (0.23, 2.43)	0.621
+ DM, –CKD5/ESKD	1.40 (0.45, 4.34)	0.560	1.34 (0.45, 3.93)	0.598
+ DM, + CKD5	1.93 (0.64, 5.83)	0.246	2.88 (0.999, 8.33)	0.050
+ DM, < 12 months	**3.15 (1.34, 7.41)**	**0.009**	1.11 (0.45, 2.75)	0.821
+ DM, > 12 months	**3.48 (1.09, 11.09)**	**0.035**	1.37 (0.41, 4.53)	0.609

Reference levels for binary variables are male sex, white race, non-basilic vein, and negative for hypertension, diabetes (DM), and CKD/ESKD. The reference level for the additive model is negative for both diabetes and CKD/ESKD. CI, confidence interval; OR, odds ratio. ESKD_w/AVF and _noAVF refer to ESKD patients with and without history of a previous AVF/AVG, respectively. Similarly, < 12 and > 12 months refer to ESKD patients separated by dialysis vintage. Bold values indicate statistical significance.

lower metalloproteinase-2 (MMP-2) expression, could explain an age-related imbalance in ECM deposition (30, 31).

The association of ESKD with increased IH is not at all surprising, but finally puts to rest a presumed notion based on comparisons with small numbers of non-CKD veins (three to 15 individuals) (3, 32–35). Our work further clarifies that this association is only evident when dialysis vintage is > 12 months or in patients with a prior history of an AVF or AVG, who also tend to have longer dialysis vintage. The independent effect of vintage IH was confirmed in ESKD patients without a previous AVF. However, a hemodynamic effect of a previous access in the arm is also likely. It is possible that the increase in IH is a cumulative response to volume overload, oxidative stress, or dialysis-related inflammation. The relationship between dialysis vintage and history of a previous AVF/AVG with increased IH underscores the importance of addressing poor access maturation and patency outcomes, as the suitability of vessels may be lower for secondary vascular accesses.

Despite the significant effects of dialysis vintage in IH, we failed to find a consistent association between CKD/ESKD stages and chronic venous fibrosis. The risk of high medial fibrosis was significantly higher in patients with diabetes and CKD5 only with respect to non-diabetic CKD5 or shorter vintage ESKD patients, but not compared to the rest of the models, suggesting differential effects of ESKD stages on the venous ECM. These results contrast the widely known association of kidney disease with increased fibrosis of kidneys, heart, arteries, and other organ systems (36, 37). However, recent studies in humans and mice have demonstrated that the profibrotic effect of CKD is not so clear-cut, and that different ECM deposition and degradation phenotypes exist depending on disease activity and progression (38–40). Creation

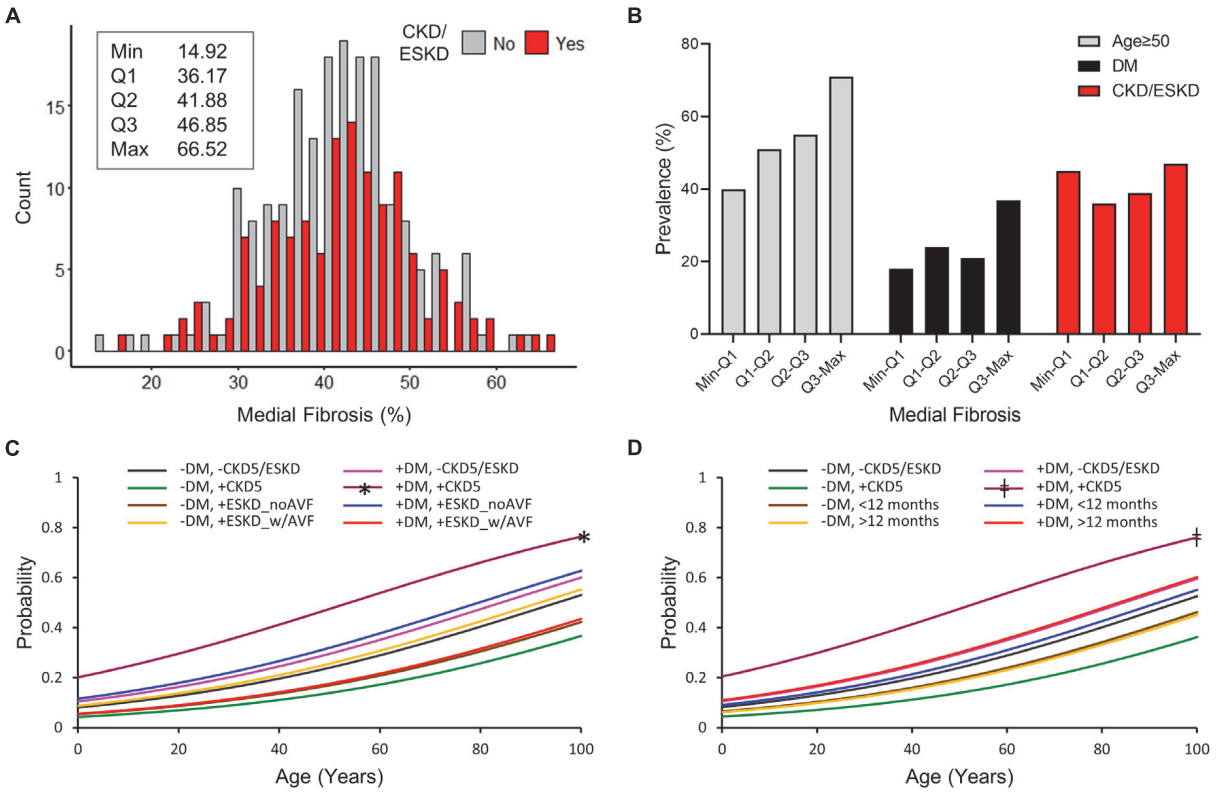

FIGURE 2
Predictors of high medial fibrosis in CKD and non-CKD veins. **(A)** Histogram of percent medial fibrosis in CKD/ESKD and non-CKD veins. The minimum, first quartile (Q1), median (Q2), third quartile (Q3), and maximum values are indicated for the overall study cohort. **(B)** Prevalence of age ≥ 50 years, diabetes, and CKD/ESKD per quartile of medial fibrosis in the overall study cohort. **(C,D)** Probability of medial fibrosis falling in the upper quartile values (≥46.85%) as predicted by age and combined status of diabetes and CKD/ESKD stages. CKD subgroups are separated according to disease stage and vascular access history **(C)** or dialysis vintage **(D)**. DM, diabetes; CKD5, stage 5 CKD; ESKD_noAVF, ESKD without previous AVF or AVG; ESKD_w/AVF, ESKD and previous AVF/AVG history. *$p < 0.05$ vs. (−) DM/(+) CKD5 and (−) DM/(+) ESKD_noAVF, ‡$p < 0.05$ vs. (−) DM/(+)CKD5 and (−) DM/ < 12 months.

of an AVF causes a profound increase in venous fibrosis in the juxta-anastomotic segment of the access (8). Our results indicate that this is a local effect that does not seem to affect ECM remodeling in more proximal veins of patients with previous AVF history.

Importantly, our study demonstrated a broad influence of diabetes in the detrimental chronic remodeling of veins by exacerbating IH and increasing medial fibrosis. This finding is of interest given the treatable nature of hyperglycemia and the potential benefits in improving vein health. A relationship between diabetes and arterial IH and fibrosis has been previously reported (2, 41–43), which has been mostly blamed on the effects of advanced glycation end-products (AGEs) on the vascular wall (44). The latter are known to increase endothelial dysfunction, oxidative stress, vascular inflammation, and angiotensin II signaling, among others (44, 45). The association of diabetes with upper quartile levels of IH and not with gradual increases mimics previous observations in carotid IH (42), and suggests an exacerbating role or independent mechanism superimposing the cellular responses to dialysis conditions. The level of AGEs in tissues is determined by glycemic control, turnover of proteins, and kidney function (46–48). Therefore, an additive vasculopathic effect of AGEs in CKD patients is highly conceivable (49). Current guidelines by the Kidney Disease Outcomes Quality Initiative for vessel preservation in pre-dialysis patients mainly refer to avoidance of vessel injury (50). However, improving vein suitability may be an additional reason for life-long glycemic control. Interestingly, unlike arteries (26, 42), hypertension was not associated with chronic venous IH or fibrosis, likely reflecting the low-pressure conditions of venous circulation.

The limitations of the study include the retrospective nature of the analyses, the lack of information on the onset of comorbidities for the CKD cohort, and the limited clinical records for organ donors which prevented us from analyzing the effects of other clinical factors. While statistical models accounted for both clinical and demographics factors, differences in the latter between the CKD and non-CKD groups may be a confounding factor to consider in future studies.

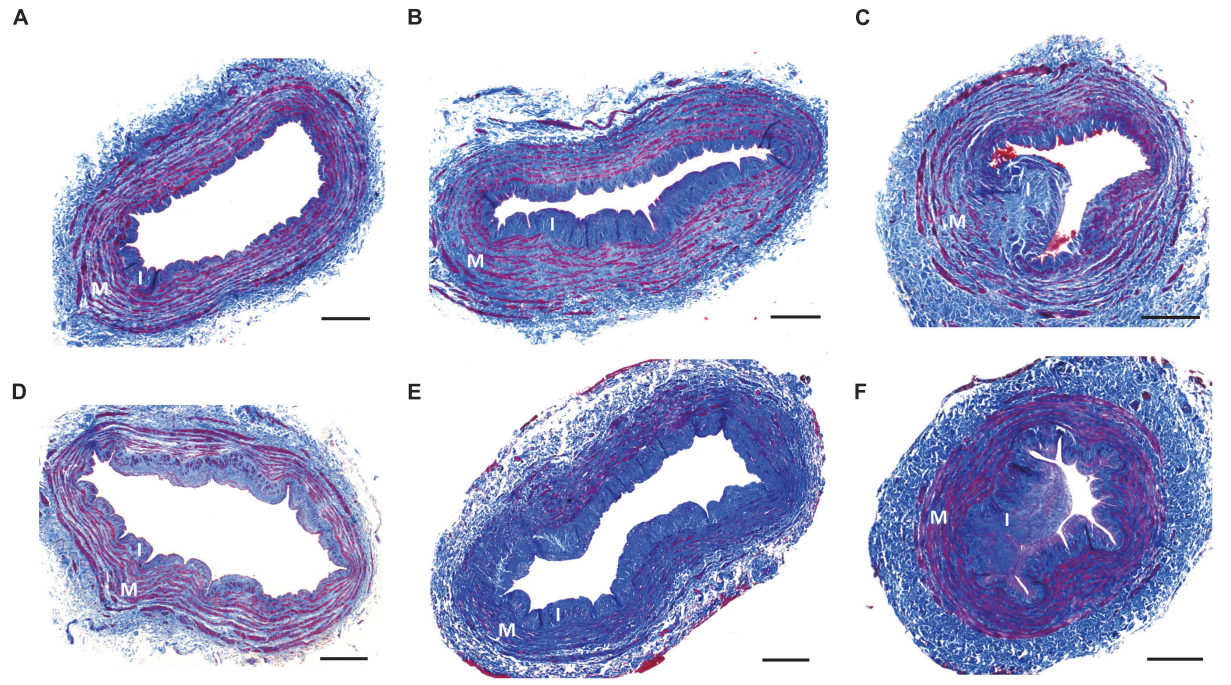

FIGURE 3
Representative vein morphometry in CKD/ESKD and non-CKD patients. Representative cross-sections of non-CKD **(A–C)** and CKD/ESKD veins **(D–F)** exemplifying mild **(A,D)**, moderate **(B,E)**, and high intimal hyperplasia **(C,F)**. Pictures in **(A,D,F)** also show cases of low medial fibrosis, whereas **(B,C,E)** present cross-sections with moderate-high fibrosis. I, intima; M, media. Scale bars = 400 μm.

Despite these limitations, to our knowledge, this is the first systematic analysis of vein morphometry in CKD and non-CKD individuals. This work improves our understanding of vascular aging and dialysis effects in upper extremity veins and identifies diabetes as a critical and manageable factor in the development of venous IH and medial fibrosis.

Data availability statement

The raw data supporting the conclusions of this article will be made available by the authors, without undue reservation.

Ethics statement

The studies involving human participants were reviewed and approved by the University of Miami Institutional Review Board. The patients/participants provided their written informed consent to participate in this study.

Author contributions

LM and RV-P contributed to the idea and study design. AS and MT were responsible for tissue collection. XL, ZZ, AC, CM, KM-P, and AA were responsible for tissue processing and data acquisition. XL, LM, and YP performed data analysis. XL, LM, and RV-P drafted the manuscript. LM, MT, AS, and RV-P were responsible for supervision and mentorship. MT, LS, and XY contributed fruitful discussions and clinical insights. All authors took part in the interpretation of the results and approved the final version of the manuscript.

Funding

This study was supported by the National Institutes of Health (grants R01-DK098511 to LS and RV-P, R01-DK121227 and R01-DK132888 to RV-P, and K08-HL151747 to LM), and the VA Merit Award (grant IBX004658 to RV-P).

Acknowledgments

We gratefully acknowledge the contribution of organ donors, their family members, and all the staff and surgical team at the Life Alliance Organ Recovery Agency for their collaboration in the collection of vascular tissues.

Conflict of interest

The authors declare that the research was conducted in the absence of any commercial or financial relationships that could be construed as a potential conflict of interest.

Publisher's note

All claims expressed in this article are solely those of the authors and do not necessarily represent those of their affiliated organizations, or those of the publisher, the editors and the reviewers. Any product that may be evaluated in this article, or claim that may be made by its manufacturer, is not guaranteed or endorsed by the publisher.

Supplementary material

The Supplementary Material for this article can be found online at: https://www.frontiersin.org/articles/10.3389/fcvm.2022.1005030/full#supplementary-material

References

1. Siddiqui MA, Ashraff S, Carline T. Maturation of arteriovenous fistula: analysis of key factors. *Kidney Res Clin Pract.* (2017) 36:318–28. doi: 10.23876/j.krcp.2017.36.4.318

2. Selvin E, Najjar SS, Cornish TC, Halushka MK. A comprehensive histopathological evaluation of vascular medial fibrosis: insights into the pathophysiology of arterial stiffening. *Atherosclerosis.* (2010) 208:69–74. doi: 10.1016/j.atherosclerosis.2009.06.025

3. Allon M, Litovsky SH, Tey JCS, Sundberg CA, Zhang Y, Chen Z, et al. Abnormalities of vascular histology and collagen fiber configuration in patients with advanced chronic kidney disease. *J Vasc Access.* (2019) 20:31–40. doi: 10.1177/1129729818773305

4. Verbeke FH, Agharazii M, Boutouyrie P, Pannier B, Guérin AP, London GM. Local shear stress and brachial artery functions in end-stage renal disease. *J Am Soc Nephrol.* (2007) 18:621–8. doi: 10.1681/ASN.2006040400

5. London GM, Marchais SJ, Guerin AP, Metivier F, Pannier B. Vascular and cardiac remodeling in end-stage renal disease. *Nefrología.* (1997) 17:17–22.

6. Kolodgie FD, Burke AP, Nakazawa G, Virmani R. Is pathologic intimal thickening the key to understanding early plaque progression in human atherosclerotic disease?. *Arterioscler Thromb Vasc Biol.* (2007) 27:986–9. doi: 10.1161/ATVBAHA.0000258865.44774.41

7. Kahn SR. The post-thrombotic syndrome. *Hematology Am Soc Hematol Educ Program.* (2016) 2016:413–8. doi: 10.1182/asheducation-2016.1.413

8. Martinez L, Duque JC, Tabbara M, Paez A, Selman G, Hernandez DR, et al. Fibrotic venous remodeling and nonmaturation of arteriovenous fistulas. *J Am Soc Nephrol.* (2018) 29:1030–40. doi: 10.1681/ASN.2017050559

9. Heckenkamp J, Lamuraglia GM. Intimal hyperplasia, arterial remodeling, and restenosis: an overview. *Perspect Vasc Surg Endovasc Ther.* (1999) 11:71–94.

10. Raffetto JD, Khalil RA. Mechanisms of lower extremity vein dysfunction in chronic venous disease and implications in management of varicose veins. *Vessel Plus.* (2021) 5:36. doi: 10.20517/2574-1209.2021.16

11. Tabbara M, Duque JC, Martinez L, Escobar LA, Wu W, Pan Y, et al. Pre-existing and postoperative intimal hyperplasia and arteriovenous fistula outcomes. *Am J Kidney Dis.* (2016) 68:455–64. doi: 10.1053/j.ajkd.2016.02.044

12. Alpers CE, Imrey PB, Hudkins KL, Wietecha TA, Radeva M, Allon M, et al. Histopathology of veins obtained at hemodialysis arteriovenous fistula creation surgery. *J Am Soc Nephrol.* (2017) 28:3076–88. doi: 10.1681/ASN.2016050598

13. Vazquez-Padron RI, Allon M. New insights into dialysis vascular access: impact of preexisting arterial and venous pathology on AVF and AVG outcomes. *Clin J Am Soc Nephrol.* (2016) 11:1495–503. doi: 10.2215/CJN.01860216

14. Cheung AK, Imrey PB, Alpers CE, Robbin ML, Radeva M, Larive B, et al. Intimal hyperplasia, stenosis, and arteriovenous fistula maturation failure in the hemodialysis fistula maturation study. *J Am Soc Nephrol.* (2017) 28:3005–13. doi: 10.1681/ASN.2016121355

15. MacRae JM, Oliver M, Clark E, Dipchand C, Hiremath S, Kappel J, et al. Arteriovenous vascular access selection and evaluation. *Can J Kidney Health Dis.* (2016) 3:2054358116669125. doi: 10.1177/2054358116669125

16. Parang P, Arora R. Coronary vein graft disease: pathogenesis and prevention. *Can J Cardiol.* (2009) 25:e57–62. doi: 10.1016/s0828-282x(09)70486-6

17. Hernandez DR, Applewhite B, Martinez L, Laurito T, Tabbara M, Rojas MG, et al. Inhibition of lysyl oxidase with beta-aminopropionitrile improves venous adaptation after arteriovenous fistula creation. *Kidney360.* (2021) 2:270–8. doi: 10.34067/kid.0005012020

18. Martinez L, Tabbara M, Duque JC, Selman G, Falcon NS, Paez A, et al. Transcriptomics of human arteriovenous fistula failure: genes associated with nonmaturation. *Am J Kidney Dis.* (2019) 74:73–81. doi: 10.1053/j.ajkd.2018.12.035

19. Charles AK, Gresham GA. Histopathological changes in venous grafts and in varicose and non-varicose veins. *J Clin Pathol.* (1993) 46:603–6. doi: 10.1136/jcp.46.7.603

20. Woodside KJ, Hu M, Burke A, Murakami M, Pounds LL, Killewich LA, et al. Morphologic characteristics of varicose veins: possible role of metalloproteinases. *J Vasc Surg.* (2003) 38:162–9. doi: 10.1016/s0741-5214(03)00134-4

21. Valdivielso JM, Rodriguez-Puyol D, Pascual J, Barrios C, Bermúdez-López M, Sánchez-Niño MD, et al. Atherosclerosis in chronic kidney disease: more, less, or just different? *Arterioscler Thromb Vasc Biol.* (2019) 39:1938–66. doi: 10.1161/ATVBAHA.119.312705

22. Xu X, Wang B, Ren C, Hu J, Greenberg DA, Chen T, et al. Age-related Impairment of Vascular Structure and Functions. *Aging Dis.* (2017) 8:590–610. doi: 10.14336/AD.2017.0430

23. Molnar AA, Nadasy GL, Dornyei G, Patai BB, Delfavero J, Fülöp GÁ, et al. The aging venous system: from varicosities to vascular cognitive impairment. *Geroscience.* (2021) 43:2761–84. doi: 10.1007/s11357-021-00475-2

24. Greaney JL, Farquhar WB. Why do veins stiffen with advancing age?. *J Appl Physiol.* (1985) 2011:11–2. doi: 10.1152/japplphysiol.01273.2010

25. Ungvari Z, Tarantini S, Donato AJ, Galvan V, Csiszar A. Mechanisms of Vascular Aging. *Circ Res.* (2018) 123:849–67. doi: 10.1161/CIRCRESAHA.118.311378

26. Harvey A, Montezano AC, Lopes RA, Rios F, Touyz RM. Vascular fibrosis in aging and hypertension: molecular mechanisms and clinical implications. *Can J Cardiol.* (2016) 32:659–68. doi: 10.1016/j.cjca.2016.02.070

27. Donato AJ, Eskurza I, Silver AE, Levy AS, Pierce GL, Gates PE, et al. Direct evidence of endothelial oxidative stress with aging in humans: relation to impaired endothelium-dependent dilation and upregulation of nuclear factor-kappaB. *Circ Res.* (2007) 100:1659–66. doi: 10.1161/01.RES.0000269183.13937.e8

28. Rossman MJ, Kaplon RE, Hill SD, McNamara MN, Santos-Parker JR, Pierce GL, et al. Endothelial cell senescence with aging in healthy humans: prevention by habitual exercise and relation to vascular endothelial function. *Am J Physiol Heart Circ Physiol.* (2017) 313:H890–5. doi: 10.1152/ajpheart.00416.2017

29. Donato AJ, Black AD, Jablonski KL, Gano LB, Seals DR. Aging is associated with greater nuclear NF kappa B, reduced I kappa B alpha, and increased expression of proinflammatory cytokines in vascular endothelial cells of healthy humans. *Aging Cell.* (2008) 7:805–12. doi: 10.1111/j.1474-9726.2008.00438.x

30. Pascual G, Mendieta C, Garcia-Honduvilla N, Corrales C, Bellón JM, Buján J. TGF-beta1 upregulation in the aging varicose vein. *J Vasc Res.* (2007) 44:192–201. doi: 10.1159/000100375

31. Perek B, Malinska A, Gasowski J, Ostalska-Nowicka D, Perek A, Jemielity M, et al. Potentially positive ageing-related variations of medial smooth muscle cells in

the saphenous veins used as aortocoronary bypass grafts. *Folia Histochem Cytobiol.* (2016) 54:91–8. doi: 10.5603/FHC.a2016.0011

32. Lee T, Somarathna M, Hura A, Wang Y, Campos B, Arend L, et al. Natural history of venous morphologic changes in dialysis access stenosis. *J Vasc Access.* (2014) 15:298–305. doi: 10.5301/jva.5000212

33. Wali MA, Eid RA, Dewan M, Al-Homrany MA. Intimal changes in the cephalic vein of renal failure patients before arterio-venous fistula (AVF) construction. *J Smooth Muscle Res.* (2003) 39:95–105.

34. Wali MA, Eid RA, Dewan M, Al-Homrany MA. Pre-existing histopathological changes in the cephalic vein of renal failure patients before arterio-venous fistula (AVF) construction. *Ann Thorac Cardiovasc Surg.* (2006) 12:341–8.

35. Monroy MA, Fang J, Li S, Ferrer L, Birkenbach MP, Lee IJ, et al. Chronic kidney disease alters vascular smooth muscle cell phenotype. *Front Biosci.* (2015) 20:784–95. doi: 10.2741/4337

36. Panizo S, Martinez-Arias L, Alonso-Montes C, Cannata P, Martín-Carro B, Fernández-Martín JL, et al. Fibrosis in chronic kidney disease: pathogenesis and consequences. *Int J Mol Sci.* (2021) 22:408. doi: 10.3390/ijms22010408

37. Briet M, Collin C, Karras A, Laurent S, Bozec E, Jacquot C, et al. Arterial remodeling associates with CKD progression. *J Am Soc Nephrol.* (2011) 22:967–74. doi: 10.1681/ASN.2010080863

38. Rasmussen DGK, Boesby L, Nielsen SH, Tepel M, Birot S, Karsdal MA, et al. Collagen turnover profiles in chronic kidney disease. *Sci Rep.* (2019) 9:16062. doi: 10.1038/s41598-019-51905-3

39. Randles M, Lausecker F, Kong Q, Suleiman H, Reid G, Kolatsi-Joannou M, et al. Identification of an altered matrix signature in kidney aging and disease. *J Am Soc Nephrol.* (2021) 32:1713–32. doi: 10.1681/ASN.2020101442

40. Freise C, Schaefer B, Bartosova M, Bayazit A, Bauer U, Pickardt T, et al. Arterial tissue transcriptional profiles associate with tissue remodeling and cardiovascular phenotype in children with end-stage kidney disease. *Sci Rep.* (2019) 9:10316. doi: 10.1038/s41598-019-46805-5

41. Nathan DM, Lachin J, Cleary P, Orchard T, Brillon DJ, Backlund JY, et al. Intensive diabetes therapy and carotid intima-media thickness in type 1 diabetes mellitus. *N Engl J Med.* (2003) 348:2294–303. doi: 10.1056/NEJMoa022314

42. Gomez-Marcos MA, Recio-Rodriguez JI, Rodriguez-Sanchez E, Patino-Alonso MC, Magallón-Botaya R, Martínez-Vizcaino V, et al. [Carotid intima-media thickness in diabetics and hypertensive patients]. *Rev Esp Cardiol.* (2011) 64:622–5. doi: 10.1016/j.recesp.2010.10.025

43. Al-Auqbi TFR, Al-Sabbagh AA, Al-Karawi IN, Maj B. Effect of hypertension on the carotid artery intima media thickness (IMT) in patients with type 2 diabetes mellitus – Across sectional study. *Int J Diabetes Res.* (2014) 3:66–70.

44. Stirban A, Gawlowski T, Roden M. Vascular effects of advanced glycation endproducts: clinical effects and molecular mechanisms. *Mol Metab.* (2014) 3:94–108. doi: 10.1016/j.molmet.2013.11.006

45. Koka V, Wang W, Huang XR, Kim-Mitsuyama S, Truong LD, Lan HY. Advanced glycation end products activate a chymase-dependent angiotensin II-generating pathway in diabetic complications. *Circulation.* (2006) 113:1353–60. doi: 10.1161/CIRCULATIONAHA.105.575589

46. Monnier VM, Sell DR, Nagaraj RH, Miyata S, Grandhee S, Odetti P, et al. Maillard reaction-mediated molecular damage to extracellular matrix and other tissue proteins in diabetes, aging, and uremia. *Diabetes.* (1992) 41:36–41. doi: 10.2337/diab.41.2.s36

47. Miyata T, Ueda Y, Horie K, Nangaku M, Tanaka S, van Ypersele de Strihou C. Renal catabolism of advanced glycation end products: the fate of pentosidine. *Kidney Int.* (1998) 53:416–22. doi: 10.1046/j.1523-1755.1998.00756.x

48. Berg TJ, Dahl-Jorgensen K, Torjesen PA, Hanssen KF. Increased serum levels of advanced glycation end products (AGEs) in children and adolescents with IDDM. *Diabetes Care.* (1997) 20:1006–8. doi: 10.2337/diacare.20.6.1006

49. Raj DS, Choudhury D, Welbourne TC, Levi M. Advanced glycation end products: a Nephrologist's perspective. *Am J Kidney Dis.* (2000) 35:365–80. doi: 10.1016/s0272-6386(00)70189-2

50. Lok CE, Huber TS, Lee T, Shenoy S, Yevzlin AS, Abreo K, et al. KDOQI clinical practice guideline for vascular access: 2019 update. *Am J Kidney Dis.* (2020) 75:S1–164. doi: 10.1053/j.ajkd.2019.12.001

frontiers | Frontiers in Cardiovascular Medicine

TYPE Original Research
PUBLISHED 11 January 2023
DOI 10.3389/fcvm.2022.1064026

OPEN ACCESS

EDITED BY
Tin Kyaw,
Baker Heart and Diabetes Institute, Australia

REVIEWED BY
Ofir Koren,
Cedars Sinai Medical Center, United States
Federico Fortuni,
Leiden University Medical Center (LUMC), Netherlands

*CORRESPONDENCE
Luca Testa
luctes@gmail.com

SPECIALTY SECTION
This article was submitted to Clinical and Translational Cardiovascular Medicine, a section of the journal Frontiers in Cardiovascular Medicine

RECEIVED 07 October 2022
ACCEPTED 20 December 2022
PUBLISHED 11 January 2023

CITATION
Testa L, Popolo Rubbio A, Squillace M, Albano F, Cesario V, Casenghi M, Tarantini G, Pagnotta P, Ielasi A, Popusoi G, Paloscia L, Durante A, Maffeo D, Meucci F, Valentini G, Ussia GP, Cioffi P, Cortese B, Sangiorgi G, Contegiacomo G and Bedogni F (2023) Patent foramen ovale occlusion with the Cocoon PFO Occluder. The PROS-IT collaborative project.
Front. Cardiovasc. Med. 9:1064026.
doi: 10.3389/fcvm.2022.1064026

Patent foramen ovale occlusion with the Cocoon PFO Occluder. The PROS-IT collaborative project

Luca Testa[1]*, Antonio Popolo Rubbio[1], Mattia Squillace[1], Flavio Albano[1], Vincenzo Cesario[1], Matteo Casenghi[1], Giuseppe Tarantini[2], Paolo Pagnotta[3], Alfonso Ielasi[4], Grigore Popusoi[5], Leonardo Paloscia[6], Alessandro Durante[7], Diego Maffeo[8], Francesco Meucci[9], Giuliano Valentini[10], Gian Paolo Ussia[11], Paolo Cioffi[12], Bernardo Cortese[13], Giuseppe Sangiorgi[14], Gaetano Contegiacomo[15] and Francesco Bedogni[1]

[1]Department of Cardiology, IRCCS Policlinico San Donato, Milan, Italy, [2]Department of Cardiac, Thoracic and Vascular Sciences, University of Padua, Padua, Italy, [3]Cardio Center, Humanitas Research Hospital, Milan, Italy, [4]Clinical and Interventional Cardiology Unit, Istituto Clinico Sant'Ambrogio, Milan, Italy, [5]Interventional Cardiology Service, Montevergine Clinic, Mercogliano, Italy, [6]U.O.C. Cardiologia-UTIC, Ospedale Santo Spirito, Pescara, Italy, [7]Cardiology Unit, Policlinico San Marco, Bergamo, Italy, [8]Fondazione Poliambulanza, Brescia, Italy, [9]Structural Interventional Cardiology, Careggi University Hospital, Florence, Italy, [10]Cardiology Intensive Care Unit and Cath Lab, Ospedale Civile SS. Filippo e Nicola, L'Aquila, Italy, [11]Unit of Cardiovascular Science, Department of Medicine, Campus Bio-Medico University, Rome, Italy, [12]Department of Cardiology, Cardiac Cath Lab, Città di Alessandria Institute, Alessandria, Italy, [13]Department of Cardiology, San Carlo Clinic, Milan, Italy, [14]Department of Biomedicine and Prevention, Tor Vergata University of Rome, Rome, Italy, [15]Department of Interventional Cardiology, Anthea Hospital, GVM Care and Research, Bari, Italy

Background: The Cocoon patent foramen ovale (PFO) Occluder is a new generation nitinol alloy double-disk device coated with nanoplatinum, likely useful in patients with nickel hypersensitivity. Early results and mid-term outcomes of this device in percutaneous PFO closure are missing.

Aims: To assess the preliminary efficacy and safety profile of PFO closure with Cocoon device in an Italian multi-center registry.

Methods: This is a prospective registry of 189 consecutive adult patients treated with the Cocoon PFO Occluder at 15 Italian centers from May 2017 till May 2020. Patients were followed up for 2 years.

Results: Closure of the PFO with Cocoon Occluder was carried out successfully in all patients, with complete closure without residual shunt in 94.7% of the patients and minimal shunt in 5.3%. Except from a case of paroxysmal supraventricular tachycardia and a major vascular bleeding, no procedural and in-hospital device-related complications occurred. No patient developed cardiac erosions, allergic reactions to nickel, or any other major complications during the follow-up. During the follow-up period, 2 cases of new-onset atrial fibrillation occurred within thirty-day.

10.3389/fcvm.2022.1064026

Conclusions: Percutaneous closure of PFO with Cocoon Occluder provided satisfactory procedural and mid-term clinical follow-up results in a real-world registry.

KEYWORDS

patent foramen ovale (PFO), embolism, translational, nanoparticle, platinum

Introduction

The presence of patent foramen ovale (PFO) can be detected in about 25% of the adult population, with implication in the pathogenesis of different medical conditions as cryptogenic stroke, decompression illness, platypnea-orthodeoxia syndrome and, although still controversial, migraine with aura (1–3). When PFO closure is indicated, percutaneous closure is recommended as the method of choice (4–6). In this regards, multiple observational studies, meta-analyses and trials have shown a benefit of percutaneous PFO closure, demonstrating favorable long-term results in terms of efficacy in preventing recurrence of stroke, improvement in quality of life and cost-effectiveness of this procedure when compared to medical therapy, thus increasing the popularity of this procedure (7–12).

Nowadays, different systems are available for percutaneous PFO closure, including a suture-based system (13, 14). Percutaneous PFO closure is considered a relatively simple procedure but, although very rarely, it has a potential risk of cardiac erosion, and nickel allergic reactions in predisposed subjects (15, 16).

The Cocoon PFO Occluder (Vascular Innovations Co. Nonthaburi, Thailand) was recently released as a novel nitinol alloy double-disk device, with a similar design to Amplatzer Occluder device (Abbott, Abbott Park, Illinois, USA). The Cocoon PFO Occluder features a specific nanoplatinum coating that should abolish the issue of nickel hypersensitivity (Ni-Hy) and smooth the microscopic geometry of the disks to minimize the risk of erosion. Initial evaluation of Cocoon septal Occluder for closure of atrial septal defects in adults and pediatric patients was recently presented, whereas procedural and follow-up data of the Cocoon PFO Occluder are missing (17).

We herein feature a nation-wide registry concerning the acute procedural data and the mid-term clinical follow-up of adult patients with PFO treated with the Cocoon Occluder.

Abbreviations: PFO, Patent Foramen Ovale; Ni-Hy, Nickel Hypersensitivity; RLS, Right-To-Left Shunting; SNAS, systemic nickel allergy syndrome; TIA, Transient Ischemic Attack; MAE(s), Major Adverse Event(s).

Methods

Patient population and study design

In this multi-center, observational registry, adult patients ≥18 years old, with a clinical indication for PFO closure according to the current guidelines, treated with the Cocoon PFO Occluder were consecutively included (4–6). All the patients treated with Cocoon PFO Occluder at the participating centers were sequentially included in the registry in a prospective way and data where then analyzed retrospectively.

Patients were eligible for the procedure if they presented a documented history of cryptogenic stroke (radiologically verified) or transient ischemic attack (TIA) in the previous 12 months, intractable migraine or need for PFO closure for professional reasons. Exclusion criteria were subjects with previous stroke or TIA with known etiology or with congenital or pre-existing neurological disorders (i.e., multiple sclerosis, epilepsy) or intra-cranial disease; subjects with atrial fibrillation/flutter or other known emboligenic heart diseases; subjects with carotid, vertebral or basilar artery stenosis >50%; subjects with previous endocarditis or at risk for endocarditis;

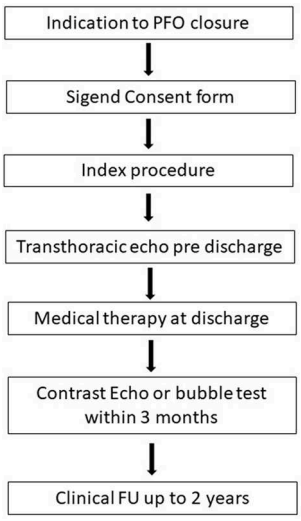

FIGURE 1
Study design flow chart.

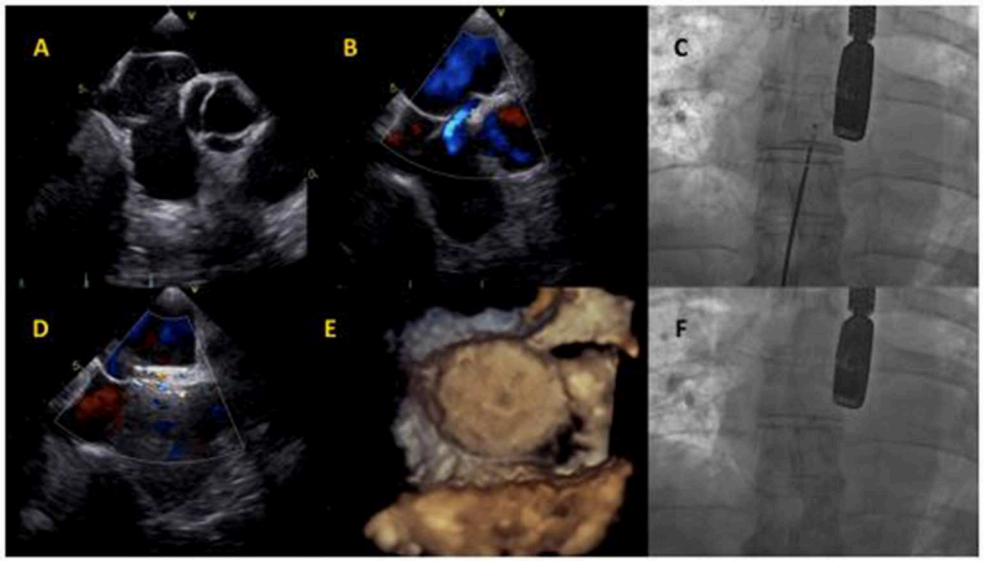

FIGURE 2
Cocoon PFO Occluder implantation. **(A)** Baseline transesophageal echocardiography showing atrial septum aneurysm and Chiari network. **(B)** Baseline interatrial shunt. **(C)** Cocoon PFO Occluder positioning at fluoroscopy. **(D)** Intraprocedural transesophageal echocardiography, showing minimal intra-device shunt. **(E)** Device assessment with 3D-echocardiography imaging. **(F)** Final device release at fluoroscopy.

subjects with contraindications to aspirin, clopidogrel or anticoagulant therapy; subjects under tutorship, curatorship or unable to take the prescribed medical therapy.

Baseline and procedural variables were collected from medical records through a web-based electronic case report form from each participating center. Follow-up data were then obtained by means of telephone calls and/or outpatients clinical visits.

For the purpose of our analysis, we considered as efficacy outcome the occurrence of effective PFO closure with a residual minimal RLS or lower in acute and at the follow-up. As regards safety outcome, we considered the occurrence of peri-procedural major adverse events (MAEs) including death, acute neurological disorders, new-onset arrhythmia, major bleeding, cardiac tamponade or complications related to the vascular access, device malposition and embolization. The secondary safety outcome was a composite of MAEs detected during the follow-up including arrhythmia, late neurological disorders, endocarditis and device-related adverse events (malposition, embolization, thrombosis, and systemic nickel allergy syndrome (SNAS).

Before the procedure, all the patients underwent contrast-enhanced transcranial Doppler ultrasound or transesophageal echocardiography with bubble test, in order to confirm the presence of the PFO and the severity of RLS. The grading of RLS through the PFO was semi-quantitative in accordance to the number of micro-bubbles detected in left atrium at rest and after Valsalva maneuver and defined as severe (≥20 bubbles or opacification), moderate (6–19 bubbles), minimal (1–5 bubbles) or no-shunt (0 bubbles) (18).

All the patients signed an informed written consent.

The registry was approved by the local ethical committees of each participating hospital and the study complied with the Declaration of Helsinki.

Device

The Cocoon PFO Occluder is an implantable self-expandable double-disk device, structurally similar to the Amplatzer Occluder device (13, 19). The two disks are linked together by a short connecting waist allowing free motion of each disc. The disc diameter range is 18 to 30 mm for the left atrium disc and 18 to 35 mm for the right atrium disc, set up in different combinations (Figure 1). Similarly to other devices for PFO closure, the Cocoon PFO Occluder presents a nitinol core structure, but the main difference lies in the nanoplatinum coating of its wire mesh, with platinum atoms up to 25 microns using nanofusion technology. According to its manufacturer's instructions for use, the nanoplatinum coating may prevent nickel leaching into the bloodstream and increase device-surface smoothing.

Procedure

All patients underwent the procedure under general anesthesia or conscious sedation, and were simultaneously studied by transesophageal echocardiography or intra-cardiac echocardiography, at discretion of each participating center.

TABLE 1 Baseline demographic and clinical characteristics of the study population.

	$N = 189$
Baseline characteristics	
Age, years	50 ± 13
Female, *n* (%)	96 (50.8)
BMI, Kg/m^2	24 (22–27)
Hypertension, *n* (%)	49 (25.9)
Diabetes, *n* (%)	4 (2.1)
Smoker, *n* (%)	18 (9.5)
Coagulation Disorders, *n* (%) • Hyperhomocysteinemia, *n* (%) • Protein C/S Deficiency, *n* (%) • Leiden V Factor Mutation, *n* (%) • Factor II Mutation, *n* (%) • MTHFR Mutation, *n* (%) • Antiphospholipid Syndrome, *n* (%) • Others, *n* (%)	14 (7.4) 5 (2.6) 2 (1.1) 1 (0.5) 1 (0.5) 1 (0.5) 1 (0.5) 3 (1.6)
Atrial septal aneurysm, *n* (%)	91 (48.1)
Family history for congenital heart disease, *n* (%)	5 (2.6)
Congenital heart disease, *n* (%)	2 (1.1)
Rope score 1–3	5%
Rope score 4–6	15%
Rope score >6	80%
Shunt at rest	
None (0 bubbles), *n* (%) Minimal (1–5 bubbles), *n* (%) Moderate (6–19 bubbles), *n* (%) Severe (≥20 bubbles), *n* (%)	40 (21.2) 49 (26.0) 35 (18.5) 65 (34.4)
History and clinical presentation	
Cryptogenic stroke, *n* (%)	80 (42.3)
Multiple cryptogenic stroke, *n* (%)	7 (3.7)
TIA, *n* (%)	61 (32.3)
Multiple TIA, *n* (%)	5 (2.6)
Paradoxical embolism, *n* (%)	7 (3.7)
Deep vein thrombosis, *n* (%)	3 (1.6)
Migraine, *n* (%)	52 (27.5)
Professional Reasons, *n* (%)	3 (1.6)

Categorical variables are expressed as n (%). Continuous variables are expressed as mean ± standard deviation (SD) or median and interquartile range (IQR), as appropriate.
BMI, Body Mass Index; TIA, Transient Ischemic Attack.

The procedure was performed as for standard for percutaneous PFO closure, with wire crossing through the PFO into the left upper pulmonary vein and delivery sheath advancing over the stiff wire, with final release of the intended device; an illustrative case is displayed in Figure 2. The patients were heparinized to achieve an activated clotting time of more than 250 s during the whole procedure. The size of the device has been selected according to the echocardiographic septum and tunnel characteristics or according to the balloon sizing and rim adequacy. When device position was optimal, the device was released by a counterclockwise rotation of the delivery cable. Also in this case, residual RLS were graded as severe (≥20 bubbles or opacification), moderate (6–19 bubbles), minimal (1–5 bubbles) or no-shunt (0 bubbles).

The patients were discharged with aspirin and/or clopidogrel and/or oral anticoagulant in accordance to their clinical history and at discretion of the physicians. In order to evaluate residual RLS, contrast-enhanced transthoracic echocardiography and transcranial Doppler follow-up were done within 3 months post procedure.

Clinical FU was evaluated and recorded up to 2 years.

Statistical analysis

Categorical and dichotomous variables were expressed as absolute numbers and percentages whereas continuous variables were expressed as mean±standard deviation (SD) or median (25^{th} to 75^{th} interquartile range–IQR), as appropriate according to their distribution. Continuous variables were analyzed for normal distribution using the Shapiro-Wilk test. The data were analyzed with SPSS statistics software (version 25, IBM Corp., Armonk, N.Y., USA).

Results

Baseline characteristics

Between May 2018 and May 2020, at 15 Italian centers, 189 patients with clinical indications for percutaneous PFO closure were treated with Cocoon PFO Occluder. Complete patient characteristics are listed in Table 1.

The mean age was 5 ± 13 years and there was a slight prevalence of female gender (50.8%). Coagulation disorders were present in just 7.4% of patients. The main indications for PFO closure were cryptogenic stroke (42.3%) and TIA (32.3%). The basal shunt was severe in 65 patients (34.4%) and almost half of the patients presented atrial septum aneurysm (48.1%).

Procedural characteristics

The procedure was performed in conscious sedation in 67.2% of patients (Table 2). Transesophageal echocardiography was the main imaging modality (80.4%). The size of the device was selected according to the echocardiographic septum characteristics (88.9%) or according to the balloon sizing (11.1%). Mean procedural time was 34 ± 20 min. The most used device was Cocoon PFO Occluder 25*18 mm (73.0%).

10.3389/fcvm.2022.1064026

TABLE 2 Procedural characteristics.

	$N = 189$
Procedural variables	
Conscious sedation, *n* (%)	127 (67.2)
General anesthesia, *n* (%)	62 (32.8)
Procedural time, min	34 ± 20
Transesophageal echocardiography, *n* (%)	152 (80.4)
Intracardiac Echocardiography, *n* (%) Balloon sizing, *n* (%)	37 (19.6) 21 (11.1)
Intra-Procedural MAEs • Death • Stroke/TIA • Atrial fibrillation • Paroxysmal supraventricular tachycardia • Ventricular tachycardia/fibrillation • Major bleeding • Cardiac tamponade • Device malposition • Device embolization	 0 (0.0) 0 (0.0) 0 (0.0) 1 (0.5) 0 (0.0) 1 (0.5) 0 (0.0) 0 (0.0) 0 (0.0)
Device employed	
• Cocoon 18∗18 mm, *n* (%)	12 (6.3)
• Cocoon 25∗18 mm, *n* (%)	138 (73.0)
• Cocoon 25∗25 mm, *n* (%)	4 (2.1)
• Cocoon 30∗30 mm, *n* (%)	28 (14.8)
• Cocoon 35∗25 mm, *n* (%)	7 (3.7)
Residual shunt	
• None (0 bubbles), *n* (%)	179 (94.7)
• Minimal (1–5 bubbles), *n* (%)	10 (5.3)
• Moderate (6–19 bubbles), *n* (%)	0 (0.0)
• Severe (≥20 bubbles), *n* (%)	0 (0.0)

Categorical variables are expressed as n (%). Continuous variables are expressed as mean ± standard deviation (SD) or median and interquartile range (IQR), as appropriate. MAEs, Major Adverse Events; TIA, Transient Ischemic Attack.

During the procedure, except a single case of paroxysmal supraventricular tachycardia and a major vascular bleeding (patient was on clopidogrel), no other significant adverse events occurred. Device embolization and recapturing or procedural cardiac erosions neither occurred. Post-procedural residual RLS was absent in most of the patients (94.7%), whereas a minimal RLS was documented in 5.3%.

Post-procedural outcome

No adverse events occurred during the hospital stay. Most of the patients were discharged with indication to dual antiplatelet therapy with aspirin and clopidogrel (97.9%), for 1–12 months (Table 3). Four patients received a short- single antiplatelet therapy with aspirin and 5 patients received an oral anticoagulant therapy in association with antiplatelet: the history of a coagulation disorder was the reason to combine the anticoagulant with the antiplatelet therapy. This therapy was kept for a month and then followed by the anticoagulant therapy alone.

TABLE 3 Discharge medical therapy.

	$N = 189$
Medical therapy	
Aspirin and clopidogrel • 1 Month • 3 Months • >3 Months Single aspirin Anticoagulant therapy	185 (97.9) 54 (28.5) 120 (64.8) 11 (6.7) 4 (2.1) 5 (2.6)
• Vitamin K antagonist • Apixaban • Dabigatran • Edoxaban • Rivaroxaban	1 (0.5) 1 (0.5) 0 (0.0) 2 (1.1) 1 (0.5)
Lifelong aspirin Lifelong clopidogrel Lifelong anticoagulant	51 (27%) 4 (2.1) 2 (1.1)

Categorical variables are expressed as n (%).

Life-long aspirin was prescribed in 27.0% of the cases, whereas life-long clopidogrel in 2.1%. Patients that were in treatment with anticoagulants before the procedure continued their standard treatment with vitamin K antagonists or direct oral anticoagulants.

The choice of the antiplatelet/anticoagulant regimen was left to the attending physician in order to mimic the real world, in the absence of clear-cut evidence on the most appropriate therapy after PFO closure.

Within 2 years post procedure, 2 cases (1.1%) of new-onset paroxysmal atrial fibrillation occurred, both within 3 weeks from the index procedure. No other major adverse events were reported. In all cases, contrast-enhanced echocardiographic and/or transcranial Doppler follow-up within 3 months after the index procedure showed absence of any severe RLS in all patients.

Discussion

Percutaneous PFO closure is a well-established therapy for paradoxical left thromboembolism (5, 20). Multiple trials and meta-analyses showed the benefit of the double-disk technology PFO closure devices (13, 14). In this context, the Cocoon PFO Occluder has been introduced with the aim of surpassing the limitations of available devices but scarce data are available and the benefit of its technical features needs to be confirmed.

The main findings of this prospective nation-wide registry can be summarized as follows:

- The novel Cocoon PFO Occluder showed good results in terms of efficacy (with absence of severe residual RLS in 100% of the cases) and safety.
- The effective closure of the PFO was confirmed in all cases by means of appropriate imaging.
- No cardiac erosion, allergic reactions or thrombotic events occurred both in the early phase and during the 2 year FU.
- 2 cases (1.1%) of early new-onset paroxysmal atrial fibrillation occurred.

Efficacy profile

The effectiveness of the Cocoon PFO Occluder in permanently closing the PFO seems to be consistent with those observed with the large RCTs concerning the Amplatzer Occluder and Gore Occluder (W. L. Gore and Associates, Inc, Newark, Delaware, USA) (6–9). Indeed, the Cocoon PFO Occluder obtained a complete resolution of the RLS in 94.7% of the cases and no ischemic events occurred up to 2 years post procedure. Previous literature concerning a limited number of cases consistently reported no recurrent events and no residual shunt over a 6-months follow-up (19, 20).

Safety profile

The nanoplatinum coating of the Cocoon PFO Occluder is supposed to soften the structure of the device, and thus minimize the risk of cardiac erosion, that is a rare but dramatic complication, more often observed with devices for the treatment of ASD (16, 21). Whether the technical features of the device actually translate in a safer tool has to be demonstrated in a head to head comparison, however, we hereby report no cases of cardiac erosion or cardiac tamponade, which is in line with previous reports with this device (17).

Potential risk reduction of Ni-Hy

The specific design of Cocoon device may supposedly address the demands for device PFO closure in patients with Ni-Hy: the nanoplatinum coating theoretically prevent nickel ions release into the bloodstream. The Ni-Hy represents the classic presentation of a T cell-mediated, delayed-type hypersensitivity response to exogenous agents. The initial step is hapten binding to a skin carrier protein. The complex ultimately produces the sensitization of T cells. Sensitized T cells encountering the antigen at any time later will then lead to the release of cytokines, which in turn leads to macrophage activation and produces the immune response (22).

In literature, the incidence and real magnitude of the device-related Ni-Hy "syndrome" is still a matter of debate, and skin reactions must be distinguished from the systemic reactions which, in extreme situations, may lead to surgical explant: this critical situation always occur weeks to months after the device implant. Preliminary studies have shown that, during the first period of endothelization after Cocoon device implantation, there was no nickel release into the bloodstream (22–26).

A way to evaluate the presence of Ni-Hy might be the use of patches before the PFO closure, although it still unclear their role on top of clinical and physical examination (27).

Contact allergy secondary to the Amplatzer (St. Jude Medical, Inc., St. Paul, Minnesota), PFO-Star (Cardia Inc., Burnsville, Minnesota), and Gore Helex devices have been described previously (28–32).

In the 3 pivotal randomized trials on https://www.sciencedirect.com/topics/medicine-and-dentistry/patent-foramen-ovale PFO closure published in 2017, which included more than 2,000 patients, only 1 device-related allergic reaction was reported among the adverse events (7–9). No device explant was reported in any of the trials. Of note, patch testing to nickel was not required in the studies and patient reported history of nickel allergy was not an exclusion criterion for any of the trials.

In a retrospective analysis of explanation rates for PFO/ASD occluder devices, 38 of 13,736 (0.28%) of patients undergoing percutaneous closure had device removal (25). Allergy was not listed as the primary cause of explanation in any cases, but among the 14 patients who required device explanation for chest pain, 7 were found to have a positive patch test for nickel.

For people who present Ni-Hy, the use of suture-mediated system may be proposed, but this technology has an 18–20% risk of significant residual RLS (33, 34), thus its use has a weak rationale.

On the other hand, whether the use of a Cocoon is the appropriate solution has to be confirmed beyond the theoretical basis.

Potential risk reduction of device thrombosis

The polypropylene filling of the Coccon occluder may be associated with a reduced device-related thrombotic risk that, according to the literature, has been estimated with other devices between 1 and 2% (6, 17, 19).

Of note, despite 7.4% of patients in our registry presented coagulation disorders, no device-related thrombotic events were recorded in the peri-procedural setting, and up to 2 years.

In a recent publication, thrombus formation on the device was the justification for surgical excision in 4 (0.03%) of the 13,736 device implants. Of the 4 devices explanted with thrombus: 3 were CardioSEAL devices (0.15% of such devices) and 1 was an Amplatzer device (0.01%) (25).

A clear understanding of the risk of thrombosis related to different PFO closure devices is quite challenging as only a large

scale direct comparison with other devices, with a comparable thrombotic risk and medical therapy might be reliable.

Arrhythmic complications

Major arrhythmic events have been previously reported in patients treated with occluder devices, with variable rates of 0.5–15%: apparently, there is a direct correlation with the size of the defect and, subsequently, with the size of the device selected that may cause a mechanical irritation and inflammatory reaction (6, 35, 36). In our registry, 1 case (0.5%) of paroxysmal supraventricular tachycardia occurred in the peri-procedural phase, whereas paroxysmal atrial fibrillation occurred after discharge within thirty-day in 2 patients (1.1%), both treated with a Cocoon PFO Occluder 25*18 mm. Due to the paroxysmal course of the arrhythmia, both cases were treated with antiarrhythmic drugs and life-long anticoagulant therapy. The incidence of AF after procedure seems to be lower than previous reports, likewise the incidence of supraventricular arrhythmias (37): overall, the lack of systematic ECG monitoring after the procedure may have led to an underestimation of the true incidence of arrhythmias.

Post-implantation antiplatelet therapy

The type and duration of antiplatelet therapy was left to physician discretion to mirror the real world setting: most patients (97.9%) received dual antiplatelet therapy for a period varying from 1 to 12 months, although the vast majority of them were on dual antiplatelet therapy for 1 to 3 months, and only 4 patients received a short-term single antiplatelet therapy, whereas 5 patients received anticoagulant therapy in association. This variability confirms the lack of a consensus about the pharmacological post-implantation approach, and highlights the need for more evidences (38–40).

Limitations

This is a prospective single arm registry and the endpoints were reported by the participating centers. The sample size of this study is relatively small, but, to the best of our knowledge, this is the largest experience so far concerning the real-world preliminary efficacy and safety profile of this new technology. The latter seems at least comparable with available and more extensively evaluated devices; the theoretical benefit in terms of increased safety has to be demonstrated.

Conclusion

The Cocoon Occluder device showed a good performance in terms of shunt resolution and recurrence of neurological ischemic events. The low rate of peri-procedural complications supports the use of the Cocoon PFO Occluder in patients with indication to PFO closure. Larger scale and comparative studies with long-term follow-up are needed in order to confirm whether the technical features of this new technology actually translate into an improved safety/efficacy profile.

Data availability statement

The raw data supporting the conclusions of this article will be made available by the authors, without undue reservation.

Ethics statement

The studies involving human participants were reviewed and approved by each participating center EC. The patients/participants provided their written informed consent to participate in this study.

Author contributions

LT and AP drafted and revised the manuscript. AP conducted the statistical analysis. LT and FB made substantial expert contributions. All authors contributed to the data collection. All authors contributed to the article and approved the submitted version.

Conflict of interest

GC was employed by GVM Care and Research.

The remaining authors declare that the research was conducted in the absence of any commercial or financial relationships that could be construed as a potential conflict of interest.

Publisher's note

References

1. Hagen PT, Scholz DG, Edwards WD. Incidence and size of patent foramen ovale during the first 10 decades of life: an autopsy study of 965 normal hearts. *Mayo Clin Proc.* (1984) 59:17–20. doi: 10.1016/S0025-6196(12)60336-X

2. Homma S, Sacco RL. Patent foramen ovale and stroke. *Circulation.* (2005) 112:1063–72. doi: 10.1161/CIRCULATIONAHA.104.524371

3. Meier B, Jüni P. Patent foramen ovale and cryptogenic stroke. *N Engl J Med.* (2013) 369:88–93. doi: 10.1056/NEJMc1305429

4. Baumgartner H, De Backer J, Babu-Narayan SV, Budts W, Chessa M, Diller GP, et al. ESC Scientific Document Group. 2020 ESC Guidelines for the management of adult congenital heart disease. *Eur Heart J.* (2021) 42:563–645. doi: 10.15829/1560-4071-2021-4702

5. Kavinsky CJ, Szerlip M, Goldsweig A, Falck-Ytter Y, Babatunde I, Morgan RL, et al. SCAI Guidelines for the management of patent foramen ovale. *JSCAI.* (2022) 1:100039. doi: 10.1016/j.jscai.2022.100039

6. Pristipino C, Sievert H, D'Ascenzo F, Mas JL, Meier B, Scacciatella P, et al. European position paper on the management of patients with patent foramen ovale. General approach and left circulation thromboembolism. *EuroIntervention.* (2019) 14:1389–402. doi: 10.4244/EIJ-D-18-00622

7. Søndergaard L, Kasner SE, Rhodes JF, Andersen G, Iversen HK, Nielsen-Kudsk N, et al. for the Gore REDUCE clinical study investigators. Patent foramen ovale closure or antiplatelet therapy for cryptogenic stroke. *N Engl J Med.* (2017) 377:1033–42. doi: 10.1056/NEJMoa1707404

8. Mas JL, Derumeaux G, Guillon B, Massardier E, Hosseini H, Mechtouff L, et al. *Patent* Foramen ovale closure or anticoagulation vs antiplatelets after stroke. *N Engl J Med.* (2017) 377:1011–21. doi: 10.1056/NEJMoa1705915

9. Saver JL, Carroll JD, Thaler DE, Smalling RW, MacDonald L, Marks DS, et al. Long-term outcomes of patent foramen ovale closure or medical therapy after stroke. *N Engl J Med*. (2017) 377:1022–32. doi: 10.1056/NEJMoa1610057

10. Leppert MH, Poisson SN, Carroll JD, Thaler DE, Kim CH, Orjuela K, et al. Cost-effectiveness of patent foramen ovale closure versus medical therapy for secondary stroke prevention. *Stroke.* (2018) 49:1443–50. doi: 10.1161/STROKEAHA.117.020322

11. Kokkinidis DG, Katsanos AH, Giannakoulas G, Singh HS, Turc G, Thijs V. Editorial: patent foramen ovale (PFO) closure for prevention of stroke. *Front Neurol.* (2021) 12:718457. doi: 10.3389/fneur.2021.718457

12. Palaiodimos L, Kokkinidis DG, Faillace RT, Foley TR, Dangas GD, Price MJ, et al. Percutaneous closure of patent foramen ovale vs. medical treatment for patients with history of cryptogenic stroke: a systematic review and meta-analysis of randomized controlled trials. *Cardiovasc Revasc Med.* (2018) 19:852–58. doi: 10.1016/j.carrev.2018.02.014

13. Moore J, Hegde S, El-Said H, El-Said H, Beekman R, Benson L, et al. Transcatheter device closure of atrial septal defects. A safety review. *JACC Cardiovasc Interv.* (2013) 6:433–42. doi: 10.1016/j.jcin.2013.02.005

14. O'Byrne ML, Levi DS. State of the art ASD closure devices for congenital heart. *Interv Cardiol Clin.* (2019) 8:11–21. doi: 10.1016/j.iccl.2018.08.008

15. Ries MW, Kampmann C, Rupprecht HJ, Hintereder G, Hafner G, Meyer J. Nickel release after implantation of the Amplatzer occluder. *Am Heart J.* (2003) 145:737–41. doi: 10.1067/mhj.2003.7

16. Sigusch HH, Zimmermann B, Kuntze T, Gerth J. Cardiac tamponade following aortic root erosion by an Amplatzer PFO-Occluder in a 41-year-old-woman: only a matter of sizing? *J Cardiol Cases.* (2020) 23:123–26. doi: 10.1016/j.jccase.2020.10.014

17. Thanopoulos BVD, Soendergaard L, Ngugen HL, Marasini M, Giannopoulos A, Bompotis GC, et al. International experience with the use of Cocoon septal occluder for closure of atrial septal defects. *Hellenic J Cardiol.* (2021) 62:206–11. doi: 10.1016/j.hjc.2020.12.009

18. Silvestry FE, Cohen MS, Armsby LB, Burkule NJ, Fleishman CE, Hijazi ZM, et al. Guidelines for the echocardiographic assessment of atrial septal defect and patent foramen ovale: from the American society of echocardiography and society for cardiac angiography and interventions. *J Am Soc Echocardiogr.* (2015) 28:910–58. doi: 10.1016/j.echo.2015.05.015

19. Srimahachota S, Sansanayudh N, Lertsuwunseri V, Cholteesupachai J, Lertsapcharoen P. New PFO device for closure of patent foramen ovale in patients who had a history of cryptogenic stroke; a report of 14 cases. *J Med Assoc Thai.* (2015) 98:S107–10.

20. Tobis J, Shenoda M. Percutaneous treatment of patent foramen ovale and atrial septal defect. *J Am Coll Cardiol.* (2012) 60:1722–32. doi: 10.1016/j.jacc.2012.01.086

21. Meier B. Closure of patent foramen ovale: technique, pitfalls, complications, and follow-up. *Heart.* (2005) 91:444–48. doi: 10.1136/hrt.2004.052258

22. Rigatelli G, Cardaioli P, Giordan M, Aggio S, Chinaglia M, Braggion G, et al. Nickel allergy in interatrial shunt device-based closure patients. *Congenit Heart Dis.* (2007) 2:416–20. doi: 10.1111/j.1747-0803.2007.00134.x

23. Apostolos A, Drakopoulou M, Gregoriou S, Synetos A, Trantalis G, Tsivgoulis G, et al. Nickel hypersensitivity to atrial septal occluders: smoke without fire? *Clin Rev Allergy Immunol.* (2022) 6:476–83. doi: 10.1007/s12016-021-08867-0

24. Badram AV, Haddad JL, Pavão RB, Novaes GC, Lago IM, de Figueiredo GL, et al. Preliminary report of serum nickel concentration after atrial septal defect occlusion with the cocoon device. *Rev Bras Cardiol Invasiva.* (2014) 22:369–74. doi: 10.1590/0104-1843000000062

25. Verma S, Tobis JM. Explantation of patent foramen ovale closure devices: a multicenter survey. *JACC Cardiovasc Interv.* (2011) 4:579–85. doi: 10.1016/j.jcin.2011.01.009

26. Spina R, Muller DWM, Jansz P, Gunalingam B. Nickel hypersensitivity reaction following Amplatzer atrial septal defect occluder device deployment successfully treated by explantation of the device. *Int J Cardiol.* (2016) 223:242–43. doi: 10.1016/j.ijcard.2016.08.112

27. Warshaw EM, Zhang AJ, DeKoven JG, Maibach HI, Belsito DV, Sasseville D, et al. Epidemiology of nickel sensitivity: retrospective cross-sectional analysis of North American contact dermatitis group data 1994-2014. *J Am Acad Dermatol.* (2019) 80:701–13. doi: 10.1016/j.jaad.2018.09.058

28. Dickison P, Harris V, Smith SD. Nickel hypersensitivity following closure of atrial septal defect: a case report and review of the literature. *Australas J Dermatol.* (2018) 59:220–2. doi: 10.1111/ajd.12787

29. Lai DW, Saver JL, Araujo JA, Reidl M, Tobis J. Pericarditis associated with nickel hypersensitivity to the Amplatzer occluder device: a case report. *Catheter Cardiovasc Interv.* (2005) 66:424–6. doi: 10.1002/ccd.20497

30. Jain M, Singh S, Cadeiras M. A case of nitinol allergy causing pericardial tamponade. *J Invasive Cardiol.* (2013) 25:E180–2.

31. Fukahara K, Minami K, Reiss N, Fassbender D, Koerfer R. Systemic allergic reaction to the percutaneous patent foramen ovale occlude. *J Thorac Cardiovasc Surg.* (2003) 15:213–4. doi: 10.1067/mtc.2003.125

32. Dasika UK, Kanter KR, Vincent R. Nickel allergy to the percutaneous patent foramen ovale occluder and subsequent systemic nickel allergy. *J Thorac Cardiovasc Surg.* (2003) 126:2112. doi: 10.1016/j.jtcvs.2003.06.005

33. Beneduce A, Ancona MB, Moroni F, Ancona F, Ingallina G, Melillo F, et al. A systematic transesophageal echocardiography study of suture-mediated percutaneous patent foramen ovale closure. *EuroIntervention.* (2022) 18:63–7. doi: 10.4244/EIJ-D-21-00242

34. Zannoni J, Popolo Rubbio A, Tusa MB, Corciu AI, Casenghi M, Cannone G, et al. Mechanism of ineffective patent foramen ovale closure using the percutaneous suture-mediated NobleStich system. *EuroIntervention.* (2022) 18:68–70. doi: 10.4244/EIJ-D-21-01021

35. Spies C, Khandelwal A, Timmermanns I, Schräder R. Incidence of atrial fibrillation following transcatheter closure of atrial septal defects in adults. *Am J Cardiol.* (2008) 102:902–6. doi: 10.1016/j.amjcard.2008.05.045

36. Chen JZJ, Thijs VN. Atrial fibrillation following patent foramen ovale closure. Systematic review and meta-analysis of observational studies and clinical trials. *Stroke.* (2021) 52:1653–61. doi: 10.1161/STROKEAHA.120.030293

37. Fortuni F, Crimi G, Leonardi S, Angelini F, Raisaro A, Lanzarini LF, et al. Closure of patent foramen ovale or medical therapy alone for secondary prevention of cryptogenic cerebrovascular events. *J Cardiovasc Med.* (2018) 19:373–81. doi: 10.2459/JCM.0000000000000648

38. Kuijpers T, Spencer FA, Siemieniuk RA, Vandvik PO, Otto CM, Lytvyn L, et al. Patent foramen ovale closure, antiplatelet therapy or anticoagulation therapy alone for management of cryptogenic stroke? A clinical practice guideline. *BMJ.* (2018) 362:k2515. doi: 10.1136/bmj.k2515

39. Nusca A, Bressi E, Colaiori I, Miglionico M, Di Sciascio G. Antiplatelet therapy in valvular and structural heart disease interventions. *Cardiovasc Diagn Ther.* (2018) 8:678–93. doi: 10.21037/cdt.2018.06.08

40. Goldsweig A, Batlivala S, Al-Azizi K, Babatunde I, Falck-Ytter Y, Morgan LM, et al. SCAI technical review on management of patent formane ovale. *JSCAI.* (2022) 1:100040. doi: 10.1016/j.jscai.2022.100040

frontiers | Frontiers in Cardiovascular Medicine

TYPE Original Research
PUBLISHED 18 January 2023
DOI 10.3389/fcvm.2023.1102525

OPEN ACCESS

EDITED BY
Jingyan Han,
Boston University, United States

REVIEWED BY
Sihai Zhao,
Xi'an Jiaotong University, China
Jiemei Wang,
Wayne State University, United States

*CORRESPONDENCE
Ming-Sheng Zhou
✉ zhoums1963@163.com

†These authors have contributed equally to this work

SPECIALTY SECTION
This article was submitted to Cardiovascular Pharmacology and Drug Discovery, a section of the journal Frontiers in Cardiovascular Medicine

RECEIVED 19 November 2022
ACCEPTED 02 January 2023
PUBLISHED 18 January 2023

CITATION
Ren H-L, Cai R, Xue R, Zhang Y, Xu Q, Zhang X, Cai RZ, Sha W, Schally AV and Zhou M-S (2023) Growth hormone-releasing hormone agonist attenuates vascular calcification in diabetic db/db mice.
Front. Cardiovasc. Med. 10:1102525.
doi: 10.3389/fcvm.2023.1102525

Growth hormone-releasing hormone agonist attenuates vascular calcification in diabetic db/db mice

Hao-Lin Ren[1†], Ruiping Cai[2,3†], Ruize Xue[2,3†], Yaoxia Zhang[2,3], Qian Xu[2,3], Xianyang Zhang[4], RenZhi Cai[4,5], Wei Sha[4], Andrew V. Schally[4,5,6,7] and Ming-Sheng Zhou[2,3*]

[1]Department of Radiology, The First Affiliated Hospital, Dalian Medical University, Dalian, China, [2]Science and Research Center, Shenyang Medical College, Shenyang, China, [3]Department of Physiology, Shenyang Medical College, Shenyang, China, [4]Veterans Affairs Medical Center, Endocrine, Polypeptide and Cancer Institute, Miami, FL, United States, [5]Miami Veterans Affairs Medical Center, South Florida VA Foundation for Research and Education, Miami, FL, United States, [6]Divisions of Medical/Oncology and Endocrinology, Department of Pathology, Medicine, Miller School of Medicine, University of Miami, Miami, FL, United States, [7]Sylvester Comprehensive Cancer Center, Miller School of Medicine, University of Miami, Miami, FL, United States

Introduction: Vascular calcification (VC) is an independent risk factor for cardiovascular diseases. VC increases mortality of all-causes. VC is one of most common cardiovascular complications in type II diabetes. So far, no therapy has been proven to be effective in treatment of clinical VC. The present study investigated the therapeutic effects of MR409, an agonistic analog of growth hormone-releasing hormone (GHRH-A), on VC in diabetic db/db mice.

Method and result: Diabetic mice were injected with MR409 subcutaneously every day for 8 weeks. Long-term treatment with MR409 improved serum lipid profile and endothelium-dependent relaxation to acetylcholine, and reduced vascular structural injury in diabetic mice without affecting serum growth hormone level. Echocardiography showed that calcium plaques present in heart valve of diabetic mice disappeared in diabetic mice after treatment with MR409. MR409 inhibited vascular calcium deposition associated with a marked reduction in the expressions of osteogenic-regulated alkaline phosphatase (ALP) and transcription osteogenic marker gene Runx2 in diabetic mice. MR409 also inhibited vascular reactive oxygen species (ROS) generation and upregulated the expressions of anti-calcifying protein Klotho in diabetic mice.

Discussion: Our results demonstrate that GHRH-A MR409 can effectively attenuate VC and heart valve calcification, and protect against endothelial dysfunction and vascular injury in diabetic mice without significantly affecting pituitary-growth hormone axis. The mechanisms may involve upregulation of anti-calcifying protein Klotho and reduction in vascular ROS and the expression of redox sensitive osteogenic genes Runx2 and ALP. GHRH-A may represent a new pharmacological strategy for treatment of VC and diabetics associated cardiovascular complications.

KEYWORDS

vascular calcification, growth hormone-releasing hormone, diabetes, oxidative stress, vascular injury

Introduction

Vascular calcification (VC) is a pathological condition, which is characterized by an abnormal deposition of calcium-phosphate in the vascular system (1). The arterial medial calcification is the most common type of VC, which is frequently found in the patients with type II diabetes, atherosclerosis and end-stage of renal diseases (ESRDs) (2). It has been reported that the prevalence of VC is as high as 41.5% in patients with type II diabetes, and 27% in the patients with ESRDs (3). The calcification in the arteries increases arterial stiffness and reduces the elasticity and compliance of the artery wall, which may increase pulse pressure, heart afterload, deteriorate peripheral tissue perfusion and thrombus formation (4). As the consequence, VC increases the incidence of thrombosis, stroke, coronary ischemic disease, and plaque rupture. VC is considered an independent risk factor for cardiovascular morbidity and mortality (5, 6).

The mechanisms of VCs are not fully understood. Like the bone remodeling, VC is an active cellular process that is regulated by various bone-related proteins, such as alkaline phosphatase (ALP), osteocalcin, osteopontin, Run-related transcription factor 2 (Runx2), and matrix vesicles (7). Some agents, such as bisphosphonate, pyrophosphate analogs, have been tested to be effective in the prevention or regression of VC in the experimental animal models. However, to date, no effective agents have been found for the treatment or regression of VC associated with human diseases (8). Therefore, there is an urgent need to develop new strategies to prevent or treat VC.

Growth hormone-releasing hormone (GHRH) is a hypothalamic neuropeptide, which binds to the G-protein coupled GHRH receptor and stimulates the secretion and synthesis of growth hormone (GH) in the pituitary gland (9). In addition to its neuroendocrine action, GHRH and its receptors are expressed in different peripheral tissues and cell types, such as cardiomyocytes, vascular smooth muscle cells, neural cells, ocular tissue and pancreas (10–13). The extrahypothalamic GHRH can regulate many cellular functions, such as cell proliferation, differentiation and survival, in various peripheral cells and organs (14, 15). In past few decades, many potent GHRH agonists has been synthesized in our laboratory. These synthetic analogs of GHRH are more stable and potent when compared with native GHRH (14). It has been shown that GHRH analog MR409 can exert therapeutic effects on experimental acute myocardial infarction, heart failure and diabetic retinopathy (11, 16, 17). More recently, Shen et al. (18) reported that MR409 can suppress vascular smooth muscle calcification *in vitro* and VC in osteoprotegerin KO mice *in vivo* by blocking reactive oxygen species (ROS)/nuclear transcription factor (NF)*k*B pathway. However, osteoprotegerin KO mice is not an animal model that mimics VC in human diseases. In the present study, we investigated the therapeutic effects of MR409 on VC in diabetic db/db mice.

Materials and methods

Animal protocols

Ten-week-old male homozygous db/db mice on a C57BL/6 background were purchased from Model Animal Research Center of Nanjing University (MARC, Nanjing, China) and housed in an animal facility at 23 ± 2°C with a 12-h light/dark cycle, C57BL/6 mice were used as a wild type (WT) control. We used 10-week-old male mice in this study, because it has been reported that sex hormones, especially estrogen, may affect VC (19), and db/db mice can develop VC about 20-week-old (the age of mice at sacrifice) (20). All animal procedures were approved by the Institute Animal Use and Care Committee of Shenyang Medical College and complies with the Guideline of the Institute Care and Use of Laboratory Animals of Shenyang Medical College. After 2 weeks of adaptation, the mice were randomly divided into 3 groups and fed a regular mouse diet, and received one of the following treatments for 8 weeks: Control group (WT): C57BL/6 mice were injected subcutaneously with vehicle solution [10% (vol/vol) propylene glycol] every day; diabetic db/db group (db/db): db/db mice received a subcutaneous injection of vehicle solution every day; db/db mice in MR409 treatment group (MR409) were administrated subcutaneously with MR409 at a dose of 15 μg/day/mouse (dissolved in 10% propylene glycol). We have shown that MR409 at a dose of 10 μg/day/mouse has therapeutic effects on experimental stroke and STZ-induced diabetic mouse models (10, 12), we used MR409 at a dose of 15 μg/day/mouse, because db/db mice have more body weight than regular mice. The number of experimental animals was based on the statistical power analysis. MR409 was synthesized by our laboratory (12, 14). At the end of the study, the mice were fasted overnight, blood was taken from the tail arteries to determine fasting blood level of glucose with an automatic blood glucose meter (Roche Accu-CHEK Active, Mannheim, Germany). After insulin tolerance test was performed, the mice were euthanized with 100 mg/kg ketamine and 20 mg/kg xylazine cocktail, and blood was withdraw through left ventricular puncture. The heart and aorta were harvested.

Insulin tolerance test

The mice were fasted for 4 h, insulin tolerance test was performed 2 days before the animals were sacrificed. Briefly, the mice were injected intraperitoneally with insulin solution (1 U insulin/kg body weight). Blood glucose levels were measured at 0 (before insulin administration), 20, 40, 60, 120, and 180 min after insulin injection using an automatic blood glucose meter (Roche Accu-CHEK Active, Mannheim, Germany).

Histological analysis

Thoracic aorta was isolated and cut into 3 mm aortic ring, which was fixed in 4% paraformaldehyde buffered solution and routinely processed for paraffin sections. The slices of 4 μm thickness was cut and mounted in the slides. The slides were stained with hematoxylin eosin (HE, Sigma Aldrich, St. Louis, MO) to evaluate the thickness of aortic wall and morphological alteration. At least four images per stained sections were examined and photographed using a Leica DM4B fluorescence microscope (Leica Microsystems Inc., Mannheim, Germany). The thickness of aortic wall (from intima to media) was measured by ImageJ software (NIH Bethesda, MD), the average thickness of aortic wall was calculated. The separated sections were stained with Masson trichrome to evaluate vascular fibrosis, the positive stained area of collagen was quantified with ImageJ software, the percentage of positive stained collagen area with total stained area was calculated. The examination of histological samples was

conducted in a blinded manner, the reviewers were not aware of the groups to which mice belonged.

Vascular reactivity

Endothelium-dependent relaxation to acetylcholine was determined by an organ chamber bath as described previously (21). Briefly, isolated thoracic aorta was cut into 3 mm aortic rings. The aortic rings were mounted on the wires connected to pressure transducer in organ chamber bath system (DMT Inc., Denmark). The rings were equilibrated under resting tension of 1 g for 1 h, then contracted twice with PSS solution containing 60 mmol/L KCL. The rings were precontracted with about 30 nmol/L of norepinephrine to reach 70% of the maximum contractile force, then cumulative concentration of acetylcholine (10^{-9}∼10^{-5} molar/L) was added to the organ bath. Maximal relaxation to acetylcholine (Emax) and the concentration of acetylcholine required for a half-maximal relaxation (ED50) were calculated using a best fit of a logistic sigmoid concentration-response curve.

Assessment of heart valve and aortic calcification with echocardiography

At the end of an 8-week treatment, the mice were subjected to ultrasound examination for determination of aortic calcification and heart valve calcification, using a high-resolution Doppler image system for small animal (Esote Medical Equipment Inco., Shenzhen, China). The mice were anesthetized with the inhalation of 1% isoflurane, and placed on a platform and heated warm to maintain body temperature. The heart valves and aortic arches were examined and imaged with B-Mode or 2D mode cursor (30 MHz) in the parasternal short-axis view with a depth setting of 2 cm. The sample volume cursor was placed at the aortic root with angle correction (37°–60°). The heart valves and aortic calcification were determined by a significant change in ultrasound density. The areas of calcification spots or plaques were quantified by using ImageJ software.

Alizarin red and Von Kossa calcium staining in mouse aortas

Alizarin red (AR) and Von Kossa (VK) were used for calcium staining of the mouse aortas. A segment of aortic arch was fixed in 10% formalin for 24 h, then dehydrated and embedded in paraffin. The section of 5-μm-thickness was cut and deparaffined. For AR staining, the slides were incubated with AR solution for 2 min (Solarbio Life Science, Beijing, China). After a quick wash in distilled water, the slides were placed under ultraviolet light until calcium phosphate turned black, followed by a counterstaining with eosin. For VK staining, deparaffined sections were stained with Von Kossa silver kits (Solarbio Life Science, Beijing, China) for 2 min. After washing with distilled water, the sections were rapidly differentiated and the nuclei stained with hematoxylin solution. Images were taken using microscope (Leica, Germany) and analyzed with ImageJ Software.

Oil red O staining and ALP staining

Fresh aortic root was frozen and embedded in OCT compound and sliced into the section of 10 μm thickness by a microtome-cryostat (Leica, Germany). The sections were briefly rinsed with distilled water and immersed in 60% isopropanol for 30 s, then incubated in oil red O working solution (Solarbio Life Science, Beijing, China) for 15 min. The sections were then de-stained with 60% isopropanol, and counterstained with hematoxylin solution. Images were captured using Leica light microscope, and the percentage of positive staining area was quantified using ImageJ software. ALP staining in aortic section was performed with ALP staining kit following manufacturer's instructions. Ten μm sections were cut, matrix solution was added to slices, and the tissue section incubated for 15 min at 37°C in dark environment. Excessive matrix solution was removed and cobalt nitrate dye added immediately and dyed for 5 min. Vulcanized solution was added and tissue sections incubated for 30 s. The slices were redyed with nuclear solid red dye for 30 s. The slices were shaken to dryness and examined by microscope.

Immunohistochemistry

Paraffin-embedded aorta was cut into 4 μm thick sections. The slides were incubated with sodium citrate buffer for 10 min in a pressure cooker for antigen retrieval. After the incubation with blocking solution of 5% goat serum in TBST at room temperature for 10 min, the sections were incubated with primary antibodies against Runx2 (1:50 diluted with TBST buffer, SC-101145, Satan Cruz Biotech., USA) or Klotho (1:50 diluted with TBST buffer, ab181373, Abcam, UK) overnight at 4°C followed by the incubation with appropriate secondary antibodies conjugated with biotin for 15 min at room temperature. The sections were then incubated with HRP labeled streptavidin for 15 min at room temperature and stained with DAB solution. The nuclei were counterstained with hematoxylin solution. The images were acquired by a Leica DM4B fluorescence microscope and analyzed with ImageJ software. The results were expressed as a percentage of positive stained areas with total selected areas.

Western blot

The whole aortas (from aortic arch to the bifurcation of abdominal aorta at femoral arteries) were lysed with RIPA lysis buffer containing a complete protease inhibitor cocktail. Protein concentrations were determined using a BCA protein assay kit (Beyotime Biotechnology, Shanghai, China). Protein samples (30 μg) were fractionated with SDS-PAGE. After electrophoretic transfer to a PVDF membrane (0.45 μm, IPVH00010, Millipore), the membranes were incubated with primary antibody against Klotho (1:1000 dilution, ab181373, Abcam) at 4°C overnight followed by the incubation with horseradish peroxidase-conjugated secondary antibody (1:5,000 dilution using blocking solution) for 2 h at room temperature, an antibody against β-actin (WH121414, ABclonal) as an internal control. The luminal chemiluminescence signals were detected with an Aplegen Omega Lum G Gel Documentation System (Aplegen Inc., Pleasanton). The band density was measured and quantified using ImageJ software.

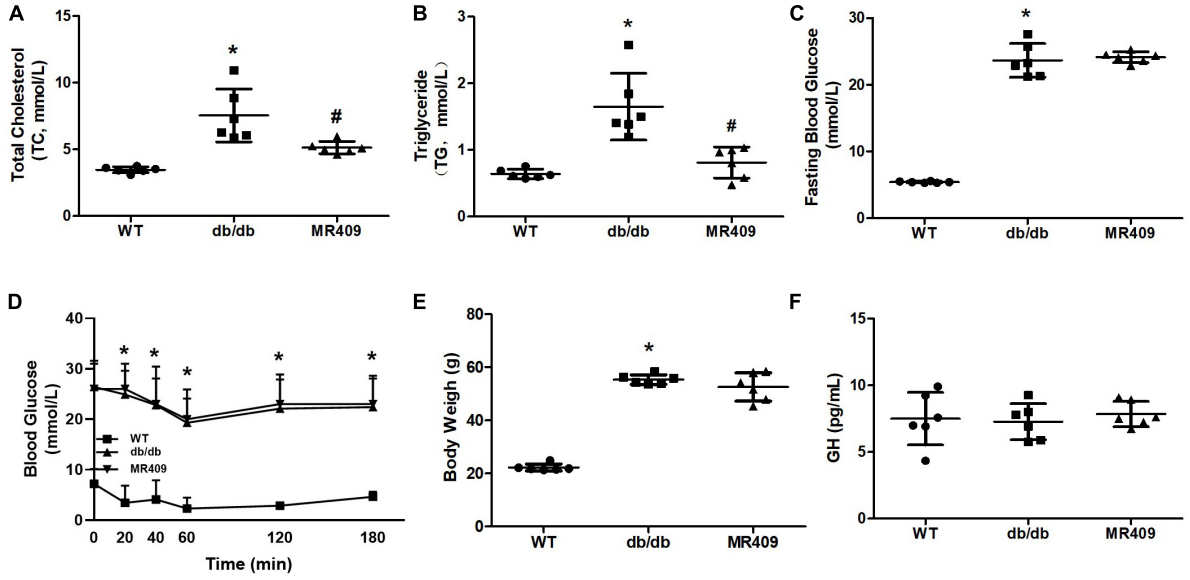

FIGURE 1
Effects of MR409 on plasma levels of total cholesterol (Ch, **A**) and total triglyceride (TG, **B**), fasting blood glucose **(C)**, insulin tolerance **(D)**, body weight **(E)** and serum level of growth hormone (GH, **F**) in diabetic db/db mice. Data is expressed mean ± SD, $n = 6$, $*p < 0.05$ diabetic mice vs. WT mice, $\#p < 0.05$ MR409 treated mice vs. diabetic mice.

Determination of serum alkaline phosphatase (ALP) activity and growth hormone (GH)

Blood was centrifuged at 5000 rpm for 10 min at 4°C. Serum ALP activity was measured using ALP assay kit following the manufacturer's instructions (Solebo Technology Co., Ltd). ALP assay kit is a p-nitrophenyl phosphate (pNPP) assay, ALP catalyzes pNPP (a phosphatase substrate) to pNP, which turns yellow at absorbance of 405 nm, which was measured using Microplate Absorbance Reader (Molecular Devices) for 15 min. One ALP unit is defined as hydrolyzation of 1 μmole of pNPP per minute at pH 9.8 at 37°C. QuantiChrom cholesterol assay kit (Coibo Bio. Inco., Shanghai, China). QuantiChrome triglyceride assay kit (Coibo Bio Inco., Shanghai, China) was used to determine serum concentration of total cholesterol, total triglyceride, respectively. Serum GH concentration was determined by mouse growth hormone enzyme-linked immunosorbent assay (ELISA) kit according to manufacturer's instructions (Cusa Bio. Inco., Wuhan, China).

Determination of superoxide (O_2^-) anion formation in aorta *in situ*

Aortic O_2^- formation was determined by oxidative fluorescent dye hydroethidine (DHE, Sigma-Aldrich, St. Louis, MO) as described (21). In brief, thoracic aorta were embedded in OCT compound and snap-frozen in the liquid nitrogen. Sections of 5 μm thickness were cut and incubated with 2 μmol/L DHE in HEPES buffer for 30 min at 37°C in a humidified chamber. The images were acquired within 30 min of DHE staining, using a fluorescence microscope (Leica Microsystems Inc., Mannheim, Germany), and the average fluorescent intensities were quantitated and expressed as percentage of control.

Statistical analysis

Statistical analysis was performed by SPSS statistical software (SPSS Inc, Chicago, IL). Data were presented as mean ± standard derivation (SD). Statistical analysis was performed by one-way or two-way ANOVA followed by the Student-Newman-Keuls test. $P < 0.05$ was considered statistically significant.

Results

Long-term treatment with GHRH-A MR409 reduced plasma lipid profile and vascular injury in diabetic db/db mice

Db/db mice at 20-week-old exhibited significant increases in fasting plasma level of total cholesterol, triglyceride and fasting blood level of glucose, impaired insulin tolerance and body weight, treatment with MR409 for 8 weeks lowered plasma lipid profile but did not significantly affect fasting blood glucose, insulin tolerance and body weight in db/db mice (**Figures 1A–E**). There was no significant difference in plasma level of GH between WT and diabetic db/db mice, and treatment with MR409 did not significantly affect plasma level of GH in diabetic mice (**Figure 1F**). HE staining showed that the thickness of aortic wall in diabetic mice significantly increased, which was prevented by MR409 treatment (**Figures 2A, B**). Masson trichrome staining revealed that diabetic mice had more positive staining area of aortic collagen and loosened elastic fiber structure, as compared with WT mice. MR409 treatment reduced aortic fibrosis and protected elastic fiber structure intact in diabetic db/db mice (**Figures 2C, D**). Lipid deposition was increased in the aorta of db/db mice, as showed by oil O staining, MR409 treatment significantly reduced aortic lipid deposition in db/db mice (**Figures 2E, F**).

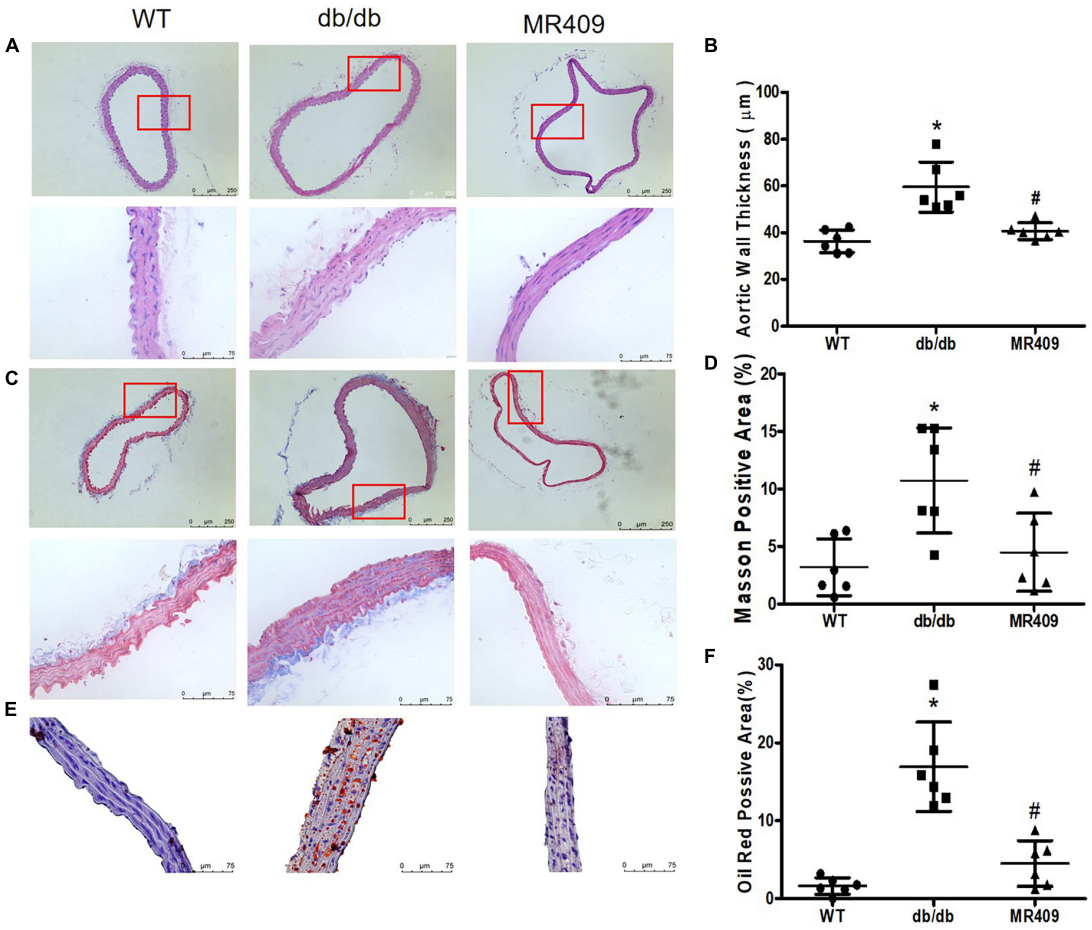

FIGURE 2
Treatment with MR409 improves vascular morphological injury in diabetic db/db mice. The representative images of cross section of aortic wall stained with hematoxylin and eosin for aortic wall thickness with a low magnification in up pane and a high magnification in low pane **(A)**, Masson trichrome for collagen content with a low magnification in up pane and a high magnification in low pane **(C)** and oil O staining for lipid deposition with high magnification **(E)**. The quantitation of aortic wall thickness **(B)**, positive collagen staining areas **(D)** and lipid deposition **(F)** in the aorta. $N = 6$, $*p < 0.05$ diabetic mice vs. WT mice, $\#p < 0.05$ MR409 treated mice vs. diabetic mice.

MR409 improved endothelium-dependent relaxation and reduced aortic ROS production in diabetic db/db mice

Endothelium-dependent relaxation to acetylcholine was significantly impaired in diabetic mice, MR409 treatment significantly improved acetylcholine-induced relaxation (**Figure 3A**). We determined aortic ROS production *in situ* by DHE oxidative fluorescence staining. As shown in **Figures 3B, C**, oxidative fluorescence intensity significantly increased in diabetic db/db mice, which was prevented by MR409 treatment.

MR409 attenuated vascular calcium deposition and the protein expressions of osteogenic-regulated molecules in diabetic db/db mice

We used a high-resolution Doppler image system for small animal to determine heart valves and vascular calcification in aortic root. The ultrasound images of heart valve or vascular calcification manifests calcified spots or plaques (white) with abnormal increase in ultrasound density. Compared with WT control mice, high brightness calcified plaques with abnormal increased ultrasound density were seen in density of aortic valves (indicated with arrowhead) of diabetic mice, which disappeared in diabetic mice treated with MR409 (**Figure 4**). Furthermore, we used alizarin red and Von Kossa calcium staining to evaluate vascular calcification in the aortic root. Vascular calcium deposition was brown in Von Kossa staining and dark red in alizarin red staining. Compared with WT mice, diabetic mice had more brown staining areas in the aortic root section with Von Kossa staining (**Figures 5A, C**) and more dark red areas with alizarin red staining ($P < 0.05$; **Figures 5B, D**). MR409 treatment significantly reduced positive vascular staining area in both Von Kossa staining or alizarin red staining ($P < 0.05$; **Figures 5B, D**) in diabetic db/db mice. These results suggest that MR409 can inhibit vascular calcification in diabetes. ALP and Runx2 are two important molecules to regulate ectopic calcification (22, 23), ALP accelerates ectopic calcification by catalyzing hydrolysis of inorganic phosphate (23), Runx-2 is a major regulator of osteocyte differentiation to drive VC processes by the regulation of osteogenesis gene expression (22). We detected serum ALP activity and aortic expression of ALP and Runx2 by immunohistochemistry. Comparing with WT

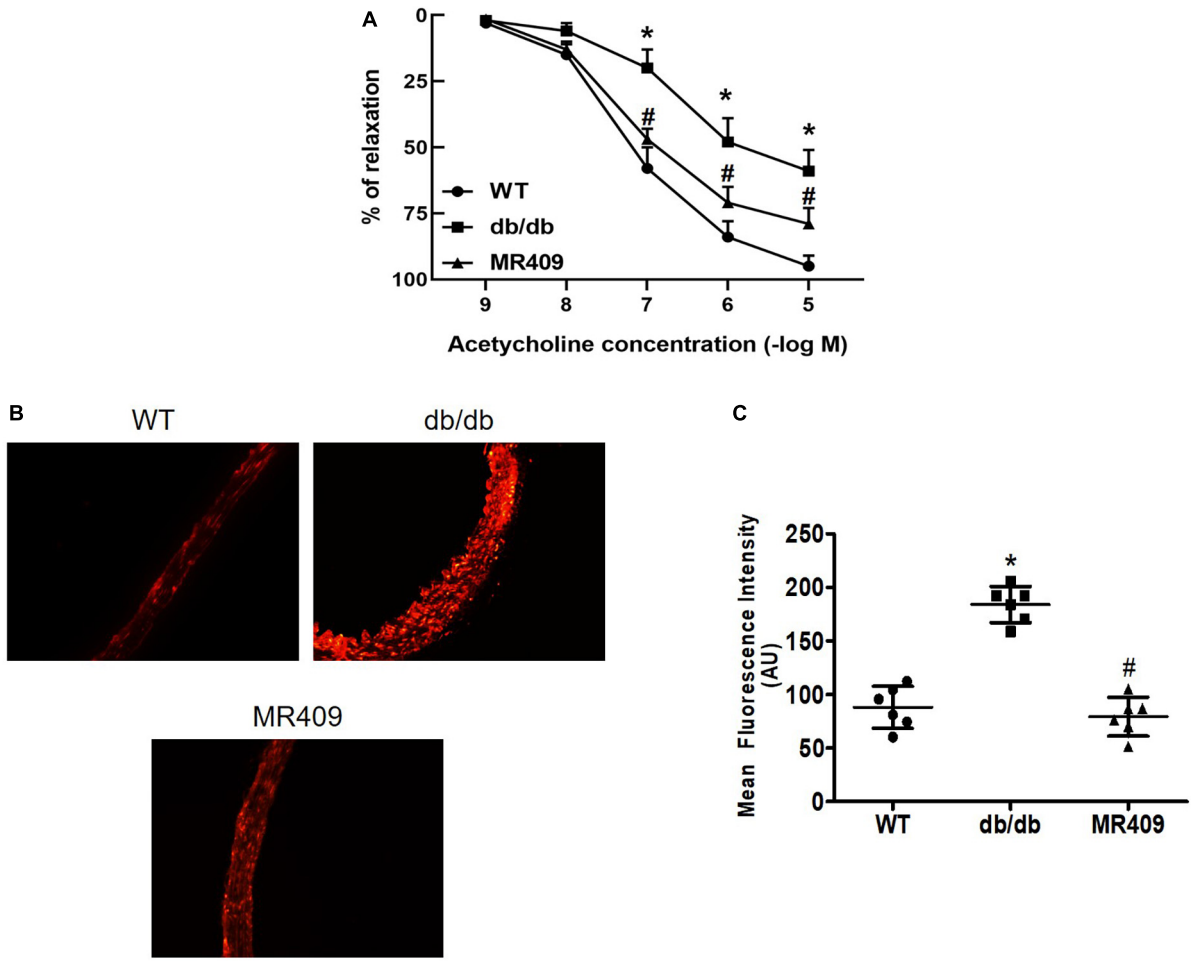

FIGURE 3
Treatment with MR409 improves endothelium-dependent relaxation to acetylcholine **(A)** and reduced reactive oxygen species (ROS) production in the aorta of diabetic db/db mice. **(B)** The representative images of oxidative fluorescence intensities in the aorta, assessed by DHE fluorescence staining, **(C)** the quantification of average oxidative fluorescence intensities. $N = 6$, $*p < 0.05$ diabetic mice vs. WT mice, $\#p < 0.05$ MR409 treated mice vs. diabetic mice.

group, serum ALP activity significantly increased in diabetic mice, MR409 treatment restored ALP activity in diabetic mice (Figure 6A). Immunohistochemistry revealed that diabetic mice had more ALP and Runx2 expression, which were reduced in diabetic mice with MR409 treatment (Figures 6B–E).

MR409 up-regulated Klotho expression in aorta of diabetic db/db mice

Klotho is an anti-aging and anti-calcifying protein, which is reduced in chronic kidney diseases and diabetic mellitus (24, 25). Klotho expression significantly decreased in the aorta of db/db mice, as determined with Western blot and immunohistochemistry. MR409 treatment significantly increased aortic Klotho expression (Figure 7).

Discussion

In the present study, we demonstrate that long-term treatment with GHRH-A MR409 significantly attenuated VC and vascular morphological injury, improved endothelial function but did not affect serum level of GH in db/db diabetic mice. The inhibitory effects of MR409 on VC was associated with a reduction in vascular ROS production and the expressions of osteogenic regulated gene Runx2 and ALP and an increase in anti-calcifying protein Klotho. These results confirm that GHRH-A may be a novel therapy for VC and VC associated vasculopathy.

Vascular calcification is a complex process that involves osteogenesis of vascular cells. VC represents a vascular aging phenotype which is commonly observed in the elderly people. Diabetes and chronic renal diseases are most common human disease associated with VC (2, 26), especially arterial medial calcification, because the patients suffer from a disturbed mineral and bone metabolism (27). Arterial medial calcification increases arterial stiffness, blood pressure and heart workload, impairs vascular compliance and vascular reactivity. Arterial medial calcification is an independent risk factor for development of stroke, cardiovascular diseases and mortality in type 2 diabetes mellitus (4, 28). Current anti-calcifying therapies may delay but can not effectively reduce existing arterial calcification and conduit vessel compliance (8). In addition, anti-calcifying

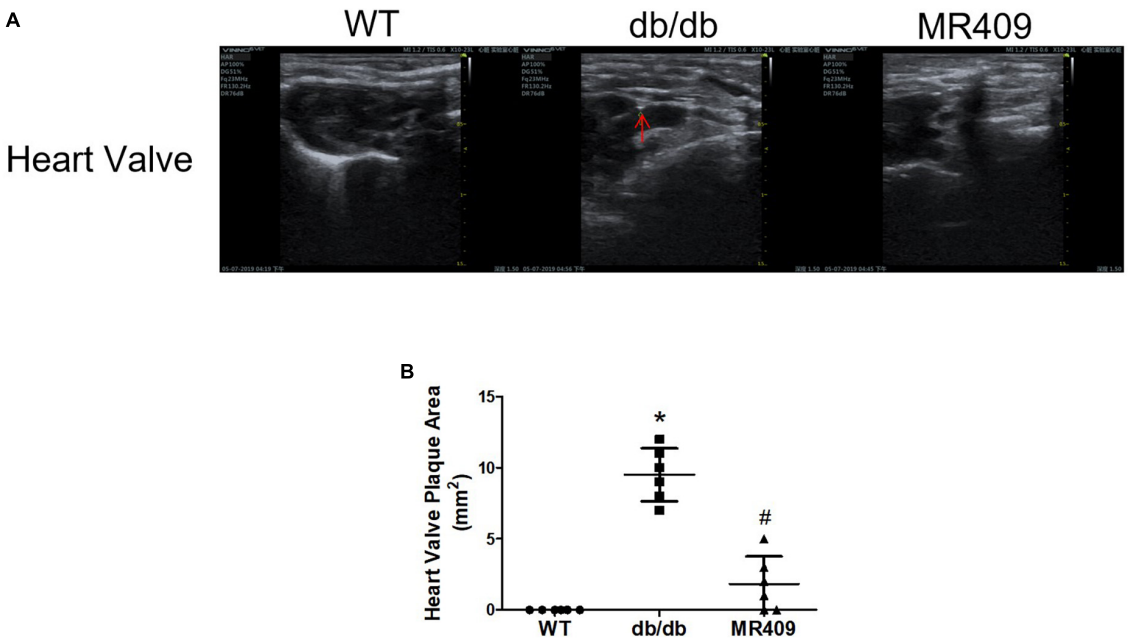

FIGURE 4
Treatment with MR409 attenuates heart valve calcification **(A)** in diabetic db/db mice. Heart valve calcification was detected with high-resolution Doppler image system for small animal. Representative images of heart valve **(A)** calcification, the quantitation of heart valve **(B)** calcification. *N* = 6, **p* < 0.05 diabetic mice vs. WT mice, #*p* < 0.05 MR409 treated mice vs. diabetic mice.

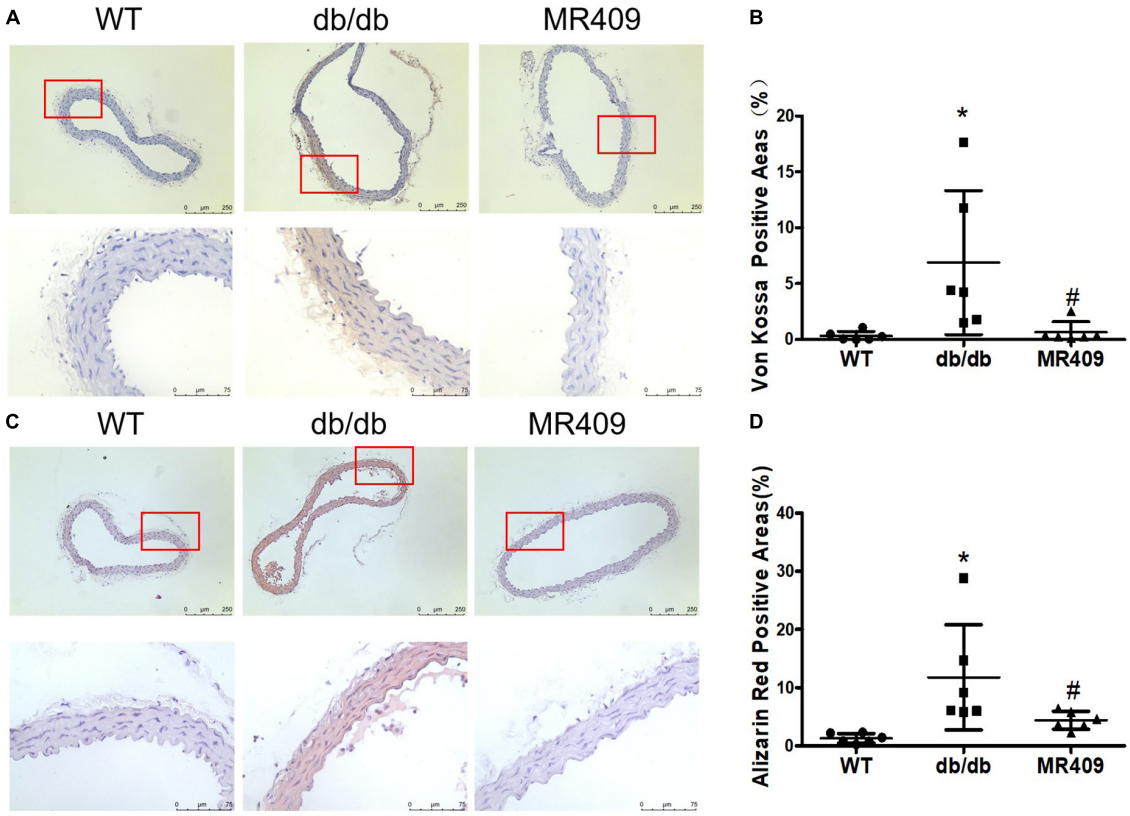

FIGURE 5
Treatment with MR409 attenuates calcium deposition in aortic root section of diabetic db/db mice. The representative images of calcium staining in the aorta by Von Kossa with a low magnification in up pane and a high magnification in low pane (brown, **A**) and alizarin red staining with a low magnification in up pane and a high magnification in low pane (dark red, **C**), the quantitation of positive calcium staining areas with Von Kossa **(B)** and alizarin red **(D)**. *N* = 6, **p* < 0.05 diabetic mice vs. WT mice, #*p* < 0.05 MR409 treated mice vs. diabetic mice.

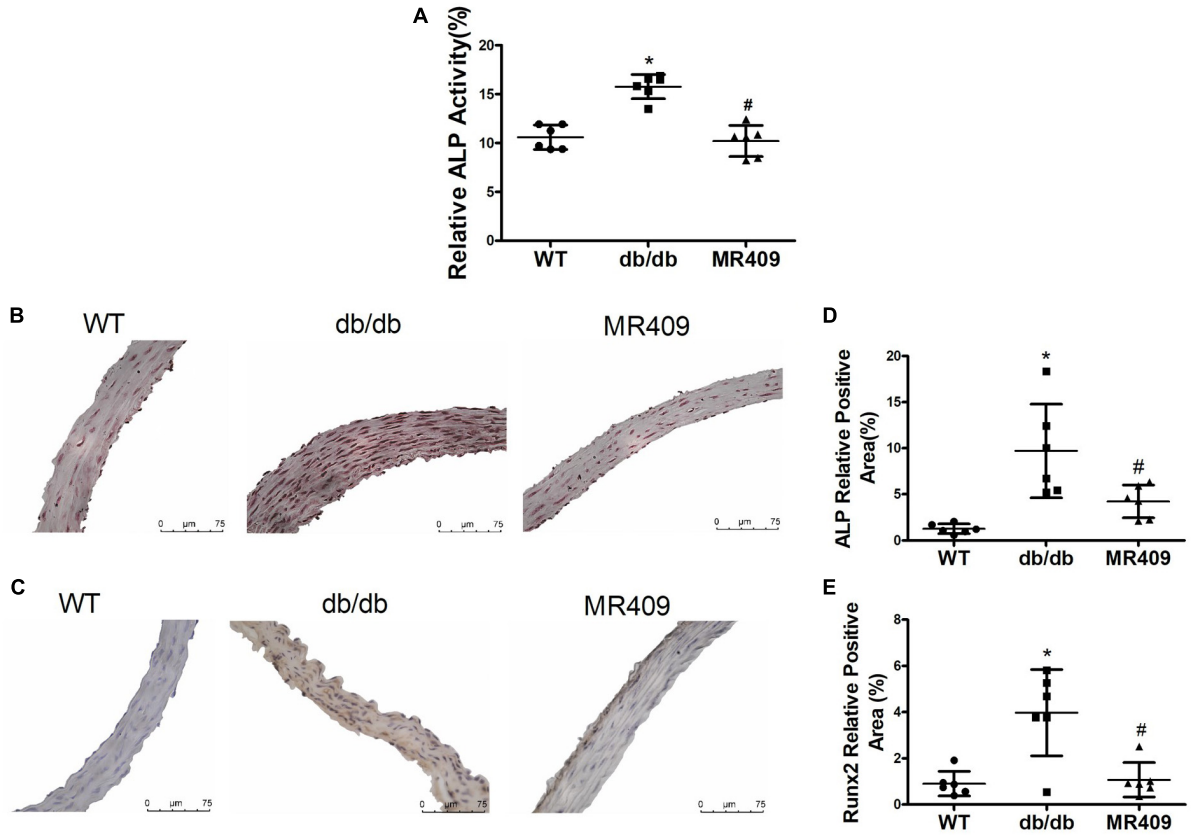

FIGURE 6
Treatment with MR409 reduces serum alkaline phosphatase (ALP) activity **(A)**, the expression of ALP **(B,D)** and Runx2 **(C,E)** in the aorta of diabetic db/db mice. The representative images of ALP **(B)** and Runx2 **(C)**, were determined by immunohistochemistry, the quantitation of positive staining areas of ALP **(D)** and Runx2 **(E)**. *N* = 6, **p* < 0.05 diabetic mice vs. WT mice, #*p* < 0.05 MR409 treated mice vs. diabetic mice.

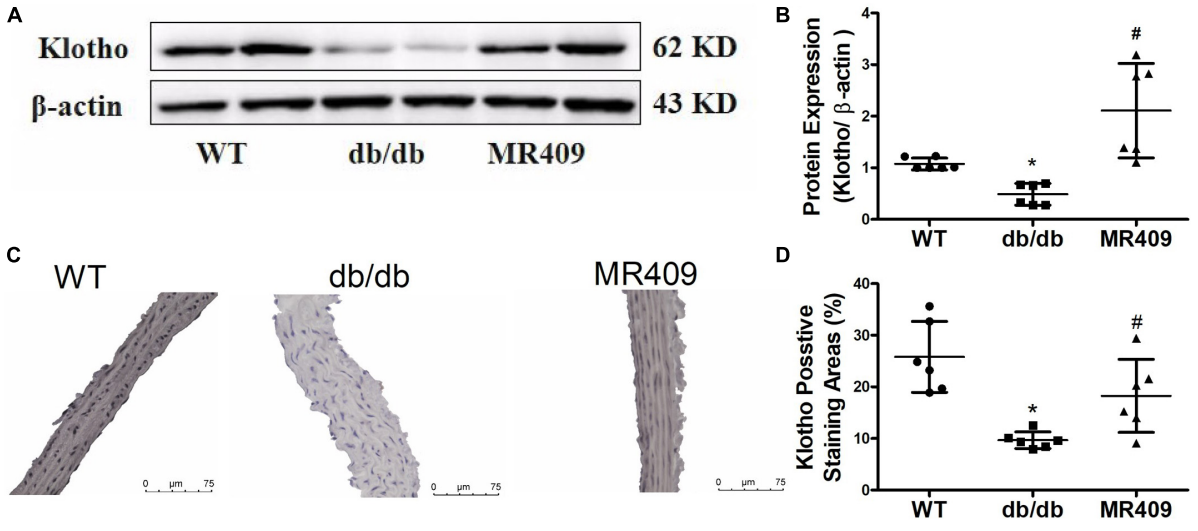

FIGURE 7
Treatment with MR409 upregulates the expression of Klotho in the aorta of diabetic db/de mice. The protein expression of Klotho was determined by Western blot **(A)**, the representative images of Klotho protein expression, determined by immunohistochemistry **(C)**, the quantitation of Klotho protein expression with Western blot **(B)** and immunohistochemistry **(D)**. *N* = 6, **p* < 0.05 diabetic mice vs. WT mice, #*p* < 0.05 MR409 treated mice vs. diabetic mice.

therapies may cause detrimental side effects at the level of bone, as the molecular and cellular process for arterial calcification is similar to physiological mineralization (5, 8). We found that diabetic db/db mice at 20-week-old developed aortic medial calcification and aortic valve calcification, which were prevented by MR409 treatment.

MR409 is a synthetic peptide of 29 amino acids with the GHRH activity site of GHRH and adjacent peptide modifications that enhance its activity and stability (14). GHRH is a hypothalamic neuropeptide, the native GHRH stimulates the release of GH by binding to GHRH receptors in pituitary gland (29). It has been reported that in addition to pituitary cells, GHRH receptors are expressed in various extrapituitary cells (10). Consistent with previous findings (18), we found that long-term treatment with MR409 reduced VC but did not affect serum level of GH in diabetic db/db mice. These results suggest that anti-calcification and vasoprotective effects of MR409 may be achieved by directly binding to its receptors in vascular cells, independent of its effects on GH-regulation pathway. As GHRH agonists are not anti-calcifying agents, MR409 may avoid the side effects of activation of GH regulatory pathways and disturbed bone mineral metabolism. Thus GHRH-A may be a safe and novel agent for VC treatment.

The molecular and cellular mechanisms of VC are complex in diabetes (2, 30). Insulin resistance, hyperglycemia and hyperlipidemia are hallmarks of diabetes (2), which could be actively involved in pathological process of VC through the production of ROS and increased proinflammatory cytokines in vascular cells (1, 31). Accumulating evidence has shown that excessive production of ROS induces osteogenic transdifferentiation of VSMCs associated with increased expression of osteogenic markers, such as Runx2, ALP, and OCN (31, 32). Runx2 is an important transcription factor that regulates osteoblast differentiation (33, 34). It has been shown that ROS induces VSMC calcification through the upregulation of Runx2, and specific expression of Runx2 in VSMCs promotes osteogenic differentiation of VSMC and atherosclerotic calcification in the ApoE$^{-/-}$ mice (32). ROS can activate redox sensitive transcription factor NF*k*B inflammatory pathway (35), which has been shown to increase expressions of osteogenic genes including Runx2 and ALP. Recently, Shen et al. (18) demonstrated that the activation of GHRH receptor signaling inhibits osteogenesis of VSMCs *in vitro* and VC *in vivo* by suppression of ROS-mediated NF*k*B/Runx2 pathway. In the present study, we found that ROS and osteogenic markers Runx2 and ALP increased in the aorta of diabetic db/db mice. MR409 treatment reduced ROS production and the expression of these osteogenic molecules, suggesting that MR409 may reduce VC *via* the inhibition of ROS/Runx2 in diabetes.

In the present study, MR409 did not affect blood level of glucose but significantly lowered serum levels of total triglyceride and total cholesterol in diabetic mice. The association of dyslipidemia and VC is well established, especially oxidized lipids or lipoprotein, such as oxidized phospholipids, which have shown to upregulate osteogenic-regulating gene expression and promote VC (36). Thus, lowering lipid profile may be another mechanism of MR409 inhibiting VC in diabetic mice.

It has been shown that anti-age protein Klotho has an important protective role against vascular dysfunction and VC (25). Klotho gene deficiency mice exhibit premature aging syndrome, accompanied with significant VC (24), and genetic overexpression of Klotho or administration of soluble Klotho rescues the Klotho-deficient phenotype and VC (37). Klotho is endowed with pleiotropic vasoprotective effects, such as the inhibition of oxidative stress and upregulation of eNOS expression in vascular cells. In addition, Klotho inhibits the osteogenic phenotype conversion of vascular progenitors or VSMCs through regulating Runx2 or mineral homeostasis (24). The patients with aging, diabetes and chronic renal diseases often have low plasma or tissue level of Klotho (38). In the present study, we found that expression of Klotho protein was downregulated in the aorta of diabetic mice, and MR409 treatment restored Klotho expression associated with reduction in vascular ROS, osteogenic protein expression of Runx2 and ALP. Thus, we surmise that attenuation of VC by MR409 may be through upregulation of Klotho, which inhibits ROS and Runx2-mediated osteogenic transdifferentiation of VSMCs in diabetes.

There are several limitations in our study. First, we used C57BL/6 mice as a wild type control group, although db/db mice are created on the background of C57BL/6 mice, C57BL/6 mice display stronger resistance to develop VC, heterozygote litters from some colony of db/db mice may be more suitable to use as the control mice. Next, although we have shown that treatment with MR409 can suppress VC and osteogenic-related genes expression in diabetic db/db mice, we have not yet determined a causal relationship between these osteogenic genes and MR409 attenuation of VC, which should be addressed in future study; Finally, we started to treat db/db mice at 12-week old, at this age, db/db mice may not develop significant VC. Thus, our results may only be applied for MR409 prevention of VC in diabetes, an intervention study that MR409 treatment was initiated after developed VC (for example, starting at 20-weeks old or late) may be required to address whether MR409 can be used to regress VC or clinically to treat VC patients.

In conclusion, the present study demonstrates for first time that treatment with GHRH-A MR409 effectively attenuates VC and heart valve calcification, accompanied by the improvement of endothelial function and vascular injury in diabetic db/db mice, an animal model that mimics type 2 diabetes in human. MR409 also increases protein expression of vascular Klotho and decreases ROS production and osteogenic genes Runx2 and ALP expressions without significant alteration in serum level of GH. These results suggest that GHRH-A MR409 could be a safe and novel approach to prevention and treatment of diabetes-induce VC and its associated vascular complications.

Data availability statement

The original contributions presented in this study are included in this article/**Supplementary material**, further inquiries can be directed to the corresponding author.

Ethics statement

The animal study was reviewed and approved by the Institutional Animal Care and Use Committee of Shenyang Medical College.

Author contributions

H-LR contributed to the experimental design, data acquisition, and statistical analysis. RPC and RX contributed to data acquisition and statistical analysis. YZ and QX contributed to the pathological experiments. XZ contributed to the experimental design. RZC and WS contributed to the synthesis of MR409. AS contributed to the experimental design and reversed manuscript. M-SZ contributed to the conception and design the work, data interpretation, and drafted

the manuscript. All authors contributed to the article and approved the submitted version.

Funding

This work was supported by the grants from the National Natural Science Foundation of China (Nos. 82270434 and 81970357) to M-SZ and Doctoral Research Foundation of Liaoning Province (2021-BS-286) to RPC.

Conflict of interest

The authors declare that the research was conducted in the absence of any commercial or financial relationships that could be construed as a potential conflict of interest.

Publisher's note

Supplementary material

The Supplementary Material for this article can be found online at: https://www.frontiersin.org/articles/10.3389/fcvm.2023.1102525/full#supplementary-material

References

1. Lee S, Lee I, Jeon J. Vascular calcification-new insights into its mechanism. *Int J Mol Sci.* (2020) 2020:21.

2. Stabley J, Towler D. Arterial calcification in diabetes mellitus: preclinical models and translational implications. *Arterioscler Thromb Vasc Biol.* (2017) 37:205–17. doi: 10.1161/ATVBAHA.116.306258

3. Lanzer P, Hannan F, Lanzer J, Janzen J, Raggi P, Furniss D, et al. Medial arterial calcification: JACC state-of-the-art review. *J Am Coll Cardiol.* (2021) 78:1145–65.

4. Lanzer P, Boehm M, Sorribas V, Thiriet M, Janzen J, Zeller T, et al. Medial vascular calcification revisited: review and perspectives. *Eur Heart J.* (2014) 35:1515–25. doi: 10.1093/eurheartj/ehu163

5. Demer L, Tintut Y. Vascular calcification: pathobiology of a multifaceted disease. *Circulation.* (2008) 117:2938–48.

6. Vieceli Dalla Sega F, Fortini F, Severi P, Rizzo P, Gardi I, Cimaglia P, et al. Cardiac calcifications: phenotypes, mechanisms, clinical and prognostic implications. *Biology.* (2022) 2022:11. doi: 10.3390/biology11030414

7. Avogaro A, Fadini G. Mechanisms of ectopic calcification: implications for diabetic vasculopathy. *Cardiovasc Diagn Ther.* (2015) 5:343–52.

8. Van den Branden A, Verhulst A, D'Haese P, Opdebeeck B. New therapeutics targeting arterial media calcification: friend or foe for bone mineralization? *Metabolites.* (2022) 2022:12.

9. Fridlyand L, Tamarina N, Schally A, Philipson L. Growth hormone-releasing hormone in diabetes. *Front Endocrinol.* (2016) 7:129. doi: 10.3389/fendo.2016.00129

10. Zhang X, Cui T, He J, Wang H, Cai R, Popovics P, et al. Beneficial effects of growth hormone-releasing hormone agonists on rat INS-1 cells and on streptozotocin-induced NOD/SCID mice. *Proc Natl Acad Sci USA.* (2015) 112:13651–6. doi: 10.1073/pnas.1518540112

11. Thounaojam M, Powell F, Patel S, Gutsaeva D, Tawfik A, Smith S, et al. Protective effects of agonists of growth hormone-releasing hormone (GHRH) in early experimental diabetic retinopathy. *Proc Natl Acad Sci USA.* (2017) 114:13248–53. doi: 10.1073/pnas.1718592114

12. Liu Y, Yang J, Che X, Huang J, Zhang X, Fu X, et al. Agonistic analog of growth hormone-releasing hormone promotes neurofunctional recovery and neural regeneration in ischemic stroke. *Proc Natl Acad Sci USA.* (2021) 2021:118. doi: 10.1073/pnas.2109600118

13. Xiang P, Jing W, Lin Y, Liu Q, Shen J, Hu X, et al. Improvement of cardiac and systemic function in old mice by agonist of growth hormone-releasing hormone. *J Cell Physiol.* (2021) 236:8197–207. doi: 10.1002/jcp.30490

14. Cai R, Schally A, Cui T, Szalontay L, Halmos G, Sha W, et al. Synthesis of new potent agonistic analogs of growth hormone-releasing hormone (GHRH) and evaluation of their endocrine and cardiac activities. *Peptides.* (2014) 52:104–12. doi: 10.1016/j.peptides.2013.12.010

15. Schally A, Zhang X, Cai R, Hare J, Granata R, Bartoli M. Actions and potential therapeutic applications of growth hormone-releasing hormone agonists. *Endocrinology.* (2019) 160:1600–12.

16. Kanashiro-Takeuchi R, Takeuchi L, Rick F, Dulce R, Treuer A, Florea V, et al. Activation of growth hormone releasing hormone (GHRH) receptor stimulates cardiac reverse remodeling after myocardial infarction (MI). *Proc Natl Acad Sci USA.* (2012) 109:559–63. doi: 10.1073/pnas.1119203109

17. Dulce R, Kanashiro-Takeuchi R, Takeuchi L, Salerno A, Wanschel A, Kulandavelu S, et al. Synthetic growth hormone-releasing hormone agonist ameliorates the myocardial pathophysiology characteristic of HFpEF. *Cardiovasc Res.* (2022). [Epub ahead of print]. doi: 10.1093/cvr/cvac098

18. Shen J, Zhang N, Lin Y, Xiang P, Liu X, Shan P, et al. Regulation of vascular calcification by growth hormone-releasing hormone and its agonists. *Circ Res.* (2018) 122:1395–408.

19. Woodward H, Zhu D, Hadoke P, MacRae V. Regulatory role of sex hormones in cardiovascular calcification. *Int J Mol Sci.* (2021) 2021:22.

20. Bostrom K, Jumabay M, Matveyenko A, Nicholas S, Yao Y. Activation of vascular bone morphogenetic protein signaling in diabetes mellitus. *Circ Res.* (2011) 108:446–57.

21. Yang X, Wang H, Huang Y, Huang J, Ren H, Xu Q, et al. Myeloid angiotensin II type 1 receptor mediates macrophage polarization and promotes vascular injury in DOCA/salt hypertensive mice. *Front Pharmacol.* (2022) 13:879693. doi: 10.3389/fphar.2022.879693

22. Lin M, Chen T, Wallingford M, Nguyen N, Yamada S, Sawangmake C, et al. Runx2 deletion in smooth muscle cells inhibits vascular osteochondrogenesis and calcification but not atherosclerotic lesion formation. *Cardiovasc Res.* (2016) 112:606–16. doi: 10.1093/cvr/cvw205

23. Haarhaus M, Cianciolo G, Barbuto S, La Manna G, Gasperoni L, Tripepi G, et al. Alkaline phosphatase: an old friend as treatment target for cardiovascular and mineral bone disorders in chronic kidney disease. *Nutrients.* (2022) 2022:14. doi: 10.3390/nu14102124

24. Hu M, Shi M, Zhang J, Quinones H, Griffith C, Kuro-o M, et al. Klotho deficiency causes vascular calcification in chronic kidney disease. *J Am Soc Nephrol.* (2011) 22:124–36.

25. Prud'homme G, Kurt M, Wang Q. Pathobiology of the Klotho antiaging protein and therapeutic considerations. *Front Aging.* (2022) 3:931331. doi: 10.3389/fragi.2022.931331

26. Yamada S, Giachelli C. Vascular calcification in CKD-MBD: roles for phosphate, FGF23, and klotho. *Bone.* (2017) 100:87–93.

27. Chen Y, Zhao X, Wu H. Arterial stiffness: a focus on vascular calcification and its link to bone mineralization. *Arterioscler Thromb Vasc Biol.* (2020) 40:1078–93. doi: 10.1161/ATVBAHA.120.313131

28. Ogunmoroti O, Osibogun O, Mathews L, Esuruoso O, Ndumele C, Okunrintemi V, et al. Favorable cardiovascular health is associated with lower prevalence, incidence, extent, and progression of extracoronary calcification: MESA. *Circ Cardiovasc Imaging.* (2022) 15:e013762. doi: 10.1161/CIRCIMAGING.121.013762

29. Devesa J. The complex world of regulation of pituitary growth hormone secretion: the role of ghrelin, klotho, and nesfatins in it. *Front Endocrinol.* (2021) 12:636403. doi: 10.3389/fendo.2021.636403

30. Ghosh S, Luo D, He W, Chen J, Su X, Huang H. Diabetes and calcification: the potential role of anti-diabetic drugs on vascular calcification regression. *Pharmacol Res.* (2020) 158:104861. doi: 10.1016/j.phrs.2020.104861

31. Toth A, Balogh E, Jeney V. Regulation of vascular calcification by reactive oxygen species. *Antioxidants.* (2020) 2020:9.

32. Furmanik M, Chatrou M, van Gorp R, Akbulut A, Willems B, Schmidt H, et al. Reactive oxygen-forming nox5 links vascular smooth muscle cell phenotypic switching and extracellular vesicle-mediated vascular calcification. *Circ Res.* (2020) 127:911–27. doi: 10.1161/CIRCRESAHA.119.316159

33. Li P, Wang Y, Liu X, Liu B, Wang Z, Xie F, et al. Loss of PARP-1 attenuates diabetic arteriosclerotic calcification via stat1/runx2 axis. *Cell Death Dis.* (2020) 11:22.

34. Li W, Feng W, Su X, Luo D, Li Z, Zhou Y, et al. SIRT6 protects vascular smooth muscle cells from osteogenic transdifferentiation via runx2 in chronic kidney disease. *J Clin Invest.* (2022) 2022:132. doi: 10.1172/JCI150051

35. He X, Wang Z, Wei L, Cheng X, Chen L, Gao F, et al. Indoxyl sulfate promotes osteogenic differentiation of vascular smooth muscle cells by miR-155-5p-dependent downregulation of matrix Gla protein via ROS/NF-kappaB signaling. *Exp Cell Res.* (2020) 397:112301. doi: 10.1016/j.yexcr.2020.112301

36. Tintut Y, Hsu J, Demer L. Lipoproteins in cardiovascular calcification: potential targets and challenges. *Front Cardiovasc Med.* (2018) 5:172. doi: 10.3389/fcvm.2018.00172

37. Yu L, Li M. Roles of klotho and stem cells in mediating vascular calcification (review). *Exp Ther Med.* (2020) 20:124.

38. Zubkiewicz-Kucharska A, Wikiera B, Noczynska A. Soluble klotho is decreased in children with type 1 diabetes and correlated with metabolic control. *Front Endocrinol.* (2021) 12:709564. doi: 10.3389/fendo.2021.7095

Frontiers in
Cardiovascular Medicine

Innovations and improvements in cardiovascular treatment and practice

Focuses on research that challenges the status quo of cardiovascular care, or facilitates the translation of advances into new therapies and diagnostic tools.

Discover the latest Research Topics

See more →

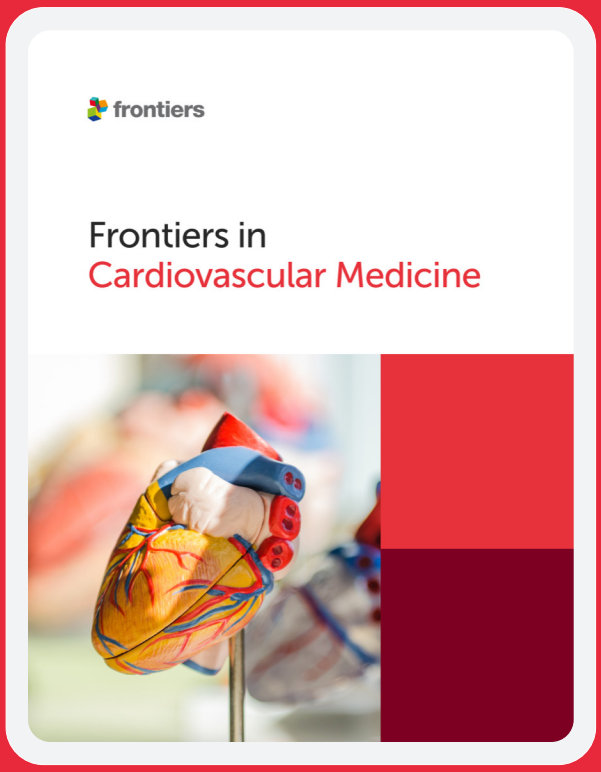

Frontiers

Avenue du Tribunal-Fédéral 34
1005 Lausanne, Switzerland
frontiersin.org

Contact us

+41 (0)21 510 17 00
frontiersin.org/about/contact